Identification and Characterization of Novel Hedgehog Signaling Pathway Inhibitors and their Cellular Targets

Dissertation

zur Erlangung des akademischen Grades eines

Doktors der Naturwissenschaften

(Dr. rer. nat.)

der Fakultät für Chemie und Chemische Biologie

der Technischen Universität Dortmund

vorgelegt von

M.Sc. Lea Kremer

geboren am 26.08.1989

in Herdecke, Deutschland

Dortmund, 05.02.2018

Die vorliegende Arbeit entstand im Zeitraum von Oktober 2013 bis Januar 2018 unter der Anleitung von Prof. Dr. Dr. h.c. Herbert Waldmann und Dr. Slava Ziegler an der Fakultät für Chemie und Chemische Biologie der Technischen Universität Dortmund und dem Max-Planck-Institut für Molekulare Physiologie Dortmund.

1. Gutachter: Prof. Dr. Dr. h.c. Herbert Waldmann

2. Gutachter: Prof. Dr. Alfred Wittinghofer

A goal is a dream with a deadline

Napoleon Hill

Results presented in this thesis contributed to the following publications:

M. Garcia-Castro, L. Kremer, C. D. Reinkemeier, C. Unkelbach, C. Strohmann, S. Ziegler,C. Ostermann, K. Kumar, "*De novo* branching cascades for structural and functional diversity in small molecules", *Nature communications* **2015**, *6*, 6516.

J. Švenda, M. Sheremet, L. Kremer, L. Maier, J. O. Bauer, C. Strohmann, S. Ziegler, K. Kumar, H. Waldmann, "Biology-oriented synthesis of a withanolide-inspired compound collection reveals novel modulators of hedgehog signaling", *Angewandte Chemie (International ed. in English)* **2015**, *54*, 5596.

L. Kremer, C. Schultz-Fademrecht, M. Baumann, P. Habenberger, A. Choidas, B. Klebl, S. Kordes, H. R. Schöler, J. Sterneckert, S. Ziegler, H. Waldmann, "Discovery of a Novel Inhibitor of the Hedgehog Signaling Pathway through Cell-based Compound Discovery and Target Prediction", *Angewandte Chemie (International ed. in English)* **2017**, *56*, 13021.

L. Kremer, E. Hennes, A. Brause, A. Ursu, L. Robke, H. T. Matsubayashi, Y. Nihongaki, I. Mejdrová, J. Eickhoff, M. Baumann, R. Nencka, P. Janning, S. Kordes, H. R. Schöler, J. Sterneckert, T. Inoue, S. Ziegler, H. Waldmann, "Phosphatidylinositol 4-kinase IIIβ is a positive Regulator of Hedgehog Signaling", *Submitted* **2018**

ACKNOWLEDGEMENTS

Obtaining a PhD is a journey that can be very exciting, demanding and, after all, extremely enriching, both on a scientific and on a personal level. I want to thank all the people who took this journey with me and contributed to its success.

First and foremost, I would like to thank Prof. Dr. Herbert Waldmann for giving me the opportunity to work in this vibrant field and on this interesting project while having access to excellent equipment and resources. I highly appreciate his encouragement and input throughout the time of my PhD. I truly value that he created a working atmosphere that stimulates independent and self-motivated work. It made me grow on so many levels.

I want to express my gratitude to Prof. Dr. Alfred Wittinghofer for being my second examiner and sharing his knowledge on primary cilia.

I am deeply grateful to Dr. Slava Ziegler, my co-supervisor and group leader who provided guidance for my scientific project but also supported my commitment in the Max Planck PhDnet and always encouraged me to develop my soft skills. Her constructive ideas, comments and suggestions have helped me to push my projects forward. Her appreciation of my work continuously motivated me to do my best. I also want to thank her for proofreading my thesis.

My special thanks go to M.Sc. Elisabeth Hennes whom I supervised during her master thesis and who contributed to this thesis with her work on the Pipinib project. Her creative ideas and suggestions were an enrichment for me and the project. Likewise, I want to thank Alexandra Brause, who worked with me during her time as a trainee and after she finished her training. Her reliability and positive personality contributed to this thesis, not only on an experimental level.

I am deeply grateful to Dr. Andrei Ursu and Dr. Lucas Robke who were the incarnate chemistry to my chemical biology projects, performed the synthesis for the Pipinib project and were always eager to discuss and advance the project. Without them, many experiments would not have been possible. Additionally, I would like to thank Dr. Miguel García-Castro, Dr. Michael Sheremet and Dr. Jakub Švenda who synthesized compounds for the other projects in this thesis. I also would like to thank Dr. Matthias Baumann and Claudia Hesse from the Lead Discovery Center for providing the two compounds, Smoothib and Pipinib, which became my main projects. I appreciate the discussions with Dr. Matthias Baumann and Dr. Peter Habenberger and the knowledge transfer concerning the Hedgehog project.

I would particularly like to thank Dr. Petra Janning, Andreas Brockmeyer, Malte Metz and Jens Warmers from the mass spectrometry team for measuring my samples, analyzing the mass spectrometry data and giving constructive feedback on my experimental design and the overall project. Additionally, I want to thank Dr. Sven A. H. Müller, Dr. Jan Hübinger, Dr. Michael Schulz and Dr. Stefano Maffini for providing training for and access to microscope and flow cytometry devices. I am thankful to the team of the Compound Management and Screening Center, especially Dr. Sonja Sievers and Dr. Claude Ostermann, for compound screening, compound handling and methodical discussions as well as sharing material and assay protocols. I am grateful to the administration and central facilities of the Max Planck Institute of Molecular Physiology. The excellent organization creates the perfect framework for science. Keeping this in mind, I want to express my gratitude to Brigitte Rose for her help and support in all administrative issues.

I would also like to thank Prof. Dr. Gisbert Schneider (ETH Zürich), Dr. Takanari Inoue (Johns Hopkins University, Baltimore) and Dr. Radim Nencka (IOCB Prague) for fruitful collaborations.

I gratefully acknowledge the International Max Planck Research School in Chemical and Molecular Biology, namely Prof. Dr. Andrea Musacchio, Christa Hornemann and Dr. Lucia Sironi, for supporting my development as a researcher through funding of conferences, seminars, scientific courses and for providing an excellent graduate course program. A very special thank you goes to Christa Hornemann and Beate Schölermann who provided continuous support (also on non-scientific matters), counselling and invaluable advice.

I would like to thank the whole department and the bio-group for creating a warm and open working atmosphere that made me enjoy my time at the institute so much more. Dr. Yasemin Akbulut, Dr. Shobhna Kapoor, Dr. Marc Schürmann and M.Sc. Tabea Schneidewind are especially acknowledged for great company, insightful comments, scientific discussions and encouragement. I also want to thank Dr. Guillaume Garivet for answering all my chemistry-related questions and being a great desk neighbor. Additionally, I would like to acknowledge all people who contributed to this thesis with input, support or experimental help, namely: Dr. Silke Brand, Dr. Javier Ceballos, M.Sc. Jana Flegel, Dr. Alexandra Friese, M.Sc. Stefanie Kösling, Dr. Luca Laraia, Christine Nowack, Dr. Sumersing Patil, M.Sc. Bernd Rathmer, M.Sc. Elena Reckzeh, Dr. Kirsten Tschapalda, Dr. Glòria Vendrell-Navarro and M.Sc. Julian Wilke.

My deepest and heartfelt appreciation goes to my parents, my partner, my sister and my brother for their everlasting support and encouragement. They have made me the person I am today. Without them, none of this would have been possible.

TABLE OF CONTENTS

1. ABSTRACT

As a major developmental pathway, Hedgehog (Hh) signaling is required for segment polarity in *Drosophila* and limb pattering in vertebrates. Since its discovery 40 years ago, several studies have identified various pathway components and helped to elucidate the underlying mechanisms of signal transduction. Nevertheless, some regulatory steps during pathway induction are not yet fully understood. Similar to other developmental pathways like Wnt, TGFβ or Notch signaling, also Hh signaling plays a central role in cancer, e.g. medulloblastoma and basal cell carcinoma. Due to the open questions concerning pathway mechanisms and the relevance in some forms of cancer, novel modulators of Hh signaling are in high demand.

Following a high-throughput screen for inhibition of Purmorphamine-induced osteogenesis, six inhibitors of Hedgehog signaling were characterized in this thesis. All compounds inhibited GLI-responsive reporter gene expression and suppressed the expression of Hh target genes. Two compounds, a withanolide A- and a pyrazolo-imidazole derivative bind to the heptahelical bundle of SMO, a membrane protein and central transducer of Hh signaling activity also known as the most druggable target of the Hh signaling pathway. The pyrazolo-imidazole derivative, termed Smoothib, impairs ciliary entry of SMO and most likely adopts a binding mode similar to that of SANT-1, a SMO antagonist that is effective against resistant SMO mutants. Four further compounds, quinoline-, indole-, azepinone- and thienopyrimidine derivatives, did not bind to the cyclopamine binding site of SMO. Screening of a kinase panel revealed that the thienopyrimidine derivative, termed Pipinib, selectively inhibits phosphatidylinositol 4-kinase IIIβ (PI4KB) in an ATP-competitive manner. This lipid kinase is required for production of phosphatidylinositol-4-phosphate (PI4P) and necessary for proper function and integrity of the Golgi apparatus as well as membrane trafficking and protein transport from the trans-Golgi network to the plasma membrane. Cellular levels of PI4P were reduced upon treatment with Pipinib, suggesting that PI4KB is inhibited by the compound in cells. PI4KB was validated as a positive regulator of Hh signaling via chemical and genetic depletion. PI4KB depletion sensitizes cells towards treatment with Pipinib, suggesting that PI4KB mediates Hh inhibition of Pipinib. Mode of action studies revealed that Pipinib impairs ciliary trafficking of PI4KB and that PI4KA inhibition only leads to minor reduction of Hh signaling. In combination with an already published role of PI4P in SMO activation, the results of this thesis lead to the conclusion that PI4KB is a major PI4-kinase source of PI4P that is required for SMO activation and transduction of Hh signaling activity.

1. KURZZUSAMMENFASSUNG

Als ein bedeutender entwicklungsbiologischer Signalweg ist der Hedgehog (Hh)-Signalweg verantwortlich für die Segmentpolarität in *Drosophila* und die Extremitätenentwicklung in Vertebraten. Seit seiner Entdeckung vor 40 Jahren wurden zahlreiche Mitglieder der zugehörigen Signalkaskade identifiziert. Nichtsdestotrotz wurden einige Schritte des Signalwegs bisher noch nicht komplett aufgeklärt. In Analogie zu anderen entwicklungsbiologischen Signalwegen spielt auch die Hh-Signaltransduktion eine zentrale Rolle in gewissen Krebserkrankungen, z.B. beim Medulloblastom und Basalzellkarzinom. Aufgrund der offenen Fragen bezüglich der Signaltransduktion und der Relevanz für die Krebsentstehung werden neue Hh-Modulatoren dringend gesucht.

Ausgehend von einem Hochdurchsatz-Screening für Inhibitoren der Purmorphamin-induzierten Osteogenese wurden im Rahmen dieser Arbeit sechs Inhibitoren des Hh-Signalwegs charakterisiert. Alle Substanzen inhibierten GLI-vermittelte Reportergen- und Hh Zielgenexpression. Ein Withanolid A- und ein Pyrazolo-Imidazol-Derivat binden an das heptahelikale Bündel von SMO, ein Membranprotein, das für die Signalweiterleitung verantwortlich ist und als am besten zu inhibierendes Zielprotein im Signalweg gilt. Das Pyrazolo-Imidazol-Derivat, genannt Smoothib, beeinträchtigt den ziliären Eintritt von SMO und bindet SMO in einem Modus, der dem bekannten SMO-Inhibitor SANT-1 gleicht, welcher Resistenzen gegenüber SMO Antagonisten überwinden kann. Vier weitere Substanzen, ein Chinolin-, ein Indol-, ein Azepinon- und ein Thienopyrimidin-Derivat binden nicht an die Cyclopamin-Bindungsstelle von SMO. Die Bestimmung der Inhibition von Kinasen ergab, dass das Thienopyrimidin-Derivat, genannt Pipinib, die Phosphatidylinositol 4-Kinase IIIβ (PI4KB) selektiv und ATP-kompetitiv inhibiert. Diese Lipidkinase ist wichtig für die korrekte Funktion und Integrität des Golgi-Apparats sowie den Membrantransport und den Transport von Proteinen vom trans-Golgi-Netzwerk zur Plasmamembran. Die Behandlung mit Pipinib führte zur Reduktion der zellulären PI4P-Pegel, was zur Annahme führte, dass PI4KB auch in Zellen durch Pipinib inhibiert wird. PI4KB wurde mittels chemischer und genetischer Depletion als positiver Regulator des Hh Signalwegs validiert. Depletion von PI4KB führte zu einer Sensibilisierung der Zellen gegenüber Pipinib. Dies spricht dafür, dass PI4KB die inhibitorische Wirkung von Pipinib auf den Hh Signalweg vermittelt. Die Substanz beeinträchtigt die ziliäre Lokalisation von SMO. Die Inhibition von PI4KA hingegen, führt nur zu einer geringen Inhibition des Hh-Signalwegs. In Kombination mit einer bereits veröffentlichten Rolle von PI4P in der Aktivierung von SMO, führen die Ergebnisse dieser Arbeit zu dem Schluss, dass PI4KB eine wichtige Quelle für PI4P darstellt, welches für die Aktivierung von SMO und die Weiterleitung des Hh-Signals entscheidend ist.

2 INTRODUCTION

2.1 Chemical Biology

Chemical biology works at the interface of chemistry and biology. It is said to be or become the major bridge between chemistry, biology and medicine[1]. In chemical biology, biological questions are answered with the tools of chemistry[1]. Small molecules are used to perturb biological systems. The observed phenotypic effects are dissected to derive new knowledge on biological processes, cellular signaling pathways and the functions of cellular components, like proteins, lipids, carbohydrates or nucleic acids. Like this, disease-relevant phenomena can be studied, and novel therapies can be discovered.

The work presented in this thesis can be assigned to the field of chemical genetics. In biology, function and relevance of proteins are typically studied via genetic removal or mutation of the respective protein and subsequent monitoring of cellular effects. The chemical biology field does the same but replaces genetic removal with chemical perturbation. This approach encompasses several advantages compared to conventional genetics. First, chemical perturbations are reversible – if a small molecule is removed, the cellular system usually can recover. Second, small molecules can be used to study essential developmental genes. If such genes would be knocked out in animal studies, the respective animal would not survive, and a study would not be possible. Third, chemical interference is fast and versatile. Different time-points, concentrations and mode of actions can be studied with one tool. Fourth and last, small molecules can cover more than proteins. They can also be employed to modulate the function of lipids, nucleic acids or carbohydrates. Of course, also the application of small molecules has limitations. On the one hand, identification of potent compounds requires screening of large compound collections or even libraries, which is connected to an immense synthetic effort. On the other hand, small molecules are rarely specific and many (off-)targets remain unknown, rendering phenotype analysis a complex and difficult process.[2,3]

Chemical genetics can be performed in two directions: forward and reverse[2,3]. Figure 1 illustrates the differences between classical and chemical genetics as well as the two directions. In forward chemical genetics, which was applied in this thesis, researchers start with a desired phenotype, e.g. perturbation of mitosis or inhibition of a signaling pathway, and then choose hit compounds that induce this desired effect in cells or organisms to identify and validate their targets[3]. Here, a major challenge is target identification and validation, which will be explained in detail in 2.1.1 and 2.1.2. This approach is often applied in academia as it enables the discovery of new (disease-relevant) proteins and processes[3].

In reverse chemical genetics, a specific protein of interest is the starting point. Typically biochemical assays are applied to directly monitor modulation of this protein. Hit compounds are chosen, if need be, optimized, and later on applied to more complex systems, i.e. cells and multicellular organisms[3]. Here the challenge lies in the identification of proper hit compounds that will be effective in living systems.

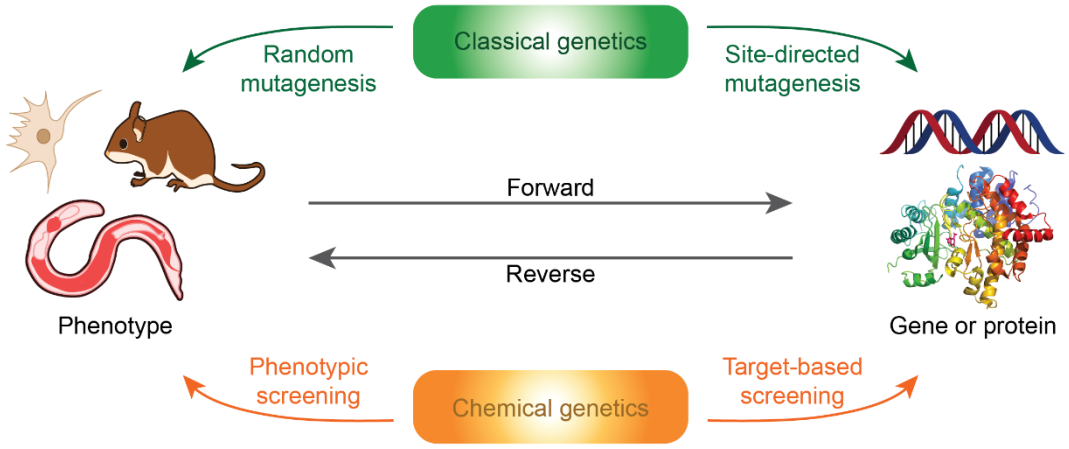

Figure 1. Classical vs. Chemical genetics. Adopted from Kawasumi and Nghiem[3]. Both fields can follow a forward or a reverse approach. The forward genetics starts with perturbation of a complex system, e.g. a living cell or organism, to induce a phenotype. Here, the challenge lies in the choice of a proper system and the identification of the target that is mainly responsible for the observed phenotype. In classical genetics, random mutagenesis is applied to induce phenotypic effects. In chemical genetics, compound collections are screened for desired phenotypes. The reverse genetics approach starts with target of interest and later on monitors target-related effects in living systems. Classical genetics uses site-directed mutagenesis, whereas chemical genetics employs target-based screening to study single targets. Especially in chemical genetics, the challenge lies in the proper choice of the screening assay format and right choice of small molecules to follow up.

In forward chemical genetics, mostly disease-relevant targets are chosen. This approach is commonly applied in the pharmaceutical industry[3], with the pitfall that many companies study the same targets, leading to a decrease in the variety of available drugs. Phenotypic screens have encountered a revival in the pharmaceutical industry but still suffer from the efforts, risks as well as unpredictable time lines and costs associated with target identification and validation[4].

2.1.1 Target identification

The identification of the target of a small molecule is a crucial step in forward chemical genetics. Several methods are available but not all techniques are applicable for all targets –

usually the success of a target identification project is based on choosing the right method. Some of the most widely used techniques will be explained in this chapter.

One of the first and still commonly applied target identification techniques is affinity chromatography. Using the small molecule as a bait, which is coupled to a solid support, potential targets are enriched from a cellular lysate. After extensive washing to remove unspecific binders, the enriched proteins are eluted from the solid support and digested for subsequent mass spectrometry. The identified peptides are then compared with a database and assigned to their parent protein. A negative probe that is similar to the bait compound but inactive in the underlying phenotypical screen is used as a control for unspecific binding. Peptides that are enriched by the compound but not by the negative control are considered as possible targets. A simplified scheme that illustrates the basic principle of this method is shown in Figure 2.

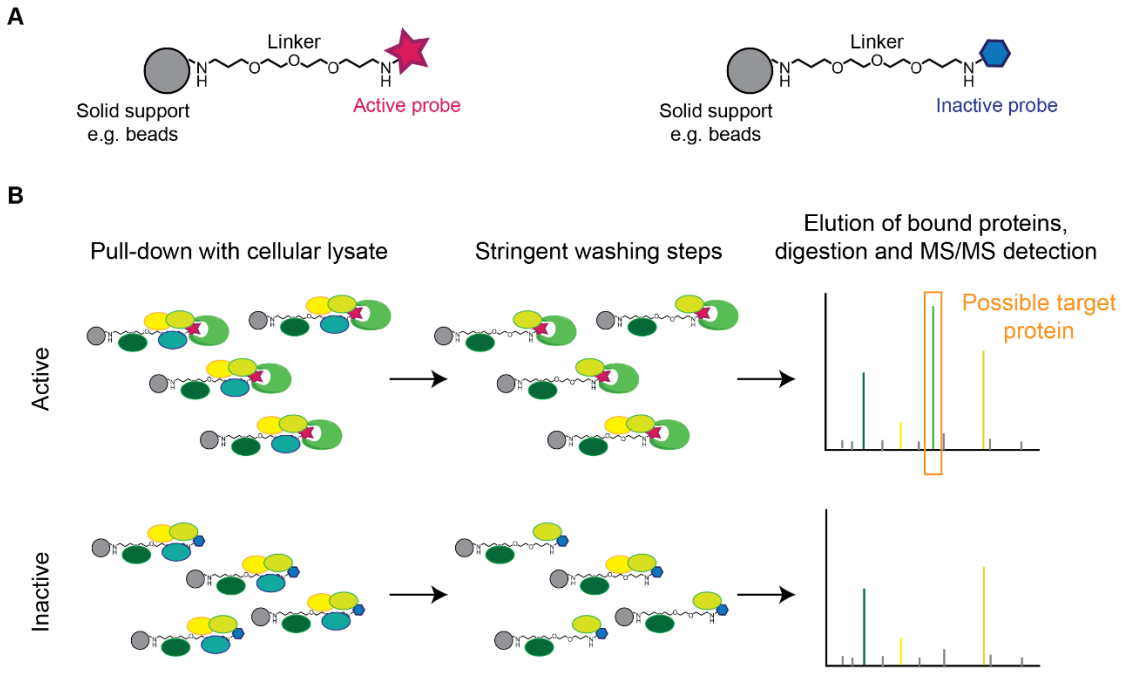

Figure 2. Affinity chromatography protein pull-down based on a small-molecule probe. A. Exemplary design of active and inactive probe. **B.** Simplified scheme of experimental steps. First, aliquots of the same lysate are incubated with either active or inactive probe. The probes are subsequently washed several times to remove unspecifically bound proteins before elution, digestion and mass spectrometry detection (MS/MS). Comparison of the spectra detected for active and inactive probe enables identification of proteins that were significantly enriched by the active probe and might be potential targets of the compound of interest.

A disadvantage of this technique is the necessity of linker attachment. To couple the compound bait to a solid support and provide sufficient space between compound and solid

support to prevent steric hindrance, a spacer, e.g. an alkyl-, or triethylene glycol-linker, has to be attached to the small molecule. To maintain compound activity after linker attachment, a position on the molecule has to be chosen that will tolerate this modification. In order to find this optimal position, the relation of compound structure to activity (structure-activity relationship, SAR) has to be known. For this, synthesis of various compound derivatives is required. This step is very laborious and does not exclude the possibility to enrich unspecific or false targets. Affinity chromatography has been advanced by the use of functional probes that could engage targets in living cells or the incorporation of heavy and light amino acids (stable isotope labeling by amino acids in cell culture (SILAC)) to enable quantification and simplify sample handling.[5]

To overcome the limitations imposed by linker attachment, modification-free target identification approaches have been developed. One of them is the cellular thermal shift assay (CETSA). This technique monitors thermal stability of a protein in presence and absence of a small molecule. Ligand binding can change the thermal stability of a protein and thus, observed changes between control and ligand-treated sample can indicate a possible interaction. For purified proteins, thermal stability assays have already been applied for decades. CETSA now uses this principle to monitor interactions in cell lysates or even living cells. Thermal stability is monitored by measuring protein solubility. Since unfolded proteins form aggregates, these insoluble components of the cell lysate can be removed via centrifugation. The remaining supernatant can be analyzed for protein abundance either via immunoblotting or mass spectrometry, thereby covering all detectable proteins of the proteasome that exhibit a melting behavior. Figure 3 depicts the basic principle of the cellular thermal shift assay. Comparison of the melting curves of compound- and control-treated samples enables identification of stabilized or destabilized proteins and thereby yields possible targets. If the technique is applied for the whole proteome, it is often called thermal proteome profiling (TPP).[6] There are first examples of *de novo* target identification and the interesting approach to identify “off-targets” of small molecules and use this information to repurpose common drugs towards further implications[7].

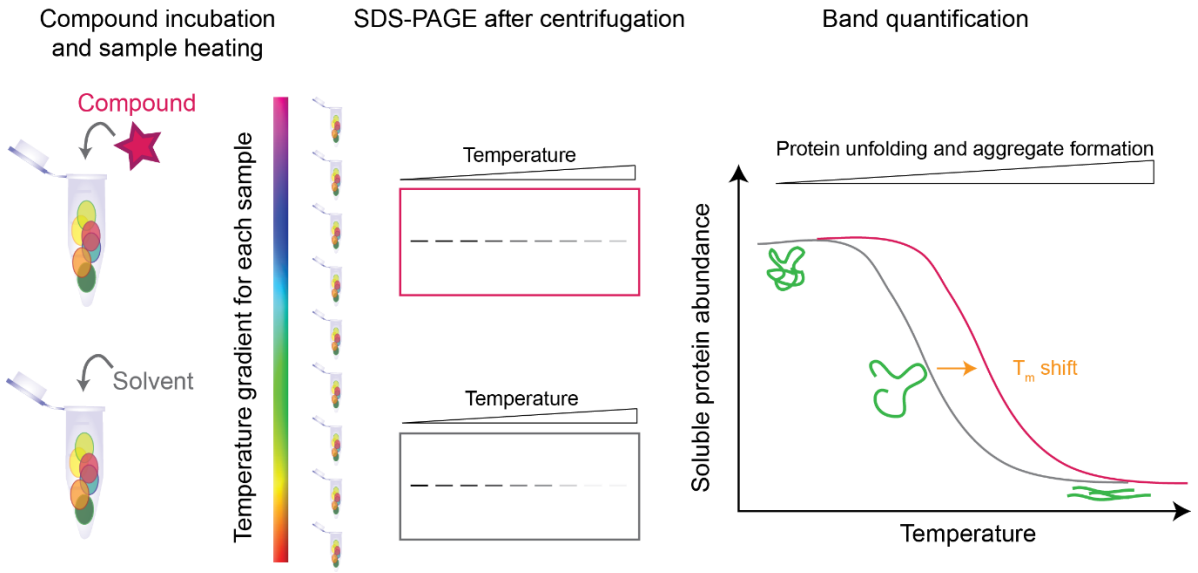

Figure 3. Cellular thermal shift assay (CETSA). Aliquots of the same lysate are either incubated with the small-molecule (compound) of interest or the solvent control. The lysates are then aliquoted and heated to increasing temperatures, before removal of insoluble proteins (aggregates) via centrifugation. A SDS-PAGE reveals the amounts of soluble protein for each temperature step. Quantification of band intensity enables generation of a melting curve and calculation of a melting temperature (T_m). Interaction with a small molecule can stabilize a protein and lead to a shift of the melting curve as well as an increase of the melting temperature.

While both affinity chromatography and CETSA require mass spectrometry analysis of protein samples to identify unknown targets, also methods that monitor changes on the genetic level can be applied. One example is the screening for compound-resistant clones. A limitation of this technique is that it is only applicable to toxic compounds. If cells that are likely to mutate, e.g. cancer cells, are incubated with medium to high concentrations of the compound, some of these cells will develop resistance-conferring mutations and survive compound treatment. If the transcriptome, i.e. the expressed RNA sequences, of these cells is sequenced and compared to the transcriptome of cells that were isolated before compound treatment, genomic mutations and/or differently expressed RNAs might provide hints on possible targets (Figure 4). This approach assumes that only mutations in compound targets will enable resistance to compound-induced toxicity. Of course, also general mechanisms like the overexpression of drug transporters or drug metabolizing enzymes can lead to resistance. To exclude this possibility, control cells can be incubated with other toxic compounds that are common substrates of drug transporters and/or induce other mechanisms that are connected to multi-drug resistance. Comparison of the obtained transcriptome data enables identification of general resistance conferring mutations and target specific alterations.[6]

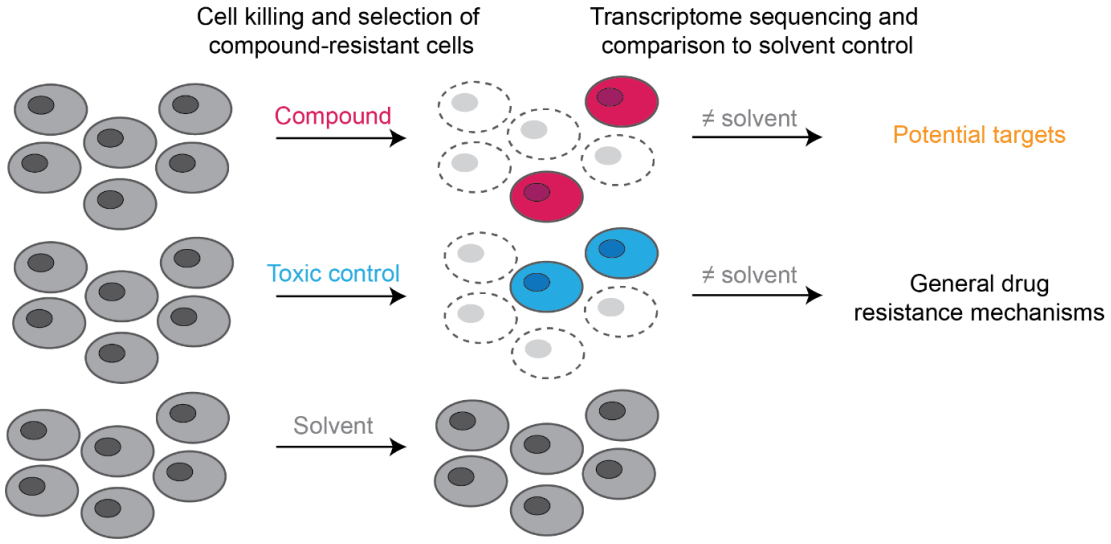

Figure 4. Compound-resistant mutant screening. Cancer cells are incubated with the compound of interest, a toxic control compound or a solvent control until toxic effects are observed. Surviving cells are isolated, expanded and their transcriptome is sequenced. Comparison with the solvent control reveals gene mutations that might cause resistance to the compound. Thus, the corresponding gene could encode the target protein of the compound. Gene mutations induced by the toxic control compound could indicate general drug resistance mechanisms and help to exclude unspecific mutations.

Furthermore, computational methods can be applied to identify possible targets. For this, databases are used to compare small-molecule structures or fragments to those of compounds with known targets. Similar compound structure often correlates with similar binding behavior and target engagement. Thus, target hypotheses can be derived.[6] The SPIDER tool, which was also applied in this thesis, is an example for an innovative advancement of this approach since it does not only compare compound structures but pharmacophore features thereby broadening the applicability of computational target prediction.[6,8]

Another interesting field is also based on the comparison of a small molecule to reference compounds with known targets. This approach, however, is not based on the compound structure but on similar phenotypic profiles[6]. In the so-called cell painting assay, which has been applied in this thesis as well, the phenotypic profile is assembled by collecting data on the morphology of cellular structures. These structures are labelled using specific markers and dyes and are monitored via automatic imaging in medium throughput.[9] Similar phenotypic/morphological profiles can be caused by similar targets and therefore might give a first hint for a target hypothesis.

While not being an experimental approach, the so-called educated guess, i.e. the use of one's experience and scientific knowledge to derive a target hypotheses, often yields important and

constructive hints towards target identification. For example, if a compound is either showing a common structural feature or exhibits a specific phenotypic profile that is common for modulation of a certain protein, this can be followed up by biochemical or biophysical binding assays and also lead to identification (or de-validation) of a possible target.

2.1.2 Target validation

If a target has been identified, e.g. by means of one of the methods described in 2.1.1, it has to be validated. This means, on the one hand, target engagement has to be confirmed and, on the other hand, it has to be verified that modulation of this target causes the observed phenotype.

Several methods can be employed to prove target engagement. The aforementioned CETSA can be carried out and detected via immunoblotting using appropriate antibodies. Like this, a dose-response curve can be recorded for a fixed temperature as a measure of compound affinity (isothermal dose response fingerprinting (ITDRF))[10]. Additionally, several biophysical methods can be used when purified protein is available, e.g. surface plasmon resonance, isothermal titration calorimetry (ITC), circular dichroism (CD) spectroscopy or fluorescence polarization, the latter however, requires a fluorescent labelling of the small molecule and thus is not modification-free. Additionally, when using a fluorescently labelled small molecule in cells that express the fluorescently tagged target protein, fluorescence resonance energy transfer (FRET) can be employed to prove target engagement in living cells. If the two fluorophores have appropriately overlapping emission and absorbance spectra, FRET can occur if the small molecule and the protein are in sufficient proximity. If the donor fluorophore is excited, it will transfer the energy to the acceptor fluorophore that, in turn, will emit fluorescent light of a distinct wavelength, serving as a detectable measure for interaction.[5]

To further verify that target engagement also occurs in cells, functional assays should be applied based on the nature and function of the target protein. Monitoring the cellular processes that are dependent on the target protein can give insights into cellular efficacy. Additionally, *in vitro* activity assays can be performed for enzymatic targets. Still, it is important to note that target engagement does not necessarily result in enzyme inhibition.[5] A compound might bind to several proteins inside the cell. The main target of a compound, however, usually induces the observed phenotype upon compound binding. To confirm a potential target as a phenotype-relevant target, one can either use structurally unrelated compounds that target the same protein or genetically deplete the protein and observe the induced phenotype. If the phenotype is the same, i.e. a phenocopy is observed, the protein is relevant

for the respective cellular process or signaling pathway. Genetic depletion can be achieved for example by means of siRNA knockdown or CRISPR-Cas-mediated knockout. Additionally, knockout mouse-derived cell lines can be applied. It must be appreciated, though, that genetic depletion is distinct from small molecule modulation and thus might also cause a different phenotype. So far, phenocopy only confirms the relevance of the respective protein for the monitored cellular process. If the phenotypic effect is caused by compound binding to a specific protein, reduction of the protein amount should increase compound potency. If a knockout of the protein was produced, compound potency should be lost due to absence of the target. Overexpression of the protein of interest can decrease compound potency due to a scavenging effect or induce a phenocopy if the protein is activated by the compound.[5] Since overexpression drastically interferes with cell physiology and the induced phenotype is dependent on protein function as well as the mode of action of the compound, the observed effects can differ from this common expectation.[11,12]

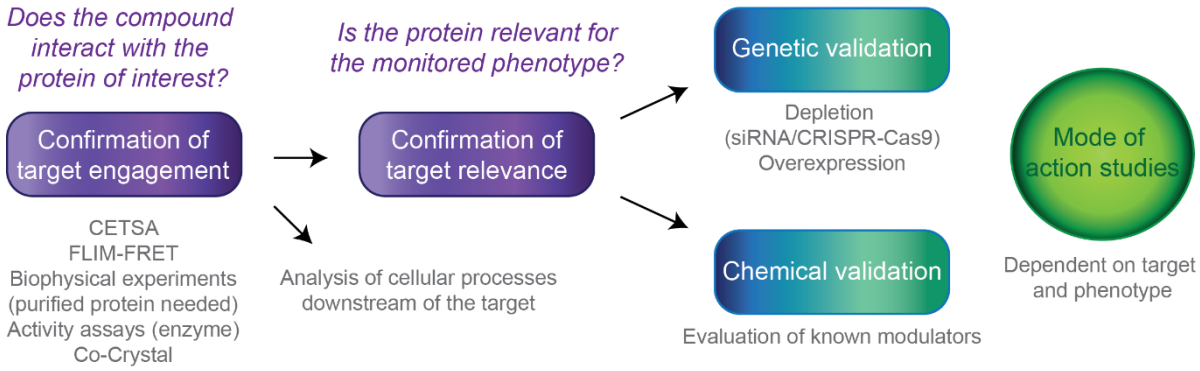

Figure 5. Target validation workflow. The first step in target validation encompasses a proof of interaction between compound and potential target. This can be accomplished by e.g. CETSA, FLIM-FRET (fluorescence lifetime-fluorescence resonance energy transfer) and, if applicable, biophysical or activity assays as well as co-crystallization. Additionally, cellular processes that are dependent on target function can be monitored to gain further proof of interaction between compound and target within cells. This step is followed by confirmation of target relevance, i.e. evaluation whether inhibition (or activation) of the target is responsible for the observed phenotype. Applied methods include genetic and chemical validation, i.e. depletion/introduction or application of inhibitors/activators of the protein of interest. Mode of action studies mark the final step of target validation and aim at elucidating how inhibition of the target causes the observed phenotype and are strongly dependent on the target protein and the respective phenotype.

The very last step of target validation includes analysis of the mode of action. This step aims at evaluating the cellular effects of target modulation and at explaining how these effects cause the observed phenotype. Appropriate experiments are strongly dependent on the target, the observed phenotype and the nature of target modulation by the compound. Figure 5 illustrates the usual target validation workflow that has also been applied in this thesis.

2.2 The Hedgehog Signaling Pathway in Vertebrates

This thesis was aimed at identifying and characterizing inhibitors of the Hedgehog (Hh) signaling pathway. This is why this pathway and its transduction and regulatory mechanisms are explained below.

Almost 40 years ago, the Hh ligand was discovered during mutational experiments in *Drosophila melanogaster*, the common fruit fly, by Christiane Nüsslein-Volhard and Eric Wieschaus[13]. It was named after the induced phenotype in mutated larvae that had spines on their backs, resembling those of a hedgehog. Further studies have led to the discovery of the underlying pathway and revealed that it is important for several developmental processes, which lead to cell patterning and differentiation during embryonic development[14]. In 1995, Nüsslein-Volhard, Wieschaus and Edward B. Lewis were awarded the Nobel Prize in medicine for their groundbreaking work in the field of developmental biology. The Hh signaling molecule fulfills the role of morphogen, i.e. secretion of Hh induces the formation of a gradient that, in concert with other morphogen gradients, contributes to tissue identity[14]. In vertebrates, three different Hh ligands, which have distinct roles in embryonic development, have been identified: Sonic hedgehog (SHH) is required for the function of the zone of polarization activity during limb and notochord development and is also found in the floor plate of the neural tube, Indian hedgehog (IHH) is responsible for bone and cartilage development while Desert hedgehog (DHH) is necessary for the development of germ cells within the testis and the formation of peripheral nerve sheaths.[14] Binding of the Hh ligands to its cellular receptor induces a signaling cascade that results in activation of transcription factors and changes the transcriptional activity of the target cell to induce cell proliferation, differentiation and determine tissue identity. The details of signal transduction are explained in the following chapters.

2.2.1 Signal Transduction

In vertebrates, several crucial signaling steps are connected to the primary cilium, a membrane protrusion that represents a defined cellular compartment and concentrates a lot of membrane receptors and signaling molecules[15,16]. In absence of a Hh ligand, the transmembrane receptor patched (PTC) inhibits through so far unknown mechanisms the ciliary localization of smoothened (SMO), a seven-pass G-protein coupled receptor-like transmembrane protein that is responsible for induction of downstream signaling[17]. Glioma-associated oncogene 2 and 3 (GLI2/3), bifunctional transcription factors and key transducers

of the Hedgehog signal, are inhibited via two mechanisms. On the one hand, suppressor of Fused (SUFU), a negative Hh regulator, prevents their nuclear localization[18]. On the other hand, phosphorylation by protein kinase A (PKA), glycogen synthase kinase 3β (GSK3β) and casein kinase I (CK1) triggers their proteasomal processing into truncated repressor forms[19]. A scheme of critical pathway steps is depicted in Figure 6.

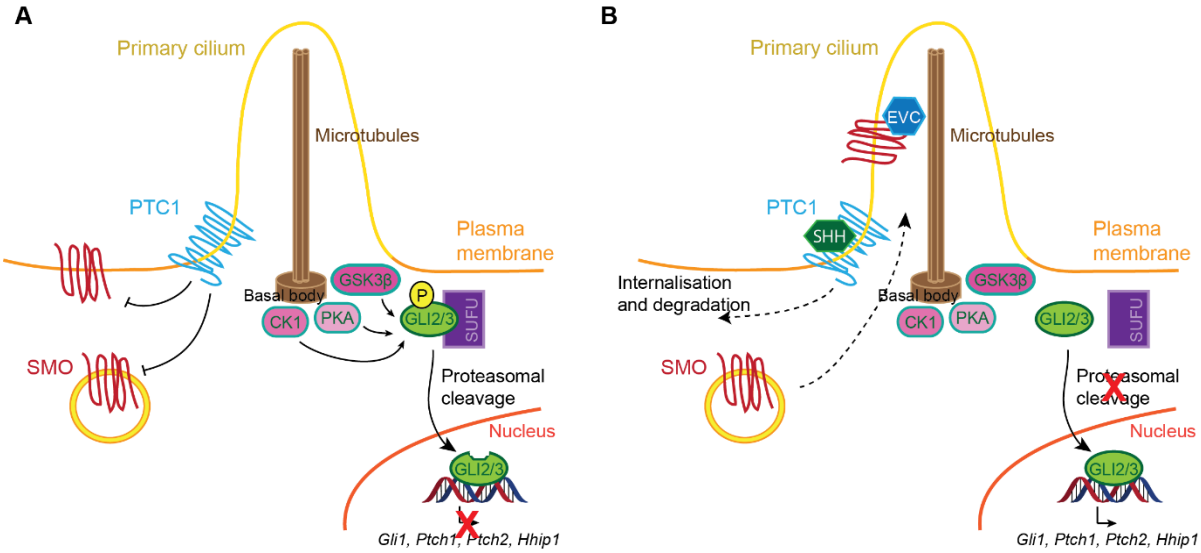

Figure 6. Simplified scheme of the Hedgehog signaling pathway in vertebrates. A. Inactive pathway. PTC1 inhibits ciliary localization of SMO. The GLI2/3 transcription factors are retained in the cytoplasm by Suppressor of Fused (SUFU) where they are phosphorylated by glycogen synthase kinase 3β (GSK3β), casein kinase 1 (CK1) and protein kinase A (PKA). This triggers proteasomal cleavage of GLI2/3 which migrate into the nucleus as transcriptional repressors and inhibit target gene expression. **B.** Active pathway. Upon binding of SHH, PTC1 is internalized and degraded. This relieves SMO repression, enabling its translocation to the primary cilium, where it interacts with several interaction partners, like EVC and EVC2, and prevents phosphorylation of GLI2/3. The transcription factors then migrate to the nucleus as full-length activators and activate expression of target genes, e.g. *Gli1*, *Ptch1*, *Ptch2* and *Hhip1*.

If SHH binds to PTC1, the receptor is inhibited, internalized and degraded[20]. This relieves inhibition of SMO, which can translocate to the cilium[21]. Here, interaction of SMO with several binding partners, like the Ellis-van Creveld proteins (EVC and EVC2)[22], recruits GLI2/3 to the cilium and leads to their dissociation from SUFU[23]. GLI2/3 subsequently translocate to the nucleus as transcriptional activators, bypassing proteasomal cleavage[19], and induce transcription of several target genes, e.g. *Gli1*, *Ptch1*, *Ptch2* and *Hhip1* (Hedgehog interacting protein 1)[24].

2.2.2 Regulation of Smoothened

Since regulation of SMO plays a central role in the Hh signaling pathway and likewise plays a central role in this thesis, the following paragraphs are dedicated to the complex and in parts still unresolved mechanisms that control SMO activity and signal transduction. The efforts of various research groups have led to profound knowledge about SMO structure, trafficking and signaling, thereby enabling the generation of several hypotheses that will be discussed below.

SMO **structure** classifies it as a class F GPCR that contains a cysteine-rich domain (CRD) at its extracellular amino terminus. This region is homologous to a region of the Frizzled (Fz) Wnt receptor and was thus suggested to possess ligand binding properties[25]. Figure 7 schematically illustrates the structure of SMO and highlights the different binding sites.

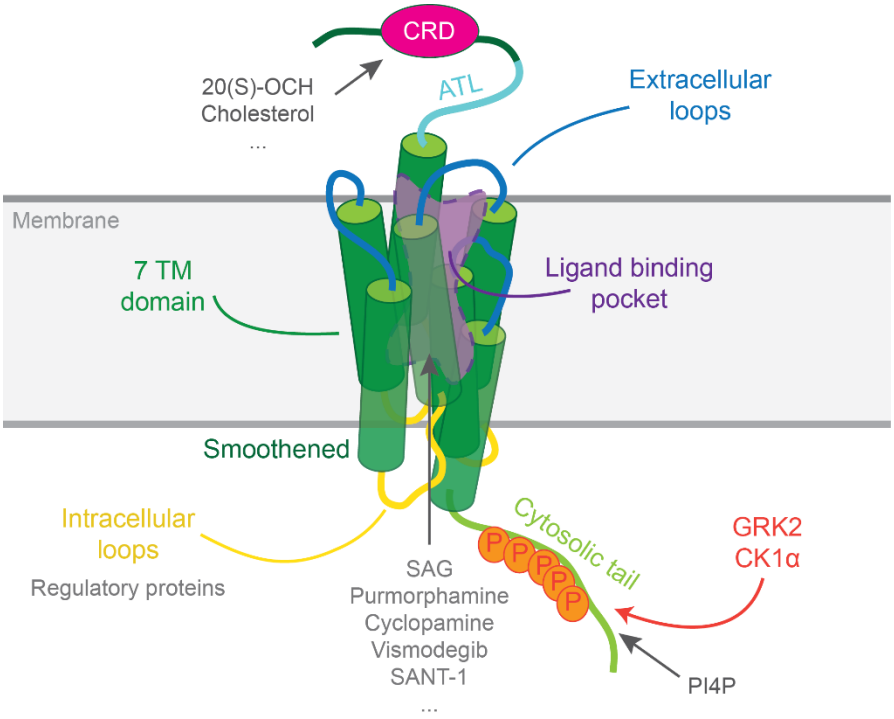

Figure 7. Structure and regulation of SMO. Three interaction sides, the cysteine-rich domain (CRD), the heptahelical bundle of the seven transmembrane (7 TM) domain containing the ligand binding pocket and the cytosolic tail are bound by several bio- and small molecules. The intracellular loops interact with regulatory downstream proteins and the cytosolic tail is phosphorylated by G-protein coupled kinase 2 (GRK) and casein kinase 1α (CK1α) which leads to receptor activation.

It was found that the oxysterol 20(S)-OHC, a SMO agonist, binds to a hydrophobic groove within the cysteine-rich domain[26]. It was further shown that an amino-terminal linker domain (ATL) at the CRD interacts with extracellular (EC) loops 1 and 3, suggesting that appropriate

positioning of the CRD towards the EC loops is important for SMO activation[27]. Additionally, the ATL coordinates binding of Smoothened Agonist (SAG), which induces movement of intracellular loop 1 (IC1) towards W535[28]. This specific amino acid is mutated in a constitutively active form of SMO (W535L) that is common in Hh-related cancers like basal cell carcinoma[29]. Thus, the interaction between IC1 and W535 is likely to be a key event during induction of SMO activity[30]. Several SMO agonists and antagonists bind within the seven transmembrane (7TM) domain highlighting the function of this substructure as a ligand binding pocket. The IC loops of GPCRs function as an interaction site with G proteins[31] and based on several studies, it was proposed that SMO IC loops interact with regulatory proteins that modulate its activity[30]. The C-terminal tail of SMO (C-tail) was shown to interact with β-arrestins, which mediate its internalization[32]. Additionally, the C-tail is hyperphosphorylated by G-protein coupled kinase 2 (GRK2) and casein kinase 1α (CK1α) upon Hh pathway activation[33]. The level of phosphorylation is proportional to the amount of Hh ligand stimulation[34], thereby representing a method to translate morphogen gradients to pathway induction[30]. Binding of PI4P to the C-tail precedes these phosphorylation events[35]. In *Drosophila*, SMO ubiquitination has an inhibitory effect on Hh signaling via SMO recycling but this was not yet confirmed for vertebrate Hh signaling.[30]

The **trafficking** of SMO to the primary cilium of vertebrate cells is believed to be the central step during pathway activation. This process typically takes place within 20 minutes after pathway induction[30], during which SMO has to pass the physical barriers of the primary cilium, i.e. the ciliary pockets and the transition zone[36]. Both PTC1 and SMO have a ciliary localization sequence (CLS) but only PTC is located in the cilium in the absence of the Hh ligand[30]. If the pathway is activated, PTC is internalized and SMO localizes to the cilium. If activated by small molecules like SAG, SMO localizes to the cilium independently of PTC, suggesting that PTC does not physically inhibit ciliary localization of SMO[30,37]. Trafficking of SMO to the cilium was suggested to be mediated either via lateral transport through the ciliary pockets, special membrane domains at the ciliary base that were suggested to play a central role in cilia associated vesicular trafficking[38], or via recycling endosomes[39]. Within the cilium, SMO occupies different locations based on its activation status. While inactive SMO is localized at the base, active SMO is found at the tip of the primary cilium[40]. It is unclear how localization within the cilium is controlled with respect to receptor activity. Since phosphoinositides define membrane identity, it was proposed that they play a role in SMO localization (see 2.2.3). As mentioned before, phosphatidylinositol-4-phosphate (PI4P) directly binds to the cytosolic tail of SMO and induces SMO phosphorylation and ciliary localization leading to pathway activation[35]. The role of PTC in SMO regulation is still

unresolved. Since PTC shares homology with the bacterial Resistance, Nodulation, Division (RND) family of small-molecule pumps[41,42] and has a sterol-sensing domain, several models for PTC-mediated SMO regulation have been suggested. It was proposed that PTC controls the abundance of either a sterol agonist, that is removed in the absence of a Hh ligand or a sterol antagonist that is enriched by PTC until induction of Hh signaling[30]. Additionally, it was assumed that PTC could also control the plasma membrane composition by regulating lipid kinases.[30]

Downstream **signaling** of SMO can be grouped into two categories: canonical and non-canonical signaling. Canonical signaling results in activation of GLI-mediated transcription and requires SMO translocation to the primary cilium[30]. How SMO activates GLI is not clear. It is known, however, that the regulation of PKA-mediated phosphorylation of GLI is dependent on the interaction between SMO and the Ellis-van-Creveld 2 (EVC2) ciliary complex[43], which controls ciliary entry and activation of GLI[44]. Non-canonical signaling does not always result in activation of GLI and does not necessarily require ciliary localization of SMO[45]. It leads to modulation of Ca^{2+} flux, RHOA/RAC activation and can induce Warburg-like metabolism via the G protein αi subunit (Gαi)[45–47]. It is not known how the decision between canonical and non-canonical signaling is made. Different possible SMO ligands that induce distinct conformations and localizations might have an influence on this decision.[30]

2.2.3 Phosphoinositides and Hedgehog signaling

Phosphoinositides are generated upon phosphorylation of phosphatidylinositol. Inositol can be phosphorylated at three different positions (3, 4 and 5) to form seven distinct phosphoinositides that can be converted into each other by the actions of various lipid kinases and phosphatases. The glycerol backbone is esterified to two fatty acid chains[48], most commonly these are arachidonic and stearic acid (Figure 8A). Phosphoinositides are known to define organelle and membrane identity and to control lipid distribution as well as endo- and exocytosis. Additionally, their discovery as signaling molecules led to the emergence of an entire new field of research.[49]

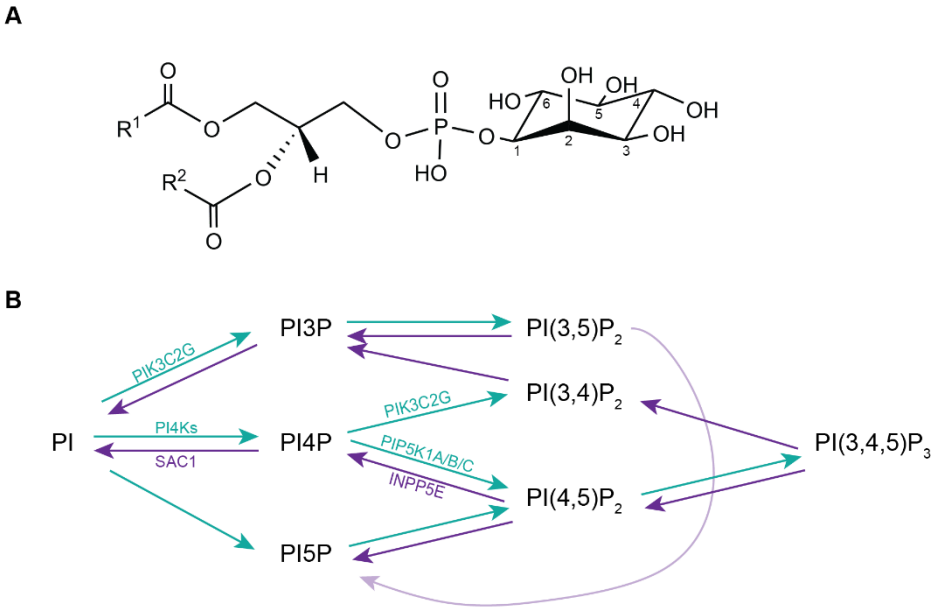

Figure 8. Phosphoinositides. A. General structure of Phosphatidylinositol. **B.** Complex network of phosphoinositides and converting lipid kinases (turquoise) or phosphatases (purple). To reduce complexity, only a few kinases and phosphatases are shown. PIK3C2G = Phosphatidylinositol-4-phosphate 3-kinase catalytic subunit type 2γ, PI4Ks = Phosphatidylinositol 4-kinases, SAC1= Suppressor of actin mutations 1-like protein, PIP5K1A/B/C = Phosphatidylinositol 4-phosphate 5-kinasae type 1α/β/γ, INPP5E = inositol polyphosphate-5-phosphatase E.

There is growing evidence that phosphoinositides are relevant for a plethora of cellular processes. Therefore, it is not surprising that they are also implicated in Hh signaling. The first hint for an implication of phosphoinositides in Hh signaling was provided by Yavari and colleagues in 2010, who reported that proper functioning of the *Drosophila* Sst4 lipid kinase, an orthologue of the vertebrate phosphatidylinositol 4-kinase IIIα (PI4KA) and source of PI4P (Figure 8B), is necessary for the membrane localization of dSMO[50]. The authors also found that siRNA knockdown of the mammalian lipid kinases PI4KA and phosphatidylinositol 4-kinase IIIβ (PI4KB) leads to inhibition of GLI dependent reporter gene expression[50]. Five years later, in 2015, two publications reported the distinct distributions of PI4P and phosphatidylinositol 4,5-bisphosphate ($PI(4,5)P_2$) within the primary cilium and the consequences for Hh signaling[51,52]. The authors revealed that PI4P is the predominant phosphoinositide in primary cilia and that knockout of the inositol polyphosphate-5-phosphatase E (INPP5E) leads to accumulation of $PI(4,5)P_2$ in the ciliary membrane. These results suggest that PI4P in the primary cilium is generated via dephosphorylation of $PI(4,5)P_2$ at the 5-position by INPP5E. Furthermore, inactivation of INPP5E also results in ciliary accumulation of tubby-like protein 3 (TULP3) and G-protein coupled receptor 161 (GPR161),

negative regulators of Hh signaling, proposing that PI(4,5)P_2 interacts with TULP3, which, in turn, recruits GPR161 to the primary cilium. One year later, in 2016, Jiang and coworkers have shown that PI4P directly interacts with the C-terminal tail of SMO and causes a conformational change that results in SMO phosphorylation and migration to the cilium, leading to activation of Hh signaling[35]. These findings emphasize that phosphoinositides play a central role at various stages of the Hh signaling pathway.

2.2.4 Phosphatidylinositol 4-kinase IIIβ

The family of phosphatidylinositol 4-kinases (PI4Ks) is subdivided into type II and type III PI4Ks. The type II PI4Ks are integral membrane proteins while type III PI4Ks are cytosolic proteins that are transiently associated with membranes to fulfill their functions[48]. Phosphatidylinositol 4-kinase IIIβ belongs to the type III PI4Ks that are evolutionary related to phosphoinositide 3 kinases (PI3Ks)[53]. The other type III PI4K is PI4KA, which is mainly localized at the endoplasmic reticulum (ER), where it is necessary for protein export from the ER[54] and the generation of the PI4P plasma membrane pool that is converted to PI(4,5)P_2[55]. PI4KB, however, is predominantly located at the Golgi apparatus, where it is required for proper formation and function of this organelle[48]. It plays essential roles in maintaining lysosomal identity[56], cytokinesis[57], ER-to-Golgi transport of ceramide[58] and vesicular trafficking within the trans-Golgi network (TGN)[48]. Several proteins recognize PI4P via a specific binding domain, i.e. the pleckstrin homology (PH) domain, e.g. the oxysterol-binding protein (OSBP), the ceramide transfer protein (CERT) or the four-phosphate-adaptor protein (FAPP), and are implicated in intra-Golgi transport[48]. PI4Ks are mainly regulated via proper recruitment to lipid membranes by their interaction partners. PI4KB is recruited to the Golgi apparatus by the GTPase ADP-ribosylation factor 1 (ARF1)[59] and the Acyl-CoA-binding domain containing protein 3 (ACBD3)[60]. Furthermore, neuronal calcium sensor 1 (NCS-1) binds and activates PI4KB[61]. Additionally, protein kinase D phosphorylates serine 294 of PI4KB[62] leading to recruitment of 14-3-3 proteins and stabilization of PI4KB kinase activity[63]. PI4KB itself is essential for recruitment of the GTPase RAB11 to the Golgi and the TGN[64], where it is necessary for membrane trafficking[48]. It was suggested that this function of PI4KB is independent of its catalytic activity.[48] Figure 9 illustrates the localization of all PI4Ks.

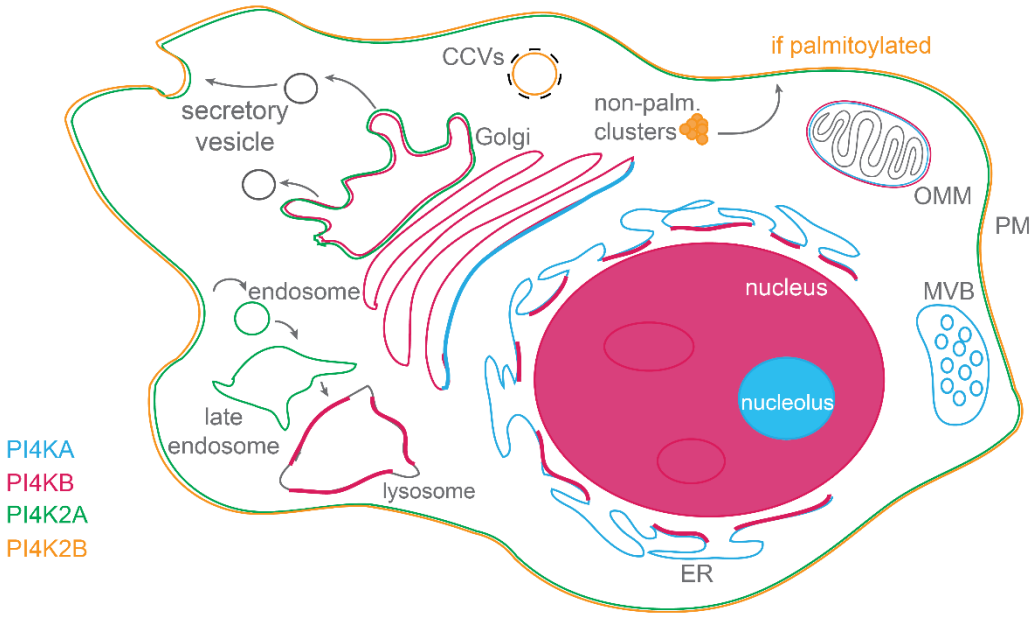

Figure 9. Cellular localization of PI4Ks. Adopted from Tan and Brill[65]. The localization of the different kinases is indicated by the color code. CCVs = clathrin-coated vesicles, non.-palm. = non-palmitoylated, OMM = outer mitochondrial membrane, MVB = multivesicular bodies.

Type III PI4Ks are relevant drug targets because they play a central role during virus infection. Positive-sense, single-stranded RNA viruses hijack type III PI4Ks to form membranous complexes rich in PI4P for replication and prevention of host defense mechanisms.[48]

2.2.4.1 Phosphatidylinositol-4-phosphate

PI4P, the product of PI4Ks, and PI(4,5)P_2 are the most abundant phosphoinositides in cells[66]. The distribution of PI4P is controlled by the localization of the different PI4Ks and the establishment of local PI4P pools.[66] The localization of PI4P is depicted in Figure 10. The best-defined role of PI4P lies in the transport of proteins/cargo from the Golgi to the PM and endosomes. Here, PI4P is essential for cargo sorting into carriers, TGN to PM transport, changes in membrane composition that enable vesicle formation and the retention of Golgi proteins[66]. Also, during transport of post-Golgi vesicles to the PM, the PI4P content of the vesicle membrane defines the different stages of vesicle maturation and finally controls fusion with the PM.

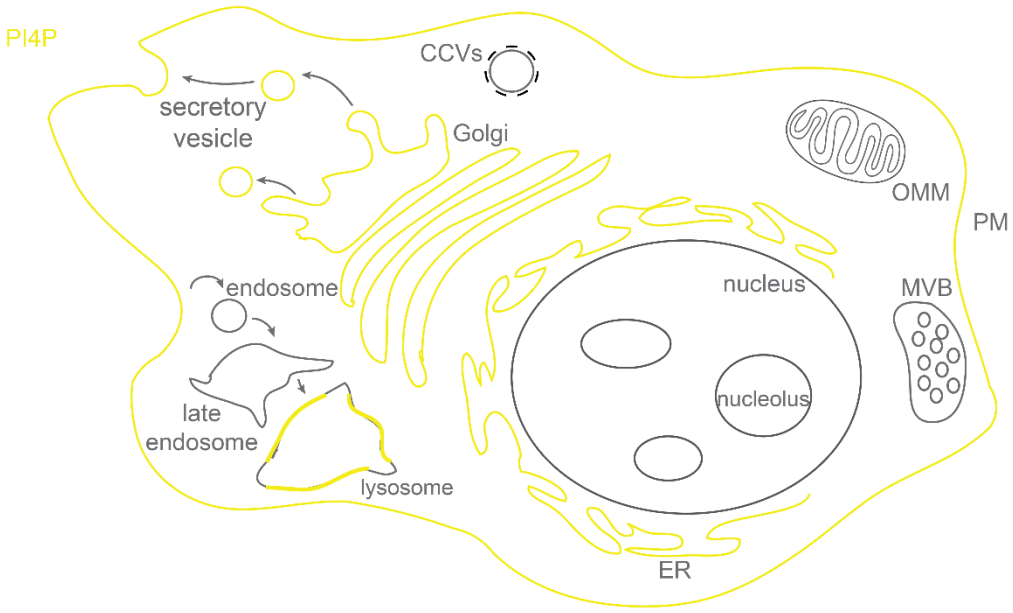

Figure 10. Cellular localization of PI4P. Adopted from Tan and Brill[65]. The localization of PI4P is indicated in yellow. CCVs = clathrin-coated vesicles, OMM = outer mitochondrial membrane, MVB = multivesicular bodies.

In yeast, the guanine-nucleotide exchange factor (GEF) Sec2 is recruited to vesicles that are rich in PI4P and activates Sec4, a small GTPase of the RAB family, which regulates vesicle transport along actin cables to the PM by Myo2 motor proteins. Thus, Sec2/Sec4 bind to vesicles/membranes with high PI4P content and regulate the transport to the PM, whereas Sec15, a component of the exocyst complex[67], binds to vesicles with low PI4P content close to the PM and mediates association with the exocyst apparatus that, in turn, mediates vesicle fusion with the PM[66].

The binding of OSBP and 12 OSBP-related proteins (ORP) to PI4P is required for intracellular transport of lipids[68]. Between ER and Golgi as well as at the ER, OSBP exchanges PI4P for sterol. For this, the SAC1 phosphatase hydrolyzes PI4P to phosphatidylinositol and the produced energy is employed for the sterol transfer[69]. ORP5 and 8 on the other hand mediate the transport of phosphatidylserine between ER and PM and are recruited to ER-PM contact sites via interaction between their PH domain and PI4P[70]. FAPP1 and FAPP2 also bind PI4P via their PH domain and form a complex with ARFs at the TGN[71]. These two proteins are necessary for glycosphingolipid metabolism and membrane sensing mechanisms.[68]

As described above, very recently, a distinct role was discovered for PI4P. The phosphoinositide binds to the SMO receptor, which, most likely enabled by the negative charge of PI4P, induces a conformational change in the C-terminal tail of SMO. This leads to

its phosphorylation by GRK2 and CK1α and migration to the primary cilium, resulting in activation of Hh signaling[35]. Additionally, the absence of PI4P from the primary cilium membrane was shown to impair proper Hh signaling[51,52].

2.2.4.2 Modulators of PI4KB

The first compound that selectively inhibited PI4KB among the class III PI-4 kinases was PIK93 (Figure 11A)[72]. Since this compound also inhibits several PI-3 kinases, it was used as a starting scaffold to synthesize other inhibitors with improved overall selectivity. Groups at Boehringer Ingelheim[73] and Novartis[74] have reported PI4KB inhibitors that have low nanomolar IC_{50} values and display selectivity among PI-4 and PI-3 kinases (Figure 11B and C).[75]

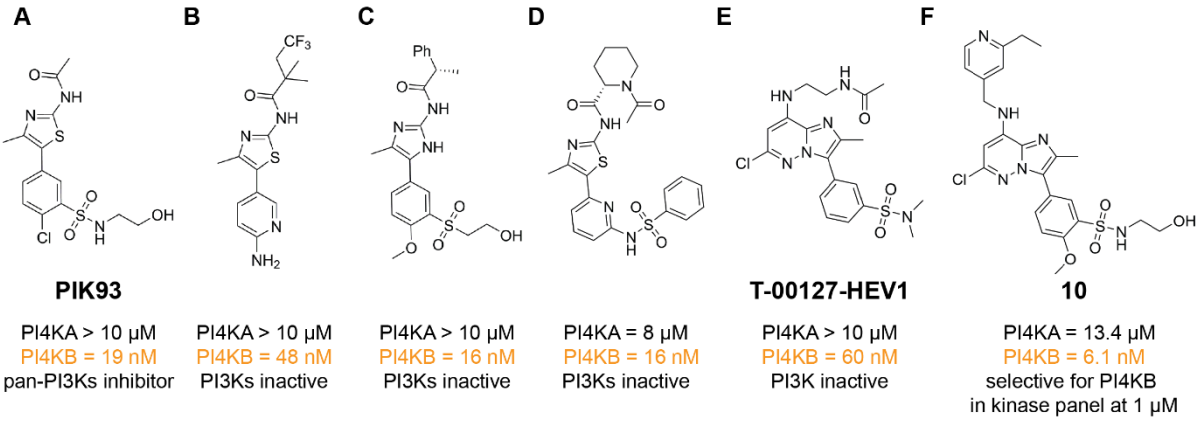

Figure 11. Selection of published PI4KB inhibitors. Adopted from Boura and Nencka[75]. Displayed values are IC_{50} values measured in *in vitro* kinase activity assays. **A.** PIK93. **B.** Compound from Boehringer Ingelheim. **C.** Compound from Novartis. **D.** Compound for AstraZeneca. **E.** T-00127-HEV1. **F.** Compound **10**.

Due to the implication of PI4KB in virus replication[48] many pharmaceutical companies had an interest in the development of potent inhibitors, which is why also AstraZeneca reported a further inhibitor based on PIK-93 (Figure 11D)[76]. Mejdrová *et al.* published inhibitors of PI4KB with further improved selectivity (Figure 11F) by combining structural elements of yet another published inhibitor of PI4KB, T-00127-HEV1 (Figure 11E)[77], and PIK93[78]. T-00127-HEV1 (compound **9**) as well as the inhibitors published by Mejdrová and colleagues (compound **10** and two derivatives: **11** and **12**) have been applied in this thesis. Several other PI4KB inhibitors have been published and were reviewed by Boura and Nencka[75].

2.2.5 Open Questions concerning the regulation of Hh signaling

The majority of open questions concerning the regulation of Hh signaling circles around SMO regulation and signal transduction and has been nicely summed up by Arensdorf *et al.*[30]

One of the most intriguing questions is how PTC regulates SMO activity and localization. Common hypotheses include PTC-mediated control of the abundance of an endogenous ligand or the lipid composition of the PM. Despite several candidates, an endogenous ligand of SMO, if it exists, has not been confirmed yet. It is likewise elusive, if several ligands are necessary and whether cooperative ligand binding at distinct binding sites is part of the activation mechanism. Furthermore, it is not clear how SMO is transported into the primary cilium and how this process is regulated. Additionally, the precise mechanism that leads to GLI activation downstream of SMO is not completely resolved, either. Last but not least, it is not known how differentiation between canonical and non-canonical signaling is accomplished and whether both pathways are equally important for embryonic development and cancer formation or progression.[30]

Complementary to genetic studies, small-molecule Hh modulators with novel targets and modes of action could help to perturb and study these pathway mechanisms. Target identification for novel compound hits may even lead to the discovery of further pathway members and might help to solve some of these open questions.

2.3 Hedgehog Signaling in Cancer Development and Progression

Being a developmental pathway that controls cell proliferation and differentiation, aberrant and deregulated Hh signaling can likewise lead to the formation of cancer. Common mutations, aberrant signaling mechanisms as well as common Hh-related cancers are described in this chapter.

2.3.1 Cancers related to Hh signaling

The first implication of Hh signaling in cancer was discovered when PTC1 mutations were found in patients with Gorlin syndrome who suffered from basal cell carcinoma (BCC, skin cancer), medulloblastoma (MB, brain tumor) and rhabdomyosarcoma (RBS, skeletal muscle cell tumor)[79,80]. BCC is the cancer with the highest frequency of mutations within the Hh signaling pathway, mostly in PTC1 or SMO[81–83]. Other common Hh-responsive tumors are

MB[84,85], pancreatic[86] and colorectal cancers[87], as well as lymphomas and multiple myeloma[88].[15] The underlying mechanisms are described in 2.3.2.

2.3.2 Aberrant Hh signaling and cancerogenesis

Except for tissue repair and regeneration, the Hh signaling pathway is quiescent in adult tissues. If the pathway gets activated due to mutations, cells and tissues can proliferate in an uncontrolled manner, leading to tumor formation[89]. Four tumor-relevant mechanisms connected to Hh signaling have been described:

2.3.2.1 Ligand-independent mechanisms

Ligand-independent mechanisms encompass all signaling variations that arise due to mutations of pathway components downstream of the Hh ligand. Gene amplifications of *Gli1* have been discovered in glioblastoma, as well as loss-of-function mutations in PTC in Gorlin syndrome and loss-of-function mutations in SUFU in basal cell carcinoma (BCC), medulloblastoma (MB) and rhabdomyosarcoma (RMS). The gain-of-function mutation of SMO (W535L), which leads to constitutive activity of the receptor, belongs to the most studied mutations in Hh signaling and is likewise common for BCC, MB and RMS. More than 70% of sporadic BCC harbor Hh specific gene alterations that can be subdivided in PTC (75%), SMO (10%) and SUFU (5%) mutations.[89]

2.3.2.2 Ligand-dependent mechanisms

Pathway deregulations that are induced by altered ligand secretion are defined as ligand-dependent mechanisms. The autocrine category describes increased Hh ligand secretion of cancer cells and binding of the Hh ligand to secreting cells, leading to activation Hh signaling to drive cell proliferation[90]. In contrast to that, the paracrine mechanism leads to secretion of Hh protein as well but the ligands target stromal cells instead of cancer cells to develop a favorable tumor microenvironment including expression of vascular endothelial growth factor and insulin growth factor that promote tumor proliferation and differentiation[91]. Reverse-paracrine secretion is defined as Hh ligand production by stromal cells to activate Hh signaling in cancer cells[92]. These Hh induction mechanisms have been reported for various types of cancer, e.g. tumors of the gastrointestinal system (gastric, colorectal, etc.) and non-solid tumors like lymphoma, as well as typical Hh-related tumors like glioblastoma.[89]

2.3.2.3 Non-canonical crosstalk

As already mentioned for SMO, non-canonical Hh signaling leads to activation of Hh pathway components but does not include the whole PTC-SMO-GLI axis[89]. Several signaling pathways have been reported to influence components of the Hh signaling pathway via crosstalk mechanisms. The main target, GLI, is regulated by e.g. transforming growth factor β (TGFβ), Kirsten rat sarcoma (KRas), mitogen activated protein kinase (MAPK) cascade, tumor necrosis factor-α (TNF-α), phosphoinositide 3-kinase (PI3K)-protein kinase B (AKT) and Wnt signaling.[89]

2.3.2.4 Cancer stem cells

Like hematopoietic stem cells, which possess the ability to self-renew, divide asymmetrically, i.e. into a differentiating and a stem daughter cell and are able to generate all cell types of the blood system (pluripotency), also most cancers contain a small subset of cells, i.e. cancer stem cells (CSCs), that is believed to be responsible for long-term tumor growth, metastasis, resistance and recurrence. These cells are the cause of the tumor's hierarchical organization and are capable of tumor initiation due to their ability to self-renew and enter a quiescent state that often results in resistance to standard therapies.[93]

Hh signaling was found to play a central role in the regulation of CSCs[94], e.g. colon carcinoma stem cells exhibit a high expression level of *Ptch1*, *Gli1* and *Gli2* and breast cancer stem cells have proven to be sensitive to Hh inhibition. Especially in the light of cancer recurrence and treatment resistance, therapeutic inhibition of Hh signaling might be beneficial.[89]

2.4 Modulators of Hedgehog Signaling

Due to its immense influence on cancer development and progression, the Hedgehog signaling pathway has become one of the most studied developmental pathways as well as an attractive therapeutic target. This led to the development of various synthetic modulators of Hh signaling. Despite the high number of modulators being published, the number of Hh targets is considerably low. Most of the known activators or inhibitors bind to SMO. Very few compounds have other targets. Some examples are introduced in this chapter.

2.4.1 Inhibitors

The very first identified Hh inhibitor was Cyclopamine (Figure 12A). It is a natural product found within *Veratrum californicum*, the California corn lily. The offspring of sheep that were feeding from this poisonous plant suffered from cyclopia and other facial phenotypes[95].

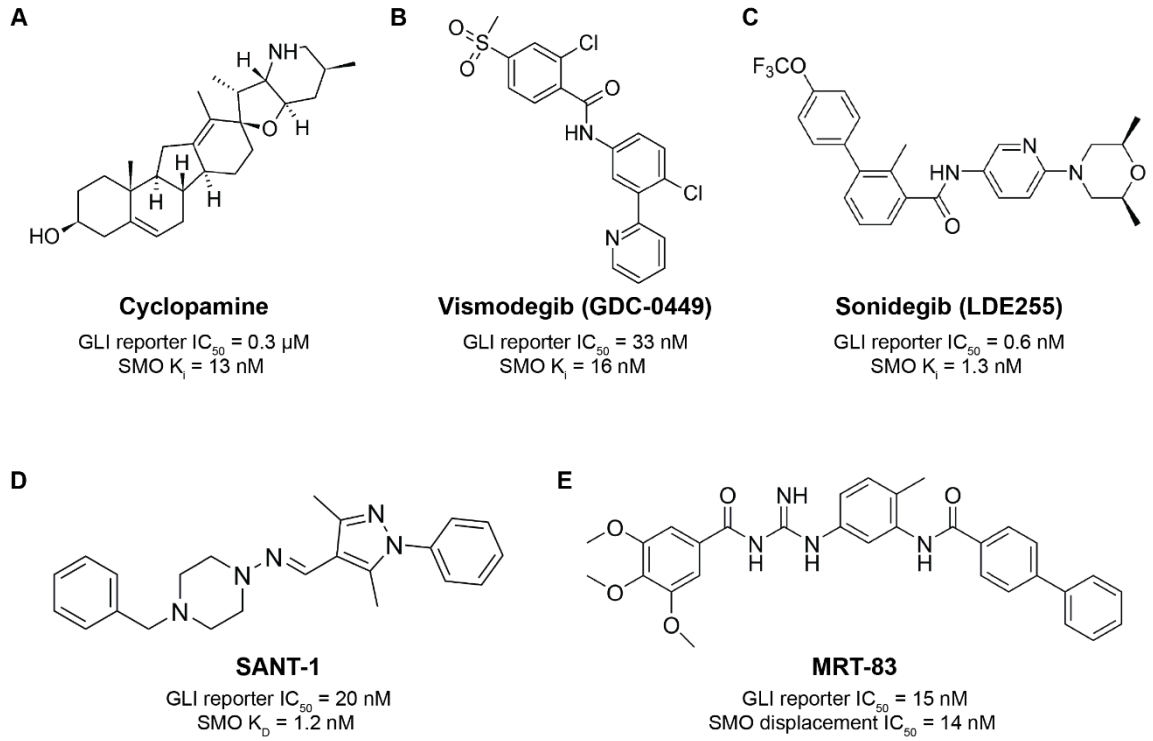

Figure 12. Selection of published SMO antagonists. A. Cyclopamine (stated values were obtained from Chen *et al.* (GLI reporter)[96] and Wang *et al.* (SMO binding)[97]). **B.** Vismodegib (GDC-0449, stated values were obtained from Wu *et al.* (GLI reporter)[98] and Wang *et al.* (SMO binding)[97]). **C.** Sonidegib (LDE255, stated values were obtained from Pan *et al.*[99]). **D.** SANT-1 (stated values were obtained from Chen *et al.*[100]). **E.** MRT-83 (stated values were obtained from Roudaut *et al.*[101]).

When mouse Hh mutants showed a similar phenotype, it was discovered that cyclopamine is the cause of the observed malformations[102]. Later on, it was discovered that cyclopamine inhibits Hh signaling by binding and inhibiting SMO[96].[15] Vismodegib (Figure 12B) was the first ("first-in-class") synthetic inhibitor of SMO[103] that was approved by the food and drug administration (FDA) for treatment of metastatic or locally advanced BCC in 2012[104]. The FDA approved one further Hh inhibitor for treatment of locally advanced BCC in 2015: Sonidegib (Figure 12C)[105]. Further SMO antagonists have followed, like SANT-1[100], MRT-83[101], Budesonide[106], DHCEO[107] and Vitamin D3[108] (the only other natural compound) to name a few (see Figure 12D-E and Figure 13A-C).[15]

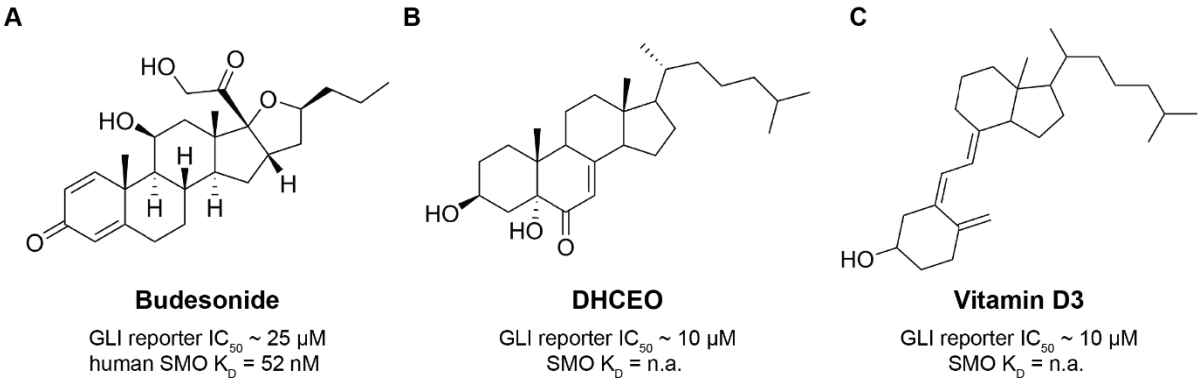

Figure 13. Selection of published SMO antagonists – continued. A**.** Budesonide (stated values were obtained from Wang *et al.* (GLI reporter value was read from curve)[106] and Rana *et al.* (SMO binding)[25]). **B.** DCHEO (stated values were obtained from Sever *et al.* (GLI reporter value was read from curve)[107]). **C.** Vitamin D3 (stated values were obtained from Bijlsma *et al.* (GLI reporter value was read from curve)[108]).

Interestingly, it was suggested that PTC transports and locally enriches Vitamin D3 to inhibit SMO, since inhibition of its synthesis impaired PTC-mediated inhibition of SMO and addition of Vitamin D3 to the medium rescued this phenotype[108]. Except for Budesonide and DHCEO (Fig. 10A and B), all so far presented SMO antagonists bind to the 7TM heptahelical domain[15] However, in contradiction to Bijlsma *et al.*[108], Linder and colleagues have published in 2015 (nine years after Bijlsma *et al.*) that calcitriol, the active form of vitamin D3, does not bind to the cyclopamine binding site, i.e. the heptahelical bundle, of SMO[109]. Budesonide binds to the cysteine-rich domain and DHCEO binds neither to the SMO CRD nor the heptahelical bundle[107].[15]

Only few Hh inhibitors with targets other than SMO have been reported. Robotnikinin (Figure 14A) and RU-SKI 43 (Figure 14B) interfere at the level of the Hh ligand. Robotnikinin does so through physical interaction with SHH that prevents its binding to PTC1[110]. RU-SKI 43 inhibits the HH-directed acyltransferase (HHAT) and thereby impairs palmitoylation and signaling potency of SHH[111]. GANT61 (Figure 14C) belongs to the small class of Hh inhibitors that target processes downstream of SMO. It prevents binding of GLI1 to its DNA target sequences and thereby inhibits target gene expression[112]. HPI1 (Figure 14D) is a Hh inhibitor that does not target SMO or its ciliary localization and acts downstream of SUFU[113]. The authors suggested that it might act on GLI phosphorylation since a GLI mutant lacking the PKA phosphorylation site was resistant to HPI-1. Still, its exact mode of action is unknown.

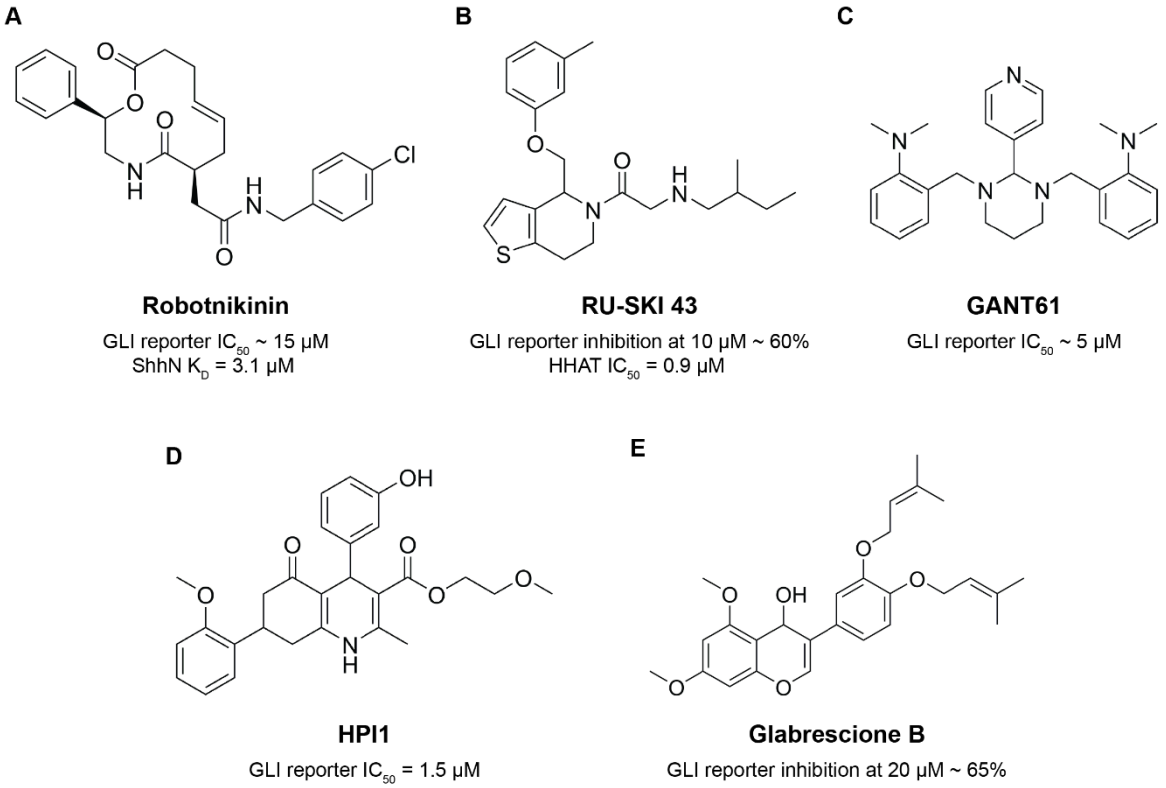

Figure 14. Hh inhibitors with targets other than SMO. A. Robotnikinin (stated values were obtained from Stanton *et al.* (GLI reporter value was estimated from titration)[110]). **B.** RU-SKI 43 (stated values were obtained from Petrova *et al.* (GLI reporter value was estimated from bar graph)[111]). **C.** GANT61 (stated values were obtained from Lauth *et al.*[112]). **D.** HPI1 (stated values were obtained from Hyman *et al.*[113]). **E.** Glabrescione B (stated values were obtained from Infante *et al.* (GLI reporter value was estimated from bar graph)[114]).

Rational design based on the structure of GLI1 led to the discovery of Glabrescione B (Figure 14E), a compound that directly binds to the GLI1 zinc finger domain, thereby inhibiting DNA binding and target gene activation[114].[15]

2.4.2 Activators

While activators are not suitable for cancer therapy, they are still important tool compounds to study pathway physiology and might be possible therapeutics for regenerative medicine. So far, all known Hh activators target SMO. Purmorphamine (Figure 15A) is the activator that was used for the majority of assays in this thesis and was found to induce differentiation of mouse mesenchymal stem cells into osteoblasts[115]. Further studies revealed that it activates Hh signaling and binds to the heptahelical bundle in the 7TM domain of SMO[116]. SMO agonist (SAG, Figure 15B) has the same mode of action[117,100].[15]

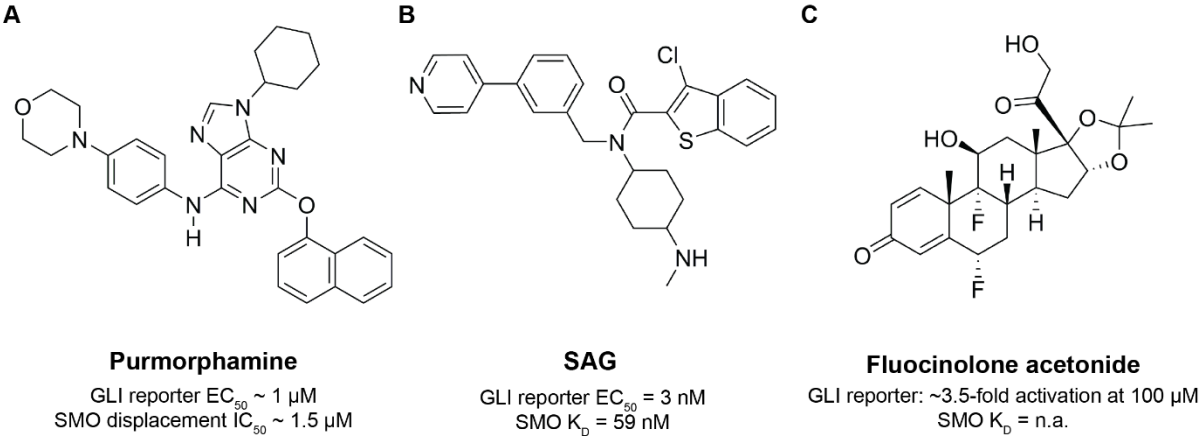

Figure 15. Hh activators – 1. A. Purmorphamine (stated values obtained from Sinha *et al.*[116]). **B.** SAG (stated values obtained from Chen *et al.*[100]). **C.** Fluocinolone acetonide (stated values obtained from Wang *et al.* (Gli reporter value was estimated from curve)[106]).

Fluocinolone acetonide (Figure 15C) also binds to the Cyclopamine-binding site of SMO but rather sensitizes cells for Shh-activation than activating the pathway on its own[106]. Another class of SMO agonists binds to the cysteine-rich domain (CRD). Two members are 20(S)-OHC oxysterol and cholesterol (depicted in Figure 16A and B). 20(S)-OHC was found to bind the CRD and activate SMO[118,119]. This discovery started a discussion if an oxysterol, being a biomolecule, could be the endogenous ligand of SMO[26].

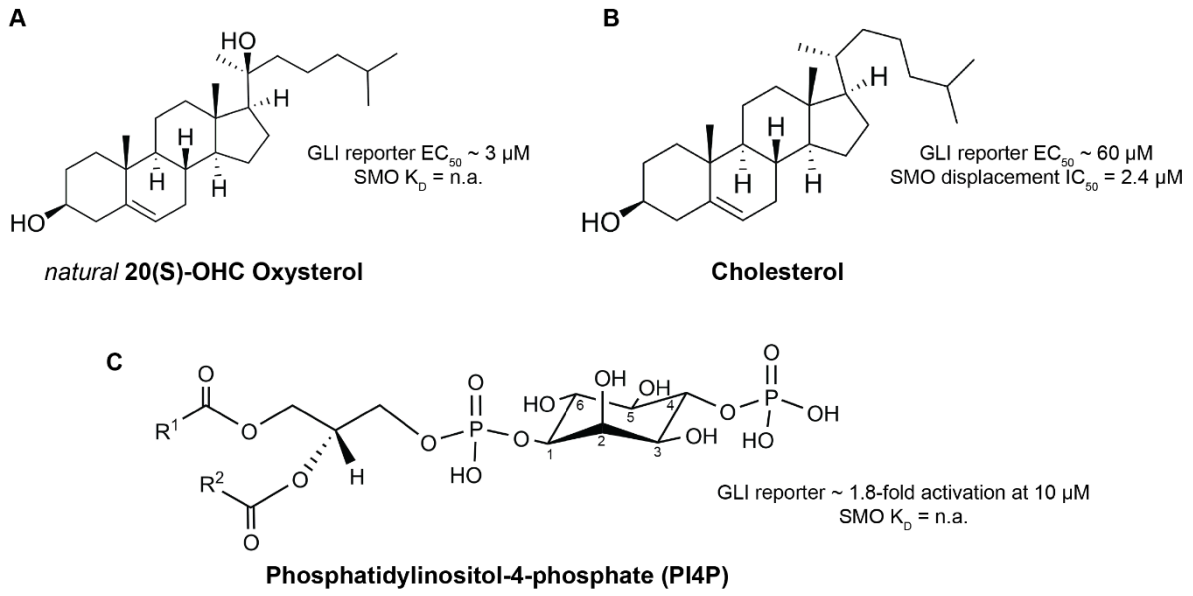

Figure 16. Hh activators -2. A. 20(S)-OHC Oxysterol (stated values were obtained from Nachtergaele *et al.*[118]). **B.** Cholesterol (stated values were obtained from Huang et al (GLI reporter value was estimated from curve)[120]). **C.** Phosphatidylinositol-4-phosphate (PI4P, stated values were obtained from Jiang *et al.* (GLI reporter value was estimated from bar graph)[35]).

However, a functional relation to endogenous Hh and SMO signaling could not be confirmed. SMO mutations that abrogate 20(S)-OHC binding to SMO did not prevent Hh activation in a way that would indicate a correlation between binding and pathway activity[121]. On top of that, endogenous 20(S)-OHC was not identified in NIH/3T3 cells, a common cell line for Hh signaling studies in vertebrates that was also used for the majority of experiments in this thesis, arguing that this oxysterol is not the natural ligand of SMO. Cholesterol, however, was found to bind the CRD of SMO as well and is highly abundant in cellular membranes. Several studies have shown a synergism between cholesterol binding to SMO and Hh ligand-mediated pathway activation[120] as well as impaired signaling after cholesterol depletion[122], suggesting that cholesterol may be the endogenous ligand of SMO.[15] Yet, since cholesterol is very hydrophobic and not well soluble in aqueous solutions, it is questionable how it can diffuse to the CRD and bind to it without a solubilizing factor. So far, such a factor or mechanism is not known.[15]

As mentioned already, the most recent candidate for an endogenous SMO ligand is PI4P (Figure 16C). It was found to bind to the C-terminal tail of SMO *in vitro* and application of exogenous PI4P led to a conformational change in SMO that induced its phosphorylation and migration to the cilium, resulting in Hh pathway activation[35].[15]

2.4.3 Unmet Needs

Despite the large number of Hh modulators, the target diversity in the pathway is very low. Most compounds target SMO and a lot of them target the same binding region, the heptahelical bundle of the 7TM domain.

Even before the FDA-approval of Vismodegib in 2012, first acquired resistances to Vismodegib treatment due to a point mutation in SMO (D473H) were reported in 2009[123]. Further studies led to the identification of several other mutations that impair efficacy of Vismodegib and other compounds that have a similar binding mode[124]. Due to that, compounds that have a different binding mode or an entirely different target, are still in high demand with regard to cancer therapy.

But also with regard to basic research, further Hh agonists or antagonists that target other proteins than SMO are of high interest to answer the open questions about Hh signaling pathway regulation (see 2.2.5). Known downstream inhibitors mostly target GLI1. Since GLI1 is also responsible for crosstalk with a lot of other important signaling pathways (see 2.3.2.3), targeting this far downstream could be a mixed blessing. On the one hand, targeting several

pathways could be beneficial in cancer treatment since most of these targets play a role in cancer metabolism. On the other hand, and for the same reason, targeting GLI could lead to an increased amount of side effects. Clinical studies could shed light on this point but, so far, only SMO antagonists have been evaluated in clinical trials[15]. At all events, the discovery of further pathway antagonists with alternative targets will be useful for the scientific community and the development of potential drug candidates.

GLI2 could be an attractive alternative target for inhibition of Hh signaling. While GLI1 functions as a signal amplifier whose expression is upregulated upon pathway activation, GLI2 and GLI3 also contain repressor domains and function as transcriptional repressors if their activator domains are cleaved of[15]. GLI3 mostly acts as a repressor and GLI2 predominantly functions as a transcriptional activator[125]. If one of them is removed, though, they can compensate each other's functions[125]. Since GLI2 acts upstream of GLI1 regulation and is a main transducer of pathway activation, it is a promising target for Hh inhibition. Nevertheless, the compensating function of GLI3 has to be considered. It has been reported that GLI2 depletion reduced migration, invasion and metastasis of osteosarcoma cells[126]. Additionally, treatment with arsenic trioxide, a toxic compound that is also used for chemotherapy and has been proposed as a treatment for Hh-driven cancers, inhibited *Gli2* transcription and reduced the invasiveness of osteosarcoma cells[126]. Darinaparsin, an arsenical that is currently evaluated in clinical trials, reduced fibrosis, also by impairing GLI2 protein expression[127], emphasizing the suitability of GLI2 as a target that, similar to GLI1, might be involved in crosstalk mechanisms.

The identification of additional SMO agonists could help to map further SMO binding sites or modes and might enable the discovery of the endogenous SMO binder. Additionally, the identification of compounds that activate Hh signaling and have alternative targets might advance the unraveling of SMO regulation and could contribute to the understanding of mechanisms required for signal transduction from SMO to GLI.

3 AIM OF THE THESIS

The Hedgehog signaling pathway is essential for embryonic development[128] and is known to be responsible for the development and progression of several cancer subtypes like basal cell carcinoma, medulloblastoma as well as colorectal and pancreatic cancer. Even though several Hh inhibitors have been developed, the low target diversity and emergence of treatment-induced and somatic mutations that impair efficacy of many Hh inhibitors, calls for the discovery of further pathway inhibitors. In addition to that, open questions concerning Hh signal transduction could be answered by new (tool) compounds with so far unknown Hh targets.

In light of this situation the aim of this thesis was the identification and characterization of novel Hh pathway modulators and their cellular targets. Initial identification of potential inhibitors (“hits”) is enabled by a high-throughput screen for inhibition of purmorphamine-induced osteogenesis at the Compound Management and Screening Center (COMAS), Dortmund. Potent hits should be confirmed and characterized using cell biology and biochemistry methods. The inhibitory potential of suitable compounds should be further characterized by establishing a structure-activity relationship (SAR) to enable compound modification for target identification experiments. Using this knowledge, probes should be synthesized to enable affinity-based enrichment of possible target proteins in biochemical assays using cellular protein lysates. If applicable, also alternative modes for target identification, like computational target prediction or enzymatic assays should be employed. Identified targets should be characterized and validated using cellular biology methods for their relevance in Hh signaling, thereby yielding new insights into the regulation of pathway mechanisms.

4 MATERIALS AND METHODS

4.1 Materials

4.1.1 Chemicals and reagents

The PI4KB inhibitors compounds **10**, **11** and **12** were kindly *provided by Dr. Radim Nencka and Dr. Ivana Mejdrová, collaboration partners at the IOCB Prague*[78]. The PI4KA inhibitor compound **16** was a *kind gift from AstraZeneca*[76] and later on *provided by Ximbio*. Compounds **5** and **6** (Smoothib and Pipinib) were *kindly provided by the Lead Discovery Center Dortmund*. All other compounds that were used in this thesis and are not mentioned in this chapter have been *synthesized by chemists of the Department of Chemical Biology at the Max Planck Institute of Molecular Physiology*.

Name	Supplier	Cat. No
2-(4-(2- hydroxyethyl)-1-piperazine ethanesulfonic acid (HEPES), ultrapure	Gerbu	1009.0250
3-(N- morpholino)propanesulfonic acid (MOPS)	Carl Roth	6979.2
4‘,6-Diamidin-2-phenylindole (DAPI)	Sigma-Aldrich	D9542
5x T4 ligase buffer	Thermo Fisher Scientific	46300018
Acetic acid (≥99.8 %)	Sigma-Aldrich	33209
Acetic acid, glacial	Fisher Chemical	A/0400PB15
Acetonitrile (AcN), HPLC grade	Fisher Chemical	A998-212
Acrylamide (30 %)	AppliChem	A1672
Ammonium bicarbonate (ABC)	Sigma-Aldrich	11213-1KG-R
Ammonium persulfate (APS)	Serva	13375
Ampicillin	Gerbu	10416.0050
Aqua-Poly/Mount	Polysciences	18606-20
Attractene	Qiagen	301005
BODIPY-cyclopamine	Carbosynth Limited	FB18988
Bovine Serum Albumine (BSA)	Serva	11945.03
Bromophenol blue, sodium salt	Carl Roth	A512.1
BSA (100x)	New England Biolabs	B9000S
Calcium chloride dehydrate ($CaCl_2 \cdot H_2O$)	Sigma	223506-500G
CDP Star reagent	Sigma-Aldrich	11685627001
Cell dissociation solution	Sigma-Aldrich	C5914

Name	Supplier	Cat. No
Cell proliferation reagent WST-1	Sigma-Aldrich	11644807001
cOmplete™, EDTA-free protease inhibitor cocktail	Sigma-Aldrich	11873580001
Cosmic calf serum (Hyclone™)	GE Healthcare/VWR	SH30087
DharmaFECT 1	Dharmacon™	T-2001-02
Digitonin	Sigma-Aldrich	D141
Dimethyl sulfoxide (DMSO)	Sigma-Aldrich	D8418
Dithioerythritol (DTE)	Gerbu	1007.0025
Dithiothreitol (DTT)	Gerbu	1008.0005
DMEM/F12 (1:1)	PAN	P04-08500
DNA loading dye (6x)	Thermo Fisher Scientific	R0611
Dulbecco's modified eagle medium (DMEM)	PAN	P04-03550
Endoproteinase GluC	Promega	V1651
Ethanol (EtOH), absolute	Fisher Chemical	E/0650DF/15
Ethanolamine (≥98 %)	Sigma-Aldrich	E9508
Ethylene glycol-bis(β-aminoethyl ether)-N,N,N',N'-tetraacetic acid (EGTA)	Carl Roth	3054.3
Ethylenediaminetetraacetic acid (EDTA) disodium salt	Gerbu	1034
ET-SSB	New England Biolabs	M2401S
Fetal bovine serum (FBS)	Gibco	10500-084
Formaldehyde solution (37 %)	AppliChem	A3592
Formic acid	J.T. Baker	6037
Fugene 6	Promega	E2691
Fugene HD	Promega	E2311
Gelatin from cold water fish skin	Sigma-Aldrich	G7765
Geneticin (G418) disulfate salt solution	Sigma-Aldrich	G8168
Glycerol	Carl Roth	3783.1
Glycin	Carl Roth	3790.2
Horse serum	PAN	P30-0702
Hyclone cosmic calf serum	Thermo Fisher Scientific	SH3008703
Hydrochloric acid (HCl)	AppliChem	A0658
Hygromycin B	Invivogen	ant-hg-1
Isopropanol	J.T. Baker	8067
Kanamycin	Gerbu	1091
L-Glutamine	PAN	P04-80100
Lipofectamine® 2000	Thermo Fisher Scientific	11668019
Lipofectamine® 3000	Thermo Fisher Scientific	L3000008

Name	Supplier	Cat. No
Lipofectamine® LTX	Thermo Fisher Scientific	15338100
Lysyl endopeptidase® (LysC)	Wako Chemicals	125-05061
Magnesium chloride ($MgCl_2$), hexahydrate	AppliChem	A3618
MEM Eagle	PAN	P04-08500
MEM-non essential amino acids (NEAA) (100x)	PAN	P08-32100
Methanol (MeOH)	Sigma-Aldrich	32213
Na-EDTA	Carl Roth	8043.2
NEBuffer™ 2	New England Biolabs	B7002S
NHS Mag sepharose beads	General Electrics Healthcare Life Sciences	28951380
Nonfat dried milk powder	AppliChem	A0830
NP-40 alternative	Calbiochem	492016
Odyssey blocking buffer (PBS)	Li-COR Biosciences	927-40000
Opti-MEM™	Thermo Fisher Scientific	31985062
PageRuler™ Plus prestained protein ladder, 10 to 250 kDa	Thermo Fisher Scientific	26620
PBS tablets	Jena Bioscience	AK-102P-L
Penicillin/Streptomycin (PenStrep)	PAN	P06-07100
PhosSTOP phosphatase inhibitors	Sigma-Aldrich	04906837001
Phusion flash high-fidelity PCR master mix	Thermo Fisher Scientific	F-548
Pierce™ protein A/G magnetic beads	Thermo Fisher Scientific	88802
Ponceau S solution (0.2 %)	Serva	3342.7
Potassium chloride (KCl)	J.T. Baker	0509
Purmorphamine	Cayman Chemical	10009634
Red Safe™ DNA stain	iNtRON	21141
RNaseZAP™, cleaning agent for removing RNase	Sigma-Aldrich	R2020
RT-PCR grade water	Thermo Fisher Scientific	AM9935
Saponin	Sigma-Aldrich	47036
ShhN protein (dissolved in 0.1 % BSA in PBS)	R&D Systems	1845-SH-100
Smoothened agonist (SAG1.3)	Calbiochem	566660
Sodium azide	Sigma-Aldrich	438456
Sodium chloride (NaCl)	VWR Chemicals	27810.295
Sodium dodecyl sulfate (SDS)	Gerbu	1012
Sodium hydroxide (NaOH)	J.T. Baker	7036
Sodium pyruvate (100 mM)	PAN	P04-43100
SsoAdvanced™Universal SYBR® Green Supermix	Bio-Rad	1725274

Name	Supplier	Cat. No
SuperSignal™ West Femto	Thermo Fisher Scientific	34095
SuperSignal™ West Pico	Thermo Fisher Scientific	34580
T4 Polymerase	New England Biolabs	M0203S
T4 Polynucleotide Kinase	New England Biolabs	M0201S
Tetramethylethylenediamine (TEMED)	Carl Roth	2367.3
Trifluoroacetic acid (TFA)	Sigma-Aldrich	106232
Tris-HCl	Carl Roth	9090.3
Triton X-100	Serva	39795.02
Trypsin, proteomics grade	Sigma-Aldrich	03708969001
Trypsin/EDTA	PAN	P10-023100
Tween 20	Fisher Bioreagents	BB337-100
UltraPure™ Agarose	Thermo Fisher Scientific	16500500
Vismodegib	Selleckchem	S1082
Zeocin	Invivogen	ant-zn-1
β-Mercaptoethanol	Serva	28625.01

4.1.2 Buffers and media

Name	Composition	Method
10x LIC (ligation independent cloning) buffer	4 mM β-mercaptoethanol in 5x T4 ligase buffer	Ligation independent cloning (LIC)
ABC buffer	20 mM ammonium bicarbonate in mH_2O	Affinity chromatography (GluC digest)
Alkylation solution	55 mM iodacetamide in 25 mM NH_4HCO_3	In-gel digestion
Alkylation solution (10x)	50 mM chloracetamide in denaturing/reducing buffer	Affinity chromatography
Binding buffer	50 mM Tris-HCl in mH_2O	Affinity chromatography
Blocking buffer A	0.5 M Ethanolamine, 0.5 M NaCl in mH_2O, pH 8.3	Affinity chromatography
Blocking buffer B	0.1 M sodium acetate, 0.5 M NaCl, in mH_2O, pH 4.0	Affinity chromatography
Buffer A	0.1% formic acid in sterile filtered mH_2O	Affinity chromatography, stage tip purification
Buffer B	0.1% formic acid in 20 % sterile filtered mH_2O and 80 % AcN	Affinity chromatography, stage tip purification

Name	Composition	Method
C3H10T1/2 growth medium	DMEM, supplemented with 10 % FBS, 6 mM L-glutamine, 1 mM sodium pyruvate, 1 % PenStrep	Cell culture
Cilia blocking and permeabilization buffer	1 % heat-inactivated horse serum, 0.1 % Triton X-100 in PBS	Immunocytochemistry (ICC), staining of cilia
Coomassie staining solution	40 % ethanol, 10 % acetic acid, 0.6 % Coomassie brilliant blue R250 in mH_2O	Coomassie staining
Coupling buffer A	0.15 M triethanolamine, 0.5 M NaCl, in mH_2O, pH 8.3	Affinity chromatography
DAOY growth medium	MEM Eagle supplemented with 10 % FBS	Cell culture
Denaturing/reducing buffer	8 M urea, 1 mM DTT in 50 mM Tris-HCl, pH 7.5	Affinity chromatography
Digest solution	0.1 µg/µl Trypsin in 10 mM HCl diluted 1/10 in 25 mM NH_4HCO_3	In-gel digestion
Fixation buffer	4 % formaldehyde in PBS	Immunocytochemistry, general fixation buffer
Fixation solution	H_2O:EtOH:Acetic acid = 5:4:1	In-gel digestion
HBS (HEPES buffered saline)	21 mM HEPES, 1.8 mM Na_2HPO_4, 137 mM NaCl, 4.8 mM KCl in Millipore filtered deionized water (mH_2O)	PI4P flow cytometry
HEK293(-T) growth medium	DMEM supplemented with 10 % FBS, 1 mM sodium pyruvate, 1x MEM-NEAA	Cell culture
IMCD3 growth medium	DMEM/F12 (1:1) supplemented with 10 % FBS	Cell culture
IP buffer	50 mM Tris-HCl (pH 7.5), 150 mM NaCl, 1mM EDTA, 0.05 % NP-40 in mH_2O	Immunoprecipitation
IP lysis buffer	25 mM Tris-HCl, pH 7.4, 150 mM NaCl, 1 mM EDTA, 1 % NP-40, 5 % glycerol, in mH_2O	Affinity chromatography (ATP probe)
Lysis buffer (pulldown)	50 mM PIPES, pH 7.4, 50 mM NaCl, 5 mM MgCl2, 5 mM EGTA, 0.1 % NP-40, 0.1 % Triton X-100, 0.1 % Tween 20, 1 mM DTT in mH_2O, supplemented with protease and phosphatase inhibitors	Affinity chromatography
Lysogeny broth (LB) medium	10 g/L Bacterial Tryptophan, 5 g/L Yeast Extract, 10 g/L NaCl in mH_2O	Bacterial culture, *prepared by the ZE biotechnology*

Name	Composition	Method
NIH/3T3 assay medium	DMEM supplemented with 0.5 % heat-inactivated cosmic calf serum	Cell culture
NIH/3T3 growth medium	DMEM supplemented with 10 % heat-inactivated cosmic calf serum, 1 mM sodium pyruvate	Cell culture
Osteogenesis lysis buffer	100 mM Tris-HCl, pH 9.5, 250 mM NaCl, 25 mM $MgCl_2$, 1 % Triton X-100 in mH_2O	Osteoblast differentiation assay
PBS-T	0.1 % Tween 20 in PBS	General washing buffer, several applications
PBS-Tx	0.1 % Triton X-100 in PBS	General washing buffer, several applications
Phosphate buffered saline (PBS)	1 PBS tablet in 500 ml mH_2O	General buffer, several applications
PI4P blocking and permeabilization buffer	3 % gelatin, 0.2 % Saponin in PBS	Immunocytochemistry, staining of PI4P
PI4P fixation buffer	1.5 % formaldehyde in PBS	Immunocytochemistry, fixation for PI4P antibody staining
Quenching buffer	50 mM NH_4Cl in PBS	Immunocytochemistry, staining of PI4P
Reaction buffer	20 mM HEPES, 150 mM NaCl, 0.1 % Triton X-100 in mH_2O	Affinity chromatography (ATP probe)
Reducing solution	50 mM DTT in 25 mM NH_4HCO_3	In-gel digestion
Resolving gel	6-12.5 % acrylamide, 1.5 M Tris-HCl (pH 8.8), 0.1 % SDS, 0.1 % APS, 0.004% TEMED in mH_2O	SDS page
Running buffer	250 mM Tris, 2 M glycin, 1 % SDS in mH_2O	SDS Page
SDS sample buffer (5x)	0.5 M Tris, 40 % glycerol, 8 % SDS, 0.4 M DTE, 0.02 % bromophenol blue in mH_2O	SDS Page
SDS sample buffer (5x) w/o	0.5 M Tris, 40 % glycerol, 8 % SDS in mH_2O	Direct lysis for SDS page and IP bead elution
Stacking gel	5 % acrylamide, 1 M Tris-HCl, pH 6.8, 0.1 % SDS, 0.1 % APS, 0.01% TEMED in mH_2O	SDS page
TAE buffer (50x)	40 mM Tris, 1 mM EDTA, 5.71 % glacial acetic acid in mH_2O	Agarose gel electrophoresis
TBS-T	0.1 % Tween 20 in TBS	General washing buffer, several applications

Name	Composition	Method
TBS-Tx	0.1 % Triton X-100 in TBS	General washing buffer, several applications
Tris-buffered saline	500 mM Tris-HCl (pH 7.5), 1.5 M NaCl, in mH_2O	General buffer, several applications
Wash buffer A	10 mM NaCl, 150 mM Tris-HCl (pH 7.4), 0.05% Tween-20 in mH_2O, sterile filtered	Proximity ligation assay
Wash buffer B	0.2 M NaCl, 0.1 M Tris-HCl (pH 7.5) in mH_2O, sterile filtered	Proximity ligation assay
Washing solution 1	25 mM NH_4HCO_3 3:1 in AcN	In-gel digestion
Washing solution 2	25 mM NH_4HCO_3 1:1 in AcN	In-gel digestion
Wet blotting buffer	250 mM Tris-HCl (pH 8.3) 192 mM Glycin (10% 10x wet blotting buffer), 20% methanol in mH_2O	Wet protein transfer
Wet blotting buffer (10x)	250 mM Tris-HCl (pH 8.3) 1920 mM Glycin in mH_2O	Wet protein transfer for immunoblotting (IB)

4.1.3 Antibodies

4.1.3.1 Primary antibodies

Antigen	Host, dilution (application)	Blocking	Supplier	Cat. No.
Acetylated Tubulin (ac-Tubulin)	Mouse, 1:5000 (ICC)	Cilia blocking and permeabilization buffer	Sigma-Aldrich	T6793
GLI3	Mouse, 1:500 (IB)	5 % nonfat dried milk in TBS	Genentech	Wen *et al.*[129]
PI4KB	Rabbit, 1:1000 (IB), 1:500 (ICC)	3 % milk in PBS (IB); PI4P blocking and permeabilization buffer (ICC)	EMD Millipore (now Merck)	06-578
PI4P	Rabbit, 1:200 (ICC)	PI4P blocking and permeabilization buffer	echelon	Z-P004
SMO	Rabbit, 1:200 (ICC)	Cilia blocking and permeabilization buffer	abcam	ab33683
β-Actin	Rabbit, 1:5000 (IB)	Li-COR blocking buffer	abcam	ab8227

4.1.3.2 Secondary antibodies

Antigen	Conjugate	Host, dilution (application)	Blocking	Supplier	Cat. No.
mouse	minus DNA probe	Donkey, 1:5 (proximity ligation assay (PLA))	PI4P blocking and permeabilization buffer	Sigma-Aldrich	DUO92004
mouse	800CW dye	donkey, 1:5,000 (IB)	Li-COR blocking buffer (PBS)	Li-COR Biosciences	926-32210
mouse	Alexa488 fluorophore	donkey, 1:500 (ICC)	Same as respective primary antibody	Thermo Fisher Scientific	A-21202
rabbit	plus DNA probe	Donkey, 1:5 (PLA)	PI4P blocking and permeabilization buffer	Sigma-Aldrich	DUO92002
rabbit	HRP	goat, 1:10,000 (IB)	5 % nonfat dried milk in PBS	abcam	ab97051
rabbit	800CW dye	donkey, 1:5,000 (IB)	Li-COR blocking buffer (PBS)	Li-COR Biosciences	926-32213
rabbit	Alexa549 fluorophore	goat, 1:500 (ICC)	Same as respective primary antibody	Thermo Fisher Scientific	A11012

4.1.4 Restriction enzymes

Name	Recognition site 5' → 3'	Supplier	Cat-No.
*Bbs*I	GAAGAC(2/6)^	Thermo Fisher Scientific	FD1014
*EcoR*I	G^AATTC	Thermo Fisher Scientific	FD0274

4.1.5 Plasmids

Name	Backbone	Insert	Source
nEGFP-PI4KB	pOpine-nEGFP	PI4KB (mouse)	Dortmund Protein Facility (DPF)
nFlag-cHis-PI4KB	TriEx4-nFlag-cHis	PI4KB (mouse)	Dortmund Protein Facility (DPF)
pGEN-SMO	pEG (EGFP removed from pEGFP-C1)	SMO (mouse)	Addgene #37673[130]
pSpCas9(BB)-2A-GFP (PX458)	PX458	SpCas9-2A-GFP	Addgene #48138[131]
SMO-BFP	Ntag-BFP	SMO (mouse, from pGEN-SMO)	LIC cloning, this thesis

4.1.6 Oligonucleotides

4.1.6.1 Primers

All primers were purchased from Eurofins MWG Operon as unmodified DNA oligos (High Purity Salt Free (HPSF) purified).

Gene	Forward (fwd) 5'→3' Reverse (rv) 5'→3'	Annealing temperature
mouse *Gak*	fwd: TGA ACC CCA AAG CTC CCA TC rv: AGA GCC AAA ACT CCA CTG CT	60 °C
mouse *Gapdh*	fwd: CAG TGC CAG CCT CGT C rv: CAA TCT CCA CTT TGC CAC TG	60 °C
mouse *Gli1*	fwd: CAC CGT GGG AGT AAA CAG GCC TTC C rv: CCA GAG CGT TAC ACA CCT GCC CTT C	60 °C
mouse *Melk*	fwd: CAA GAA GAT AAT GTT GAC TCA CCT C rv: GTG AGG TGA TCG TAC TGC CA	60 °C
mouse *Pi4kb*	fwd: AAG TCA GAT GCT ACG GCC AG rv: CGG ACA GGG GAA CTG AAT GAA T	60 °C
mouse *Pik3c2g*	fwd: AAT ATC AAG AAG ACA TTT GGA GCC rv: CTT CCT GTG GTT CAG TGC GA	60 °C
mouse *Pip5k1c*	fwd: GCC TCA GAT GAG GAG GAT GC rv: GAA GTT ATG TGT CGC TCT CGC	60 °C
mouse *Ptch1*	fwd: CTC TGG AGC AGA TTT CCA AGG rv: TGC CGC AGT TCT TTT GAA TG	60 °C
mouse *Ttk*	fwd: AGA TTC TCA GGT TGG CAC AGT rv: CCC CAA GGA CCA GAC ATC AC	60 °C
SMO-BFP cloning	fwd: CTCGAGCTCAAGCTTCGAATTACCATGGCCGCTGGCCGCCCCGTG rv: GGTACCGTCGACTGCAGAATTAGGAAGTCCGAGTCTGCATCCAA	72 °C
Deletion primers	fwd: CCTGGTGTGTGATGTATGTTGT rv: AAAAGGAGGGTAAGGAGTATGTG	58 °C
Non-deletion primers	fwd: AGGAGGTAAGCAGTCAGTAGC rv: TATAATCTGCTGGTCCAACTT	55 °C

4.1.6.2 siRNA target sequences

All siRNAs were purchased from Dharmacon.

Gene	Sequence 5'→3'	Cat. No.
Gak Pool (mouse)	GAGGGAGGCUGCAGGCUAA	J-052494-05
	GACCAAACAGCAAGACUUA	J-052494-06
	UGGCAGAGAGUAUGCAUUA	J-052494-07
	CCUGGAUGCUUGUGAUAUU	J-052494-08
Gapdh control (mouse)	GUGUGAACCACGAGAAAUA	D-001830-02-05

Gene	Sequence 5'→3'	Cat. No.
Melk Pool (mouse)	GAGAGGAGGUGCCGUUCAA	J-059459-05
	AUGACGAACUCCUCAAAUA	J-059459-06
	GGACAGGUGGCUUUGCAAA	J-059459-05
	CGAAGAUUCCAGUUAGUAA	J-059459-08
Non-targeting	UGGUUUACAUGUCGACUAA	D-001810-01-05
Pi4kb (mouse)	UGGCAUGAUUGAACCAGUA	J-056390-07
Pik3c2g Pool (mouse)	GAUCACUUAUGGAUGCCUA	J-065486-05
	AAAGUCAGGUCACAUGUUU	J-065486-06
	GAAACAGUAUCAUCUGACU	J-065486-07
	GCUCGUAUUUCACAUCCAA	J-065486-08
Pip5k1c Pool (mouse)	CGGGAGAGACUACGUAUAA	J-042927-09
	GCUUCUAUGCAGAGCGCUU	J-042927-10
	GCAGCACGGUGUUCCGGAA	J-042927-11
	UCGAUCAGCAGGAGCGAGA	J-042927-12
Ttk Pool (mouse)	GAGCUACCGCAACGAGAUA	J-047162-05
	GCAGCUCCUUGGAUGAUUA	J-047162-06
	UCAGUUAACGGAAGAAUUU	J-047162-07
	GAUGGAAUGCUAAAGCUAA	J-047162-08

4.1.6.3 Guide sequences for CRISPR-Cas9 (4.2.2.3)

All guide sequences were designed using the CRISPR design tool (http://crispr.mit.edu/)[132] in combination with the sgRNA design tool of the Broad Institute, version 1.0@6673fa0 of the Genetic Perturbation Platform (GPP) Web Portal (https://portals.broadinstitute.org/gpp/public/analysis-tools/sgrna-design)[133] and the E-CRISP tool (http://www.e-crisp.org/E-CRISP/)[134].

Name	Target	Sequence 5' → 3'
2a	PI4KB Exon 1	CGTCATCACGGAGGGGGTCG
4b	PI4KB Exon 3	GATGGCAATCGGCAAACGGC
5a	PI4KB Exon 1	CCCATTAACCAACTCCAGCG
5b	PI4KB Exon 3	GGCTGGCTTTGACCACCACG
7a	PI4KB Exon 1	AGCCCATCAGGGAATAATGG
8b	PI4KB Exon 3	TGTGGGGCACACGGACCACG

4.1.7 Cell lines

Name	Description	Culture conditions	Source
3T3-PI4KB-KD	NIH/3T3 cells with a CRISPR-Cas9-mediated knockdown of PI4KB	NIH/3T3 growth medium, 37 °C, 5% CO_2	this thesis
C3H10T1/2	Mouse mesenchymal stem cells	C3H10T1/2 growth medium, 37 °C, 5% CO_2	ATCC®, CCL-226™
DAOY	Human medulloblastoma	DAOY growth medium, 37 °C, 5% CO_2	ATCC®, HTB-186™
HEK293	Human embryonic kidney	HEK293(-T) growth medium, 37 °C, 5% CO_2	ATCC®, CRL-1573™
HEK293-T	Human embryonic kidney cells transformed with SV-40 large T-antigen	HEK293(-T) growth medium, 37 °C, 5% CO_2	ATCC®, CRL-11268™
IMCD3-Flp-in	Mouse (transgenic), kidney, medulla/collecting duct, genome contains flp-in cassette to facilitate stable transfections	IMCD3 growth medium, 37 °C, 5% CO_2	parental: ATCC®, CRL-2123™
NIH/3T3	Mouse embryonic fibroblasts	NIH/3T3 growth medium, 37 °C, 5% CO_2	DZMS, ACC-59
Shh-LIGHT2	NIH/3T3 cells, stably transfected with a Gli-responsive firefly luciferase reporter plasmid[135] and a pRL-TK constitutive Renilla-luciferase expression vector (Promega)	NIH/3T3 growth medium (supplemented with 400 µg/ml G418 and 150 µg/ml Zeocin), 37 °C, 5% CO_2	Taipale *et al.*[130]

4.1.8 Bacterial strains

Name	Description	Source
One Shot OmniMAX™ 2 T1	Chemically competent *Escherichia Coli*	Thermo Fisher Scientific, # C854003

4.1.9 Kits

Name	Supplier	Cat. No.
DC protein assay	Bio-Rad	5000112
Dual-Glo® luciferase assay system	Promega	E2980
Duolink detection reagents orange	Sigma-Aldrich	DUO92007
EndoFree plasmid maxi kit	Qiagen	12362
MycoAlert™ mycoplasma detection kit	Lonza	LT07-318

Name	Supplier	Cat. No.
Pierce™ kinase enrichment kit with ATP probe	Thermo Fisher Scientific	88310
Pierce™ silver stain kit	Thermo Fisher Scientific	24612
PureLink™ quick gel extraction and PCR purification combo kit	Thermo Fisher Scientific	K220001
QIAprep spin miniprep kit	Qiagen	27104
QuantiFast SYBRgreen kit	Qiagen	204054
QuantiTect reverse transcription kit	Qiagen	205311
Quick Ligation™ kit	New England Biolabs	M2200S
QuickExtract DNA extraction solution	Epicentre	QE09050
RNeasy mini kit	Qiagen	74104

4.1.10 Machines and devices

Description	Name	Supplier
Accessories for SDS gel preparation	Mini-PROTEAN® Short Plates	Bio-Rad
Accessories for SDS gel preparation	Mini-PROTEAN® Spacer Plates with 1.0 mm Integrated Spacers	Bio-Rad
Accessories for SDS gel preparation	Mini-PROTEAN® Comb, 10-well, 1.0 mm, 44 µL	Bio-Rad
Accessories for SDS gel preparation	Mini-PROTEAN® Comb, 15-well, 1.0 mm, 26 µL	Bio-Rad
Agarose gel reader	Gel Logic 200 imaging system	Kodak
Automated cell imaging system	IncuCyte®	EssenBio
Buffer dam for SDS gel electrophoresis	Mini Cell Buffer Dam	Bio-Rad
Clean bench for affinity chromatography	MSC-Advantage 1.2	Thermo Fisher Scientific
Clean bench for cell culture	NU-437-400E	ibs tecnomara
Confocal Microscope	Leica SP8	Leica Microsystems CMS
Device for running SDS gels and wet protein transfer	Mini-PROTEAN® Tetra Cell	Bio-Rad
Device for SDS gel preparation	Mini-PROTEAN® Tetra Cell Casting Module	Bio-Rad
DNA/RNA bench	UV-Air Clean 2 workstation (UVC/T-M-AR)	LTF Labortechnik
Fine scale	Analytical Plus	Sartorius

Description	Name	Supplier
Flow cytometer	FACS LSRII Flow Cytometry System	Becton Dickinson
Flow cytometer and cell sorter	FACS Aria Fusion Flow Cytometry System	Becton Dickinson
Handheld automated cell counter	Scepter™	Millipore
Holder for SDS gels	Mini-PROTEAN® Tetra Electrode Assembly	Bio-Rad
Holder for wet protein transfer	2-Gel Tetra and Blotting Module	Bio-Rad
Horizontal rotor	RM5	neolab
Imaging system	Odyssey Fc	Li-COR Biosciences
Incubator	Nuaire NU-5500E	IBS integra biosciences
Large table-top centrifuge	5810R	eppendorf
Laser microscope	DeltaVision	General Electrics
Magnetic rack for affinity chromatography	MagRack6	General Electrics Healthcare Life Sciences
Mass spectrometer	Q Exactive™ Plus or Q Exactive™ HF Hybrid Quadrupole-Orbitrap equipped with a nano-spray source	Thermo Fisher Scientific
Multi-channel pipettes, 10 and 100 µL	Research Plus	eppendorf
nano-HPLC system	Ultimate™ 3000 RSLC nano-HPLC system	Thermo Fisher Scientific
One-channel pipettes 10, 100, 200 and 1000 µL	Research Plus	eppendorf
Over-head rotor	Rotator SB3	Stuart
Pipetting controller	accu-jet® pro pipette controller	Brand
Plate reader	Tecan Infinity M200	Tecan
Power supply	PowerPac™ Basic Power Supply	Bio-Rad
qRT-PCR cycler	iQ5	Bio-Rad
qRT-PCR cycler	CFX96 Touch™ Real-Time PCR Detection System	Bio-Rad
Scale	CP3202S	OHAUS
Spectrophotometer	Nanodrop 2000c	Thermo Fisher Scientific
Stage tip syringe	Insertion of filter paper into low binding tips for purification of peptides	MPI Dortmund, self-made
Stop-and-go-extraction (Stage) tip centrifuge	Sonation Tomy mini personal	Sonation lab solutions

Description	Name	Supplier
Syringe for sample loading during SDS gel electrophoresis	Hamilton™ syringe, #702	Sigma-Aldrich
Table-top centrifuge	5415R	eppendorf
Table-top centrifuge	5415D	eppendorf
Table-top centrifuge	5424R	eppendorf
Table-top centrifuge	5430	eppendorf
Thermomixer	Thermomixer comfort 1.5 mL	eppendorf
Thermoshaker	Thermomixer comfort 2.0 mL	eppendorf
Ultracentrifuge	Optima™ MAX-XP Ultracentrifuge	Beckmann Coulter
Ultrasound bath	Sonorex Super	Bandelin
Ultrasound device	Sonoplus	Bandelin
UV transilluminator	UST-20M-8K	Biostep
Vacuum centrifuge	Concentrator plus	eppendorf
Widefield fluorescence microscope	Zeiss Observer Z1	Zeiss

4.1.11 Other material and consumables

Name	Supplier	Cat. No.
0.5 mL tubes (standard)	Sarstedt	72.704
1.5 mL tubes (standard)	Sarstedt	72.706
10 µL pipette tips (standard)	Sarstedt	70.1130.100
1000 µL pipette tips (standard)	Diagonal	297800500
15 mL falcon tubes	Sarstedt	62.554.502
2 mL tubes (standard)	Sarstedt	72.695.500
200 µL pipette tips (standard)	Diagonal	32120000
24-well plate (transparent, standard)	Sarstedt	83.3922
384-well plate (white)	Greiner	78108
3M™ Empore™ high performance extraction disks, C18 (octadecyl) – stage tip membrane	Fisher Scientific	221547
4–20% Mini-PROTEAN® TGX™ precast protein gels, 10-well, 50 µl	Bio-Rad	4561094
5 mL tubes	eppendorf	0030119401
50 mL falcon tubes	Sarstedt	62.547.254
6-well plate (transparent, standard)	Sarstedt	83.3920
96-well plate (transparent, standard)	Sarstedt	83.3924
96-well plate (white, clear bottom)	Greiner	655098

Name	Supplier	Cat. No.
BD Falcon™ cell scraper, 18 cm	BD Biosciences	353085
C18 PepMap 100 column (5 µm, 100 Å, 300 µm ID * 5 mm)	Dionex, Thermo Fisher Scientific	160454
C18 PepMap 100 column (3 µm, 100 Å, 75 µm ID * 25 cm)	Dionex, Thermo Fisher Scientific	164261
CoolCell® LX cell freezing container	BioCision	BCS-405
Cryo vials	Sarstedt	72.379.992
Falcon® 5mL round bottom polystyrene test tube, with cell strainer snap cap for flow cytometry	Corning Life Sciences	352235
Fisherbrand™ cover glasses: circles (Ø 12 mm)	Fisher Scientific	12-545-80
Glass slides, 76 x 26 mm	Diagonal	02 1102
Hard-Shell® 96-Well PCR plates, low profile, thin wall, skirted, white/clear	Bio-Rad	HSP9601
Immobilon-FL PVDF Membrane	Millipore	IPFL00010
Improved Neubauer cell counting chamber	Brand	7178 05
KIMTECH® Science precision tissues	Carl Roth	AA63.2
Microseal® 'B' PCR plate sealing film, adhesive, optical	Bio-Rad	MSB1001
PCR tubes	Sorenson	16960
Pico Tip emitter (ID 20 µm, Tip-ID 10 µm)	New Objective	FS3602010CE5
Pierce™ spin Columns - screw cap	Thermo Fisher Scientific	69705
Poly-D-Lysine coated coverslips	neoLab	9930002
Protein LoBind Tubes 0.5 mL	eppendorf	0030108094
Protein LoBind Tubes 1.5 mL	eppendorf	0030108116
Protein LoBind Tubes 2.0 mL	eppendorf	0030108132
QIAshredder	Qiagen	79656
SafeSeal tips premium 10 µL, sterile	Biozym Scientific	693010X
SafeSeal tips premium 100 µL, sterile	Biozym Scientific	692066X
SafeSeal tips premium 1000 µL, sterile	Biozym Scientific	692078X
SafeSeal tips premium 200 µL, sterile	Biozym Scientific	692069X
Serological pipette 1 mL	Sarstedt	86.1251.001
Serological pipette 10 mL	Sarstedt	86.1254.001
Serological pipette 25 mL	Sarstedt	86.1685.001
Serological pipette 5 mL	Sarstedt	86.1253.001
Sorenson™ low binding aerosol barrier tips, 10 µL	Sigma-Aldrich	Z719404

Name	Supplier	Cat. No.
Sorenson™ low binding aerosol barrier tips, 1000 µL	Sigma-Aldrich	Z719463
Sorenson™ low binding aerosol barrier tips, 200 µL	Sigma-Aldrich	Z719447
Sorenson™ low binding tips, 200 µL w/o aerosol barrier (for stage tip preparation)	Sigma-Aldrich	Z719595
SuperSep Phos-tag™ (50 µmol/L), 12.5%, 17 wells, 83 x 100 x 3.9 mm	Wako Pure Chemical Industries	195-17991
T175 cell culture flask	Sarstedt	83.3912.002
T25 cell culture flask	Sarstedt	83.3910.002
T75 tissue culture flask	Sarstedt	83.3911.002
Ultracentrifuge tubes, polycarbonate, thick wall, 8x34mm vials	Beckman Coulter	343776
Whatman® gel blotting paper, Grade GB005	Sigma-Aldrich	WHA10426994
Zeba™ spin desalting Columns, 7K MWCO, 5 mL	Thermo Fisher Scientific	89892

4.2. Methods

4.2.1 Molecular biology methods

All experiments with bacteria were performed using sterile equipment, if necessary under selection pressure of the respective antibiotic, and close to a Bunsen burner to prevent contamination. If not stated otherwise, standard consumables were used.

4.2.1.1 Polymerase Chain Reaction (PCR)

To amplify DNA, a polymerase chain reaction (PCR) was carried out using the Phusion Flash PCR Master mix following the manufacturer's instructions. In all reactions, a primer concentration of 0.5 µM was used, as well as 1x Master Mix in a total volume of 20 or 50 µL. The total reaction volume was obtained via addition of RT-PCR grade water. The annealing temperatures are listed in 4.1.6.1.

4.2.1.2 Agarose gel electrophoresis

In order to identify a DNA fragment of interest, the products of a PCR or a restriction enzyme reaction were separated via agarose gel electrophoresis. The applied current leads to migration of the negatively charged DNA molecules through the agarose mesh towards the positively charged anode. Since large DNA fragments migrate slower than small fragments,

size dependent separation occurs. To prepare the agarose gel, 0.5-2 % (depending on the size of the DNA of interest) agarose was suspended in 1x TAE buffer and dissolved via heating in a microwave. Subsequently, 1:20,000 Red Safe™ DNA stain was added and the agarose solution was filled into a chamber for polymerization (30 min). The DNA samples were supplemented with 6x DNA loading dye at a 1/6 dilution, loaded onto the gel and separated at a voltage of 4 V per cm (distance between anode and cathode). The DNA bands were visualized using UV light.

4.2.1.3 DNA extraction

DNA Extraction from an agarose gel or a PCR reaction mixture was carried out with the help of the PureLink™ Quick Gel Extraction and PCR Purification Combo Kit following the manufacturer's instructions.

4.2.1.4 Heat shock transformation

Transformation of chemically competent cells was performed to introduce a plasmid into bacterial strains. For this, One Shot OmniMAX™ 2 T1 (50 µL) were thawed and incubated with 10 ng of plasmid on ice for 30 min. Afterwards, the cells were transferred to 42 °C for 2 minutes (heat shock) and again transferred to ice for another minute. LB medium was added to obtain a total volume of 1 mL and the culture was shaken at 350 rpm and 37 °C for 1 h. Subsequently, the culture was spun down at 23,000 x g for 5 min. The supernatant was removed, and the pellet was resuspended in 100 µL LB medium. This cell suspension was then added to three agar plates, which were supplemented with the respective selection antibiotic, in different volumes (e.g. 10, 30 and 60 µL). After overnight incubation at 37 °C, the plates were scanned for clones which were, in case of an established plasmid, expanded (4.2.1.6) for further use or, in case of a cloning project, screened in a colony PCR (4.2.1.5).

4.2.1.5 Colony PCR

A colony PCR was carried out to verify successful cloning. After transformation of a cloned plasmid, colonies were picked with a pipette tip, suspended in autoclaved mH_2O and heated for 10 minutes at 95 °C to destroy the bacterial cell wall and release the DNA. This solution was then used as a template in a PCR (4.2.1.1) employing corresponding primers to check for the presence of the desired insert.

4.2.1.6 Plasmid amplification

To amplify a plasmid of interest, positive clones or cells from a glycerol stock were inoculated in an LB culture (supplemented with the respective selection antibiotic) and incubated overnight at 37 °C.

4.2.1.7 Plasmid isolation

After amplification, the plasmid of interest was isolated employing the EndoFree Plasmid Maxi Kit or the QIAprep Spin Miniprep Kit, depending on the culture volume, according to the manufacturer's instructions. The dried DNA pellet was dissolved in autoclaved mH_2O and the plasmid concentration was determined using the Nanodrop 2000 spectrophotometer.

4.2.1.8 DNA sequencing

DNA sequencing was performed by the StarSEQ sequencing service employing the Sanger sequencing technique.

4.2.1.9 Ligation Independent Cloning (LIC)

For this cloning technique, the insert is equipped with overhangs that are complementary to the insertion site on the target vector. Like this, site-directed insertion and subsequent ligation aided by bacterial DNA ligases is achieved.

Complementary overhangs are introduced by a PCR (4.2.1.1) using primers that contain both sequences complementary to the insertion site on the target vector and sequences that are complementary to the start and end sequence of the insert. The resulting amplicon contains the full insert sequence which is flanked by sequences that are complementary to the insertion site. The 5' overhangs, which are necessary for insertion, are created by a T4 polymerase that has a 5'→3' exonuclease activity. When the linearized vector and the insert are then mixed and transformed into competent bacteria, the bacterial ligases complete the cloning process and the plasmid can be isolated after bacterial amplification. Positive clones are identified via colony PCR (4.2.1.5), verified via sequencing (4.2.1.8), expanded and stored as glycerol stocks at -80 °C.

The protocol has been adapted from Arens *et al.*[136]. To clone the coding sequence of mouse SMO into the nTag-BFP vector, the primers given in 4.6.1 were used and a PCR was carried out according to the conditions described in 4.11.1. The insert was separated on an agarose gel (4.2.1.2) and purified (4.2.1.3). The nTag-BFP vector was linearized using the *EcoR*I

restriction enzyme according to the manufacturer's instructions. To create 5' overhangs, an exonuclease digest using the T4 polymerase was carried out for equimolar amounts (50-100 ng) of both linearized vector and the mSMO insert (see Table 1) for 30 min at 22 °C. 10 mM dATP was added to the reaction at a ratio of 1/10 (v/v) to stop the reaction because addition of dNTPs prevents degradation of double stranded DNA by T4 polymerase.

Table 1. Reaction set up for exonuclease digest

Component	Vector	Insert
DNA	50-100 ng	equimolar amount
NEBuffer™ 2 (5x)	0.5 µL	
T4 Polymerase	0.25 µL	
BSA (100x)	0.1 µL	
100 mM DTT	0.5 µL	
PCR clean water	fill up to 10 µL	

After the exonuclease digest, vector and insert were mixed, supplemented with 1/10 (v/v) 10x LIC buffer and incubated at 22 °C for another 30 min. The reaction was stopped with 1 µL 100 mM EDTA (pH 6.8) for 30 min at 22 °C. The hybridized plasmid was transformed into chemically competent One Shot OmniMAX™ 2 T1 cells (4.2.1.4).

4.2.1.10 Gateway cloning for CRISPR-Cas9 experiments

The CRISPR-Cas9 technique employs the Cas9 nuclease to induce DNA double strand breaks at specific sites in the genome and thereby leads to mutations in desired genes. To achieve double strand breaks at specific sites, so-called single guide RNAs (sgRNAs) build a complex with the Cas9 nuclease and guide it according to complementary base pairing to its site of action. To obtain specific sgRNAs and transfect them together with the Cas9 enzyme into a cell line of interest, the designed guide sequences (4.1.6.3) had to be cloned into the sgRNA scaffold inside the Cas9 vector for subsequent co-expression in target cells. The gateway cloning protocol of the Zhang lab was followed[131]. Oligos were designed according to the scheme depicted in Figure 17.

5‘ – CACCGNNNNNNNNNNNNNNNNN – 3‘
3‘ – CNNNNNNNNNNNNNNNNNNCAAA – 5‘

Figure 17. Oligo design for CRISPR-Cas9 cloning. “N” are bases of the guide sequence.

The target vector pSpCas9(BB)-2A-GFP (PX458) was digested with the restriction enzyme *Bbs*I for 30 min at 37 °C according to the manufacturer’s instructions. The linearized plasmid was purified using the PureLink™ Quick Gel Extraction and PCR Purification Combo Kit again according to the manufacturer’s instructions. Next, the oligos were annealed and phosphorylated. For this, 100 µM of each oligo were mixed with 1x T4 ligation buffer and 0.5 µL T4 Polynucleotide kinase and the reaction volume was filled up to 10 µl with autoclaved mH_2O. The reaction mixture was incubated first at 37 °C for 30 min and then at 95 °C for 5 min before ramping down to 25 °C at steps of 5 °C per minute. To ligate the oligo and the linearized vector, 50 ng of the vector and 1 µL of the oligo reaction mixture were supplemented with 5 µl 2x quick ligation buffer (from the Quick Ligation™ kit, New England bioloabs) and filled up to 10 µl with autoclaved mH_2O. After addition of 1 µl Quick Ligase (from the Quick Ligation™ kit, New England bioloabs), the reaction mixture was incubated at room temperature (RT) for 10 min and transformed into chemically competent One Shot OmniMAX™ 2 T1 cells (4.2.1.4).

4.2.2 Cell biology methods

Handling of living cells was carried out under sterile conditions using appropriate sterile equipment and a clean bench. If not stated otherwise, standard consumables were used.

4.2.2.1 Cell culture and seeding

All cell lines were maintained at 37 °C and 5 % CO_2. Cells were passaged either at 90-95 % confluence or, in case of NIH/3T3 and derived cell lines, below 80 % confluence. For this, medium was removed, and the cell layer was washed with PBS. After removal of PBS, Trypsin/EDTA was added at a minimal volume (e.g. 1 mL for a T75 flask) and the flask was panned to allow equal distribution of the solution. Approximately half of the volume of Trypsin/EDTA was removed directly after panning and the cells were incubated at 37 °C for 2 to 5 min until detachment was observed. Cells were then resolved using the respective growth medium (e.g. 4-5 mL for a T75 flask). An appropriate volume of cell suspension was then added to a new flask in a total volume of 5 (T25), 13 (T75) or 25 (T175) mL.

If the cells had to be seeded for an experiment, the obtained cell suspension was collected in a 50 mL falcon tube and cells were counted using either a Neubauer counting chamber, employing trypan blue staining to identify dead cells, or a Scepter™ automated cell counting device (based on impedance). The necessary dilution was carried out in growth medium, depending on the required cell number per well or dish, and the diluted cell suspension was filled into the wells or dishes.

I Cryo-conservation of cells

To cryo-conserve cells, a cell suspension was obtained as described in 4.2.2.1. The suspension was supplemented with 10 % DMSO (and 10 % heat inactivated cosmic calf serum for NIH/3T3 cells) and aliquoted into cryo vials. The vials were placed in a freezing container and incubated at -80 °C for several hours. After this, the vials were transferred to the vapor phase of a liquid nitrogen tank for long-term storage.

II Thawing of cryo-conserved cells

To thaw cryo-conserved cells, a falcon with 5 mL growth medium was prepared. The desired vial was removed from the vapor phase of the liquid nitrogen tank and incubated in a water bath at 37 °C until most of the content was thawed and only a small ice clump was visible. The vial was then transferred to the clean bench and added to the growth medium in the prepared falcon tube. The cells were pelleted by centrifugation at 1000 x g for 5 min and resuspended in 5 mL fresh growth medium. This suspension was transferred to T75 cell culture flask and the volume was filled up to 13 mL. In case of NIH/3T3 and Shh-LIGHT2 cells, the suspension was transferred to a T25 cell culture flask. The cells were left to grow for several days and only used for experiments after another round of passaging.

III Mycoplasma assay

Mycoplasma are atypical bacteria that do not possess a cell wall.[137] Due to this, they are resistant to various types of antibiotics. Owing to their small size, they are also not visible under a conventional widefield microscope. To still ensure that all cell lines used for experiments do not carry a contamination, monthly mycoplasma tests were carried out employing the MycoAlert™ Mycoplasma Detection Kit according to the manufacturer's instructions.

4.2.2.2 Transfection

All transfections were carried out using the lipofection technique following the manufacturer's protocol. Table 2 shows the conditions used in the respective experiments.

Table 2. Transfection conditions

Experiment	Reagent	Nucleic acid	Ratio DNA [µg] : Reagent [µL]	Incubation time [h]
CRISPR-Cas9 transfection	Lipofectamine 3000	1 µg/mL	1:2	48
nEGFP-PI4KB transfection	Lipofectamine LTX	0.36 µg/mL (osteogenesis) or 0.5 µg/mL (target genes)	1:2	24 (osteogenesis) or 48 (target genes)
nFlag-cHis-PI4KB transfection	Lipofectamine LTX	titration: 0.14, 0.28, 0.58, 1.15, 1.38 µg/mL	1:2	24
siRNA transfection	DharmaFECT 1	30 nM (PI4KB) 50 nM (other)	1:500 dilution	24 (osteogenesis) or 48 (target genes)
Smo binding assay	Fugene HD	1 µg/mL	1:3	48

4.2.2.3 Generation of PI4KB knockout cells using the CRISPR-Cas9 approach

The Clustered Regularly Interspaced Short Palindromic Repeats (CRISPR) system conveys adaptive immunity against invading phages/plasmids in bacteria and archaea.[138] The system consists of the CRISPR arrays, short direct repeats that are interspaced by non-repetitive spacer sequences, and the CRISPR associates (Cas) genes.[138] Spacers and direct repeats are transcribed into single guide RNAs (sgRNAs) that are incorporated into the Cas proteins (including nucleases) and direct these proteins to specific DNA sequences (e.g. phage mRNA or DNA) via complementary base pairing. The targeted DNA sequences are then degraded and a possible phage infection is prevented.[138] This natural defense mechanism has been utilized for gene editing. First examples have been described by Emmanuelle Charpentier and Jennifer Doudna as well as Feng Zhang.[139,140] For this, a plasmid has been engineered that contains the Cas9 nuclease and an sgRNA scaffold. This scaffold can be equipped with a guide RNA sequence of choice via gateway cloning (4.2.1.10). If this cloned plasmid is then transfected into the desired cell line, both nuclease and sgRNA are co-expressed. If the sgRNA is incorporated into the Cas9 nuclease, it directs the enzyme to the genomic sequence of choice where double strand breaks are induced that lead to error prone repair mechanisms. In most cases, mutations are inserted, which abrogate expression of the respective gene and lead to a knockout.[141,142] Bauer *et al.* have described a dual approach in which two sites of a gene are targeted to induce large deletions and facilitate screening of possible clones via

simple PCR reactions.[143] This approach was applied to induce a knockout of PI4KB in NIH/3T3 cells.

I Transfection and GFP-sorting

To apply the aforementioned dual approach, NIH/3T3 cells were transfected with the successfully cloned plasmids (4.2.1.10), using the guide sequences given in 4.1.6.3. Cas9-GFP plasmids containing sequences that target sites in exon 1 and exon 3 where transfected in pairs (2a + 4b, 5a + 5b, 7a + 8b), as specified in 4.2.2.2, to induce large deletions. After 48 h incubation at 37 °C and 5% CO_2, the cells were trypsinized, collected in growth medium, centrifuged, washed with PBS and filtered through a FACS tube cap filter. The cells were then sorted for GFP signal using the FACS Aria Fusion Flow Cytometry System (488/445 laser line) to only obtain successfully transfected cells. The top 10% of GFP-positive cells were re-plated into a 10 cm dish at a very high dilution to allow growth of single clones. Cells at a higher density were seeded into a 6-well plate to use these bulk cells for optimization of screening primers.

II Single cell clone selection and isolation of genomic DNA

A few hours after seeding, the dish was checked for single cells. All single cells were marked and observed over a period of several days. Once the selected colonies consisted of approx. 30 to 50 cells, the cells were trypsinized. The detachment of the cells was monitored under the microscope. As soon as the cells rounded off, they were transferred into a 24-well plate with an Eppendorf pipette. After reaching approx. 80% confluence, both bulk cells and single cell clones were trypsinized and collected in growth medium. The cells were pelleted by centrifugation at 1000 g for 5 min and resuspended in 50 µL of DNA extraction solution. The samples we incubated at 65 °C for 6 min, followed by 2 min at 98 °C to extract the genomic DNA (gDNA).

III Screening for genomic deletions

The optimized deletion and non-deletion primers given in 4.1.6.1 were used in a PCR (4.2.1.1) and the PCR products were analyzed via agarose electrophoresis (4.2.1.2) to screen for large deletions. Positive clones were expanded for assessment of protein levels using an anti-PI4KB antibody after cell lysis (4.2.2.10-I), SDS-PAGE (4.2.3.2) and immunoblotting (4.2.3.4). Clones that were validated on protein level were expanded, cryo-conserved (4.2.2.1-I) and used for further experiments.

4.2.2.4 Osteoblast differentiation assay

The osteoblast differentiation assay is employed to evaluate the effect of small molecules on osteogenesis, a process that is positively influenced by HH pathway activity. When osteogenesis is induced, the enzyme alkaline phosphatase (ALP) is expressed, which is why the activity of this enzyme is an indirect measure of HH signaling activity. For the assay, $2.4x10^4$ ($8x10^3$) C3H10T1/2 mesenchymal stem cells per well were seeded into a white 96-(384-)well plate and incubated at 37 °C and 5% CO_2 overnight. After 24 h, compounds were added to the cells. For this, the small molecules were prediluted first in DMSO, then in medium. The medium in the plate was removed and replaced with 80 (15) µL fresh medium. 10 (5) µL of the 10 (5)x compound or DMSO solution as well as 10 (5) µL of 15 (7.5) µM Purmorphamine was added to the respective wells. The total DMSO concentration did not exceed 0.5%, the final Purmorphamine concentration was 1.5 µM. After 96 h incubation at 37 °C and 5% CO_2, the cells were lysed, and the activity of alkaline phosphatase was assessed using the CDP star reagent and a Tecan Infinite M200 plate reader according to the manufacturer's instructions. The activity of ALP in DMSO-Purmorphamine-treated cells was set to 100%. To obtain IC_{50} values, nonlinear regression was performed using a four-parameter fit (GraphPad Prism 6, GraphPad Software, USA).

4.2.2.5 GLI reporter gene assay

The GLI reporter gene assay is an orthogonal approach to the osteoblast differentiation assay and employs stably transfected NIH/3T3 cells (Shh-LIGHT2[130]) that express a GLI-responsive firefly luciferase[135] and, as a control, a Renilla luciferase under the control of the constitutively active thymidine kinase promotor. The firefly luciferase is only expressed upon HH pathway activation and the Renilla luciferase is constitutively expressed, serving as a control for viability and gene expression. For the assay, $2.5x10^4$ Shh-LIGHT2 cells per well were seeded in a transparent 96-well plate and incubated at 37 °C and 5% CO_2 overnight. After 24 h, compounds were added as described in 4.11.3. Instead of 1.5 µM, the final Purmorphamine concentration was 2 µM. After 48 h of incubation at 37 °C and 5% CO_2, luciferase activity was measured by means of the Dual-Glo® Luciferase Assay System according to the manufacturer's instructions. The firefly signal was normalized to the Renilla luciferase signal and the value for DMSO-Purmorphamine-treated cells was set to 100 %. To obtain IC_{50} values, nonlinear regression was performed using a four-parameter fit (GraphPad Prism 6, GraphPad Software, USA).

4.2.2.6 Gene expression analysis

In order to analyze the relative cellular expression levels of a gene of interest, messenger ribonucleic acid (mRNA) levels have to be determined as they are a quantitative measure of gene transcription. For this, cellular RNA is isolated and converted into complementary deoxyribonucleic acid (cDNA) via a reverse transcription reaction to produce a DNA template that can be amplified in a quantitative reverse transcription PCR (qRT-PCR). This special form of a PCR reaction enables quantitative detection of DNA by using a DNA intercalating dye and gene-specific primers. The signal of the dye is measured in real time during the experiment and intensifies as increasing amounts of DNA are produced. For data analysis, an intensity threshold is defined, which is employed to compare amplification speed between samples, as determined by the cycle at which a sample crosses this threshold (C_T-value). Samples that have a low cDNA concentration for a respective gene (i.e. mRNA level) will pass the threshold later (with higher C_T-values) than samples with a high cDNA concentration. To translate C_T-values into relative expression values, the $\Delta\Delta C_T$-method[144] was applied. In this method, the C_T-value of the employed reference gene (in this case *Gapdh*) is subtracted from the corresponding C_T-value of the gene of interest (ΔC_T). Next, the ΔC_T-value of the control sample is subtracted from all other ΔC_T-values ($\Delta\Delta C_T$). To retrieve expression values, $2^{-\Delta\Delta C_T}$ is calculated.

Before RNA was isolated, all surfaces and devices were cleaned with RNaseZAP™ to remove RNases and protect the sample RNA from degradation. SafeSeal tips, Protein LoBind tubes (PCR clean) and a DNA hood (for reverse transcription and qRT-PCR) were used to prevent contaminations and ensure sample integrity.

I RNA isolation

NIH/3T3 or DAOY cells were seed at $2x10^4$ cells/well in a 24-well plate and incubated for approx. 24 h at 37 °C and 5% CO_2. On the next day, compounds or DMSO (solvent control) and Purmorphamine were added. For this, the small molecules were prediluted, first in DMSO then in medium, and the medium on the cells was exchanged for 500 µL compound/DMSO medium, supplemented with 2 µM Purmorphamine or 0.2% DMSO. After 48 h incubation at 37 °C and 5% CO_2, total RNA was isolated using the RNeasy kit according to the manufacturer's instructions. For homogenization of the RNA lysates, QIAshredder columns were used at 16,000 x g for 2 min.

II Reverse transcription

The isolated RNA was transcribed into cDNA using the QuantiTect reverse transcription kit using random primers that were supplied with the kit according to the manufacturer's instructions.

III Quantitative reverse transcription PCR (qRT-PCR)

The qRT-PCR was carried out by employing the QuantiFast SYBR green kit or the SsoAdvanced™Universal SYBR® Green Supermix according to the manufacturer's instructions. The used primers and corresponding annealing temperatures are listed in 4.1.6.1. The reactions were carried out on an CFX96 or iQ5 Bio-Rad PCR cycler. To retrieve relative gene expression levels, the $\Delta\Delta C_T$-method[144] was applied as described in 4.2.2.6. DMSO-Purmorphamine-treated cells were used as control sample and the calculated value for this sample was set to 1. If applicable, nonlinear regression was performed using a four-parameter fit (GraphPad Prism 6, GraphPad Software, USA) to obtain IC_{50} values.

4.2.2.7 Flow cytometry

I SMO binding assay

To evaluate whether a compound binds to the SMO protein, a displacement assay with a fluorescently labelled SMO binder (BODIPY-cyclopamine[116]) was performed. The procedure was adopted from Chen *et al.*[96]. For this, HEK293-T cells were seeded in a 6-well plate at $3x10^5$ cells/well and incubated for approx. 24 h at 37 °C and 5% CO_2. On the next day, the cells were transfected as stated in 4.2.2.2 with the pGEN-SMO or the SMO-BFP plasmid. After 48 h at 37 °C and 5% CO_2, the cells were treated with compounds or DMSO (solvent control). For this, the small molecules were prediluted first in DMSO then in medium, and the medium on the cells was exchanged for 3 mL compound/DMSO medium, supplemented with 5 nM BODIPY-cyclopamine or 0.05% DMSO (solvent control). After 5 h incubation at 37 °C and 5% CO_2, cells were detached using PBS (since HEK293T cells attach loosely to the tissue culture plate, application of Trypsin/EDTA is not necessary), collected in 1.5 mL Eppendorf tubes, centrifuged at 129 x g and resuspended in 500 µL PBS. After repeating this washing step once more, the cell suspension was passed through the lid filter of a FACS tube and subjected to flow cytometry employing the BD LSR II Flow Cytometer (BD Biosciences, USA) (laser line: 488 nm, emission filter: 530/30 for BODIPY and laser line: 405 nm, emission filter: 450/50 for BFP). Data were analyzed with the FlowJo software, version 7.6.5 (Tree Star Inc., USA).

II PI4P levels

To assess cellular levels of PI4P upon compound treatment, cells were stained with an anti-PI4P antibody and analyzed via flow cytometry. For this, NIH/3T3 cells were seeded in a 6-well plate at $1x10^5$ cells/well and incubated at 37 °C and 5% CO_2 overnight. After approx. 24 h, cells were treated with the compounds or DMSO (solvent control) for another 48 h. For this, the small molecules were prediluted first in DMSO, then in medium, and the medium on the cells was exchanged for 3 mL compound/DMSO medium, supplemented with 2 µM Purmorphamine or 0.2 % DMSO (solvent control). Subsequently, cells were washed with PBS, trypsinized and collected in growth medium. The cells were centrifuged at 1000 g for 5 min and resuspended in 200 µL PBS. To fix the cells, 800 µL of a PBS/formaldehyde solution (final concentration of formaldehyde: 3%) were added and the suspension was incubated at room temperature (RT) for 10 min. Afterwards, the fixation solution was removed via centrifugation (5 min at 1000 x g), the pellet was resuspended in 1 mL 20 µM digitonin in HBS buffer and incubated at RT for 5 min. The digitonin solution was removed via centrifugation (5 min at 1000 g), replaced with 300 µL antibody solution (anti-PI4P 1:200 in HBS buffer) and incubated at 37 °C for 30 min. The antibody solution was removed via centrifugation (5 min at 1000 g) and the pellet was washed twice with 500 µL HBS before addition of 300 µL secondary antibody solution (anti-mouse-Alexa Fluor 488 1:500 in HBS buffer) and incubation at 37 °C for 20 min. Cells were then centrifuged for 5 min at 1000 g, resuspended in 500 µL HBS and passed through the lid filter of a BD FACS tube. All samples were subjected to flow cytometry employing the BD LSR II Flow Cytometer (BD Biosciences, USA) (laser line: 488 nm, emission filter: 530/30 for alexa-488). Data were analyzed with the FlowJo software, version 7.6.5 (Tree Star Inc., USA).

4.2.2.8 Immunocytochemistry (ICC)

I SMO trafficking assay

For evaluation of SMO localization with respect to the primary cilium, fluorescence microscopy after immunostaining of fixed cells was carried out. The staining protocol was adopted (with modifications) from Rohatgi *et al.*[17] NIH/3T3 cells were seeded in a 24-well plate containing Ø 12 mm coverslips at a concentration of $3x10^4$/well. After approx. 24 h of incubation at 37 °C and 5% CO_2, the medium was changed to assay medium to starve the cells and induce ciliation. After 24 h, compounds were added. For this, the small molecules were prediluted, first in DMSO then in assay medium, and the medium on the cells was exchanged for 500 µL compound/DMSO medium. After another 24 h, compounds and Hh

activator were added. For this, the small molecules were prediluted, first in DMSO then in assay medium, and the medium on the cells was exchanged for 500 µL compound/DMSO medium, supplemented with 2 µM Purmorphamine or 0.2% DMSO (solvent control) or 2 µg/ml ShhN protein (0.1% BSA in PBS as a negative control). After 24 h incubation at 37 °C and 5% CO_2, the cells were fixed with ice-cold cilia fixation solution for 10 min at gentle shaking and washed with cold PBS for 5 min at gentle agitation. To block unspecific binding sites, the samples were incubated with cilia blocking buffer for 30 min before addition of primary antibodies against SMO and acetylated tubulin (see 4.1.3.1 for description and dilution details) in cilia blocking buffer. After incubation at 4 °C overnight, the samples were washed twice with PBS-Tx for 5 min at gentle agitation and incubated with secondary antibodies (anti-rabbit-Alexa Fluor 594, anti-mouse-Alexa Fluor 488, see 4.1.3.2 for details) and 1 µg/ml DAPI in cilia blocking buffer for 45 min at RT and gentle agitation. Finally, the cells were washed twice with PBS-Tx for 5 min and once with PBS for another 5 min before they were mounted on glass slides for microscopic examination. Imaging was performed with a DeltaVision Elite System (GE Healthcare, UK) equipped with an IX-71 inverted microscope (Olympus, Japan), UPLanSApo 100x/1.4 NA (Olympus) and a pco.edge sCMOS camera (PCO-TECH Inc., USA). Images were acquired as Z-sections (using the softWoRx software from DeltaVision) and converted into maximal intensity projections TIFF files for illustrative purposes. Furthermore, images were taken on a Leica SP8 confocal microscope, equipped with 63x 1.4 NA objective (Leica Microsystems CMS GmbH, Mannheim, Germany). Also here, images were acquired as Z-sections and converted to maximal intensity projections using the software ImageJ[145] for illustrative purposes. Quantification was carried out employing ImageJ. For this, acetylated tubulin-positive cilia were marked, and the intensity of the anti-Smoothened antibody was measured within this area. Statistical significance was assessed using an unpaired t-test (GraphPad Prism 6, GraphPad Software, USA) with a confidence level of 95 % (*=p<0.05, **=p<0.005, ***=p<0.0005, ****=p<0.0001).

II SMO binding assay

The assay was adopted from Sinha *et al.*[116]. HEK293-T cells were seeded into 24-well plates containing poly-D-Lysine coated Ø 12 mm coverslips at a concentration of $1.5x10^4$/well. After approx. 24 h of incubation at 37 °C and 5% CO_2, the cells were transfected with the pGEN-SMO plasmid as described in 4.2.2.2. Two days after transfection, cells were fixed in cilia fixation buffer for 10 min, treated with PBS containing 10 mM glycine and 0.2% sodium azide for 5 min and washed with PBS. Fixed cells were then treated with the compound or DMSO in assay medium supplemented 5 nM BODIPY-cyclopamine or 0.05 % DMSO (solvent control) for 4 h at RT. Afterwards, coverslips were washed with PBS and incubated with

1 µg/ml DAPI in PBS for 10 min at RT. Coverslips were then washed again with PBS and mounted onto glass slides. Samples were examined by means of fluorescence microscopy using the Zeiss Observer Z1 (Carl Zeiss, Germany) and a Plan-Apochromat 63x/1.40 Oil DIC M27 objective.

III PI4P staining

NIH/3T3 cells were seeded into 24-well plates containing Ø 12 mm coverslips at a concentration of $2x10^4$/well. After approx. 24 h of incubation at 37 °C and 5% CO_2, the compounds were added. For this, the small molecules were prediluted, first in DMSO then in assay medium, and the medium on the cells was exchanged for 500 µL compound/DMSO medium. After an incubation of 2, 6, 24 or 48 h, cells were fixed in PI4P fixation buffer for 15 min, quenched with PI4P quenching buffer for 10 min and washed with PBS for 5 min. After blocking with PI4P blocking buffer for 30 min at RT, the primary antibody against PI4P (see 4.1.3.1 for description and dilution details) was added in PI4P blocking buffer. After incubation at 4 °C overnight, the samples were washed with PBS for 5 min at gentle agitation and incubated with the secondary antibody (anti-mouse-Alexa Fluor 488, see 4.1.3.2 for details) and 1 µg/ml DAPI in PI4P blocking buffer for 45 min at RT and gentle agitation. Finally, the cells were washed two times with PBS for 5 min before they were mounted on glass slides for microscopic examination. Samples were examined by means of fluorescence microscopy using the Zeiss Observer Z1 (Carl Zeiss, Germany) and a Plan-Apochromat 63x/1.40 Oil DIC M27 objective.

IV Proximity Ligation Assay (PLA)

The proximity ligation assay[146] is a technology that detects close proximity of two proteins of interest in cells by combining antibody and PCR techniques. This approach employs secondary antibodies that are modified with DNA oligos (PLA-probes). If the PLA-probes bind to the two primary antibodies against two desired proteins, the DNA oligos will bind to each other via complementary base pairing if the proteins are close enough to each other (40 nm maximum distance). Subsequent addition of a ligase and a polymerase results in a rolling circle amplification of the DNA. The simultaneous incorporation of fluorescently labelled dNTPs that are provided in the master mix leads to generation of an intense, dot-like fluorescent signal that can be detected via fluorescence microscopy.

NIH/3T3 cells were seeded and treated with compounds as described in 4.2.2.8-I. Fixation and primary antibody staining were performed as in 4.2.2.8-I as well. One day after addition of the primary antibodies, the samples were washed two times for 5 min with PBS. Meanwhile, the PLA probes were diluted 1:5 in blocking buffer and incubated at RT for 20 min. A humidity

chamber was pre-heated to 37 °C. After washing, the coverslips were removed from the 24-well plate and transferred to the humidity chamber. From here on, all washing steps were performed with a volume of 65 µL and all reagent incubation steps had a volume of 40 µL. The PLA solution was vortexed and added to the coverslips, which were then incubated at 37 °C for 1 h. The ligation mix was prepared according to the manufacturer's instructions and added to the coverslips after two times washing with wash buffer A. After incubation for 30 min at 37 °C, the coverslips were washed twice for 2 min with wash buffer A. The amplification solution, including the fluorescent dNTPs and the polymerase, was prepared according to the manual and added to the coverslips for 100 min at 37 °C. Next, the coverslips were washed two times for 10 min with wash buffer B, including 1µg/ml DAPI in the second washing step. Finally, the samples were washed with 0.01x wash buffer B and mounted on glass slides. Images were taken on a Leica SP8 confocal microscope, equipped with 63x 1.4 NA objective (Leica Microsystems CMS GmbH, Mannheim, Germany). Images were acquired as Z-sections and converted to maximal intensity projections using the software ImageJ[145] for illustrative purposes. Quantification was carried out employing ImageJ. For this, the PLA dots ("PLA events") were counted using the "analyze particles" tool after setting an appropriate threshold to enable identification of the single events. Using the same tool, the nuclei were counted as well. PLA events per cell were calculated by dividing the total number of PLA events by the number of nuclei per image. Statistical significance was assessed using an unpaired t-test (GraphPad Prism 6, GraphPad Software, USA) with a confidence level of 95 % (*=p<0.05, **=p<0.005, ***=p<0.0005, ****=p<0.0001).

4.2.2.9 Live-cell imaging and confluence monitoring using the IncuCyte Live-cell Analysis system

Cells were seeded at $8x10^3$ (NIH/3T3 cells) or $1.5x10^3$ (DAOY cells) per well in 96-well plates. After incubation overnight, cells were treated with 2 µM Purmorphamine or DMSO and the compounds or DMSO as a control. Over an incubation time of approx. 72 h, the cells were monitored by the IncuCyte® automated cell imaging system that acquired phase contrast images every 60 min (NIH/3T3) or every 2 h (DAOY). The confluency of the obtained images was then quantified using the IncuCyte® Zoom software and plotted against the time to derive growth curves.

4.2.2.10 Cell lysis

For analysis of cellular protein levels after cell seeding and treatment or transfection, lysates had to be generated. To do so, several methods were applied:

I Direct lysis in SDS Sample Buffer

After removal of the medium, an appropriate amount of 1x SDS sample buffer w/o was added to the cells. To obtain a high protein concentration, the volume of buffer was as low as possible but big enough to cover the well/dish and allow appropriate handling, e.g. 60 µL for a 24-well plate. If the cells were plated in a 6-well plate, a cell scraper was used to collect the lysate. If the cells were plated in a 24-well plate, the lysate was collected with an Eppendorf pipette and transferred to a 1.5 mL Eppendorf tube. The lysate was then sonicated and the protein concentration was determined by means of a DC protein assay (4.2.3.1) as per the manufacturer's instructions. After addition of 0.8 mM DTE and 0.2% Bromophenol blue, the samples were boiled at 95 °C and 350 rpm for 5 min and stored at -20 °C until further usage.

II Lysis via Freeze-Thaw Cycling

The cells were washed with PBS, trypsinized and collected in growth medium. After centrifugation at 1000 g for 5 min, the pellet was resuspended in PBS and shock-frozen in liquid nitrogen. The cells were then thawed at RT and again shock-frozen in liquid nitrogen. This procedure was repeated two more times. In case of lysate preparation for CETSA, the lysate was centrifuged at 100,000 x g for 25 min at 4 °C in an ultracentrifuge. The concentration of the lysate supernatant was determined by means of a DC protein assay (4.2.3.1) as per the manufacturer's instructions. Prepared lysates were again shock-frozen in liquid nitrogen and stored at -80 °C until further usage.

4.2.2.11 Smo Receptor Membrane Binding Assay at SB Drug Discovery, UK

Compound binding to SMO was evaluated in a radioligand displacement assay. For this, membrane preparations from a SMO-expressing cell line (Multispan Inc, 14 µg per well) were incubated with different concentrations of the compound or DMSO and 7 nM [^{3}H] Cyclopamine until an equilibrium was reached. To measure Cyclopamine binding to SMO, free and bound radioactive ligand were separated using a Packard Filtermate Harvester and glass filter plates. Radioactivity was then assessed employing a Packard Topcount. Data were normalized to DMSO-treated membranes.

4.2.2.12 Medulloblastoma Growth Assay at Exiris Srl, Italy

The medulloblastoma growth assay measures the influence of small molecules on the proliferation of medulloblastoma cells that carry a heterozygous deletion of the *Ptch1* gene. The cells were isolated from medulloblastoma tumors of postnatally irradiated *Ptch1*$^{+/-}$ mice and resuspended in Neural Progenitor Basal Medium (NPMM) supplemented with growth factors (NPMM BulletKit, Lonza, #CC-3209). Viable cells were then seeded at 1x10^4 per well in a 96-well plate and incubated with or without 0.3 µM SAG1.3 and different concentrations of the compound. After incubation for 72 h, DNA was stained with BrdU for 24 h. The amount of incorporated BrdU was determined via the Cell Proliferation ELISA, BrdU (chemiluminescent, Sigma Aldrich, Roche, #11669915001) and normalized to DMSO. For determination of IC_{50} values, data was fitted with a three-parameter logistic equation using the KaleidaGraph 3.5 software.

4.2.2.13 PI4P Sensor Experiment performed by collaboration partners at the Johns Hopkins University in Baltimore, USA

Dr. Takanari Inoue and Dr. Yuta Nihongaki, collaboration partners at the Johns Hopkins University in Baltimore, USA, carried out the PI4P sensor Experiment. A YFP-PH(FAPP1) construct, which specifically binds to PI4P via its pleckstrin homology (PH) domain, and a GT-CFP plasmid (Clontech), which encodes the N-terminal 81 amino acids of human -1,4-galactosyltransferase tagged with ECFP as a marker for the Golgi apparatus, were transiently transfected into HeLa cells using FuGENE HD (Promega, E2311). After transfection, the cells were plated at 2-3x10^4 cells per well on Lab-Tek 8-well chambered coverglasses (Thermo Fisher Scientific, 155411PK), which were coated with poly-D-Lysine (Sigma, P6407). Cells were maintained in imaging medium (DMEM, corning, 17-205-CV) supplemented with 1% Pen-Strep, 1x GlutaMAX and 10% FBS for 16-24 h. After addition of compound or DMSO control, cells were imaged every minute for a duration of 30 to 60 min. During image acquisition, a temperature of 37 °C, an atmosphere of 5% CO_2 and humidity were maintained by a stage top incubator and lens heater (Tokai Hit). Images were acquired using a Neo Fluore 40x objective (Zeiss) mounted on an inverted Axiovert 200 microscope (Zeiss). Excitation was conducted by means of diode lasers and a semiconductor laser (COHERENT, OBIS 445 nm LX 75 mW, OBIS 514 nm LX 40 mW) fiber-coupled (OZ optics) to the spinning disk confocal unit (CSU10; Yokogawa) mounted with a triple-band dichroic mirror (Di01-T442/514/647, Semrock). Signals were processed with appropriate filter sets for CFP and YFP (Chroma Technology) and fluorescence images were captured with a CCD camera

(Orca ER, Hamamatsu Photonics) controlled by the Metamorph 7.8 imaging software (Molecular Devices). Image quantification was performed using ImageJ. The intensity of YFP-PH(FAPP1) was quantified within the area of the GT-CFP Golgi marker to retrieve Golgi-intensities of the PI4P sensor. Cytosolic intensities of the sensor were determined by taking arbitrary region scans inside the cell without covering nucleus and endomembranes.

4.2.2.14 Cell Painting Assay performed at the Compound Management and Screening Center (COMAS), Dortmund

The cell painting assay was performed by the COMAS, Dortmund. The cell painting assay was carried out as described in Bray *et al.*[9] with slight modifications. U2OS cells (ATCC) were seeded at $2x10^3$ cells/well in in 384 well plates (PerkinElmer, CellCarrier-384 Ultra) and incubated for 4 h at 37 °C and 5% CO_2 (DMEM containing 10% fetal calf serum (PAN Biotech, 131206), 1% L-Glutamine (PAN Biotech, P04-80100), 1% Sodium Pyruvate (Gibco 11360-0930) and 1% non-essential amino acids (Gibco, 11140-035)). Compounds were added using Echo 520 acoustic dispenser (Labcyte) with a final screening concentration of 10 and 20 µM. Compound treatment continued for approx. 20 h at 37°C, 5% CO_2. After compound incubation, mitochondria were stained with the MitoTracker staining solution (MitoTracker Deep Red (Thermo Fisher Scientific, M22426)), which was applied to living cells because the MitoTracker dye is only taken up by active mitochondria. For this, media was aspirated form the plates with 10 µL residual volume and 25 µL of 100 nM Mitotracker solution was added followed by incubation for 30 min in the dark at 37 °C. Next, cells were fixed by addition of 7 µL of 18.5% Formaldehyde, to give a final concentration of 3.7% (v/v), and incubated at room temperature (RT) for 20 min. Plates were then washed three times with 70 µL PBS with final aspiration (Biotek Washer Elx405). Next, 25 µL of 0.1% (v/v) Triton X-100 in PBS was added and the cells were incubated in the dark at RT for 15 min to enable permeabilization. Plates were again washed three times with 70 µL PBS with final aspiration. Next, a staining solution containing 5 µL/mL phalloidin solution (Thermo Fisher Scientific, A12381), 25 µg/mL ConcanavalinA (Thermo Fisher Scientific, C11252), 5 µg/mL Hoechst 33342 (Sigma, B2261-25mg), 1.5 µg/mL WGA-Alexa594 conjugate (Thermo Fisher Scientific, W11262), 1.5 µM SYTO 14 solution (Thermo Fisher Scientific, S7576) and 1% BSA was prepared in PBS. 25 µL of staining solution were added to each well and incubated in the dark at RT for 30 min. Plates were washed three times with 70 µL PBS with no final aspiration. Imaging was carried out using an ImageXpress Micro XL High-Content Screening System (Molecular Devices) at 20x magnification. Nine pictures were taken from every well with a camera binning of 2. Image

analysis was carried out using the Cell Profiler Pipeline[9]. Per-image mean values for all parameters were calculated in Cell Profiler during processing of the images.

Further processing was performed with a custom KNIME workflow [https://www.knime.org/, with the HCS Tools extensions provided by the Max Planck Institute of Molecular Cell Biology and Genetics (MPI-CBG)]. Outliers among the 9 image sites per well were removed and the relevant parameters were determined in a three-step procedure: 1. Parameters that have a high coefficient of variation (>= 10 %) for the controls were removed. 2. Parameters that have a low coefficient of variation (<= 10 %) over all test compounds were removed. 3. Highly correlated parameters were filtered out by a Correlation Filter. The remaining parameters were normalized to Percent-of-Control (POC) and toxic compounds (reducing the cell count to 55 % or less of the control) were filtered out. Principal-Component-Analysis (PCA) was performed and the compounds were plotted with the first three components of the PCA using DataWarrior [http://www.openmolecules.org/datawarrior/].

4.2.3 Biochemical Methods

4.2.3.1 DC Protein Assay

To determine the protein concentration of a lysate or protein mixture, a DC protein assay was performed. The colorimetric assay determines protein concentration based on the interaction of copper ions with peptide bonds and the oxidation of basic amino acids.[147] In combination with a BSA standard dilution series, the protein concentration of the sample can be calculated. The assay was carried out in duplicates according to the manufacturer's instructions.

4.2.3.2 SDS-polyacrylamide gel electrophoresis (PAGE)

An SDS-PAGE was conducted to analyze proteins or protein mixtures and lysates. For this, SDS polyacrylamide gels with different percentages (depending on the size of the protein of interest) were loaded with the proteins or proteins mixtures/lysates supplemented with 5x SDS sample buffer at a 1/5 dilution. Since SDS and DTT in the sample buffer as well as the boiling at 95 °C lead to denaturation, reduction and a homogenous negative charge of the proteins, a size-dependent separation in the polyacrylamide mesh is achieved upon application of current. Large proteins migrate slower than small proteins, leading to the formation of several protein bands.

The SDS polyacrylamide gel was prepared according to the recipe in 4.1.2 and addition of APS and TEMED induced polymerization. First, the resolving gel was filled into the polymerization chamber (short and 1 mm spacer plates, fixed in the Mini-PROTEAN® Tetra Cell Casting Module). After incubation for 20 min, the stacking gel was added, and the comb was inserted before incubation for 15 min. After polymerization, the comb was removed, and the gel pockets were rinsed with mH_2O. The Mini-PROTEAN® Tetra Cell was assembled and 1x running buffer was filled into the tank and between the gels as indicated by the mark. The protein samples as well as 7 µL of PageRuler™ Plus prestained protein ladder (marker, M) were loaded with a Hamilton syringe so that the individual protein amount was the same in all pockets. All protein samples had to be supplemented with 1/5 5x SDS sample buffer and boiled at 95 °C for 5 min. After loading, a voltage of 80 V was applied for 30 min to allow slow migration through the stacking gel (5% acrylamide) and generation of protein stacks. Afterwards, the current was increased to 130 V and kept until the running front reached the end of the gel. The glass slides were separated, and the gel was either transferred into a tank with mH_2O or transfer/wet blotting buffer. The protein bands were detected either via immunoblotting using specific antibodies or via Coomassie staining.

4.2.3.3 Silver Staining

To visualize all proteins in an SDS polyacrylamide gel, the gel was stained with the Pierce™ Silver Stain Kit according to the manufacturer's instructions. Images were taken with a digital camera (Leica SUMMARIT H1:2.2/27 ASPH).

4.2.3.4 Immunoblotting

Immunoblotting techniques employ primary and corresponding secondary antibodies to detect a protein of interest. For this, the proteins must be transferred from an SDS polyacrylamide gel onto a suitable membrane that allows antibody binding and detection. In this thesis, the wet blotting technique was used for all protein transfers.

I Wet blotting protein transfer

After electrophoresis, the gel was equilibrated in 1x wet blotting buffer for approx. 10 min. The Immobilon-FL PVDF membrane was activated by incubation in methanol for 30 s. The plastic holder belonging to the transfer cassette was placed in a big tank filled with 1x wet blotting buffer. One fiber pad was placed on top of the white site of the plastic holder and one piece of prewetted filter paper was added on top, followed by the activated membrane (the sandwich was flattened with a plastic roller to remove bubbles) and the equilibrated gel. The

sandwich was completed by adding another piece of filter paper (flattened again) and another fiber pad. The plastic holder was then closed and inserted into the cassette, which was placed inside the blotting tank. The second plastic holder was assembled like the first, the cooling unit and a magnetic stir bar were added, and the tank was filled with 1x wet blotting buffer until the indicated mark. The whole tank was placed on top of a magnetic stirrer and a voltage of 100 V was applied for 85 min to complete the transfer.

II Immunostaining and detection

After the protein transfer, the membrane is stained with Ponceau S solution to ensure successful blotting. If the stain is positive, the membrane is washed with mH_2O, cut according to the used antibodies and corresponding protein sizes and filled into 50 ml falcon tubes. After 1 h of blocking, primary antibodies are added and the membranes are incubated overnight at 4 °C. On the next day, the membranes are washed twice in PBS for 10 min and incubated with a corresponding secondary antibody, coupled to horseradish peroxidase (HRP, for chemiluminescent detection) or near-infrared dyes (680RD or 800CW, Li-COR antibodies, for fluorescent detection) (4.1.3.2) for 1 to 1.5 h at RT. After two more 10 min washing steps, the membrane is either directly imaged (in case of secondary antibodies coupled to 680RD or 800CW) or incubated with SuperSignal™ West Femto or SuperSignal™ West Pico reagent according to the manufacturer's instructions (for HRP-coupled antibodies). All images were taken on an Odyssey Fc imaging system.

4.2.3.5 Cellular Thermal Shift Assay (CETSA)

This assay is based on the biophysical principle of protein thermal stability that has been used in melting temperature shift assays for a long time already. If a protein is heated up, its tertiary structure unfolds, and hydrophobic structures are exposed to the solvent. This process can be monitored by differential scanning calorimetry (DSC), which monitors the phase transition during unfolding by measuring the energy change via detection of a temperature change in the surrounding solvent.[148] An advancement of this technique is the thermal shift assay or differential scanning fluorimetry (DSF) that monitors protein unfolding by means of a fluorescent dye, e.g. SYPRO orange, whose interaction with hydrophobic protein structures leads to an increase of quantum yield that is detectable via fluorescence spectroscopy.[149] The cellular thermal shift assay, in contrast to the precursor assays, does not use purified proteins but cells or cellular lysates and is thereby performed under more physiological conditions.[150] Protein unfolding is not detected via energy changes or a fluorescence dye but by monitoring protein precipitation. Unfolded proteins will aggregate with each other due to hydrophobic

interactions. If the protein sample is then centrifuged, insoluble proteins will be pelleted. Separation of the protein supernatant on an SDS-PAGE enables detection and quantification of the remaining soluble proteins. When the soluble protein amount is plotted against a temperature range, a melting curve can be generated and the melting temperature (T_m) can be calculated (inflection point of the melting curve). If a protein is bound by a ligand, e.g. a small molecule, its thermal stability can be affected, leading to a shift of the melting curve and a change of the melting temperatures.[149,150]

To perform the CETSA, lysates were generated as described in 4.2.2.10-II. Two aliquots of 600 µL lysate (900 µg) were incubated with a compound at a concentration of 50 µM or DMSO at 0.5% for 10 min. Each lysate was then aliquoted in nine PCR tubes and heated to several temperatures (40.3, 44.5, 50.6, 54, 55.6, 57.1, 58.6, 63.7 and 66.9 °C) for 3 min. After heating, the samples were incubated at RT for another 3 min and transferred to ultracentrifuge vials. Ultracentrifugation was carried out at 100,000 g and 4 °C for 25 min. The supernatant was transferred to 1.5 mL tubes, shock frozen in liquid nitrogen and stored at -80 °C. For analysis via SDS-PAGE, 5x SDS sample buffer was added at 1/5 dilution and the samples were boiled at 95 °C and 350 rpm for 5 min. Afterwards, SDS-page (4.2.3.2) and immunoblotting (4.2.3.4) for the protein of interest were carried out. The bands of the protein of interest were quantified with the Image Studio software (Version 4.0.21, Li-COR Biosciences, ©2014). The band intensities were plotted against the temperature and non-linear regression was performed using a four-parameter fit (GraphPad Prism 6, GraphPad Software, USA) to calculate the melting temperature.

4.2.3.6 Affinity chromatography for target identification

Affinity chromatography is a procedure that separates certain components of a mixture from the bulk by specific interaction with a solid phase. In this thesis, the method was applied to isolate protein binding partners of small molecules from a protein mixture (also called “pull-down”). For this, the small molecule or antibody was attached to a solid phase and incubated with a lysate. After stringent washing, the bound proteins were eluted and either analyzed via immunoblotting or mass spectrometry. Two different approaches were applied: Enrichment of ATP binding proteins was achieved by using an ActivX Desthiobiotin-ATP Probe and a small molecule as a competitor. In the second approach, the compound itself was employed as a small-molecule probe to identify its binding partners.

All steps were performed in a clean bench to prevent contamination with external peptides or proteins, e.g. keratin. Additionally, equipment (pipette tips and tubes) with low protein binding

surfaces were used to maximize protein retrieval. Whenever a mass spectrometry measurement was done, each sample was prepared in technical triplicates.

I Affinity chromatography using an ActivX Desthiobiotin-ATP probe

The Pierce™ Kinase Enrichment Kit with ATP Probe (Thermo Fisher Scientific) was used for this method.

Ia.) Generation of Lysates

NIH/3T3 cells were seeded in eight T175 cell culture flasks and incubated at 37 °C and 5% CO_2 until they reached 100% confluence. Medium was removed, and cells were washed with 5 mL ice-cold PBS before addition of 1.5 mL cell dissociation solution. The cells were incubated at 37 °C and 5% CO_2 for 15 min and collected in growth medium (10 mL per flask). All suspensions were pooled in two 50 mL falcon tubes. Washing, lysis and desalting were carried out as described in the kit protocol. Protein concentration was measured by means of the DC protein assay (4.2.3.1) and the lysate was aliquoted at 1 mg per tube.

Ib.) Pulldown

The reaction volume (corresponding to 1 mg of protein) was filled up to 485 µL per sample with reaction buffer. After addition of 10 µL 1 M $MgCl_2$ and incubation for 1 min at RT, 100 and 200 µM compound (or 1% DMSO, control) was added and incubated for 1 h at RT. The lyophilized desthiobiotin ATP probe was resolved in ultrapure water as described in the kit protocol. 5 µM of the probe (10 µL of a 0.25 mM stock solution) was added to each sample and incubated for 10 min at RT. Afterwards, 490 µL 8 M urea in IP lysis buffer, as well as 50 µL 50% high capacity streptavidin agarose resin slurry, was added to each sample. After incubation for 1 h at RT on an overhead rotor at 10 rpm, the samples were centrifuged at 1000 x g for 1 min to pellet the resin. The supernatant was removed carefully and the pellet was resuspended in 500 µL 4 M urea in IP lysis buffer. The resin was washed two more times with 500 µL 4 M urea. Bound proteins were eluted by addition of 40 µL 5x SDS sample buffer and heating to 95 °C for 5 min at 500 rpm. The samples were subjected to an SDS-PAGE and proteins were either detected via immunoblotting (Ic.)) or mass spectrometry (Id.)).

Ic.) Immunoblot Detection

For immunoblot detection, SDS page and immunoblotting were carried out as described in 4.2.3.2 and 4.2.3.4.

Id.) In-gel Digestion

Before proteins can be detected via mass spectrometry, they must be digested to shorter peptide sequences. To achieve this, in-gel digestion is performed. To remove detergents and EDTA, the samples were loaded onto a precast TGX 4-20% gel, which was run for approx. 15-30 min at 80 V until the complete sample was inside the gel. The gel was then transferred into a glass petri dish, rinsed with fixation solution and cut below the running front and in between the pockets. The single gel pieces were transferred to Protein LoBind tubes and incubated in 500 µL fixation solution overnight. On the next day, the fixation solution was replaced by 200 µL washing solution 1 and shook for 30 min at 600 rpm and 37 °C. Afterwards, washing solution 1 was removed and 200 µl of washing solution 2 were added prior to a 15 min incubation at 600 rpm and 37 °C. Washing solution 2 was then replaced by 200 µL reducing solution and incubated for 45 min at 600 rpm and 37 °C before removal and addition of 200 µL alkylating solution. After 1 h of incubation at RT in the dark, the alkylating solution was replaced by 200 µL washing solution 2 and the gel pieces were shaken for 15 min at 600 rpm and 25 °C. After one repetition, all liquid was removed and 100 µL AcN were added to dehydrate the gel. AcN was removed and the gel was dried by leaving the opened tube in a closed clean bench for 30 min. Subsequently, 75 µl of digest solution were added to the dried gel piece and incubated for 15 min at 600 rpm and RT before addition of another 75 µL 25 mM NH_4HCO_3 and incubation overnight at 350 rpm and 30 °C.

On the next day, 10 µL concentrated TFA was added to each sample to stop the digestion reaction. To extract the peptides from the gel, all samples were sonicated on ice for 30 min. After addition of 75 µL AcN, the samples were incubated for 15 min at 350 rpm and 25 °C. The supernatant was transferred to a new LoBind tube and another 75 µL AcN were added to the gel pieces and incubated for 15 min at 350 rpm and 25 °C. Both supernatants were combined and concentrated in a vacuum centrifuge for 3-6 h at 30 °C. If a pellet was visible after concentration, this was most likely due to salt contaminations and a stop-and-go-extraction (stage) tip sample purification (4.2.3.6.-IIe.)) was performed to remove such contaminations.

Ie.) Nano-HPLC/MS/MS

The Nano-HPLC/MS/MS measurement *was performed by the Mass spectrometry group of the MPI Dortmund, namely Andreas Brockmeyer, Malte Metz and Petra Janning.*

After tryptic digestion and purification, the protein fragments were analyzed by nano-HPLC-MS/MS using an Ultimate™ 3000 RSLC nano-HPLC system and a Q Exactive™ Plus or Q Exactive™ HF Hybrid Quadrupole-Orbitrap mass spectrometer equipped with a nano-spray

source (all Thermo Fisher Scientific). For this, the lyophilized tryptic peptides were dissolved in 20 µL 0.1 % TFA and 3 µL of these samples were injected and enriched onto a C18 PepMap 100 column (5 µm, 100 Å, 300 µm ID * 5 mm) using 0.1% TFA and a flow rate of 30 µL/min for 5 min. Afterwards, the peptides were separated on a C18 PepMap 100 column (3 µm, 100 Å, 75 µm ID * 25 cm) using a linear gradient starting with 95% solvent A/5% solvent B and increasing to 70.0% solvent A/30.0% solvent B in 90 min with a flow rate of 300 nL/min (solvent A: water containing 0.1% formic acid, solvent B: acetonitrile containing 0.1% formic acid). The nano-HPLC was coupled to the mass spectrometer using a standard coated Pico Tip emitter (ID 20 µm, Tip-ID 10 µM). A mass range of m/z 300 to 1,650 was acquired with a resolution of 70,000 for a full scan, followed by up to ten high-energy collision dissociation (HCD) MS/MS scans of the most intense at least doubly charged ions with a resolution of 17,500 for the samples analyzed on the Q Exactive Plus. For samples analyzed on the Q Exactive HF the same mass range was used and a resolution of 60,000 for a full scan, followed by up to fifteen HCD-MS/MS scans of the most intense at least doubly charged ions with a resolution of 16,000.

If.) Data Analysis

Data analysis *was performed by the Mass spectrometry group of the MPI Dortmund, namely Andreas Brockmeyer, Malte Metz and Petra Janning.*

Protein identification and relative quantification were performed using MaxQuant[151] v.1.5.3.30 or v.1.5.6.5, respectively, including the Andromeda search algorithm and searching the mouse reference proteome of the UniProt database. Briefly, a MS/MS ion search was performed for full enzymatic trypsin cleavages allowing two miscleavages. For protein modifications carbamidomethylation was chosen as fixed and oxidation of methionine and acetylation of the N-terminus as variable modifications. The mass accuracy was set to 20 ppm for the first and 6 ppm for the second search. The false discovery rates for peptide and protein identification were set to 0.01. Only proteins for which at least two peptides were quantified were chosen for further validation. Relative quantification of proteins was carried out using the label-free quantification algorithm implemented in MaxQuant. All experiments were performed in technical triplicates. Statistical data analysis was performed using Perseus[152], label-free quantification (LFQ) intensities were logarithmized (log2). Samples resulting from affinity purification using the small molecule as a competitor were grouped together and samples resulting from affinity purification using DMSO as solvent control as well. Proteins which were not at least three times quantified in at least one of the groups were filtered off. Missing values were imputed using small normal distributed values and a t-test was

performed. Proteins which were statistically significant outliers and enriched in the samples treated with DMSO over the ones treated with compound competitor were considered as hits.

II Affinity chromatography using a small-molecule probe

The small-molecule probes that were used in this approach *were synthesized by Dr. Lucas Robke, MPI Dortmund and Dr. Andrei Ursu, MPI Dortmund.*

IIa.) Generation of Lysates

NIH/3T3 cells were seeded in eight T175 cell culture flasks and incubated at 37 °C and 5% CO_2 until they reached 100% confluence. After washing two times with PBS, the cells were detached using cell dissociation solution. After detachment, the cells were collected in growth medium (7 mL per flask) and pooled in 50 mL falcon tubes. The suspension was centrifuged at 2000 g for 5 min and the pellet was washed with PBS three times. Then, 4 mL of pulldown lysis buffer were added to each pellet and the solutions from different falcon tubes were pooled. The lysate was then passed subsequently through a 0.9 Ø and a 0.45 Ø cannula and collected in a 15 mL falcon tube, before incubation on ice for 40 min with vortexing every 10 min. The lysate was aliquoted at 2 mL and centrifuged at full speed for 20 min at 4 °C. For determination of the protein concentration using the DC protein assay (4.2.3.1), the supernatants were pooled and afterwards aliquoted at 1 mL for storage at -80 °C.

IIb.) Compound Immobilization

Since magnetic beads were used for this approach, all separation steps (removal of buffer/lysate from the beads) were achieved by placing the vials into a magnetic rack. Each sample was prepared in triplicates.

Before the starting the pulldown experiment, the active and inactive probes had to be coupled to the solid phase, i.e. the beads. For this, both active and inactive probes were diluted to 10 µM in 550 µL coupling buffer A. Next, 25 µL of the NHS magnetic sepharose beads were filled into protein LoBind tubes and the buffer was removed. Then, 500 µL cold equilibration buffer were added to the beads, the vials were inverted, and the buffer was removed again. Immediately after removal, 500 µL of the probe dilution were added to the beads and the vials were incubated on an overhead rotator for 2.5 h at force 16 to couple the probes to the beads. Afterwards, residual active groups were quenched by alternating incubations with blocking buffer A and B (both at 500 µL, overhead rotator). First, blocking buffer A was added for 5 min, then, after removal of blocking buffer A, blocking buffer B was added for 5 min as well. Afterwards, blocking Buffer A was added for 15 min followed by subsequent 5 min incubations

with blocking buffer B, A and again B. The quenching was completed by a 10 min incubation in lysis buffer.

In case of a competition experiment with the unmodified compound, the lysate was pre-incubated with an excess of compound, i.e. 200 µM, to block target binding sites, or with 1% DMSO as a control on an overhead rotator for 2.5 h at 4 °C. In this case, all samples contained beads coupled to the active probe – three bead-samples were mixed with a DMSO-pre-incubated lysate and three others were mixed with a compound-pre-incubated lysate.

IIc.) Pulldown

After coupling and, when applicable, pre-incubation of the lysate with unmodified compound or DMSO, 500 µL of the lysate (i.e. a total protein amount of 1 mg or more) were added to the beads and incubated on an overhead rotator for 1 h at RT with force 16. Afterwards, the beads were washed with lysis buffer supplemented with 25 mM $MgCl_2$ for 10 min and then washed two more times with PBS for 10 min each, to remove detergents and EGTA.

IId.) On-bead Digestion

To release bound proteins, an on-bead digestion was carried out, meaning that the digestion enzymes were directly added to the beads and liberated the bound proteins by cleaving the respective peptide bonds. Before digestion could take place, the bound proteins had to be reduced and alkylated. For this, 50 µl Denaturing/reducing buffer were added to the beads and incubated at RT in a thermomixer for 30 min at 350 rpm. Next, 5.55 µL of 10x Alkylation solution were added before incubation at RT for another 30 min at 350 rpm. LysC was added at 1 µg and the samples were incubated for 30 min at 350 rpm and 37 °C. The supernatant was then transferred to a protein LoBind tube and 165 µl 50 µM Tris (pH 7.5) containing 1 µg trypsin were added to the beads, followed by a 30 min incubation at 350 rpm and 37 °C. Finally, both supernatants were combined, another 2 µg of trypsin were added, and the mixture was incubated overnight at 350 rpm and 37 °C. On the next day, the digestion was terminated by adding 2 µL concentrated TFA.

IIe.) Stop-and-Go-Extraction (Stage) Tip Sample Purification

The stage tip sample purification was performed to remove possible contaminants from the peptide samples. For this, a stage tip was prepared by placing two layers of 3M™ Empore™ High Performance Extraction Disks, C18 (Octadecyl) into a low binding 200 µL pipette tip using a special stage tip syringe, which has been prepared by the workshop of the MPI Dortmund, to trump out the membrane and insert it into the tip. The membrane contains chromatographic beads immobilized in a Teflon meshwork that holds back the peptides but

not possible contaminants, which can be washed out. Later on, the peptides can be eluted with fresh and contamination-free buffer.[153] To activate the membrane, 100 µL methanol were added to the tips and removed via centrifugation in a stage tip centrifuge (as for the following steps). Next, the stage tips were washed first with 100 µL buffer B and then twice with 100 µL buffer A. Afterwards, the samples were loaded to the tips, incubated for 1 min and centrifuged. Then the tips were washed again with 100 µL of buffer A and the samples were eluted by adding two times buffer B, incubating the tips for 1 min, centrifuging them in a conventional centrifuge for 5 min at 6,010 g and collecting the eluate in fresh lo-bind tubes. Finally, the samples were dried in a vacuum centrifuge for 2 h at 30 °C

IIf.) MS/MS Measurement

The Nano-HPLC/MS/MS measurement *was performed by the Mass spectrometry group of the MPI Dortmund, namely Andreas Brockmeyer, Malte Metz and Petra Janning.*

After tryptic digestion and purification, the protein fragments were analyzed by nano-HPLC-MS/MS using an Ultimate™ 3000 RSLC nano-HPLC system and a Q Exactive™ Plus or Q Exactive™ HF Hybrid Quadrupole-Orbitrap mass spectrometer equipped with a nano-spray source (all Thermo Fisher Scientific). For this, the lyophilized tryptic peptides were dissolved in 20 µL 0.1% TFA and 3 µl of these samples were injected and enriched onto a C18 PepMap 100 column (5 µm, 100 Å, 300 µm ID * 5 mm) using 0.1% TFA and a flow rate of 30 µL/min for 5 min. Afterwards, the peptides were separated on a C18 PepMap 100 column (3 µm, 100 Å, 75 µm ID * 25 cm) using a linear gradient starting with 95% solvent A/5 % solvent B and increasing to 70.0% solvent A/30.0% solvent B in 90 min with a flow rate of 300 nL/min (solvent A: water containing 0.1% formic acid, solvent B: acetonitrile containing 0.1% formic acid). The nano-HPLC was coupled to the mass spectrometer using a standard coated Pico Tip emitter (ID 20 µm, Tip-ID 10 µM). A mass range of m/z 300 to 1,650 was acquired with a resolution of 70,000 for a full scan, followed by up to ten high energy collision dissociation (HCD) MS/MS scans of the most intense at least doubly charged ions with a resolution of 17,500 for the samples analyzed on the Q Exactive Plus. For samples analyzed on the Q Exactive HF the same mass range was used and a resolution of 60,000 for a full scan, followed by up to fifteen HCD-MS/MS scans of the most intense at least doubly charged ions with a resolution of 16,000.

IIg.) Data Analysis

Data analysis *was performed by the Mass spectrometry group of the MPI Dortmund, namely Andreas Brockmeyer, Malte Metz and Petra Janning.*

Protein identification and relative quantification were performed using MaxQuant[151] v.1.5.3.30 or v.1.5.6.5, respectively, including the Andromeda search algorithm and searching the mouse reference proteome of the UniProt database. Briefly, a MS/MS ion search was performed for full enzymatic trypsin cleavages allowing two miscleavages. For protein modifications carbamidomethylation was chosen as fixed and oxidation of methionine and acetylation of the N-terminus as variable modifications. The mass accuracy was set to 20 ppm for the first and 6 ppm for the second search. The false discovery rates for peptide and protein identification were set to 0.01. Only proteins for which at least two peptides were quantified were chosen for further validation. Relative quantification of proteins was carried out using the label-free quantification algorithm implemented in MaxQuant. All experiments were performed in technical triplicates. Statistical data analysis was performed using Perseus[152], Label-free quantification (LFQ) intensities were logarithmized (log2) and samples resulting from affinity purification using the active molecule bound to solid support were grouped together and samples resulting from affinity purification using the inactive control molecule bound to solid support as well. Proteins which were not at least three times quantified in at least one of the groups were filtered off. Missing values were imputed using small normal distributed values and a t-test was performed. Proteins, which were statistically significant outliers and enriched in the samples resulting from affinity enrichment using the active molecule bound to the solid support, were considered as hits. In case of a competitive pulldown, proteins, which were statistically significant outliers and enriched in the samples treated with DMSO over the ones treated with compound competitor, were considered as hits.

4.2.3.7 Kinase Activity or Binding Measurements at Thermo Fisher Scientific

The majority of kinase activity measurements and the kinase panel screen were performed at SelectScreen™ (Thermo Fisher Scientific). Here, three different assays were conducted. The principles of the assays are described in the following:

I Adapta Assay

The Adapta assay is a fluorescence resonance energy transfer (FRET)-based ATP-depletion assay, wherein the formation of ADP is monitored. First, the kinase reaction is allowed to take place, mostly for 60 min. Next, the reaction is stopped with EDTA and a FRET pair, consisting of a europium-labelled anti-ADP antibody and an Alexa647-labelled ADP tracer, are added to the solution. The ADP generated due to ATP hydrolysis by the kinase replaces the tracer from the antibody and disrupts the energy transfer leading to a low FRET signal. If the kinase

is inhibited by a small molecule, less ADP is generated, resulting in less replacement and higher FRET signal. Data were normalized to DMSO-treated samples.

II Lantha Assay

The Lantha assay is a FRET-based displacement assay that assesses binding of a small molecule to a kinase. The FRET pair consists of a europium-labelled antibody that binds to a tag on the kinase of interest and an Alexa647-labelled tracer, based on an ATP-competitive kinase inhibitor. If both the antibody and the tracer bind to the kinase, FRET occurs. If a small molecule displaces the tracer, the FRET signal decreases. Data were normalized to DMSO-treated samples.

III Z'Lyte Assay

The Z'Lyte assay measures kinase activity by monitoring the conversion of a synthetic peptide substrate in a FRET-based manner. For this, the peptide substrate is labeled with a fluorophore at each end that together make up a FRET pair. After the kinase reaction took place, a developing reagent containing a protease, which cleaves all non-phosphorylated substrate peptides and disrupt FRET, is added. Phosphorylation prevents cleavage by the protease and sustains FRET. If the kinase is inhibited, though, phosphorylation is reduced leading to increased cleavage and lower FRET. Data were normalized to DMSO-treated samples.

Kinases or assay formats that were not available for screening at SelectScreen™ were tested at Reaction Biology, Eurofins or SignalChem. The principle of the assays is described in the following sections.

4.2.3.8 Kinase Assays at Reaction Biology and Eurofins

At Reaction Biology, kinase activity is measured via monitoring ATP consumption in a radiometric manner. For this, ^{33}P-ATP is added to the kinase reaction and after 2 h at RT, the reaction mixture is spotted onto P81 ion exchange paper to separate kinase substrate, which has been phosphorylated and carries radiolabeled phosphate, and ^{33}P-ATP. The amount of radiolabeled substrate is then measured by scintillation counting. Data were normalized to DMSO-treated samples. Eurofins uses the same assay principle in a filter-binding radiometric kinase activity assay.

4.2.3.9 K_i Determination at SignalChem

At SignalChem, the luminescent ADP-Glo kinase assay was performed to measure ATP consumption, which is proportional to kinase activity. Different concentrations of compound were titrated against different ATP concentrations. Relative light units (RLU) were converted to ATP conversion rate using standard ATP conversion curves and reaction velocities were calculated based on the amount of ATP transferred in the reactions. For determination of K_i and the mode of inhibition, the ATP concentration was plotted against the velocity in a Michaelis-Menten saturation curve.

4.2.4 Computational methods

4.2.4.1 Computational target prediction performed by collaboration partners at the ETH Zürich

*Computational target prediction was performed for compound **5**, Smoothib, by Prof. Gisbert Schneider and his coworkers at the ETH Zürich* as described in Kremer *et al.*[154]. The SPiDER software tool[155], short for self-organizing map–based prediction of drug equivalence relationships, was used to predict possible targets for Smoothib. The software employs a ligand-based method that identifies possible target proteins by comparing the compound of interest to other substances with known targets. In this case, the COBRA database of bioactive compounds was employed[156]. Similarity is not calculated based on structural features but based on topological pharmacophore features, termed chemical advanced template search (CATS) descriptors[157], combined with physicochemical properties and other topological indices, termed MOE QSAR descriptors[158]. Additionally, the Target Inference GEneRator (TIGER) software tool[159], which only compares pharmacophore patterns, was employed as well. To perform the software-based prediction, the compound was drawn in a structure-data file (SDF) v2 format and entered into both software tools. The results were manually analyzed and compared by Prof. Gisbert Schneider and his coworkers to retrieve a list of potential targets.

4.2.4.2 Molecular Docking of Smoothened and Smoothib performed by a collaboration partner at the Lead Discovery Center, Dortmund

Molecular docking was performed by Dr. Carsten Schultz-Fademrecht at the Lead Discovery Center Dortmund according to the procedure described in Kremer *et al.*[154]. The Schrodinger

Suite 2017-1 was used to screen different crystal structures of SMO in complex with various antagonists that were derived from the Protein Data Bank (PDB, http://www.rcsb.org/pdb/) for possible binding positions of Smoothib. The employed structures are listed under the following PDB codes: 4JKV, 4N4W, 4O9R, 4QIM and 5L7I. To screen the transmembrane domain for docking, the cytochrome b562 insert was removed and only chain A was kept in case of dimeric structures (4JKV and 5L7I). As a first step, the X-ray is cleaned up by adding hydrogen atoms, removing water molecules, fixing bond orders, optimizing protonation states and hydrogen bond networks and finally performing a minimization under constraints by OPLS3 force-field (Schrodinger utility “Protein Preparation Wizard”). Smoothib was likewise prepared for docking by adding hydrogen atoms and generating tautomeric and ionization states (Schrodinger utility “LigPrep”). All structures were minimized using the OPLS3 force-field. The protein grid necessary for docking experiments was generated by the “Receptor Grid Preparation (Glide)”. The Van der Waals radius scaling factor was set to 0.50 with a partial charge cutoff of 0.25. The site of the enclosing box was set to 25 Å. The actual docking of SMO and Smoothib was performed by using the “Ligand docking” utility. Under Setting, XP (extra precision), Dock flexibly, sample nitrogen inversions, sample ring conformation and Epik state penalties to docking score were selected and amide bonds were penalized for nonplanar conformation.

5 RESULTS

5.1 Quinoline, indole and azepinone derivatives as Hh inhibitors

Applying a *de novo* branching cascades approach, 61 molecules *have been synthesized by Dr. Miguel Garcia-Castro*.[160] These molecules were screened for biological activity at the Compound Management and Screening Center (COMAS), Dortmund and were found to be active in various pathways, one of them being the Hh signaling pathway. The chemical structures of the three most active compounds, a quinoline (compound **1**), indole (compound **2**) and an azepinone (compound **3**) derivative are shown in Figure 18A. The corresponding results for inhibition of Hh signaling-dependent osteogenesis are depicted in Figure 18B.

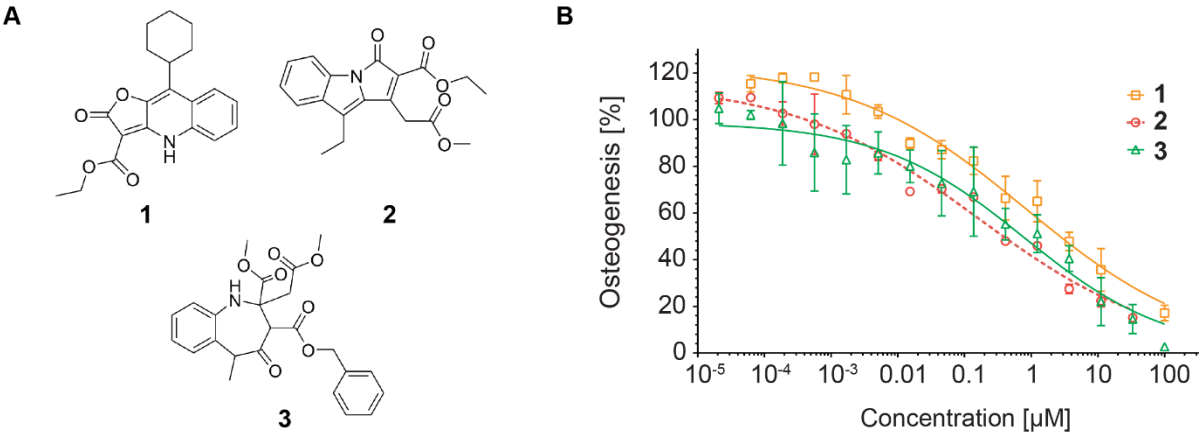

Figure 18. Diverse scaffolds inhibit Hh signaling-dependent osteogenesis. A. Chemical structures of compounds **1**, **2** and **3**. **B.** Osteogenesis assay. C3H10T1/2 cells were treated with 1.5 µM Purmorphamine and various concentrations of the compounds or DMSO as a control for 96 h before measuring alkaline phosphatase activity using the CDP-Star reagent in a luminescent readout. Data were normalized to Purmorphamine-DMSO-treated cells and are mean values of biological replicates (n=3) ± standard deviation (SD).

Compounds **1**, **2** and **3** inhibited osteogenesis with IC_{50} values of 1.0 ± 0.9 µM, 0.2 ± 0.0 µM and 0.5 ± 0.6 µM, respectively. Since the Hh agonist Purmorphamine was used to induce osteogenesis, inhibition of this process is an indirect proof of Hh signaling pathway inhibition.

5.1.1 Confirmation of Hh inhibition

Osteogenesis is a complex process that is, additionally to Hh signaling, controlled by Wnt and bone morphogenetic protein (BMP) signaling[161], to name only a few. To confirm inhibition of Hh signaling, a GLI reporter assay was performed. For this, a stable cell line, Shh-LIGHT2 cells (see 4.1.7), was used. In this cell line, firefly luciferase expression is induced upon Hh

signaling pathway activation, whereas Renilla luciferase expression serves as a control for transcriptional activity and overall cell viability. Within this assay, all three compounds have shown inhibition of reporter expression (Figure 19A). However, with IC_{50} values of 5.7 ± 3.4 µM, 45.0 ± 9.5 µM and 31.6 ±6.7 µM, the potency was drastically decreased. Even though compound **1** retained a one-digit micromolar IC_{50}, Hh signaling pathway inhibition only reached a maximum of 40 % in the reporter gene assay.

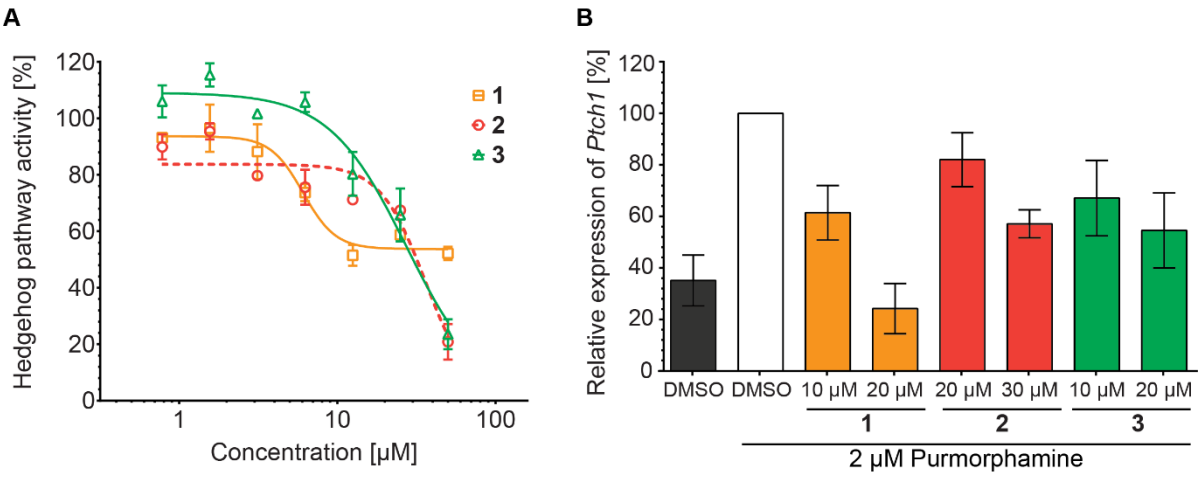

Figure 19. Diverse scaffolds were confirmed as Hh signaling pathway inhibitors. A. GLI reporter gene assay. Shh-LIGHT2 cells were treated with 2 µM Purmorphamine and the compounds or DMSO as a control for 48 h. The Hh-dependent firefly luciferase signal was divided by the control signal of the Renilla luciferase. Data were normalized to Purmorphamine-DMSO-treated cells and are mean values of biological replicates (n=3) ± SD. **B.** Evaluation of target gene expression. NIH/3T3 cells were treated with 2 µM Purmorphamine (Purm) and the compounds or DMSO as a control for 48 h. Using primers for *Ptch1* as a Hh target gene and *Gapdh* as a reference gene, qRT-PCR was carried out to retrieve expression levels. Data were normalized to Purmorphamine-DMSO-treated cells and are mean values of biological replicates (n=3) ± SD.

In reporter gene assays, gene expression activity is indirectly measured via luciferase activity. To obtain a direct measure for Hh signaling pathway activity and to further characterize inhibition of Hh signaling, expression of the Hh target gene *Ptch1* was assessed via qRT-PCR (Figure 19B). All compounds showed dose-dependent inhibition of target gene expression with medium to low potency. Compound **1** reduced expression of *Ptch1* to 60 and 25% at 10 and 20 µM, respectively, showing a slightly increased potency compared to the GLI reporter gene assay. Compounds **2** and **3** reduced *Ptch1* expression to 60% at 30 µM, showing reduced potency compared to the GLI reporter gene assay. Compared to the osteoblast differentiation assay, all compounds showed a drastically decreased potency in the GLI reporter gene assay and the evaluation of *Ptch1* expression.

5.1.2 Quinoline, indoline and azepinone derivatives do not target SMO

Since various known Hh inhibitors bind to the membrane protein SMO (2.4.1), a displacement assay was employed to evaluate binding of compounds **1**, **2** and **3** to SMO. BODIPY-labelled Cyclopamine, a known SMO binder that targets the heptahelical bundle inside the transmembrane part of the protein[96], was used as a displacement probe. If the probe is added to SMO-expressing cells, it will bind to SMO and lead to a green fluorescence signal. If a compound is added simultaneously, a decrease in BODIPY-related fluorescence indicates that the compound competes with BODIPY-cyclopamine for binding to SMO and thus can be considered as a SMO binder. The fluorescence signal can either be detected via fluorescence microscopy or flow cytometry. Results obtained with both detection methods are shown in Figure 20.

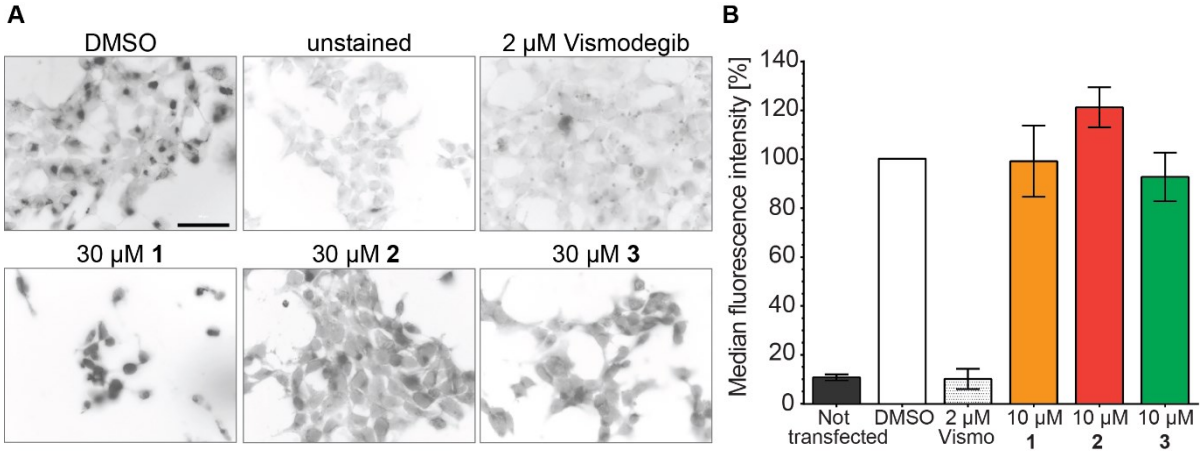

Figure 20. Compounds 1, 2 and 3 do not bind to Smoothened. A. Smo-binding assay using fluorescence microscopy. HEK293-T cells were transfected with a SMO expression construct and, after 48 h, fixed and treated with 5 nM BODIPY-cyclopamine and the compounds or DMSO as a control for 4 h. Cells were then washed and mounted for image acquisition. Images are representative biological replicates (n=2, scale bar: 50 µm). **B.** Smo-binding assay using flow cytometry. HEK293-T cells were transfected as described in A. After 48 h of transfection, cells were treated with 5 nM BODIPY-cyclopamine and the compounds or DMSO as a control for 5 h. Cells were then detached, washed and filtered for flow cytometry. Data were normalized to DMSO-treated cells and are mean values of biological replicates (n=3) ± SD.

In both experimental settings, compounds **1**, **2** and **3** did not displace BODIPY-cyclopamine from SMO. Nevertheless, compound **1** led to reduced cell confluence when used at 30 µM (Figure 20A), which is why a lower concentration of 10 µM was used in the flow cytometry approach (Figure 20B). But even at this slightly toxic concentration of 30 µM, compound **1** did not lead to a decrease in fluorescence which was confirmed by the quantitative approach. Compounds **2** and **3** did not reduce cell confluence but showed a redistribution of

fluorescence in the microscopy images (Figure 20A). Quantification via flow cytometry, however, showed that overall fluorescence intensity did not decrease. These results rather point at a downstream effect on protein localization than a competition for binding to SMO.

Since none of the compounds bound to SMO; their target was still unknown. To identify possible targets, affinity chromatography should be performed to enrich possible protein targets from cell lysates. For this, a structure activity relationship (SAR) study would be necessary to attach a linker and couple the compound to a solid support for the pull-down experiment. For two reasons, this approach was not feasible for this project. On the one hand, the synthesis route, being *de novo* branching cascades, was not designed for SAR-based synthesis and neither suitable derivatives nor established synthesis routes to make them were available. On the other hand, the compounds had a medium to low potency in the GLI reporter gene assay. In many cases, cellular potency decreases with attachment of a bulky linker. Therefore, compounds **1**, **2** or **3** were not considered for a target identification study.

Data presented in this chapter have contributed to the publication "*De novo* branching cascades for structural and functional diversity in small molecules" by Garcia-Castro *et al.*[160].

5.2 A Withanolide A derivative as Hh inhibitor

Withanolides are natural steroids that are mostly isolated from plants like *Withania somnifera*, commonly known as ashwagandha or Indian ginseng, and have been shown to be biologically active in various pathways and physiological processes.[162] According to the principles of biology-oriented synthesis (BIOS), scaffolds that already show biological activity are pre-validated by nature and pose attractive starting point for synthesis of new bioactive small molecules.[163] Due to that, *Dr. Jakub Švenda and Dr. Michael Sheremet synthesized* a compound collection of Withanolide A derivatives[164], which was screened for biological activity in various assays at COMAS. The most active analogue, compound **4** (Figure 21A), inhibited osteogenesis with an IC_{50} of 1.8 ± 0.6 µM. This activity was confirmed in a GLI reporter gene assay with an IC_{50} of 3.2 ± 0.7 µM (Figure 21B).

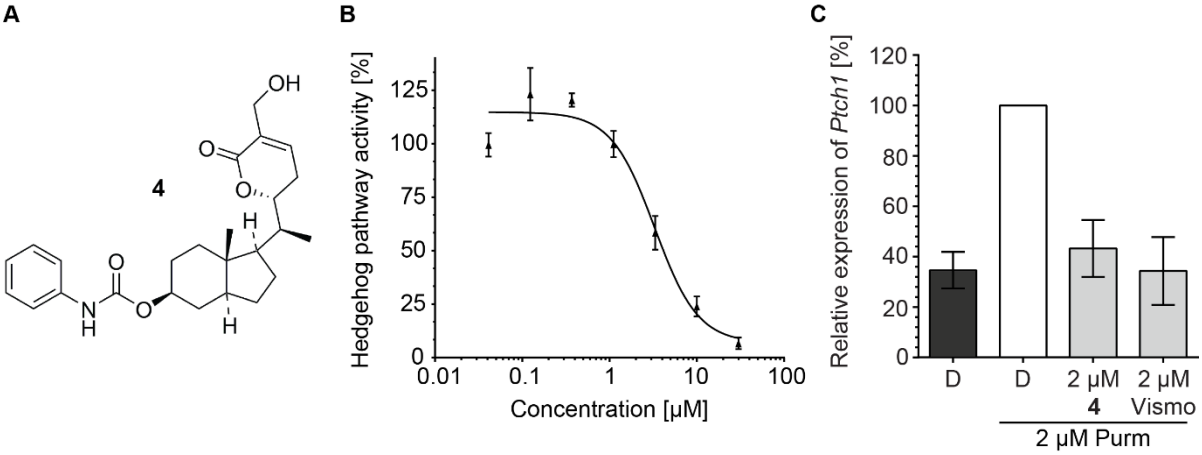

Figure 21. Compound 4 inhibits Hh signaling. A. Structure of compound **4**. **B.** GLI reporter gene assay. Shh-LIGHT2 cells were treated with 2 µM Purmorphamine and the compounds or DMSO as a control for 48 h. The Hh dependent firefly luciferase signal was divided by the control signal of the Renilla luciferase. Data were normalized to Purmorphamine-DMSO-treated cells and are mean values of biological replicates (n=3) ± SD. **C.** Evaluation of target gene expression. NIH/3T3 cells were treated with 2 µM Purmorphamine (Purm) and the compounds or DMSO as a control for 48 h. Using primers for *Ptch1* as a Hh target gene and *Gapdh* as a reference gene, qRT-PCR was carried out to retrieve expression levels. Data were normalized to Purmorphamine-DMSO-treated cells and are mean values of biological replicates (n=3) ± SD (D=DMSO, Vismo=Vismodegib, Purm=Purmorphamine).

To confirm Hh signaling pathway inhibition, the expression of the Hh target gene *Ptch1* was assessed by means of qRT-PCR (Figure 21C). Compound **4** reduced expression of *Ptch1* by 57% at 2 µM, almost to the level of unstimulated cells or cells that were treated with Vismodegib, a known Hh signaling pathway inhibitor and SMO binder.

5.2.1 Withanolide A derivative binds to SMO

As already described in 5.1.2, the membrane protein SMO is a common target of Hh signaling pathway inhibitors. For this, as a first step in compound characterization, binding to SMO was evaluated using the aforementioned BODIPY-cyclopamine displacement assay.

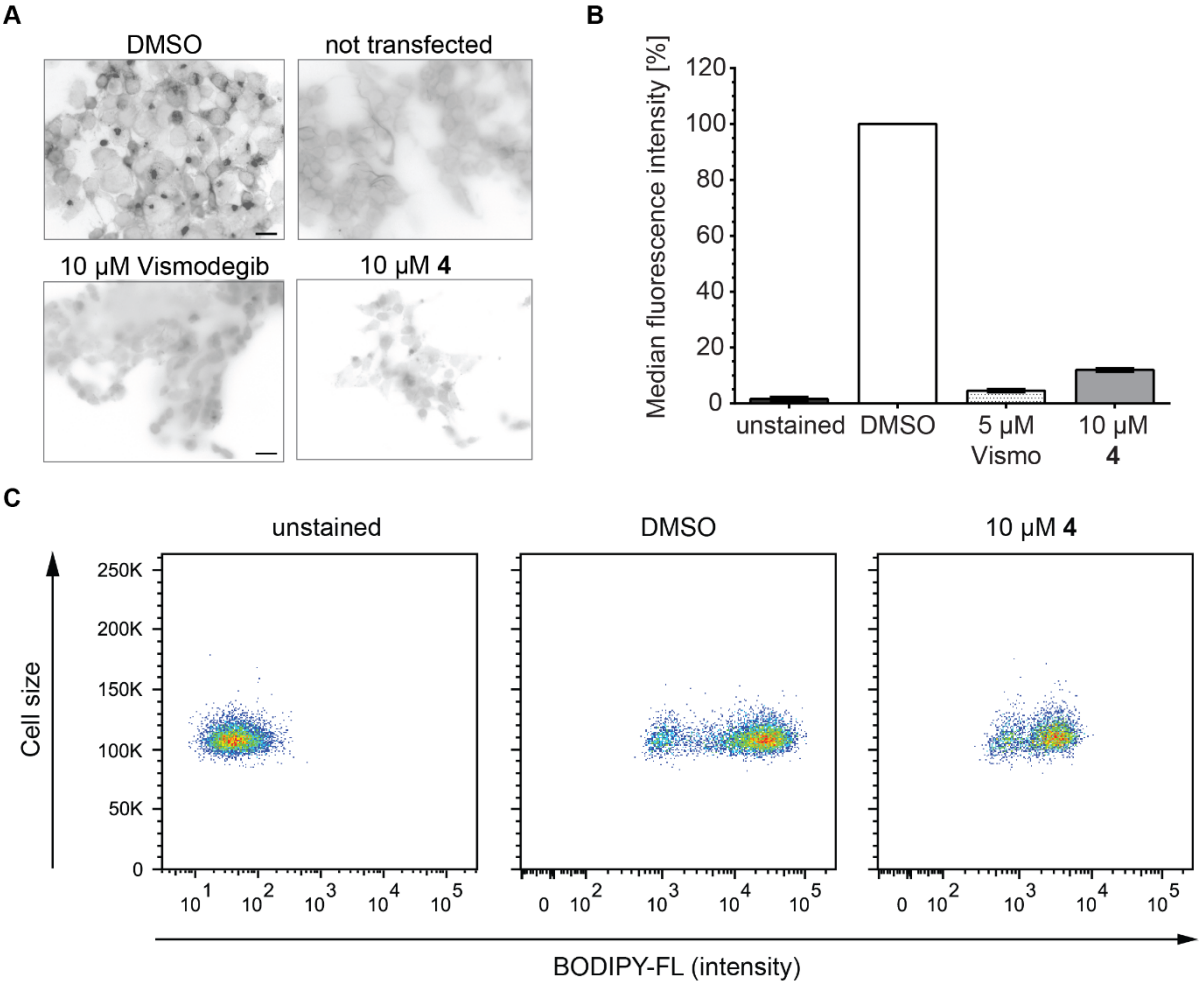

Figure 22. Compound 4 binds to SMO. A. SMO-binding assay detected via fluorescence microscopy. HEK293-T cells were transfected with a SMO expression construct and, after 48 h, fixed and treated with 5 nM BODIPY-cyclopamine and the compounds or DMSO as a control for 4 h. Cells were then washed and mounted for image acquisition. Images are representative of biological replicates (n=3, scale bar: 25 µm). **B.** Smo-binding assay detected via flow cytometry. HEK293-T cells were transfected as described in A. After 48 h of transfection, cells were treated with 5 nM BODIPY-cyclopamine and the compounds or DMSO as a control for 5 h. Cells were then detached, washed and filtered for flow cytometry. Data were normalized to DMSO-treated cells and are mean values of biological replicates (n=3) ± SD, Vismo=Vismodegib. **C.** Intensity histograms underlying the quantification in B. Data are representative of biological replicates (n=3).

Compound **4** efficiently replaced BODIPY-cyclopamine from SMO with a potency comparable to that of Vismodegib (Figure 22A). Quantitative data gained by flow cytometry analysis of BODIPY-cyclopamine related fluorescence confirmed the observations of the fluorescence microscopy experiments (Figure 22B and C). These results suggest that compound **4** binds to the Cyclopamine binding site of SMO, i.e. the heptahelical bundle in the transmembrane (TM) domain[96]. In a further SMO binding assay using ^{3}H-cyclopamine and membrane preparations of a SMO-expressing cell line *performed by SB Drug Discovery*, binding affinity was measured and revealed a K_i of 0.057 ± 0.01 µM for compound **4**.

Data in this chapter have contributed to the publication “Biology-Oriented Synthesis of a Withanolide-Inspired Compound Collection Reveals Novel Modulators of Hedgehog Signaling” by Švenda *et al.*[164]

5.3 A pyrazolo-imidazole derivative as Hh inhibitor

Screening a library of 336,639 compounds for inhibition of osteogenesis at the *Lead Discovery Center (Dortmund)* led to the identification of two potent Hh inhibitors, compound **5**, termed Smoothib and compound **6**, termed Pipinib. This chapter will focus on the pyrazolo-imidazole derivative Smoothib, whereas data on Pipinib will be presented in chapter 5.4. Compound structure and the results of the osteogenesis assay are illustrated in Figure 23. Smoothib was found to be a potent inhibitor of osteogenesis with an IC_{50} of 46 ± 10 nM.

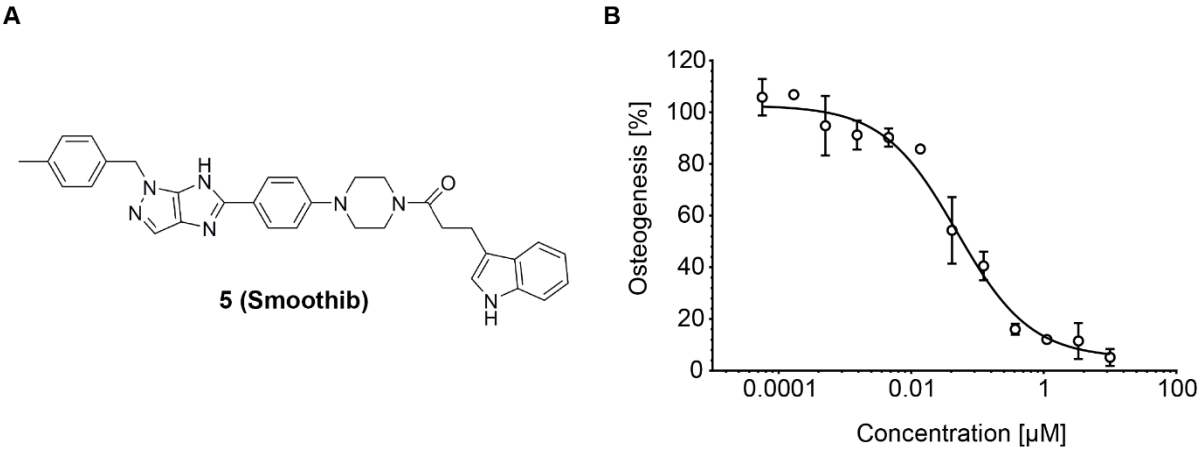

Figure 23. Compound 5 (Smoothib) inhibits osteogenesis. A. Chemical structure of Smoothib. **B.** Osteogenesis assay. C3H10T1/2 cells were treated with 1.5 µM Purmorphamine and various concentrations of the compounds or DMSO as a control for 96 h before measuring alkaline phosphatase activity using the CDP-Star reagent in a luminescent readout. Data were normalized to Purmorphamine- DMSO-treated cells and are mean values of biological replicates (n=3) ± standard deviation (SD).

Similar to the other small molecules that were characterized in this thesis, additional assays were performed to confirm inhibition of Hh signaling (5.3.1).

5.3.1 Confirmation of Hh inhibition

Both GLI reporter gene activity and expression of the *Ptch1* and *Gli1* Hh target genes were evaluated after treatment with Smoothib to confirm inhibition of Hh signaling (Figure 24).

Smoothib dose-dependently inhibited GLI reporter expression in Shh-LIGHT2 cells (Figure 24A). The graph shows all four repetitions of the experiment because the assay-to-assay variability produced single curve progressions that were too distinct to fit them into a mean curve. The mean IC_{50} value of 1.4 ± 1.0 µM, however, shows a reproducibility of compound potency. Additionally, curves obtained when activating the pathway with 0.1 µM Smoothened Agonist (SAG), another Smoothened binder that induces Hh signaling[100], resulted in a mean curve (IC_{50}=2.3 ± 0.1 µM) that lies in the same range as the curves obtained when employing 2 µM Purmorphamine for pathway activation.

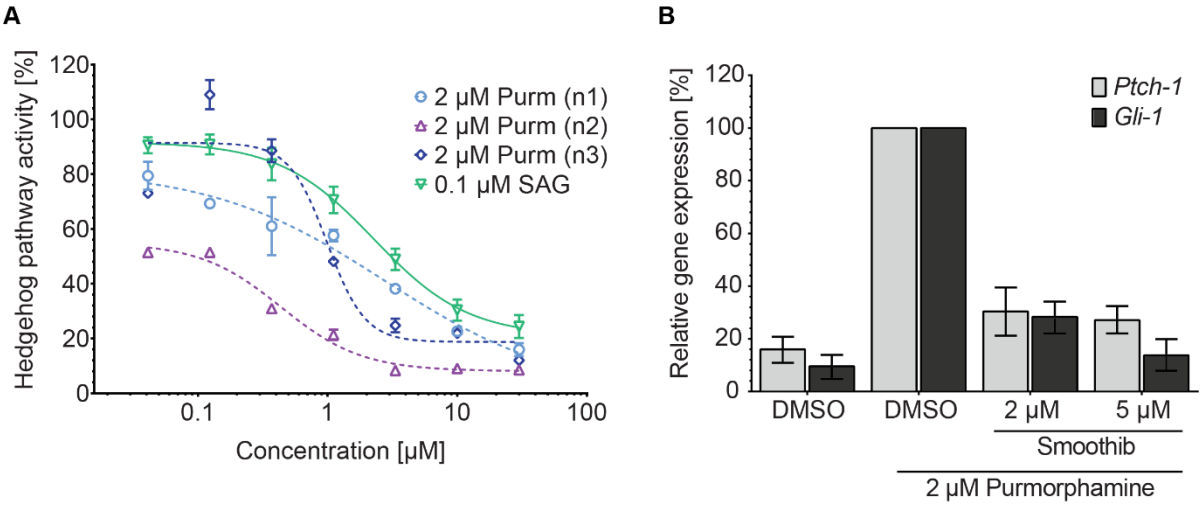

Figure 24. Smoothib is a confirmed Hh signaling inhibitor. A. GLI reporter assay. Shh-LIGHT2 cells were treated with 2 µM Purmorphamine or 0.1 µM SAG and the compound or DMSO as a control for 48 h. The Hh dependent firefly luciferase signal was divided by the control signal of the renilla luciferase and normalized to Purmorphamine- DMSO-treated cells. Curves show three biological repetitions of the experiment (Purmorphamine activation (n=3)), each being mean values of three technical replicates ± SD as well as mean values of biological replicates (n=3) ± SD (SAG activation). **B.** Evaluation of target gene expression. NIH/3T3 cells were treated with 2 µM Purmorphamine and the compounds or DMSO as a control for 48 h. Using primers for *Ptch1* and *Gli1* as Hh target genes and *Gapdh* as a reference gene, qRT-PCR was carried out to retrieve expression levels. Data were normalized to Purmorphamine-DMSO-treated cells and are mean values of biological replicates (n=3) ± SD.

Evaluation of target gene expression confirmed all preceding experiments. Also here, expression of Hh target genes *Gli1* and *Ptch1* was inhibited to approx. 65 and 70% following treatment with 2 and 5 µM Smoothib (Figure 24B). Taken together, Smoothib can be considered as a verified inhibitor of Hh signaling.

5.3.2 Smoothib binds to SMO and inhibits its ciliary entry

To retrieve an initial hint for a possible target of Smoothib, *computational target prediction was carried out by Prof. Gisbert Schneider and his coworkers at the ETH Zürich* using the SPiDER software[155]. This software compares the structure of the query compound to other drugs with known targets (COBRA database of bioactive compounds)[156] and thereby delineates possible targets of the query compound based on structure similarity. Here, SMO was identified with the highest confidence (p<0.001) as possible target of Smoothib. To validate this target hypothesis, the Smoothened displacement assay, described in 5.1.2, was performed (Figure 25). The immunofluorescence images are depicted in Figure 25A. Smoothib led to an almost complete reduction of BODIPY-cyclopamine fluorescence at a concentration of 30 µM. Quantification via flow cytometry confirmed a dose dependent reduction of fluorescence with an approximate EC_{50} of 12.7 ± 0.8 µM (Figure 25B). These results lead to the conclusion that Smoothib binds to the Cyclopamine binding site of SMO. To find further proof that Smoothib is a SMO antagonist, SAG, the aforementioned SMO agonist (K_i (SMO binding) = 8.4 nM, EC_{50} (osteogenesis) = 3 nM))[100,165], was co-administered with Smoothib at an excess, i.e., 1 µM (in comparison to 0.1 µM "optimal activation")[100] in the GLI reporter assay (Figure 25C). If Smoothib binds to the heptahelical bundle of SMO, both compounds will compete for binding to the receptor. This would result in a shift of the curve to the right and an increase of the IC_{50} value because higher concentrations of Smoothib will be required to achieve inhibition. Indeed, in the presence of an excess of SAG, Smoothib titration led to a shallower curve that was not completed at 30 µM, in contrast to cells treated with 0.1 µM SAG. Since the curve at 1 µM SAG is not complete, it is not possible to calculate the IC_{50} value. However, one can estimate, that this value is greater than 10 µM. Compared to the IC_{50} value obtained when employing 0.1 µM SAG (2.3 ± 0.1 µM), a drastic decrease of compound potency is observed, referring to a competition for binding to SMO. Added verification was achieved in a proliferation assay, *carried out by Exiris Srl*, which uses cells derived from medulloblastoma of postnatally irradiated *Ptch*$^{+/-}$ mice. As these cells express only one copy of PTC, the Hh signaling pathway is constitutively active and addition of a pathway activator is not necessary to induce signaling. Smoothib alone efficiently inhibited cell growth with an IC_{50} value of 81.7 ± 14.7 nM (Figure 25D). Also in these cells, addition of the SMO binder SAG, even though it is not required for pathway activation, lead to a 15-fold decrease of compound potency (1.2 ± 0.1 µM), validating that Smoothib binds to SMO. Similar to compound **4**, SMO binding was also confirmed for Smoothib in a binding assay using ^{3}H-cyclopamine and membrane preparations of a SMO-expressing cell line that was

performed by SB Drug Discovery. Measurement of the binding affinity revealed a K_i of 202 nM.

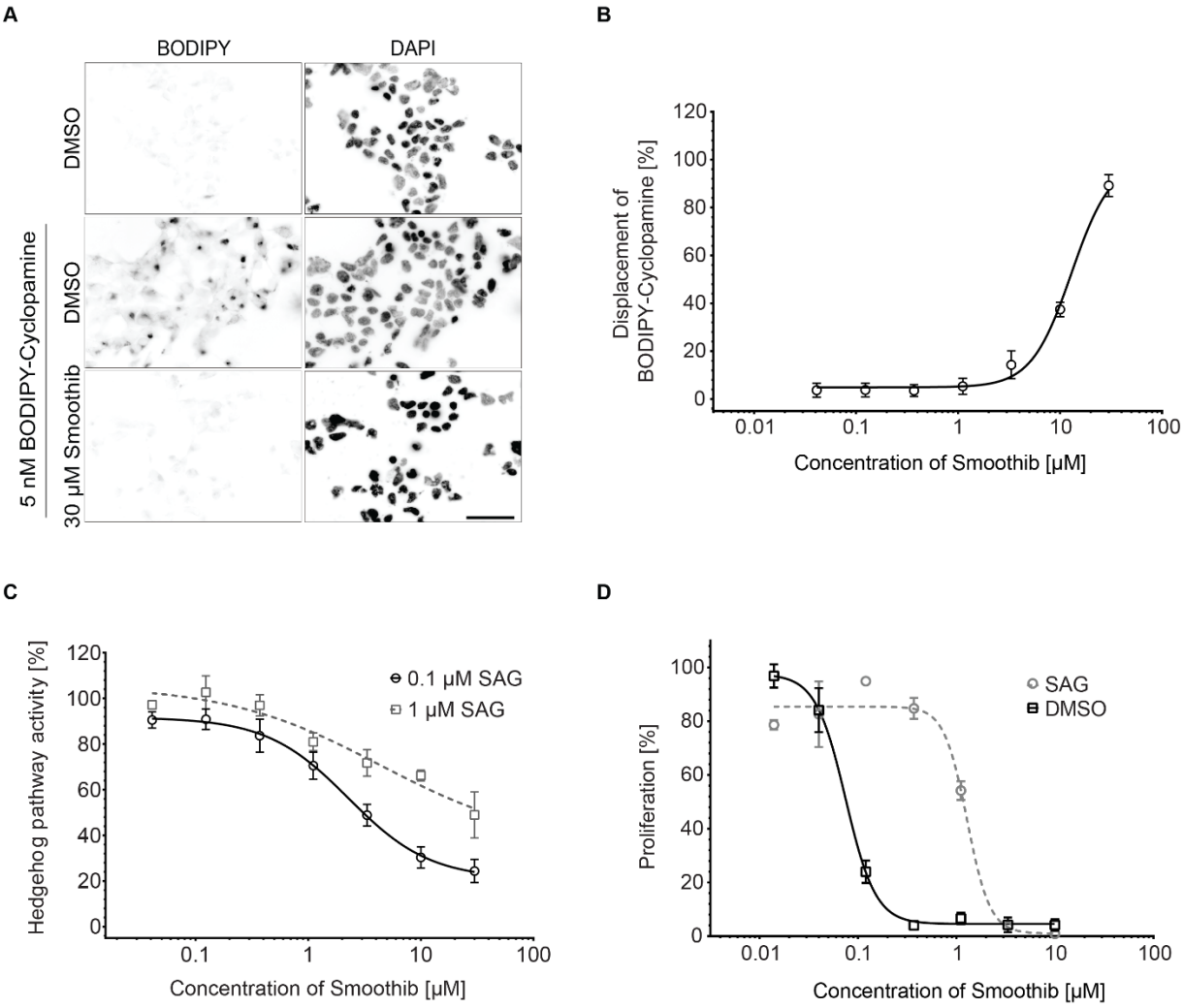

Figure 25. Smoothib binds to SMO. A. SMO-binding assay detected via fluorescence microscopy. HEK293-T cells were transfected with a SMO expression construct and, after 48 h, fixed and treated with 5 nM BODIPY-cyclopamine and the compound or DMSO as a control for 4 h. Cells were then treated with DAPI, washed and mounted for image acquisition. Images are representative of biological replicates (n=3, scale bar: 50 µm). **B.** SMO-binding assay detected via flow cytometry. HEK293-T cells were transfected as described in A. After 48 h of transfection, cells were treated with 5 nM BODIPY-cyclopamine and the compound or DMSO as a control for 5 h. Cells were then detached, washed and filtered for flow cytometry. Data are mean values of biological replicates (n=3) ± SD. **C.** SAG competition assay. Shh-LIGHT2 cells were treated with 0.1 and 1 µM SAG and the compound or DMSO as a control for 48 h. The Hh dependent firefly luciferase signal was divided by the control signal of the renilla luciferase and normalized to SAG-DMSO-treated cells. Data are mean values of biological replicates (n=3) ± SD. **D.** *Ptch*$^{+/-}$ medulloblastoma proliferation assay. *Ptch*$^{+/-}$ cells were treated with 0.3 µM SAG or DMSO and the compounds or DMSO as a control for 72 h. BrdU was added for another 24 h to stain viable cells which were determined by means of the Cell Proliferation ELISA BrdU chemiluminescent assay. Data were normalized to DMSO-treated cells and are mean values of biological replicates (n=3) ± SD.

In some cases, interaction of a small molecule with SMO impairs the receptor's migration to the primary cilium. To investigate whether this is also true for Smoothib, intracellular localization of SMO was monitored via immunofluorescence (Figure 26). Using antibodies against the ciliary marker acetylated tubulin and against SMO, it was possible to track the presence of SMO in the primary cilium after treatment with 2 µM Purmorphamine. Simultaneous application of 2 µM Smoothib reverted this phenotype, pointing out that Smoothib, like Vismodegib, impairs ciliary trafficking of SMO (Figure 26A). The visual impression was verified via quantification of the pixel intensity of SMO inside the cilia. Here, Pipinib led to a significant decrease of ciliary SMO intensity that corresponds to the intensity of non-activated cells (Figure 26B).

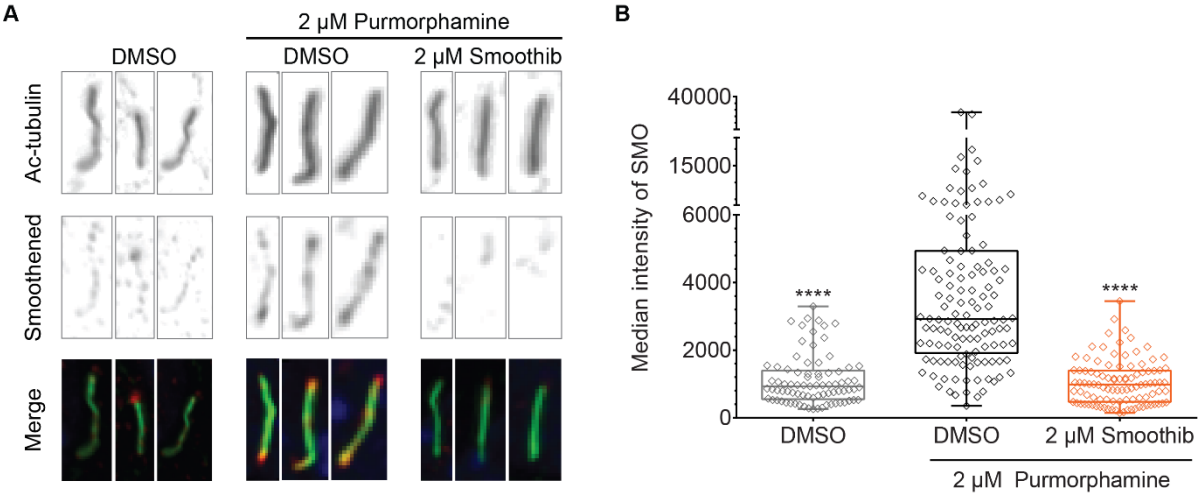

Figure 26. Smoothib inhibits ciliary trafficking of SMO. A. Smoothened trafficking assay. NIH/3T3 cells were treated with 2 µM Purmorphamine and Smoothib or DMSO as a control for 24 h in assay medium to induce simultaneous ciliation. Cells were then fixed, permeabilized, blocked and incubated with antibodies against acetylated tubulin (ac-tubulin) and SMO as well as DAPI to visualize the nucleus. Representative images of independent experiments (n=3) are shown. **B.** Quantification of SMO ciliary intensity. More than 100 cilia were quantified using the software ImageJ. For this, each cilium was marked according to the ac-tubulin stain and the pixel intensity of SMO was quantified. Data are shown as median intensity throughout the cilium; each dot represents a single cilium. The plot is representative of independent experiments (n=3). Statistical significance was assessed using an unpaired t-test with a confidence level of 95% (****: $p<0.0001$).

To assess the binding mode of Smoothib, *Dr. Carsten Schultz-Fademrecht from the Lead Discovery Center, Dortmund,* performed a molecular docking study using Glide as part of the Schrödinger suite. Figure 27 shows the obtained binding position.

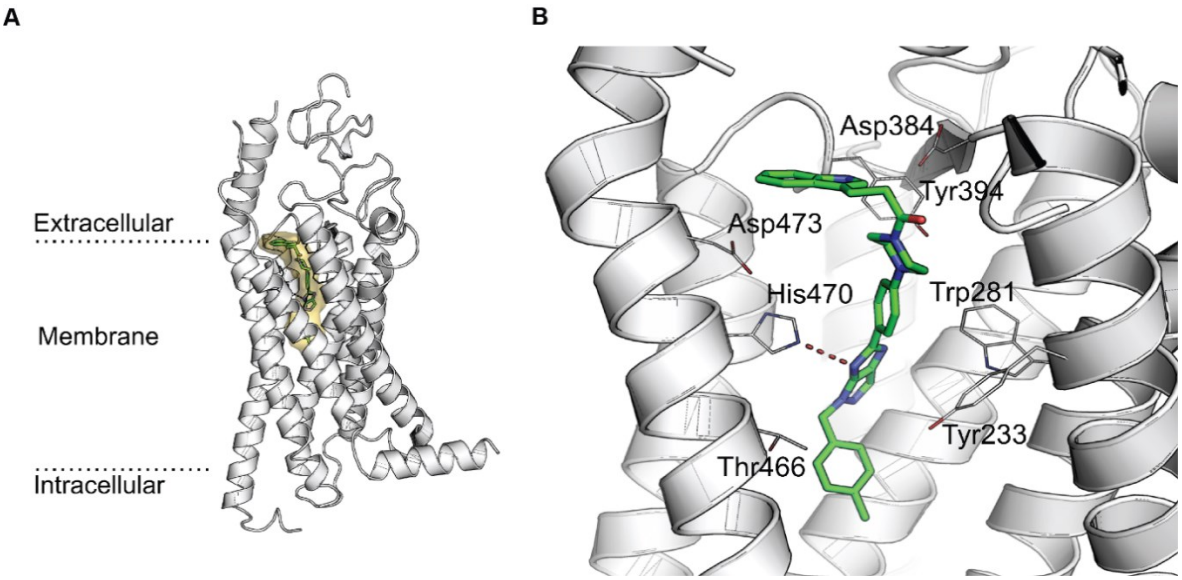

Figure 27. Smoothib binds to the heptahelical bundle of SMO – docking-based putative binding mode. A. Overview image of the binding region of Smoothib. The SMO receptor structures that was obtained in complex with SANT-1 (PDB: 4N4W) was used. **B.** Zoom-in on the binding site.

The best position was retrieved in a docking model based on the X-ray structure of SMO in complex with SANT-1[100] (PDB: 4N4W) with a glide xp gscore of -10.003. Smoothib delves deep into the cavity of Smoothened's heptahelical domain, in a similar way to SANT-1 (Figure 27A). A hydrogen bond between H470 and the nitrogen atom of the pyrazolo-imidazole moiety of Smoothib could be identified. This binding mode suggests that Smoothib forms π-π stacking interactions with Trp281, Phe391, and His470 (Figure 27B).[154]

Data in this chapter have contributed to the publication "Discovery of a Novel Inhibitor of the Hedgehog Signaling Pathway through Cell-based Compound Discovery and Target Prediction" by Kremer *et al.*[154].

5.4 A thienopyrimidine derivative as Hh inhibitor

As already described in 5.3, screening a library of 336,639 compounds for inhibition of osteogenesis at the *Lead Discovery Center, Dortmund*, led to the identification of two potent Hh inhibitors, compound **5**, termed Smoothib and compound **6**, termed Pipinib. Smoothib was introduced in chapter 5.3. This chapter will focus on the thienopyrimidine derivative Pipinib. Compound structure and the results of the osteogenesis assay are illustrated in Figure 28. Pipinib (Figure 28A) was found to be a potent inhibitor of osteogenesis with an IC_{50} of 0.6 ± 0.3 µM (Figure 28B).

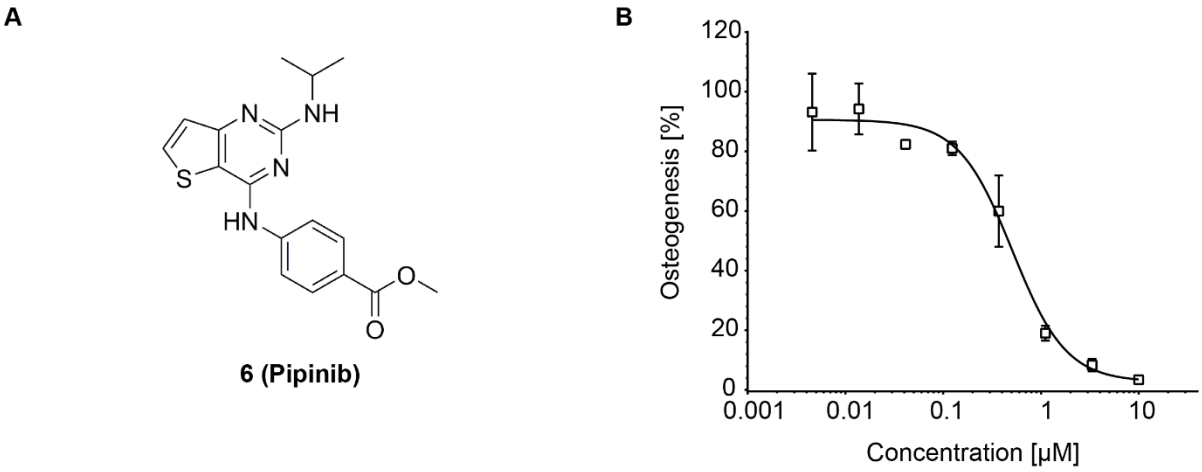

Figure 28. Compound 6 (Pipinib) is an inhibitor of osteogenesis. A. Chemical Structure of compound **6**. **B.** Osteogenesis assay. C3H10T1/2 cells were treated with 1.5 µM Purmorphamine and various concentrations of the compound or DMSO as a control for 96 h before measuring alkaline phosphatase activity using the CDP-Star reagent in a luminescent readout. Data were normalized to Purmorphamine-DMSO-treated cells and are mean values of biological replicates (n=3) ± SD.

Similar to all other osteogenesis hits presented in this thesis, also Pipinib had to be confirmed as a Hh inhibitor using orthogonal assays (5.4.1).

5.4.1 Confirmation of Hh inhibition

To confirm inhibition of Hh signaling, a GLI reporter gene assay was performed and expression of the Hh target genes *Ptch1* and *Gli1* was evaluated. GLI reporter activity was inhibited with an IC_{50} value of 1.7 ± 0.1 µM (Figure 29A). Already a concentration of 5 µM was sufficient to inhibit expression of *Ptch1* and *Gli1* to 24 and 16%, respectively (Figure 29B). An increase of the concentration of Pipinib to 10 µM reduced the expression of both Hh target genes even further, showing a dose-dependent effect. When titrating Pipinib, this dose dependent effect was confirmed and IC_{50} values of 3.1 ± 0.9 µM and 4.1 ± 1.6 µM were obtained for *Ptch1* and *Gli1*, respectively (Figure 29C). These results validate Pipinib as an inhibitor of Hh signaling. To further characterize pathway inhibition, levels and length of the GLI3 transcription factor were monitored via immunoblotting.

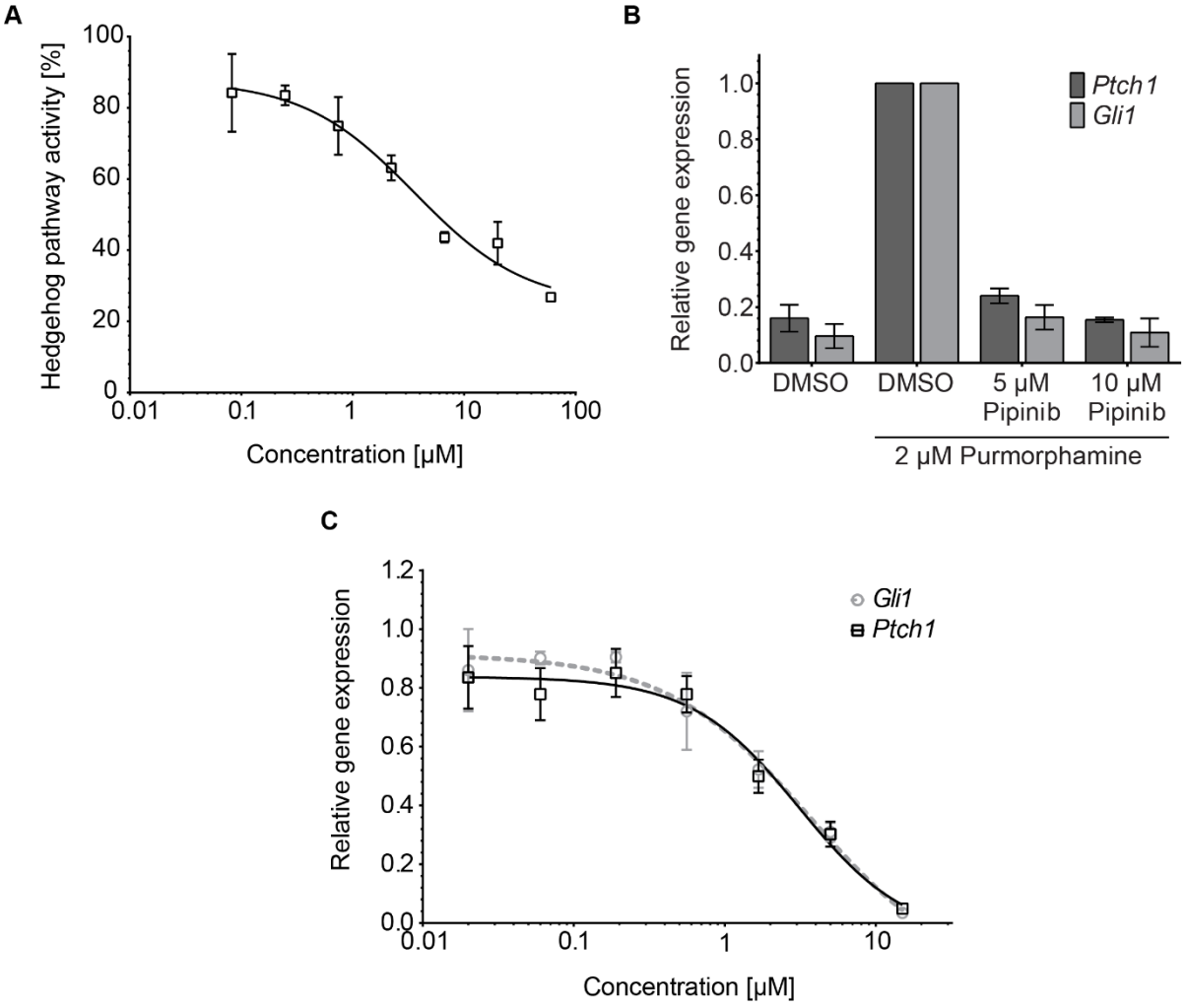

Figure 29. Pipinib inhibits Hh signaling pathway. A. GLI reporter assay. Shh-LIGHT2 cells were treated with 2 µM Purmorphamine and the compound or DMSO as a control for 48 h. The Hh dependent firefly luciferase signal was divided by the control signal of the renilla luciferase and normalized to Purmorphamine-DMSO-treated cells. Data are mean values of independent experiments (n=3) ± SD. **B.** Evaluation of target gene expression. NIH/3T3 cells were treated with 2 µM Purmorphamine and the compounds or DMSO as a control for 48 h. Using primers for *Ptch1* and *Gli1* as Hh target genes and *Gapdh* as a reference gene, qRT-PCR was carried out to retrieve expression levels. Data were normalized to Purmorphamine-DMSO-treated cells and are mean values of biological replicates (n=3) ± SD. **C.** Evaluation of target gene expression applying a titration of Pipinib. Experiments were carried out as described in C. Data were normalized to Purmorphamine-DMSO-treated cells and are mean values of biological replicates (n=3) ± SD.

As detailed in 2.2.1, the GLI2 and GLI3 transcription factors are proteolytically processed if the Hh signaling pathway is inactive. In this case, GLI2 and GLI3 are phosphorylated by protein kinase A (PKA), casein kinase 1 (CK1) and glycogen synthase kinase 3β (GSK3β)[15]. Phosphorylation targets the transcription factors for proteolytic processing resulting in a truncated repressor version (85 kDa)[129]. Due to that, the abundance of the full-length activator (GLI3-F) and the truncated repressor version of GLI3 (GLI3-R) are a protein level measure for Hh signaling activity. An increased level of the repressor version points towards an

inhibited or inactive pathway, whereas a decrease of GLI3-R abundance hints at pathway activation.

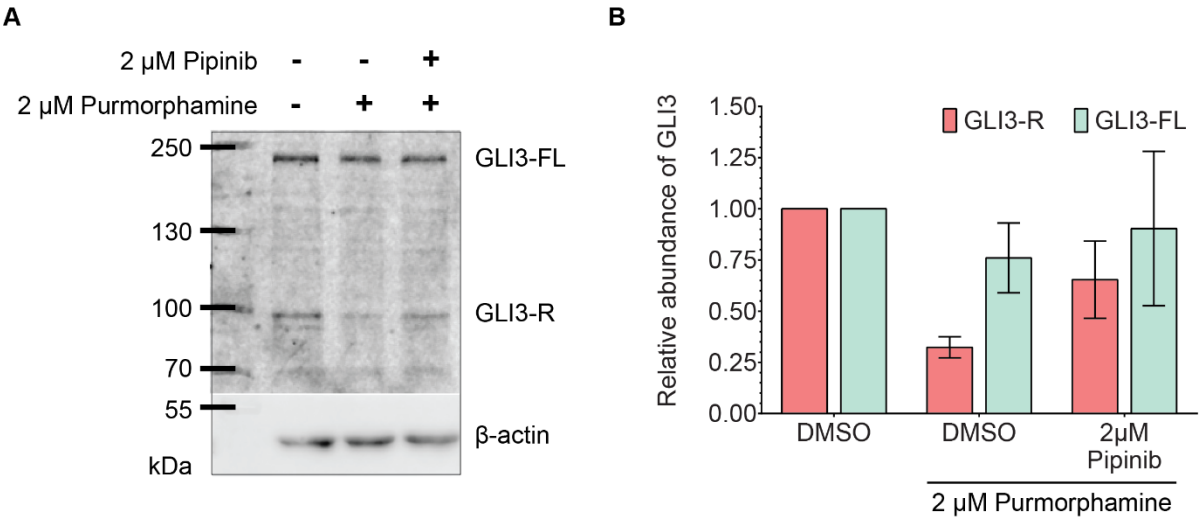

Figure 30. Pipinib increases protein levels of GLI3-R. A. Evaluation of GLI3 protein levels. NIH/3T3 cells were serum starved for 8 h and treated with 2 µM Purmorphamine and 2 µM Pipinib or DMSO as a control for 16 h. Cells were lysed, proteins were separated via SDS-PAGE, transferred onto a PVDF membrane, which was then blocked and stained with antibodies against GLI3 and β-actin as a loading control. The depicted blot is representative of independent experiments (n=3). **B.** Quantification of protein bands from A and two further blots. Bands were quantified using the Image studio software (Li-COR Biosciences). The band intensity of the GLI3 repressor (GLI3-R) or the full-length version of GLI3 (GLI3-FL) was normalized to the respective β-actin band and the respective DMSO sample was set to 1. Data are mean values of independent experiments (n=3) ± SD.

As expected, treatment with 2 µM Purmorphamine led to a decrease of GLI3-R levels (Figure 30A, quantification in Figure 30B). Co-treatment with 2 µM Pipinib reverted this phenotype and led to an increase of GLI3-R, confirming pathway inhibition by Pipinib on the protein level. The band intensity of GLI3-F drops slightly with pathway activation and increases weakly with inhibition (Figure 30A, quantification in Figure 30B).

5.4.2 Pipinib does not target SMO

As part of the compound characterization, it was investigated whether Pipinib binds to SMO. Even at a concentration of 20 µM, Pipinib was not able to displace BODIPY-cyclopamine from SMO (Figure 31A).

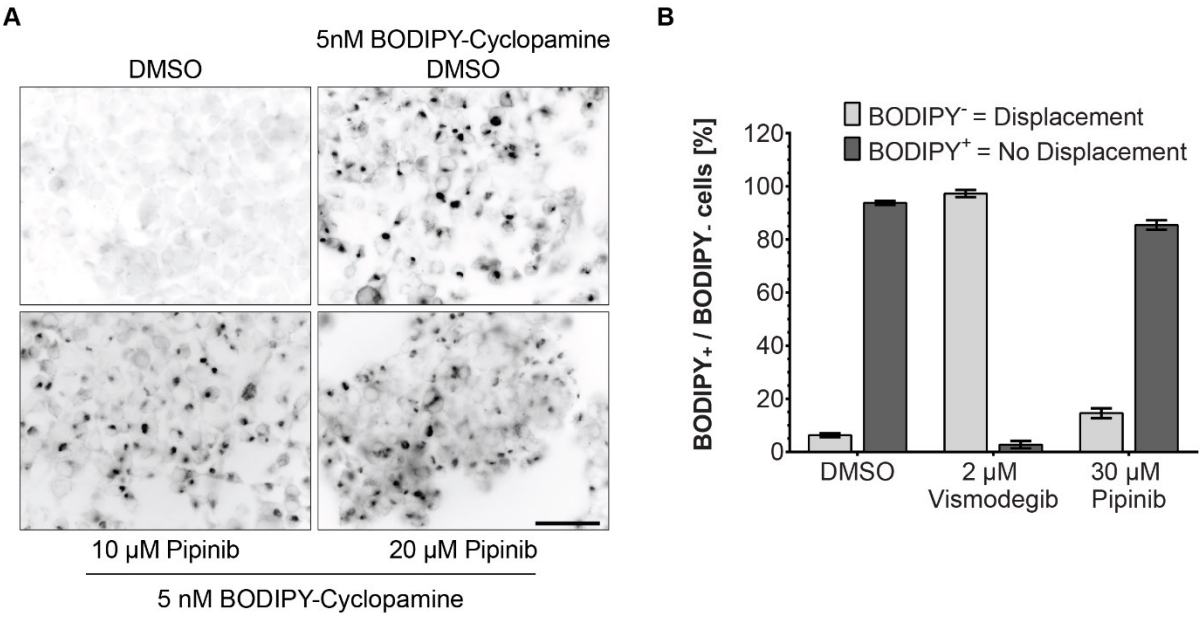

Figure 31. Pipinib does not bind to the Cyclopamine binding site of SMO. A. SMO-binding assay detected via fluorescence microscopy. HEK293-T cells were transfected with a SMO expression construct and, after 48 h, fixed and treated with 5 nM BODIPY-cyclopamine and the compound or DMSO as a control for 4 h at RT. Cells were then washed and mounted for image acquisition. Images are representative of biological replicates (n=3, scale bar: 50 µm). **B.** SMO-binding assay detected via flow cytometry. HEK293-T cells were transfected as described in A. After 48 h of transfection, cells were treated with 5 nM BODIPY-cyclopamine and the compounds or DMSO as a control for 5 h. Cells were then detached, washed and filtered for flow cytometry. Data are mean values of biological replicates (n=3) ± SD.

Also quantification of BODIPY-related fluorescence by means of flow cytometry revealed that Pipinib did not displace BODIPY-cyclopamine, whereas Vismodegib led to an almost complete displacement (Figure 31B). Based on these experiments, it can be concluded that Pipinib does not bind to the Cyclopamine binding site of Smoothened.

5.4.3 Pipinib is a kinase inhibitor and inhibits PI4KB

Being a potent inhibitor of Hh signaling that does not bind to the Cyclopamine binding site of SMO, Pipinib is appropriate for a target identification project. There are plenty of approaches and strategies to identify the target of a small molecule, e.g. computational target prediction, affinity chromatography or drug resistance sequencing[6]. In the case of Pipinib, a scan of the compound scaffold already gave a first hint: The structure contains three nitrogen atoms (Figure 32A) that are well suitable to build hydrogen bonds with the typical hinge region of protein kinases (Figure 32B).[166]

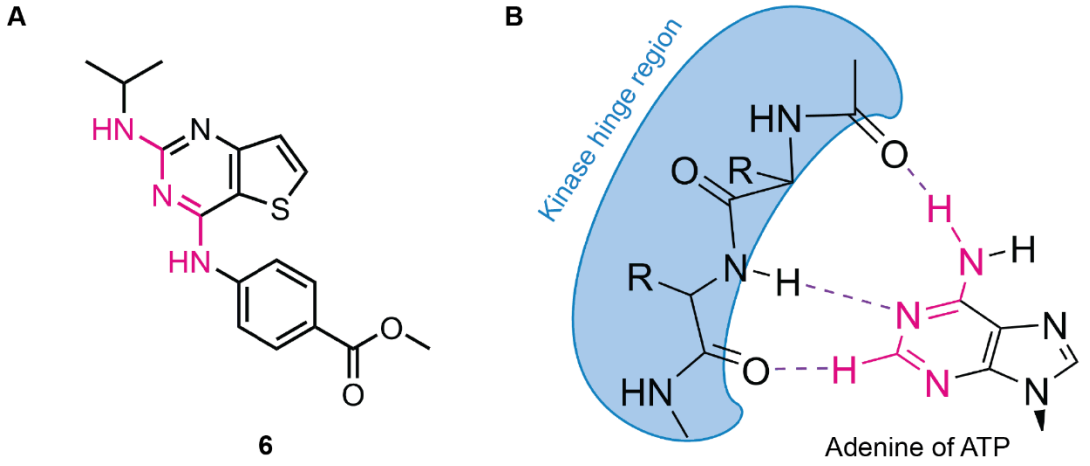

Figure 32. Typical kinase inhibitors and Pipinib. A. Chemical structure of Pipinib (compound **6**). The possible hinge region interacting residues are highlighted in pink. **B.** Typical hinge region of protein kinases (blue) and the structure of adenine from adenosine triphosphate (ATP). The interacting residues are highlighted in pink.

Since its structure suggested that Pipinib might bind to kinases, the evaluation of kinase inhibition was chosen as the first step to identify the target of Pipinib.

5.4.3.1 Kinase panel results – nine hits

A panel of 456 kinases was screened for Pipinib-mediated inhibition or binding at SelectScreen™ (Thermo Fisher Scientific). Pipinib was tested at a concentration of 10 µM and was found to inhibit nine kinases that were inhibited to more than 50% (Table 3).

Table 3. Kinase panel hits (inhibition of enzymatic activity (i)/or tracer displacement (d, binding assay) > 50 %). Assays were performed at SelectScreen™, Thermo Fisher Scientific, employing a compound concentration of 10 µM. The results of the whole panel can be reviewed in the appendix (12.2).

Kinase	inhibition/displacement [%]
Phosphatidylinositol 4-kinase IIIβ (PI4KB)	76 ± 2 (i)
Cyclin G associated kinase (GAK)	73 ± 1 (d)
Ttk protein kinase (TTK)	69 ± 3 (i)
Mitogen-activated protein kinase 8 (MAPK8 (JNK1))	65 ± 2 (d)
Phosphatidylinositol 4-phosphate 5-kinasae type 1γ (PIP5K1C)	56 ± 0 (i)
Myosin light chain kinase family member 4 (MYLK4)	53 ± 1 (d)
Phosphatidylinositol-4-phosphate 3-kinase catalytic subunit type 2γ (PIK3C2G)	53 ± 3 (i)
G protein-coupled receptor kinase 7 (GRK7)	53 ± 3 (i)
NUAK family SNF1-like kinase 1 (NUAK1)	51 ± 2 (i)

Since all experiments for Hh inhibition were carried out in mouse cells, GRK7 was excluded as a Hh relevant target because it is not expressed in this organism.[167] For MAPK8 and MYLK4, only binding of a tracer, which is based on an ATP-competitive kinase inhibitor, was found to be affected. To investigate, whether the kinases were inhibited as well, the enzymatic activity was measured in the presence of 10 µM Pipinib (Table 4).

Table 4. Further kinase activity measurements to assess inhibition. Biochemical kinase assays were performed at SelectScreen™ (MAPK8) and Reaction Biology (MYLK4).

Kinase	Inhibition [%]
Mitogen-activated protein kinase 8 (MAPK8 (JNK1))	8 ± 4
Myosin light chain kinase family member 4 (MYLK4)	41.5 ± 0.1

For the remaining kinases, IC_{50} values were obtained. For PI4KB, an IC_{50} value of 2.2 ± 0.8 µM was measured (Figure 33A). Since three other PI-4 kinases (PI4KA, PI4K2A, and PI4K2B) are also expressed in cells and catalyze the same reaction, the production of PI4P, the activity of these kinases was also measured in presence of Pipinib. No activity was observed against the other PI4 kinases (Figure 33A). In general, Pipinib was fairly selective against all tested lipid kinases (Table 5).

Table 5. Tested lipid kinases. Assays were performed at SelectScreen™, Thermo Fisher Scientific, employing a compound concentration of 10 µM. All measurements in this table have been made in the adapta activity assay.

Kinase	mean inhibition [%]	SD
PI4K2A (PI4K2 alpha)	11	1
PI4K2B (PI4K2 beta)	-2	2
PI4KA (PI4K alpha)	-8	1
PI4KB (PI4K beta)	76	2
PIK3C2A (PI3K-C2 alpha)	12	2
PIK3C2B (PI3K-C2 beta)	10	4
PIK3C2G (PI3K-C2 gamma)	53	3
PIK3C3 (hVPS34)	25	5
PIK3CA E545K/PIK3R1 (p110 alpha E545K/p85 alpha)	10	1
PIK3CA/PIK3R1 (p110 alpha/p85 alpha)	-15	4
PIK3CA/PIK3R3 (p110 alpha/p55 gamma)	1	7
PIK3CB/PIK3R1 (p110 beta/p85 alpha)	8	0

Kinase	mean inhibition [%]	SD
PIK3CB/PIK3R2 (p110 beta/p85 beta)	5	6
PIK3CD/PIK3R1 (p110 delta/p85 alpha)	-2	1
PIK3CG (p110 gamma)	23	4
PIP5K1C	56	0

For PIP5K1C and PIK3C2G, compound titration revealed IC_{50} values of 4.1 ± 0.9 µM and 3.5 ± 0.7 µM, respectively (Figure 33B). GAK was the only kinase for which no activity assay was available. Thus, the displacement of a tracer, which is based on an ATP-competitive kinase inhibitor, was measured (Figure 33C) and an EC_{50} value of 0.8 ± 0.2 µM was obtained.

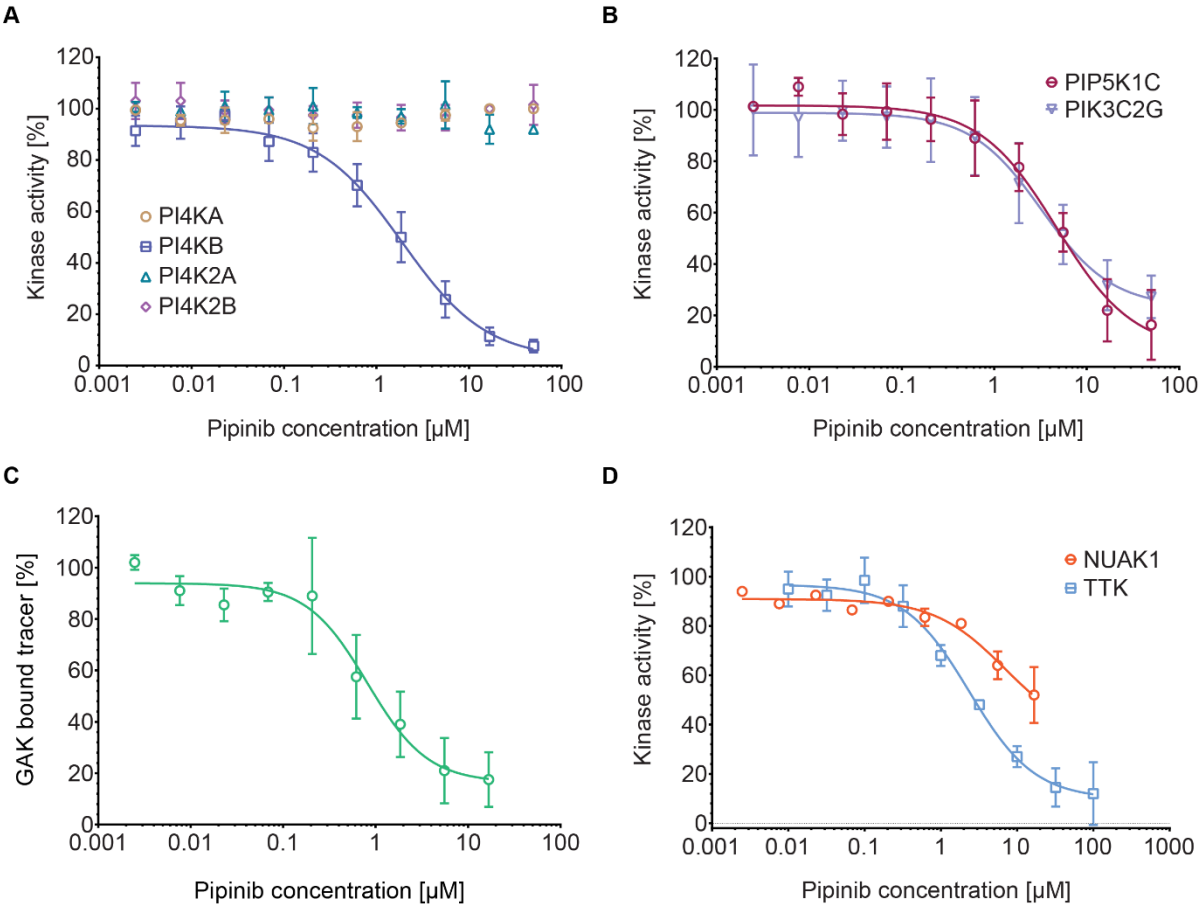

Figure 33. Titration of Pipinib against kinase activity/tracer binding for the kinase panel hits. All measurements were performed by SelectScreen™. **A.** Adapta activity assay for inhibition of PI4KB (n=5) and for other PI-4 kinases (n=2, all at ATP Km). **B.** Adapta activity assay for inhibition of PIP5K1C (n=3) and PIK3C2G (n=4, both at 10 µM ATP). **C.** Pipinib was measured in the Lantha FRET-based displacement assay (SelectScreen™) that assesses binding to GAK (n=2). **D.** Pipinib was measured in the Z'Lyte kinase activity assay (SelectScreen™) that monitors the conversion of a synthetic peptide substrate in a FRET-based manner against NUAK1 (n=1). To measure TTK activity, a radiometric kinase assay (Eurofins) was performed employing 45 µM γ-[^{32}P]-ATP (n=2). All data are mean values ± SD.

For inhibition of TTK activity an IC_{50} value of 2.5 ± 0.7 µM was obtained, whereas for NUAK1, no IC_{50} value could be calculated due to an incomplete curve (Figure 33D). It can be estimated that the approximate IC_{50} value is greater than 16.7 µM, the highest measured concentration. Since Pipinib was not as active against NUAK1 as expected from the panel results, it was excluded as a relevant cellular target. When performing a literature search on the five remaining potential targets, it was found that the *Drosophila* homologue of PI4KA (Sst4) is relevant for the membrane localization of SMO in *Drosophila* and that knockdown of mammalian PI4KA and PI4KB in mouse Shh-LIGHT2 cells led to reduced GLI reporter gene expression.[50] As PI4KB was the only kinase with a known connection to Hh signaling, this kinase was chosen for further characterization.

To investigate how Pipinib mediates inhibition of PI4KB, kinetic measurements were performed at SignalChem wherein four different concentrations of Pipinib were titrated against six different concentrations of ATP within a kinase activity assay for PI4KB. The consumption of ATP by PI4KB was assessed using ^{33}P-ATP in combination with an ADP-Glo assay. Using standard ATP conversion curves, ATP consumption was converted to ATP conversion rate and used to calculate the velocity (pmol phosphate transferred per liter per second) at different compound and ATP concentrations; tables containing all underlying raw data can be found in the appendix (12.3)). Using Michaelis-Menten kinetics, saturation curves were plotted to calculate K_m, V_{max} and K_i (Figure 34A). Thereby, a K_i value of 10.2 ± 2.3 µM was obtained. In order to derive a mode of inhibition from this data, the change of V_{max} and K_m dependent on compound concentration was monitored. The comparison of these variables gives information about whether an enzyme is inhibited competitively, i.e. competing with the substrate for binding to the catalytic center, non-competitively, i.e. substrate-independent enzyme inhibition, or uncompetitively, i.e. inhibition only occurs if the enzyme has bound its substrate.[168,169] If both K_m and V_{max} of the PI4KB enzyme reaction are plotted against the concentration of Pipinib, an increase of both parameters can be observed (Figure 34B). However, V_{max} shows a high standard deviation for a compound concentration of 10 µM. If this data point is excluded, V_{max} only shows a minor decrease. An increase of K_m while V_{max} is largely unchanged, fits to the behavior of a competitive enzyme inhibitor. This observation is supported by the Lineweaver Burk plot. Originally, this technique was applied to calculate V_{max} and K_m, before non-linear regression was applicable. For a competitive inhibitor, the regression lines of control and inhibitor are expected to intersect at the Y-axis. This can be observed for Pipinib in Figure 34C. The zoom-in (Figure 34D) shows that not all regression lines intersect in one point at the Y-axis. In fact, all curves except the 50 µM curve intercept close to the y-axis on its right-hand side. The 50 µM curve intersects the DMSO curve close

to the y-axis on its left-hand side. A non-competitive inhibitor, however, would lead to an intersection on the left-hand-side the X-axis and an uncompetitive inhibitor would produce parallel lines. Considering both visualization methods (Figure 34B and D), a competitive mode of inhibition is most likely.

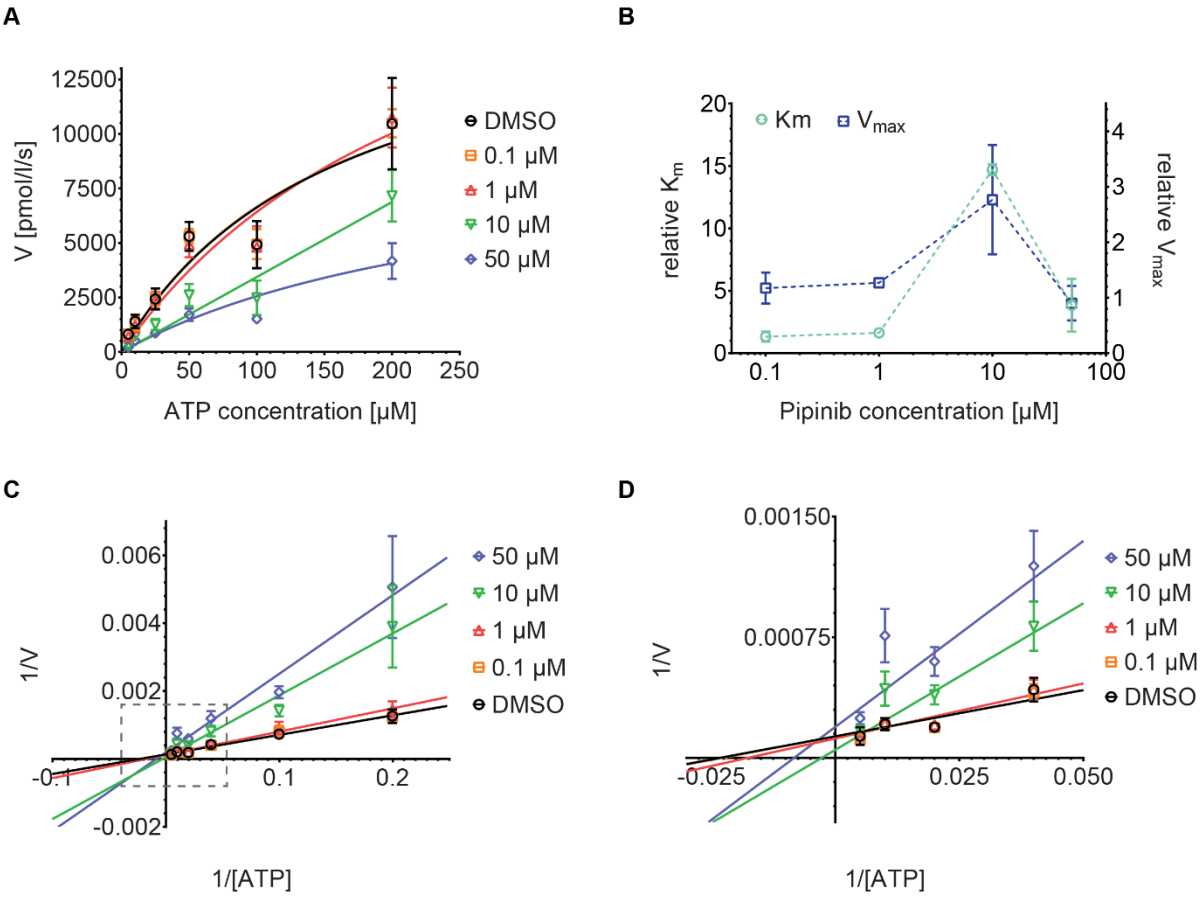

Figure 34. Kinetic measurements for determination of the mode of PI4KB inhibition. A. Michaelis-Menten kinetics. ATP consumption by PI4KB was measured at six different ATP and four different Pipinib concentrations. The reaction velocity (pmol phosphate transferred per liter per second) was plotted against the ATP concentration creating a curve for each applied compound concentration. Data are mean values of independent experiments (n=3) ± SD. **B.** Variation of V_m and K_{max} for different concentrations of Pipinib. Data are mean values of independent experiments (n=3) ± SD. **C.** Lineweaver Burk plot (inverse of the ATP concentration against the inverse of the reaction velocity) of the data presented in A. Data are mean values of independent experiments (n=3) ± SD. **D.** Zoom-in on the indicated area in C (grey dashed rectangle). The corresponding raw data and the processed data are available in the appendix (12.3).

5.4.3.2 ATP-based kinase enrichment and competition

ATP competitive inhibitors can be characterized in a competitive ATP-based kinase enrichment assay. As described in 4.2.3.6-I, the ATP-based kinase enrichment is a special form of a protein pull-down, wherein an ATP-probe is used to enrich ATP binding proteins. If

an ATP competitive inhibitor, like Pipinib, is added to the lysate before the pull-down, possible targets can be identified. If proteins are bound by the inhibitor, binding of the ATP probe and thereby enrichment of that protein is impaired. This results in reduced enrichment of target proteins compared to a solvent control (Figure 35A). When this assay was carried out using 100 and 200 µM Pipinib, a dose-dependent decrease of PI4KB enrichment could be observed via immunoblot detection (Figure 35B).

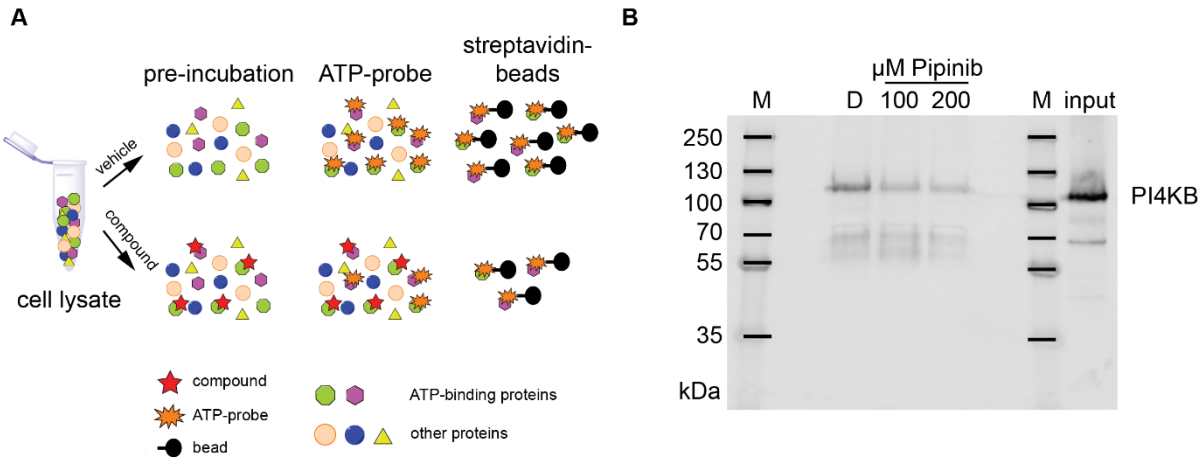

C

n1	n2	n3	count identified
Pi4kb	Pi4kb	Pi4kb	3
Acaa2			1
	Acad10		1
	Cav1		1
Cdc42			1
	Commd2		1

*ratio vehicle/compound significantly >1

Figure 35. ATP-probe kinase enrichment assay. A. Assay principle. Cell lysate is incubated with a compound or vehicle control before treatment with a desthiobiotin ATP probe. When streptavidin beads are added to this mixture, they bind to desthiobiotin and enable enrichment of ATP-binding proteins. Proteins that are bound by an ATP-competitive inhibitor, however, cannot be bound by the ATP probe and will be enriched to a lesser extent compared to the vehicle control. **B.** ATP-probe kinase enrichment detected via immunoblotting. NIH/3T3 cell lysate was incubated with 100 and 200 µM Pipinib or 0.5% DMSO as a control before addition of 5 µM desthiobiotin-ATP and subsequent capture using streptavidin beads. Bound proteins were eluted and separated via SDS-PAGE, transferred onto a PVDF membrane, which was then blocked and stained with an antibody against PI4KB. A representative blot of independent experiments (n=5) is shown. **C.** ATP-probe kinase enrichment detected via MS/MS. The assay was carried out as described in B, with the exception that only 200 µM of Pipinib was used. Bound proteins were eluted and run on an SDS gel until the lysate was taken up. The gel pieces were then fixed, alkylated and digested using trypsin. Peptides were analyzed by nano-HPLC-MS/MS. Peptides were identified and quantified using MaxQuant. Statistical significance was assessed with a t-test. Statistically significant outliers that were enriched in the samples treated with DMSO over the ones treated with compound competitor were considered as hits. Statistically significant hits of independent experiments (n=3) are displayed in the table.

Because immunoblot detection only enables monitoring of one or few proteins at a time, mass spectrometry detection was applied to investigate the effect of Pipinib on the enrichment of ATP binding proteins in a proteome-wide manner. Like this, the specificity of Pipinib could be assessed and other possible binding partners could be identified. In three independent repetitions of the experiment, PI4KB was the only protein to be significantly less enriched in presence of Pipinib (ratio DMSO/Pipinib=8.4 ± 4.3). Other proteins were enriched as well, but this enrichment was not reproducible (Figure 35C). Even though these results indicate a selective behavior of Pipinib, only ATP binding proteins are covered by this technique. This is why, as a complementary approach, small-molecule probe-based affinity chromatography was performed (5.4.3.3).

5.4.3.3 Small-molecule probe-based affinity chromatography

In this approach, Pipinib itself is used a probe to enrich its binding proteins. Before Pipinib can be applied as a probe, a linker has to be attached to couple the compound to a solid phase. However, linker attachment can cause loss of compound activity. To identify the optimal attachment position for a linker, the establishment of a structure-activity relationship (SAR) is required.

5.4.3.3.1 SAR of Pipinib

To enable an SAR study, *Dr. Andrei Ursu and Dr. Lucas Robke re-synthesized* Pipinib and additionally synthesized 16 derivatives of Pipinib that were derivatized at positions R^1 and R^2 (Table 6). Pipinib, entry **1**, displayed the highest activity of all derivatives. None of the introduced modifications led to an increase of bioactivity as measured by the osteogenesis assay. At position R^1, replacing the isopropylamine with various primary amines containing 3 to 7 carbon atoms lead to a minor decrease in biological activity (Table 6, entries **2**, **3**, **4**, **5** and **8**). Even a minor increase of the steric bulkiness of the isopropylamine leads to a 8- to 11-fold drop in biological activity (Table 6, entries **6** and **7**). Substitution with secondary amines such as pyrrolidine or piperidine does neither improve nor impair biological activity (Table 6, entries **9** and **10**). Substitution with morpholine, however, lead to mild cytotoxicity (Table 6, entry **11**). For variation at R^2, the primary amines that did not significantly alter the osteogenesis activity (Table 6, entries **1**-**6**) were selected. The para-carboxylic acid methyl ester substitution was replaced with a nitrile to introduce a less bulky functional group. In total 5 derivatives have been synthesized (Table 6, entries **12**-**16**) and analyzed in the osteogenesis assay. Here, the same conclusions that were made for entries 1, 3, 4, 5 and six, can be drawn. Again, the isopropylamino substitution (see entry **12**) represents the

biologically most active derivative across this series, emphasizing the key role played by this group in the cellular context and pointing out to a rather restricted panel of available chemical modifications. Even though the biological activity of Pipinib could not be improved, the SAR study indicated that R^1 might be suitable for installing a triethylene linker containing a free primary amine by nucleophilic substitution.

Table 6. Structure-activity relationship of Pipinib (Entry 1). Entries **2** to **16** were retrieved via derivatization of Pipinib at positions R^1 and R^2. Compound activity was assessed via an osteoblast differentiation assay. For this, C3H10T1/2 cells were incubated with 1.5 µM Purmorphamine and the compounds or DMSO as a control for 96 h. The activity of alkaline phosphatase was assessed by means of a luminescence readout. DMSO was set to 100%. Data are mean values of independent experiments (n=3) ± SD. Viability was measured in the same setting using a CellTiter Glo Kit (Promega). Values > 10 µM were obtained when the inhibition achieved up to a concentration of 10 µM was not sufficient to calculate an IC_{50} value. A compound was considered as "inactive" if no toxicity was observed up to the maximum applied concentration of 10 µM. Osteo.=Osteogenesis.

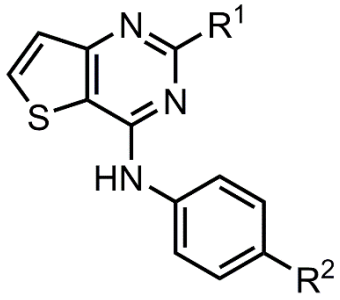

No.	R^1	R^2	Osteo. IC_{50} [µM]	Viability IC_{50}[µM]
1	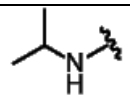	COO Me	0.6 (±0.3)	inactive
2	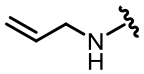	COO Me	2.9 (±0.2)	> 10
3	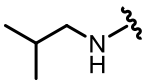	COO Me	3.4 (±0.1)	> 10
4	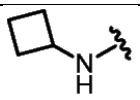	COO Me	3.8 (±0.2)	> 10
5	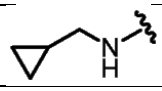	COO Me	3.4 (±0.3)	8.0 (±0.6)
6	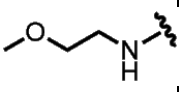	COO Me	4.9 (±0.5)	inactive
7	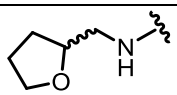	COO Me	6.8 (±0.3)	inactive
8	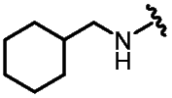	COO Me	7.7 (±1.4)	> 10

No.	R^1	R^2	Osteo. IC_{50} [µM]	Viability IC_{50}[µM]
9	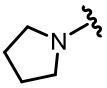	COO Me	2.1 (±0.5)	> 10
10	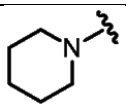	COO Me	3.0 (±0.1)	> 10
11	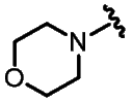	COO Me	2.9 (±0.1)	6.8 (±0.1)
12	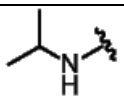	CN	2.4 (±0.2)	inactive
13	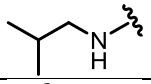	CN	6.5 (±0.4)	inactive
14	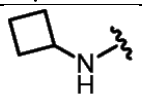	CN	4.0 (±0.3)	inactive
15	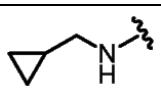	CN	3.8 (±0.1)	> 10
16	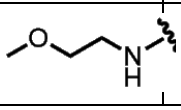	CN	6.3 (±0.7)	inactive

5.4.3.3.2 Evaluation of active and inactive small-molecule probes

Based on these results, *Dr. Andrei Ursu and Dr. Lucas Robke synthesized two pull-down probes*. One of them ("active") was designed to contain a linker and be active as a Hh inhibitor. The other ("inactive") contained the linker and only a core scaffold that was expected to not inhibit Hh signaling (Figure 36A and B, respectively) and will serve as a negative control in the affinity chromatography experiments.

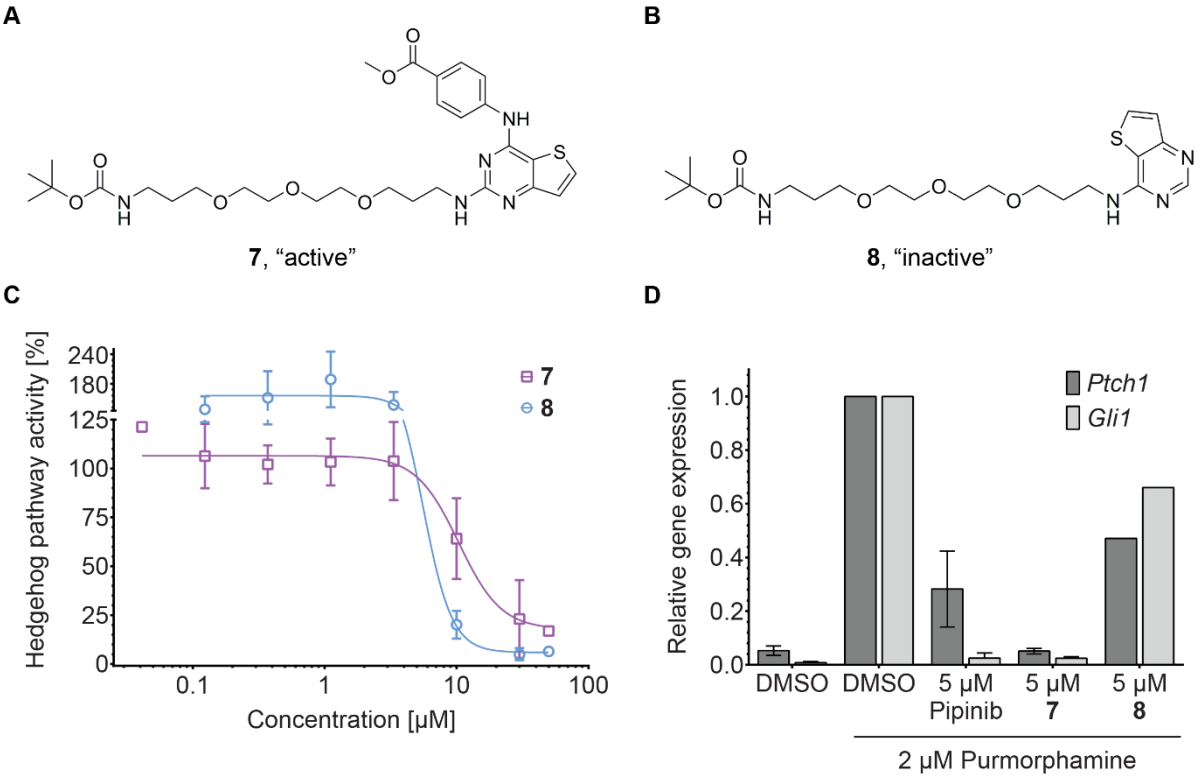

Figure 36. Evaluation of small-molecule probes for target identification via affinity chromatography. A. Chemical structure of the Boc-protected active probe, compound **7**. **B.** Chemical structure of the Boc-protected inactive probe, compound **8**. **C.** GLI reporter gene assay. Shh-LIGHT2 cells were treated with 2 µM Purmorphamine and the compounds or DMSO as a control for 48 h. The Hh dependent firefly luciferase signal was divided by the control signal of the renilla luciferase and normalized to Purmorphamine-DMSO-treated cells. Data are mean values ± SD of biological replicates (n=5 active probe; n=2, inactive probe). **D.** Evaluation of target gene expression. NIH/3T3 cells were treated with 2 µM Purmorphamine and the compounds or DMSO as a control for 48 h. Using primers for *Ptch1* and *Gli1* as Hh target genes and *Gapdh* as a reference gene, qRT-PCR was carried out to retrieve expression levels. Data were normalized to Purmorphamine-DMSO-treated cells and are mean values of biological replicates (n=2, active probe; n=1, inactive probe) ± SD.

To ensure that these probes are indeed active (compound **7**) and inactive (compound **8**), their phenotypic effects on osteoblast differentiation, GLI reporter activity and the expression of Hh target genes were evaluated. Osteogenesis was inhibited with IC_{50} values of 3.8 ± 0.2 µM and 8.3 ± 0.5 µM for the active and inactive probe, respectively. While the active probe was

slightly toxic to the cells (viability IC_{50}=8.3 ± 0.5 µM), the inactive probe did not exhibit toxicity. These values indicate that the active probe, even though being less active than the parent compound, is still displaying an inhibitory effect. The inactive probe has a strongly reduced potency as compared to the parent compound. Assessment in the GLI reporter assay (Figure 36C) showed pathway inhibition by both probes with an IC_{50} value of 9.6 ± 2.6 µM for the active probe and an IC_{50} value of 6.2 ± 2.7 µM for the inactive probe. In contrast to the osteoblast differentiation assay, both compounds inhibited GLI reporter expression with similar potency. However, taking into account the curves in Figure 36C, the inactive probe (compound **8**) leads to a rapid drop of reporter activity at 10 µM resulting in a steep curve. This is can be caused by unspecific inhibition, e.g. through aggregate formation[170]. In accordance with that, comparison of parent compound, active and inactive probe for inhibition of Hh target gene expression (Figure 36D) shows that the inactive probe only leads to mild inhibition of Hh signaling, while the active probe is more potent than the parent compound. When tested for inhibition of PI4KB at a concentration of 10 µM, the inactive probe was indeed inactive (-6 ± 2% inhibition) whereas the active probe was only slightly less active than the parent compound (62 ± 0% inhibition). Considering all results as a whole, the probes were considered appropriate for affinity chromatography experiments.

5.4.3.3.3 Pull-down results

In general, the small-molecule probe-based affinity chromatography (pull-down) follows the same principle as the ATP probe-based affinity chromatography. Lysates are incubated with a probe that has been coupled to beads. The probe on the beads binds to proteins within the lysate and thereby captures potential targets. The beads are then washed several times to remove unspecific binding partners. The proteins are then eluted and analyzed via immunoblot or digested into smaller peptide fragments and analyzed via mass spectrometry. To distinguish specific binding from unspecific binding, an inactive probe, which does not or only weakly induce the phenotype of the parent compound, is used. Only proteins that are specifically enriched in the active probe sample are considered as targets. To gain further proof, in a second approach, the lysate can be pre-incubated with the free parent compound as a competitor. Thus, proteins that bind to the parent compound will not or to a lesser extent bind to the probe, resulting in reduced enrichment compared to a DMSO pre-treated lysate that is likewise incubated with the active probe. Both described approaches were applied in this thesis.

To assess the performance of the pull-down probes, all eluted proteins were separated via SDS-PAGE and stained with a silver stain (Figure 37A).

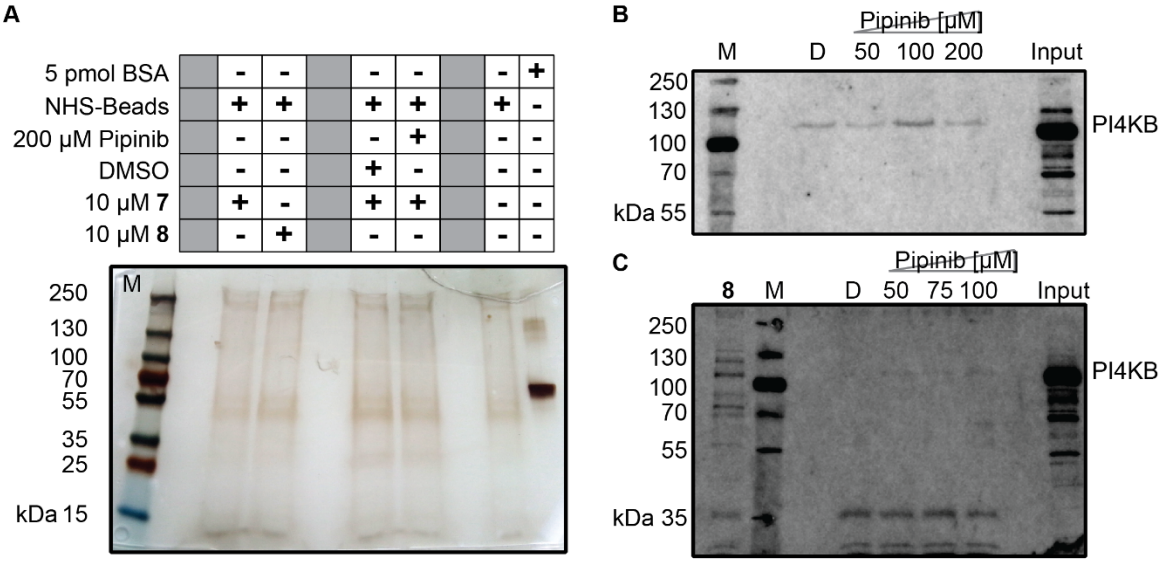

D

Name	n1	n2	competition	detected by MS/MS?
	identified peptides active/inactive		DMSO/ Pipinib	
Ribosyldihydronicotinamide dehydrogenase [quinone]	16 / 0	12.3 / 0	9.8	3/3
Mitogen-activated protein kinase 9/ Mitogen-activated protein kinase 10	13.3	2.3	**n.i.**	2/3
Sepiapterin reductase	13.9	1.4	**n.c.**	3/3
Heme-binding protein 1	4.7 / 0	4 / 0	5.5	3/3
Flavin reductase (NADPH)	3.7	1.5	**n.c.**	3/3
GRAM domain-containing protein 4	**n.i.**	5 / 0	**n.i.**	1/3
Transmembrane 7 superfamily member 3	**n.i.**	3.8	**n.i.**	1/3
Liprin-beta-1	**n.e.**	4.8	**n.c.**	3/3
Nucleoside diphosphate kinase, mitochondrial	**n.e.**	3/0	**n.c.**	3/3
Fatty acid desaturase 1	**n.e.**	3.0	**n.c.**	3/3
Ferrochelatase;Ferrochelatase, mitochondrial	**n.i.**	2.0	**n.i.**	1/3
Total proteins identified	1472	1557	1768	
PI4KB	**n.i.**	**n.i.**	**n.i.**	0/3

n.i. = not identified **n.e.** = not enriched **n.c.** = no competition

Figure 37. Results of the small molecule probe affinity chromatography. A. Silver stain of eluted proteins. De-protected active and inactive probe were coupled to NHS-magnetic beads and incubated with NIH/3T3 cell lysate. The beads were then washed, and proteins were eluted via heating in 5x SDS sample buffer and separated via SDS-PAGE. In case of lanes 5 and 6, the lysates were pre-incubated either with DMSO or with 200 µM Pipinib. Protein bands were detected by means of a silver stain. (n=1) **B.** Immunoblot detection of PI4KB after affinity chromatography. The experiment was carried out as described in A. Lysates were pre-incubated with DMSO (D), 50, 100 or 200 µM Pipinib. Eluted proteins were separated via SDS-PAGE, transferred onto a PVDF membrane, which was then blocked and incubated with an anti-PI4KB antibody (n=1). **C.** Repetition of B, including a sample using beads with an inactive probe (**8**). Here, the lysates were pre-incubated with 50, 75 or 100 µM Pipinib (n=1). **D.** Mass spectrometry detection of the affinity chromatography experiments. The experiment was carried out as described in A. After washing, on-bead digestion followed by stage-tip purification was carried out and peptides were detected via MS/MS (n=2, without competitor; n=1, competition). The column on the right summarizes how often the respective protein was detected by the mass spectrometry measurement, e.g. 1/3=identified once in three experiments.

With the naked eye, no obvious difference is visible: neither between active and inactive probe nor between active probe plus DMSO and active probe plus Pipinib as a competitor. The probe bands are not differing clearly from the beads only sample, either, suggesting unspecific binding and emphasizing the necessity of an inactive control probe. In many cases, differences between active and inactive probe are too small to be observed visually but still big enough to be detectable via MS/MS. Since one possible target of Pipinib was PI4KB, this protein was detected via immunoblotting after a pulldown with the positive probe using lysates that were pre-incubated with different concentrations of Pipinib (Figure 37B and C). While in a first run, PI4KB was pulled down with the positive probe and competed by 50 and 200 µM Pipinib (Figure 37B), this behavior could not be reproduced when the experiment was repeated (Figure 37C). Nevertheless, the probes were applied for proteome-wide detection via mass spectrometry. Again, PI4KB was not detected in any of the experiments (Figure 37D). In total, 12 potential binding partners were identified. Of these, two proteins were enriched in both pull-down experiments and competed by free Pipinib. These proteins are ribosyldihydronicotinamide dehydrogenase (NQO2), a detoxification oxidoreductase and heme-binding protein 1 (HEBP1), a scavenger for possibly toxic free porphyrinogens. So far, no connection to Hh signaling is known and considering their biological functions, it is rather unlikely that these proteins are relevant for Hh signaling. While they might be target proteins of Pipinib, they are most likely not relevant for Pipinib-mediated inhibition of Hh signaling.

Furthermore, Sepiapterin reductase and Flavin reductase were enriched in both repetitions of the pull-down but not competed by free Pipinib, which is why they were not regarded as specific binding partners. Mitogen-activated protein kinase 9 and 10 (MAPK9/ MAPK10) were also enriched in both pull-downs. Unfortunately, these proteins were not identified in the competition experiment. Because of that, it is not possible to judge whether this interaction is specific. In the kinase panel, the enzymatic activity of MAPK9 was inhibited by Pipinib (10 µM) to 8.7 ± 2.2% and MAPK10 was inhibited to -8.65 ± 2.7%. This low extent of inhibition led to the exclusion of these two kinases as primary targets of Pipinib. Liprin-beta-1, Nucleoside diphosphate kinase (mitochondrial) and Fatty acid desaturase 1 were only significantly enriched in one pulldown and not competed by free Pipinib and were thus excluded as targets. GRAM domain-containing protein 4 (GRAMD4), Transmembrane 7 superfamily member 3 (TM7SF3) and Ferrochelatase (mitochondrial, FECH) were enriched in the second pull-down but could not be identified in the other two experiments. Based on these results, it is not possible to decide whether these proteins are possible targets. GRAMD4 is a mitochondrial pro-apoptotic protein that mimics the proto-oncogene p53 and mediates p73-induced apoptosis.[171] While no direct role for GRAMD4 in Hh signaling is known, it was reported that

the GLI2 promotor region contains binding sites for p73.[172] Since p73 is upstream of GRAMD4, no relevance of GRAMD4 for Hh signaling can be concluded based on the current literature. TM7SF3 is an orphan transmembrane receptor that was reported as an inhibitor of cytokine-induced death of pancreatic beta cells.[173] It was recently shown that this plasma membrane receptor is controlled by p53 and inhibits ER stress, unfolded protein response (UPR) as well as caspase 3/7 activation and thus is a pro-survival homeostatic factor.[174] Also for TM7SF3, no direct implication in Hh signaling is known. FECH catalyzes the insertion of iron into protoporphyrin IX[175] and is the final enzyme of the heme biosynthetic pathway. Also for FECH, no direct connection to Hh signaling is known. Because PI4KB is the only potential target with a known connection to Hh signaling[50], it was chosen for further studies.

5.4.4 Pipinib reduces intracellular levels of PI4P

Based on the results described above, PI4KB was chosen for further investigation. To confirm that the enzyme is inhibited *in cellulo*, the levels of its product, PI4P, were assessed after Pipinib treatment. Using an anti-PI4P antibody, cellular PI4P was monitored by means of immunofluorescence (Figure 38A). Over a time course of 6 or 24 h, Pipinib led to a concentration dependent decrease of PI4P levels. Already 2 µM Pipinib led to a changed PI4P staining, i.e. reduced PI4P intensity and narrower distribution compared to DMSO. This effect intensified with increasing concentrations and time. At 15 µM Pipinib, the PI4P stain is densely concentrated close to the nucleus and not distributed throughout the cell. PI4P is normally found at the Golgi apparatus and on post-Golgi vesicles[66]. The observed concentration of PI4P close to the nucleus, i.e. at the Golgi, and its absence from vesicles is an indication of a disturbed PI4P metabolism, which could be caused by inhibition of PI4KB. Inhibition of other PI 4-kinases is less likely to be the cause of this phenotype because they were not inhibited by Pipinib *in vitro*. It cannot be excluded that activation of 4-phosphatases (e.g. SAC1) contributes to this phenotype. However, considering the known function of Pipinib as an inhibitor of PI4KB, it is rather unlikely that it also acts as an activator of 4-phosphatases. When overall PI4P levels were monitored via flow cytometry, a decrease of approx. 40% was observed for 5, 10 and 15 µM Pipinib (Figure 38B). However, no concentration dependency was observed, maybe because a minimum threshold of cellular PI4P was reached already at 5 µM Pipinib. Compound **9**, a published PI4KB inhibitor[176] (Figure 38C), did not lead to a reduction of PI4P levels at a concentration of 5 µM. Since no selectivity data across the kinome is available for compound **9**, this could likely be a cause of unselectivity or poor permeability properties.

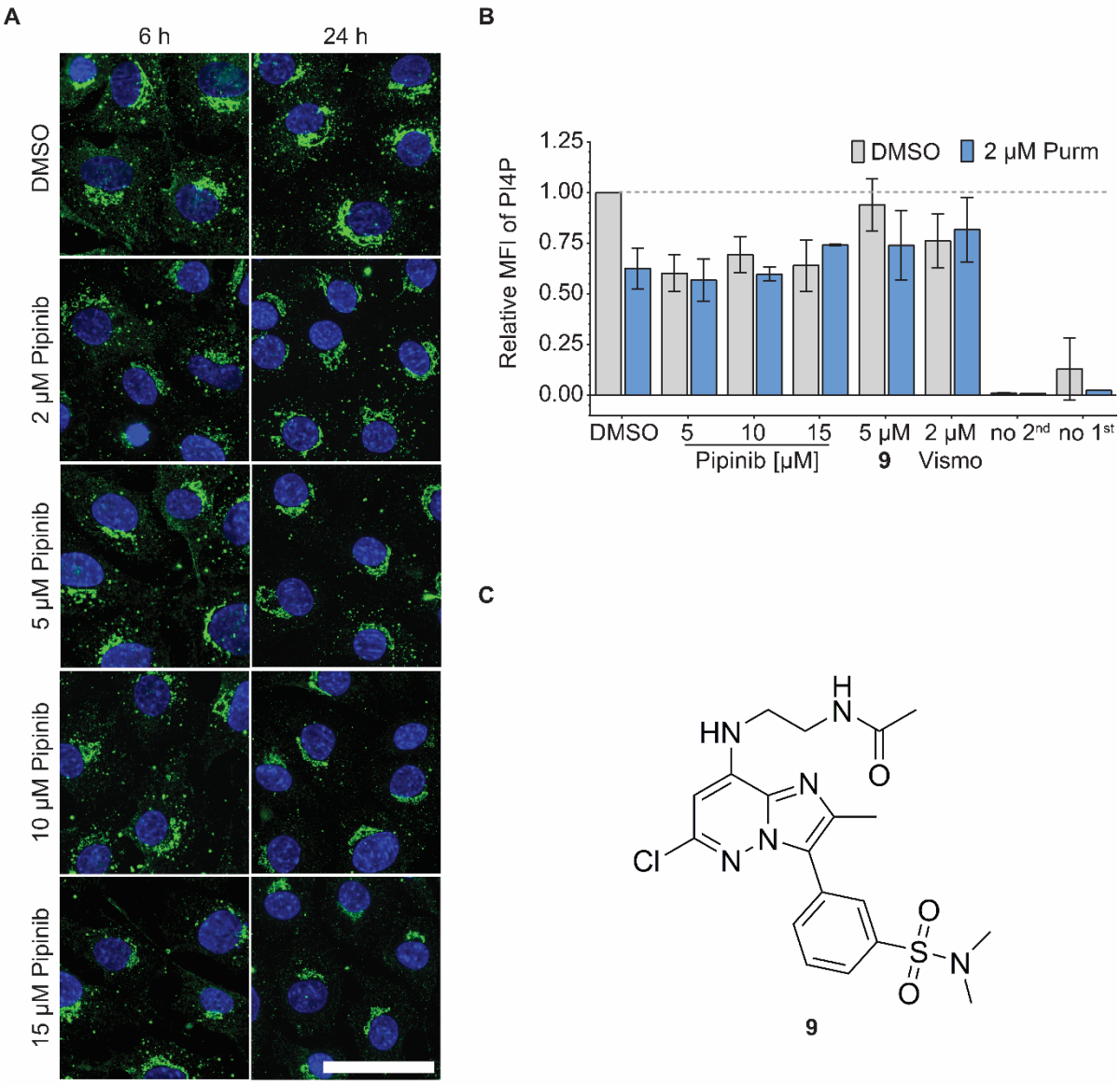

Figure 38. Assessment of cellular PI4P. A. PI4P assessment via fluorescence microscopy. NIH/3T3 cells were treated with different concentrations of Pipinib or DMSO as a control for 6 and 24 h. Cells were then fixed, permeabilized and blocked before treatment with a primary antibody against PI4P and subsequent incubation with an Alexa488 secondary antibody (green) and DAPI as a nuclear marker (blue). Representative images of biological replicates (n=3) are shown. Scale bar: 50 µm. **B.** PI4P assessment via flow cytometry. NIH/3T3 cells were treated with the compounds or DMSO as a control for 48 h. Cells were then detached, washed, fixed, permeabilized and blocked before incubation with primary and secondary antibodies as detailed in A. Data were normalized to DMSO-treated cells and are mean values of biological replicates (n=4) ± SD. **C.** Structure of compound **9**.

Vismodegib, a Hh inhibitor and Smoothened binder, did not reduce PI4P levels either, suggesting that cellular amounts of PI4P are not controlled by Hh signaling. Addition of Purmorphamine lead to a reduction of PI4P levels. Additional treatment with Pipinib did not lead to a further decrease of PI4P. One possible explanation is that Hh activation leads to consumption of PI4P and, similar to the absence of a concentration dependency for Pipinib

treatment, the resulting levels are already at a threshold that cannot be lowered further. Another reason for this observation could be the generation of PI4P by other PI 4-kinases that are not inhibited by Pipinib.

Dr. Takanari Inoue and Dr. Yuta Nihongaki, collaboration partners at the Johns Hopkins University in Baltimore, USA, have applied a PI4P sensor to monitor PI4P in living cells (Figure 39). HeLa cells were transfected with an EYFP-PH(FAPP1) construct that leads to expression of the PI4P binding pleckstrin homology (PH) domain of the Phosphatidylinositol-4-phosphate adapter protein 1 (FAPP1) protein.[177] This domain specifically binds to PI4P and is therefore suitable to detect PI4P in living cells when it is fused to a fluorescent protein like the enhanced yellow fluorescent protein (EYFP).

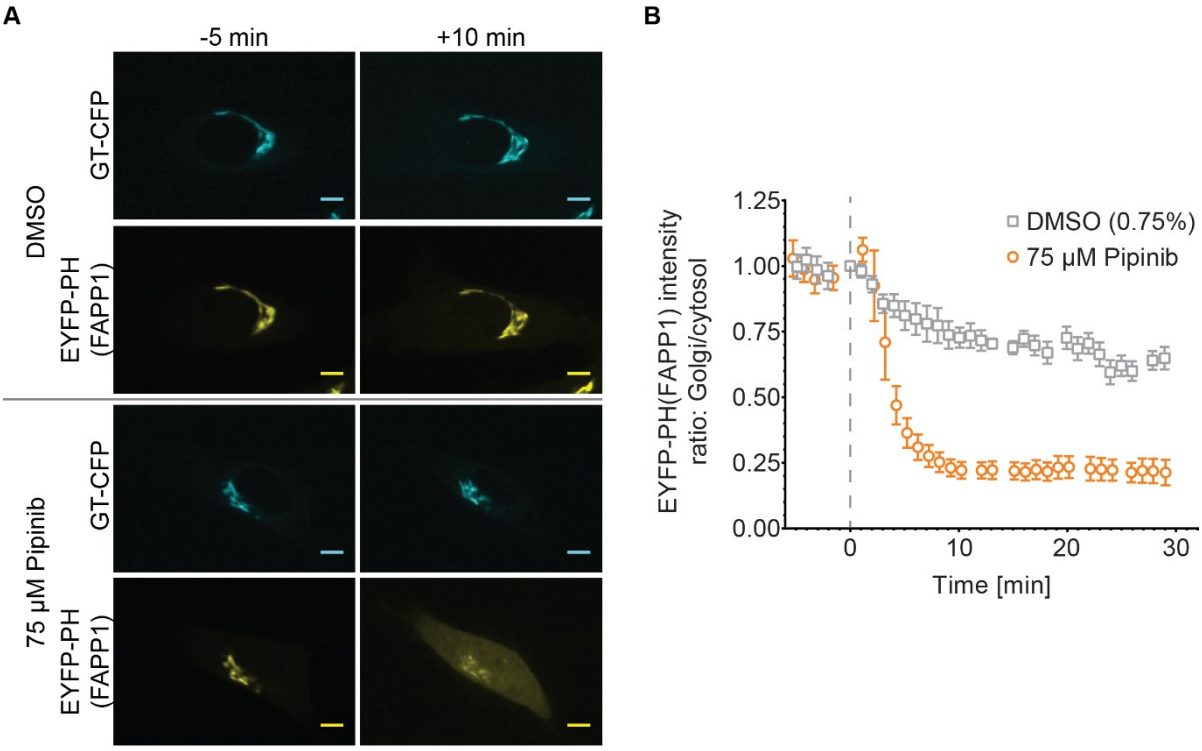

Figure 39. Assessment of PI4P in living cells. A. PI4P sensor experiment. HeLa cells were transfected with an EYFP-PH(FAPP1) and a GT-CFP construct overnight. Cells were treated with 75 µM Pipinib or DMSO as a control and monitored in real-time for 30 min. Images are representative of 8 measured cells. Scale bar: 10 µm. **D.** Quantification of FAPP1-sensor intensity from C. The FAPP1 intensity ratio between Golgi and cytosol is plotted against the time. Compound addition is marked with a grey dashed line. Data were normalized to time point 0 and are mean values of eight measurements ± standard error of the mean (SEM).

Additionally, cells were transfected with a GT-CFP construct to induce expression of β1,4-galactosyltransferase (GT), which is a Golgi membrane protein and thus used as a marker for the Golgi apparatus[178], fused to cyan fluorescent protein (CFP). Application of 75 µM

Pipinib lead to a drastic and rapid redistribution of PI4P throughout the cell over a time course of 30 min (Figure 39A and B). The usually Golgi-localized pool of PI4P is distributed all over the cytosol, while still being accumulated at the Golgi with decreased intensity. This influence on intensity and distribution of the sensor emphasizes Pipinib's effect on intracellular PI4P. It has to be noted that 75 µM is a high compound concentration and observed effects might be unspecific. Nevertheless, in combination with the results obtained with the anti-PI4P antibody (Figure 38A and B) the findings in Figure 39C are likely to be a consequence of PI4KB inhibition.

5.4.4.1 Pipinib induces morphological changes of the Golgi apparatus and mitochondria

Further insights into the cellular effects of Pipinib were gained by means of the so-called cell painting assay. This assay monitors morphological changes induced after 20 h of compound treatment via staining with several cell compartment markers. The applied markers are MitoTracker dye to stain mitochondria, fluorescently labelled wheat germ agglutinin (WGA) to label the Golgi apparatus as well as the plasma membrane[179], fluorescently labelled phalloidin to stain the cytoskeleton, SYTO 14 dye to stain cytoplasmic RNA and nucleoli, fluorescently labelled Concanavalin A to stain the endoplasmic reticulum (ER) and Hoechst to stain DNA, i.e. the nucleus. Due to careful fluorophore selection, all organelles/structures can be detected in one well. After image acquisition, the images are computationally analyzed for changes between compound-treated samples and the DMSO control. The parameters which are analyzed include the correlation, i.e. co-localization, of different stains, the overall object intensity, shape and surrounding as well as the radial distribution of objects within the image. On top of that, granularity and texture (i.e. the sharpness of the objects, smooth vs. textured) of the images are evaluated. Only parameters that are significantly decreased or increased compared to the DMSO control are reported.

By means of this assay, a morphological profile of Pipinib was created. The overall induction of morphological changes was 5.5%, which is considered as a low value. This argues for a rather selective mode of action, since unselective compounds tend to induce many changes in various organelles because they target many different cellular mechanisms.

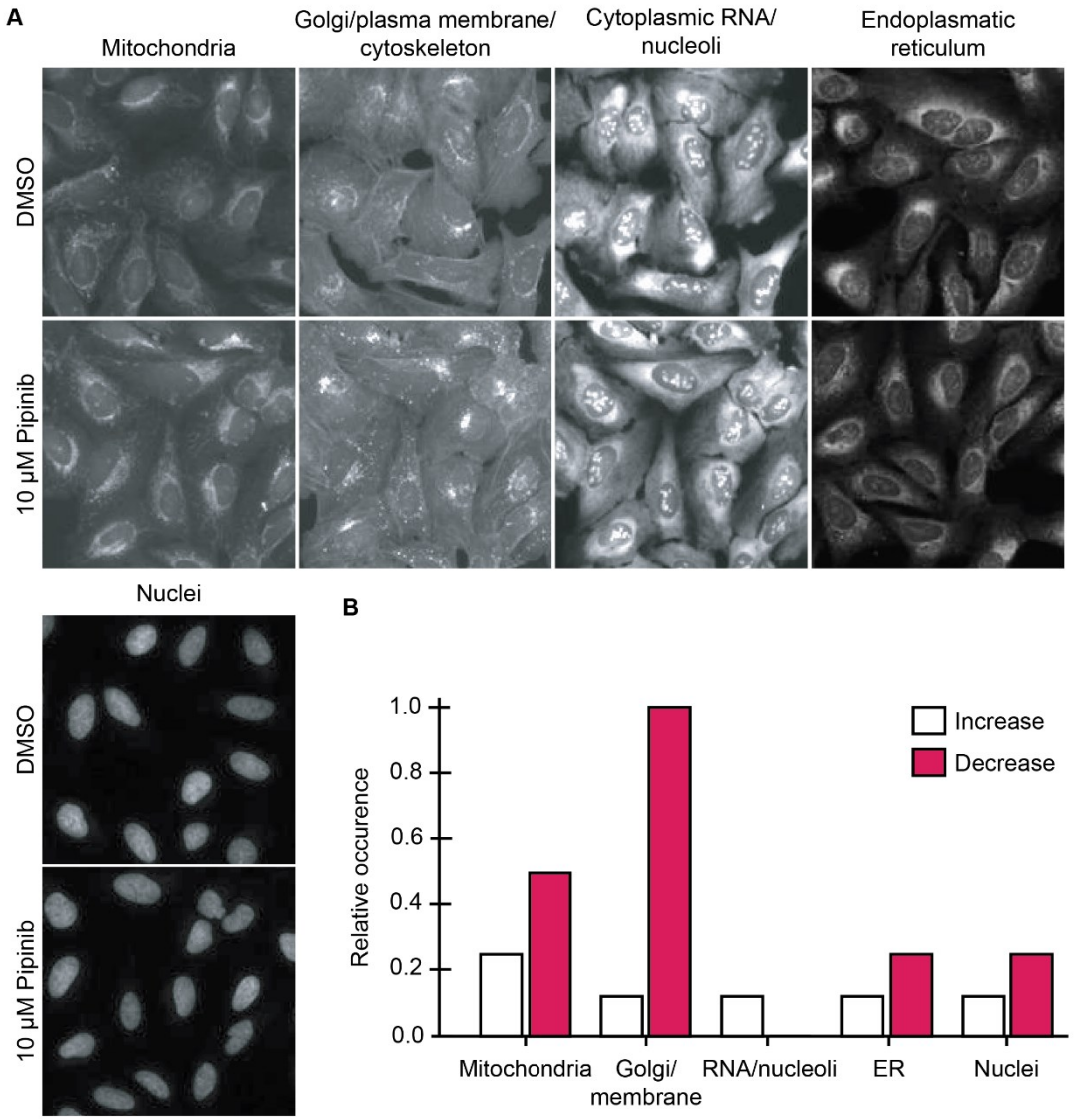

Figure 40. Cell painting assay for Pipinib. A. Fluorescence microscopy images. U2OS cells were treated with 10 µM Pipinib or DMSO as a control for 20 h. Living cells were then treated with MitoTracker and imaged. After that, cells were fixed, permeabilized and stained with WGA-Alexa594 (Golgi, membrane), phalloidin-594 (cytoskeleton), Syto14 (RNA, nucleoli), Concanavalin A-Alexa488 (ER) and Hoechst before automatic image acquisition. Images are representative of 27 acquisitions per condition (9 per well, 3 wells, n=1). **B.** Image analysis output for A. The image analysis was performed with the Cell Profiler software and a custom KNIME workflow. Relative occurrence of increased or decreased parameters is illustrated respective to the compartment of appearance.

At a first glance, the images presented in Figure 40A look similar for Pipinib and DMSO. The computational image analysis, however, has identified several changes with a maximum in the Golgi apparatus and the plasma membrane. The second highest number of changes was found for mitochondria (Figure 40B). Indeed, upon closer inspection, one can see an intensified mitochondrial stain for Pipinib-treated cells as well as an increased area of the staining within each cell. For the WGA-Golgi stain, Pipinib-treated cells show a decreased

staining area for the Golgi apparatus, resembling a contracted phenotype, while displaying several dot like structures in the cytosol. This phenotype might be induced by inhibition of PI4KB since this enzyme is not only important for the generation of PI4P but also for the structural integrity of the Golgi apparatus.[180]

In addition to novel small molecules, also reference compounds with known target proteins or modes of action are tested in the cell painting assay. If the morphological profiles of test compounds are computationally compared with reference profiles, reference compounds with a similar profile can give further hints for a target hypothesis. For Pipinib, four reference compounds were identified that exhibited more than 40% similarity. The respective compound structures can be found in Figure 41.

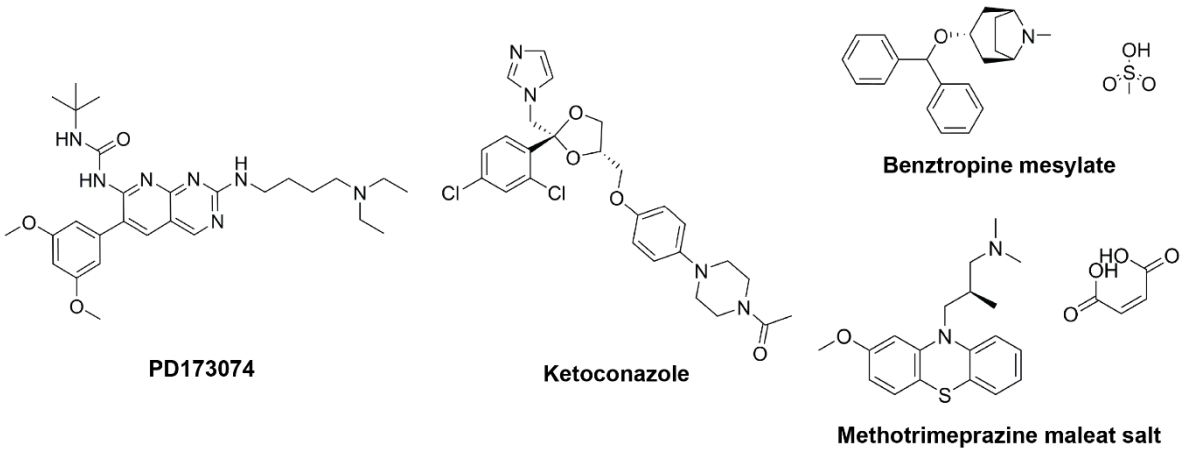

Figure 41. Reference compounds that induced a similar morphological profile to Pipinib.

A characterization of these molecules and Pipinib, including published targets, activity on osteoblast differentiation (osteogenesis), cell painting as well as structure similarity and morphological induction, is available in Table 7. The highest similarity was found for PD173074, an inhibitor of growth factor (receptor)s, insulin receptors, dual specificity mitogen-activated protein kinase kinase 1, Src kinase and protein kinase C. While inhibition of PI4KB was not evaluated, it is inhibiting several kinases and thus could also be an inhibitor of the lipid kinase. Additionally, it was found to inhibit Purmorphamine-induced osteoblast differentiation which is another common feature of Pipinib and PD173074. The second highest similarity was calculated for ketoconazole, an inhibitor of various cytochrome enzymes, steroid 5-α-reductase-2, UDP-glucuronosyltransferase 1-1 and androgen receptor. For this compound, osteoblast differentiation was not evaluated. The third and fourth highest

similarity of approx. 40% was retrieved for benztropine mesylate and methotrimeprazine maleate salt. The first is an antagonist of the muscarinic acetylcholine receptor M1, the latter was found to inhibit the mitochondrial permeability transition pore, geminin, lysine-specific demethylase 4A, isocitrate dehydrogenase NADP cytoplasmic and glucagon-like peptide receptor. For both compounds, inhibition of osteoblast differentiation was not tested.

Table 7. Comparison of biologically similar reference compounds and Pipinib. Known targets for the similar compounds were retrieved from the ChEMBL database. Abbreviations: Biol. similar. = biological similarity, Struct. similar. = structural similarity, osteo. = osteogenesis FGFR = fibroblast growth factor receptor, VEGF = vascular endothelial growth factor, EGFR = epidermal growth factor receptor, MAP2K1 = dual specificity mitogen-activated protein kinase kinase 1, Src = neuronal proto-oncogene tyrosine-protein kinase Src, PKC = protein kinase C, UGT1A1 = UDP-glucuronosyltransferase 1-1, KDM4A = lysine-specific demethylase 4A, n.d. = not determined.

Compound	Biol. similar. [%]	Struct. similar. [%]	Induc-tion [%]	Known and putative targets	Inhibition of osteogenesis?
PD173074	50	18.4	4.2	FGFR, VEGF, EGFR, insulin receptor, MAP2K1, Src, PKC	97% (osteo.) 90% (viability)
Ketoconazole	41.7	14.7	5.5	Various cytochrome enzymes (CYP2D6, CYP1A2, etc.), steroid 5-α-reductase-2, UGT1A1, androgen receptor	n.d.
Benztropine mesylate	40.9	12.4	4.6	Muscarinic acetylcholine receptor M1	n.d.
Methotrime-prazine maleat salt	40.6	20.9	9.1	Mitochondrial permeability transition pore, geminin, KDM4A, isocitrate dehydrogenase NADP cytoplasmic, glucagon-like peptide receptor	n.d.
Pipinib	-	-	5.5	**PI4KB**, PIP5K1C, PIK3C2G, GAK, TTK, NQO2, HEBP1, GRAMD4, TM7SF3, FECH	98% (osteo.) 58% (viability)

In conclusion, the cell painting assay revealed the morphological phenotype of Pipinib and confirms an effect on the Golgi apparatus and suggests interference with the mitochondria. The known targets of the similar reference compounds gave hints for further targets. However, considering the kinase panel results, further kinases can be excluded as targets. There is evidence for a cooperation of Hh, growth factor receptor, MAPK cascade, PKC and KRas signaling in cancer.[181] If any of these pathways is upregulated, this can lead to modulation of GLI1 and GLI2 stability and activity[181]. In non-transformed cells however, these

signaling pathways should be in control and thereby their inhibition is unlikely to have an effect on Hh signaling. In contrast, there is a connection between mitochondrial metabolism and Hh signaling but it is rather Hh signaling that controls mitochondria fragmentation[182], abundance and activity[183] as well as respiration[184] and not vice versa. A feedback mechanism could still have an influence on Hh signaling but this kind of regulation has not been confirmed so far. Muscarinic acetylcholine receptors are mainly expressed in central neurons and peripheral muscles but are unlikely to have an implication in canonical Hh signaling.[128] Considering these results and the current literature, PI4KB is still the most probable target with relevance to Hh signaling.

5.4.5 Pipinib increases thermal stability of PI4KB

The data described above provide evidence that Pipinib binds to PI4KB. It has been confirmed as an inhibitor in a biochemical assay and it was found to compete with ATP for binding to PI4KB. To further validate target engagement, a cellular thermal shift assay (CETSA) was carried out. When performing the CETSA for PI4KB, a temperature dependent decrease of protein content due to precipitation was observed and a melting temperature of 52.6 ± 0.6 °C was retrieved for an NIH/3T3 lysate that has been pre-incubated with DMSO (Figure 42A and B).

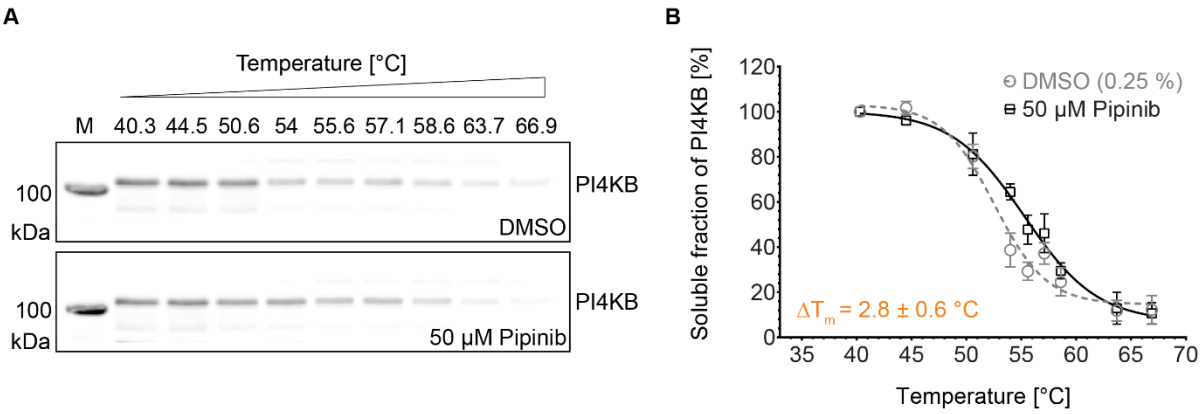

Figure 42. Pipinib treatment leads to thermal stabilization of PI4KB. A. Immunoblot detection of PI4KB solubility. NIH/3T3 cell lysate was incubated with 50 µM Pipinib or 0.25% DMSO as a control for 10 min. The lysate was then aliquoted and heated to several temperatures before ultracentrifugation to remove insoluble proteins. The supernatant was separated via SDS-PAGE, transferred to a PVDF membrane, which was then blocked and stained with an antibody against PI4KB. This blot is representative of independent experiments (n=3). **B.** Quantification of PI4KB band intensity from A and two further repetitions. Band intensity was quantified using the Image studio software and normalized to the 40.3 °C sample. Data are mean values of independent experiments (n=3) ± SD.

When the same lysate was pre-incubated with 50 µM Pipinib, an increase in protein stability, leading to a shift of the melting curve to the right-hand side and an increased melting temperature of 55.3 ± 0.2 °C was observed (Figure 42A and B). Over three repetitions of this experiment, a mean temperature change of 2.8 ± 0.6 °C was detected, suggesting a thermal stabilization of PI4KB by Pipinib.

Titration of Pipinib at 54 °C, i.e. the temperature for which the biggest shift of the curve was observed, should show a dose-dependent stabilization of PI4KB. This approach is also called isothermal dose-response fingerprinting (ITDRF). Indeed, experiments with Pipinib yielded a dose-dependent stabilization curve (Figure 43A and B).

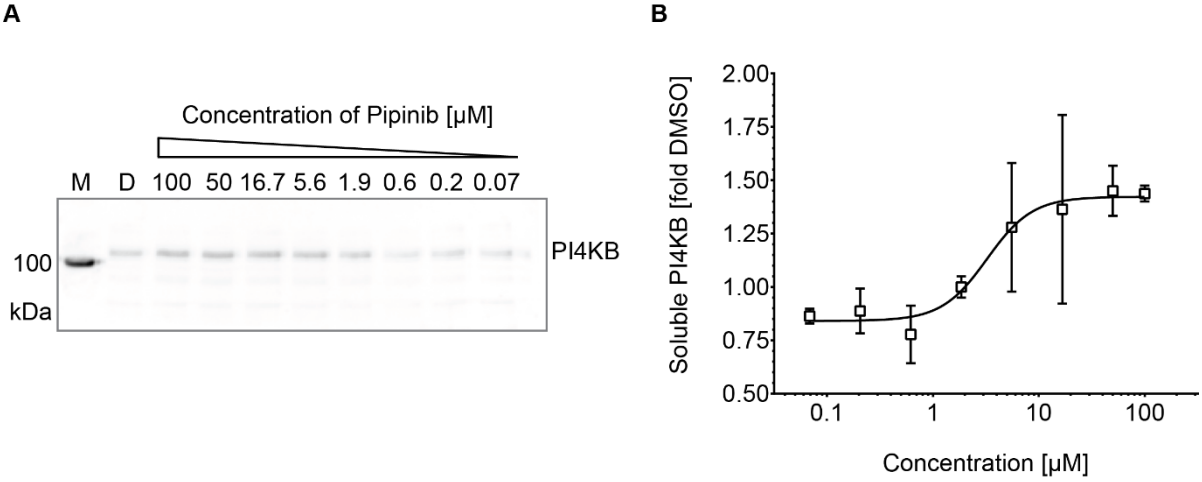

Figure 43. Isothermal titration curve. A. Immunoblot detection of PI4KB solubility. NIH/3T3 cell lysate was aliquoted and incubated with different concentrations of Pipinib or DMSO (D) as a control for 10 min. The lysates were then heated to 54 °C before ultracentrifugation to remove insoluble proteins. The supernatant was separated via SDS-PAGE, transferred to a PVDF membrane, which was then blocked and stained with an antibody against PI4KB. This blot is representative of independent experiments (n=4). **B.** Quantification of PI4KB band intensity from A and three further repetitions. Band intensity was quantified using the image studio software and normalized to the DMSO-treated sample. Data are mean values of independent experiments (n=4) ± SD.

Even though two data points exhibit a large standard deviation, an overall trend towards increased stability for increased concentrations of Pipinib was observed. *The ITDRF experiments were performed by Alexandra Brause.*

5.4.6 PI4KB depletion leads to Hh inhibition and sensitizes cells towards Pipinib

To investigate whether interference with PI4KB function inhibits Hh signaling, two approaches can be applied. On the one hand, other, structurally unrelated, inhibitors can be evaluated for

effects on Hh signaling. On the other hand, PI4KB expression can be downregulated before assessing Hh signaling pathway activity. In this thesis, both approaches were applied.

5.4.6.1 Application of structurally unrelated PI4KB inhibitors

Dr. Radim Nencka and Dr. Ivana Mejdrová, collaboration partners at the IOCB Prague, provided three published and selective inhibitors of PI4KB, compounds **10**, **11** and **12** (Figure 44A)[78]. These compounds are PI4KB inhibitors, derived from compound **9**[77] and PIK93, a PI 3,4-kinase inhibitor[72] (both also in Figure 44A). They potently inhibit PI4KB activity with IC_{50} values of 6.1 nM, 19.1 nM and 5.3 nM, respectively. Evaluation of these next generation PI4KB inhibitors in an osteogenesis screen at COMAS returned IC_{50} values of 0.2 ± 0.04 µM, 2.1 ± 0.3 µM and 0.1 ± 0.01 µM for compounds **10**, **11** and **12**, respectively. Unfortunately, the compounds were found to be equally or even more potent in decreasing cell viability with IC_{50} values of 0.1 µM, 0.7 µM and 0.03 µM, respectively.

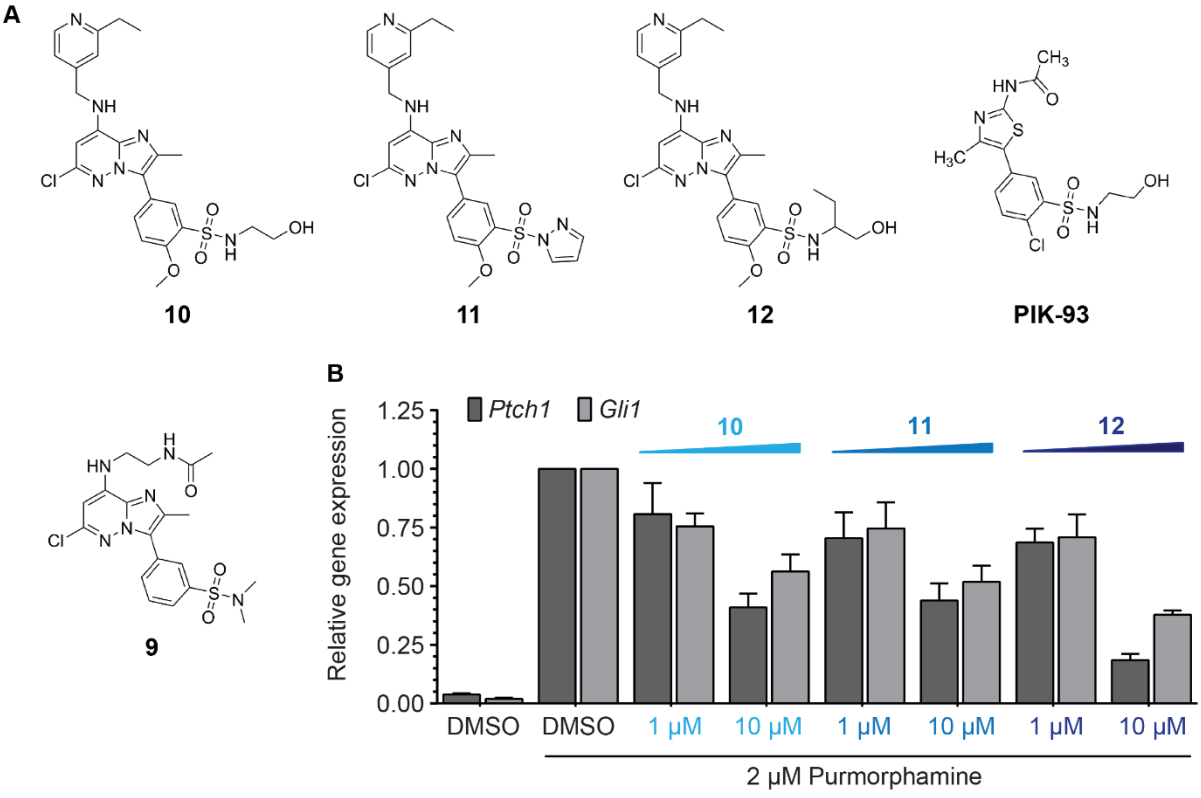

Figure 44. Effects of PI4KB inhibitors on Hh signaling. A. Chemical structures of next generation PI4KB inhibitors (compounds **10**, **11** and **12**), a first generation PI4KB inhibitor (compound **9**) and PIK-93, a PI 3,4-kinase inhibitor. **B.** Evaluation of Hh target gene expression. NIH/3T3 cells were treated with 2 µM Purmorphamine and the compounds or DMSO as a control for 48 h. After this, the cells were lysed, RNA was isolated and reverse transcribed into cDNA: Using primers for *Ptch1* and *Gli1* as Hh target genes and *Gapdh* as a reference gene, qRT-PCR was carried out to retrieve expression levels. Data are mean values of biological replicates (n=3) ± SD.

Since osteogenesis is an indirect assay and measured over a long incubation time of 96 h, Hh target gene expression (48 h treatment) was evaluated as an orthogonal approach. All three PI4KB inhibitors were found to inhibit Hh signaling in a dose-dependent manner (Figure 44C). Compound **13**, being most active against PI4KB, was also most potently inhibiting Hh target gene expression. Remarkably, compared to their PI4KB IC_{50} values, high concentrations of **10**, **12** and **13** are required to induce Hh signaling pathway inhibition. Of course, *in vitro* activity cannot be compared to inhibition in a complex cellular context. Lower potency in cells can be explained by permeability hindrance, compound processing by cellular enzymes or unspecific binding to other proteins, which reduces the effective cellular concentration.

5.4.6.2 Genetic depletion of PI4KB

5.4.6.2.1 siRNA-mediated depletion of PI4KB

Small interfering RNA (siRNA) was used to lower the expression of PI4KB in C3H10T1/2 cells, which were used in the osteoblast differentiation assay, and NIH/3T3 cells, which were used to determine Hh target gene expression. The siRNA binds to messenger RNAs (mRNAs) via complementary base pairing and induces their degradation. Because the mRNA cannot be translated into a protein anymore, protein levels decrease over time. Using this technique, a knockdown efficiency of 95.4% and 96.8% was achieved using 7.5 and 10 nM PI4KB siRNA in C3H10T1/2 cells, respectively (Figure 45A and B). When testing four different concentrations of Pipinib after Hh signaling pathway activation with 2 µM Purmorphamine, treatment with PI4KB siRNA increased the inhibitory effect of Pipinib by approx. 2-fold at concentrations of 0.1 and 0.4 µM, i.e. 35% inhibition (NT siRNA) was increased to 75% (PI4KB siRNA), resulting in a stronger inhibition of osteogenesis (Figure 45B). At higher compound concentrations, inhibition of osteogenesis was similar in cells treated with PI4KB and non-targeting siRNA. A possible explanation is that the maximum inhibition achievable with Pipinib was already reached at that concentration under wildtype PI4KB expression levels and that a further decrease of protein levels would not amplify this effect. It was further noted that overall pathway activity was slightly decreased upon PI4KB knockdown, even though this was not observable for all repetitions of the experiment, leading to a high standard deviation. To determine IC_{50} values for inhibition of osteogenesis after PI4KB knockdown, a titration of Pipinib was performed in cells at two different siRNA concentrations of 7.5 nM (Figure 45D) and 10 nM (Figure 45E). For both siRNA concentrations, osteogenesis activity was reduced for all tested compound concentrations compared to non-targeting siRNA. For 7.5 nM PI4KB siRNA, it was not possible to fit a curve for IC_{50} determination. For 10 nM, IC_{50}

values of 4.9 ± 8.3 µM and 0.2 ± 1.8 µM were obtained for PI4KB and non-targeting siRNA, respectively. Thus, an increased compound potency after PI4KB depletion, i.e. a sensitization of these cells towards Pipinib treatment, can be assumed.

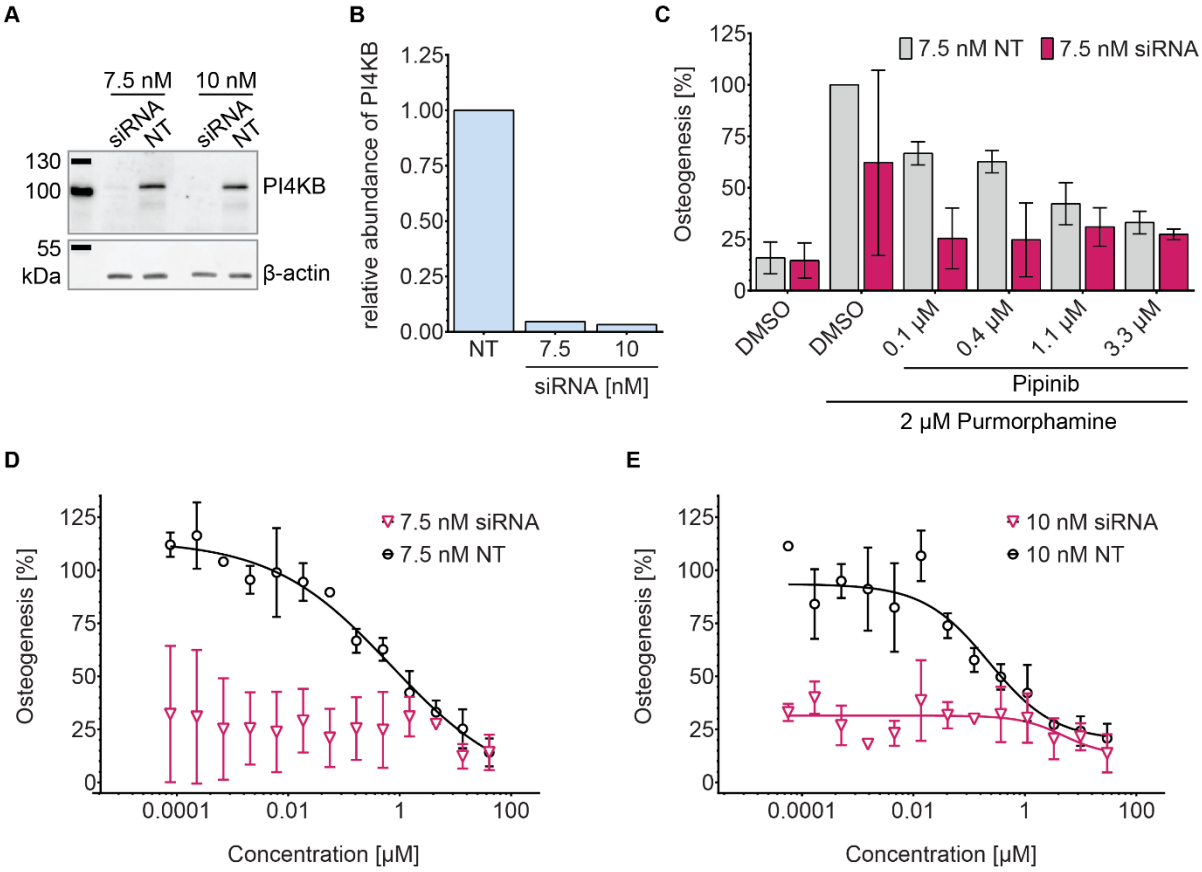

Figure 45. PI4KB depletion via siRNA in C3H10T1/2 cells. A. Knockdown efficiency determined via immunoblotting. C3H10T1/2 cells were transfected with PI4KB siRNA (siRNA) or non-targeting siRNA (NT, control) for 24 h and subsequently treated with the compounds or DMSO for 96 h. Cells were then lysed and proteins were separated on an SDS-PAGE. Proteins were transferred onto a PVDF membrane, which was then blocked and incubated with an anti-PI4KB antibody as well as an IR800CW secondary antibody. **B.** Quantification of protein bands from A. PI4KB intensity was normalized to β-actin band intensity and the NT sample was set to 1 (n=1). **C, D and E.** Osteoblast differentiation assay. Cells were treated as described in A. After lysis, as a measure of osteogenesis, alkaline phosphatase activity was detected. Data were normalized to NT-Purmorphamine-DMSO-treated cells and are mean values of biological replicates (n=3) ± SD. **C.** The Bar graph shows induction of osteogenesis for selected concentrations of Pipinib. **D and E.** Dose-response curves for Pipinib in cells treated with 7.5 nM siRNA (D) or cells treated with 10 nM siRNA (E).

In NIH/3T3 cells, PI4KB levels were decreased by 66 ± 9% (Figure 46A and B). For Hh target gene expression, decreased levels of *Ptch1* and *Gli1* mRNA could be detected upon knockdown with PI4KB siRNA (Figure 46C). At a concentration of 10 µM, there was a hint for a slightly increased compound potency but due to high standard deviations, no definite

conclusion could be drawn (this work was *performed by M.Sc. Elisabeth Hennes, MPI Dortmund, as part of her Master thesis*).

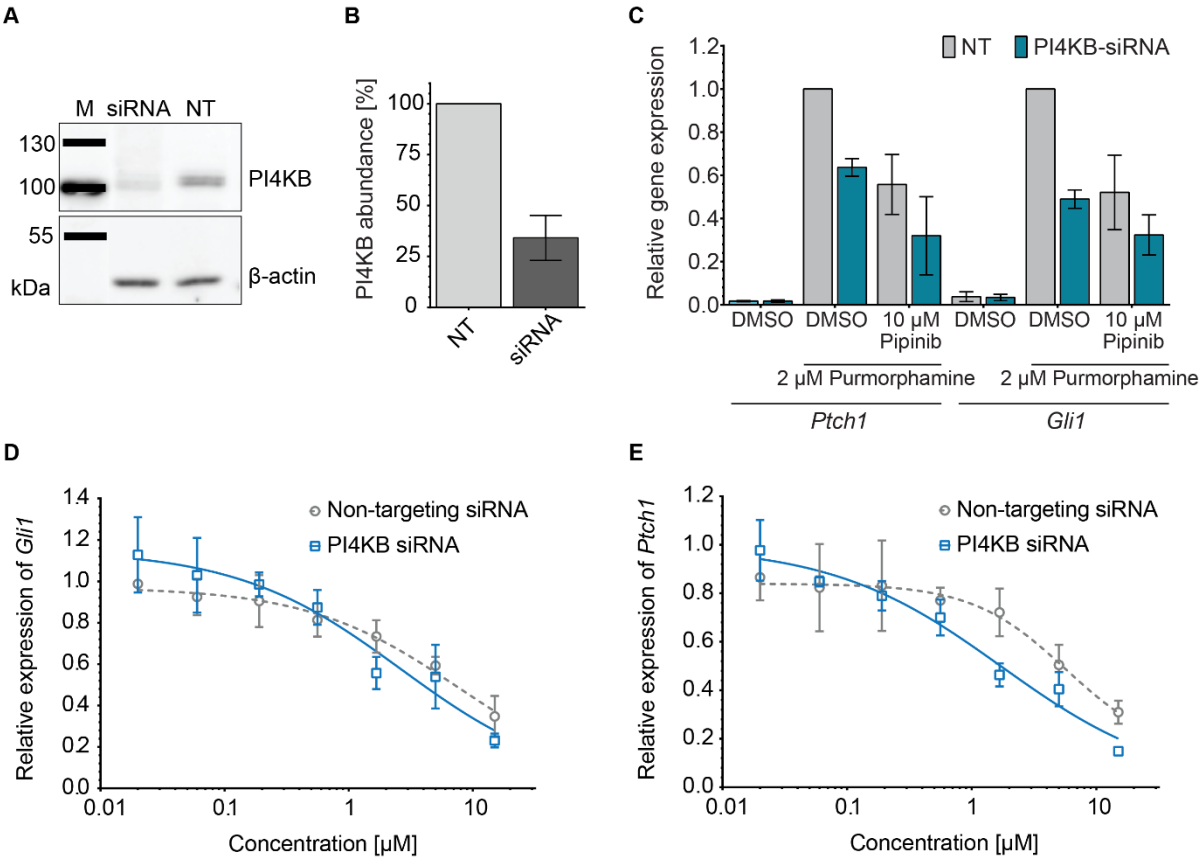

Figure 46. PI4KB depletion via siRNA in NIH/3T3 cells. A. Knockdown efficiency determined via immunoblotting. NIH/3T3 cells were transfected with 30 nM siRNA for 48 h before DMSO (control) treatment for another 48 h. Cells were then lysed and proteins separated via SDS-PAGE before transfer onto a PVDF membrane and subsequent blocking and staining of the membrane with primary (anti-PI4KB, anti-β-actin) and secondary (anti-rabbit-IR800CW) antibodies. **B.** Quantification of protein bands from A. PI4KB intensity was normalized to β-actin intensity and the NT sample was set to 100%. Data are mean values of biological replicates (n=3) ± SD. **C, D and E.** Evaluation of Hh target gene expression. NIH/3T3 cells were treated as described in A. After compound/DMSO treatment, cells were lysed, RNA was isolated, transcribed into cDNA and employed in qRT-PCR using primers for Hh target genes *Ptch1* and *Gli1* as well as *Gapdh* (reference). Data are mean values of biological replicates (n=3) ± SD. **C.** The Bar graph shows induction of target gene expression for selected concentrations of Pipinib. Data were normalized to NT-Purmorphamine-DMSO-treated cells. **D and E.** Expression of *Gli1* (D) and *Ptch1* (E) after Pipinib titration. Data were normalized to the respective Purmorphamine-DMSO sample.

Considering the threshold effect observed in C3H10T1/2 cells (Figure 45C), Pipinib was also titrated in NIH/3T3 cells before determination of Hh target gene expression levels. PI4KB depletion led to a decrease of the IC_{50} value from 7.3 ± 2.4 µM to approx. 1.6 ± 0.5 µM for *Gli1* and from 5.2 ± 2.5 µM to approx. 1.6 ± 0.3 µM for expression of *Ptch1* (Figure 46D and

E). These results confirm the increased potency of Pipinib after siRNA knockdown of PI4KB in C3H10T1/2 cells.

5.4.6.2.2 CRISPR-Cas9-mediated depletion of PI4KB

As a further proof that PI4KB is required for proper Hh signaling, a complete knock-out of PI4KB via the CRISPR-Cas9 technique was attempted in NIH/3T3 cells. If PI4KB is the main target of Pipinib, a complete removal of this protein is expected to impair Hh signaling while compound efficacy should be lost.

As described in 4.2.2.3, the CRISPR-Cas technique uses the Cas9 nuclease, which is directed to specific sites in the DNA via a small guiding RNA (sgRNA), to induce double strand breaks in the DNA. These DNA lesions lead to error prone DNA repair, which, in many cases, results in gene silencing. Using sgRNAs that are complementary to the genomic sequence of a gene of interest, the system can be exploited to create knockout cell lines. For this thesis, the CRISPR-Cas technique was employed to create a PI4KB knockout cell line derived from NIH/3T3 cells. Simultaneous application of two different sgRNAs should induce a large deletion of 9094 bp in the PI4KB genomic sequence (Figure 47A).

To screen for positive clones that contain the deletion, two primer sets were used. The deletion primers (D) target genomic DNA (gDNA) outside of the deletion region and, thus, produce a large fragment of 10,234 bp in case of a negative clone (non-deletion) and a small fragment of 1,458 bp in case of a positive clone (deletion, Figure 47B). The other set of primers (non-deletion primers, N) targets the deletion region and, thus, does not produce a fragment in case of a positive clone while a 2377 bp fragment will be obtained in case of a negative clone (Figure 47C).

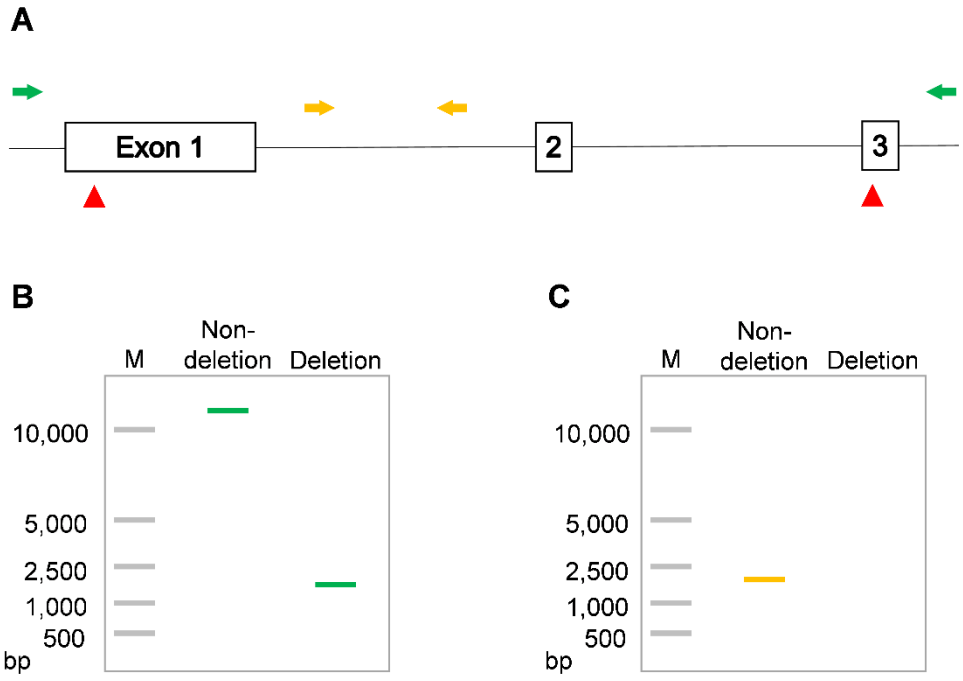

Figure 47. Design of deletion and non-deletion primers. A. Primer location on the PI4KB locus. The Cas9 nuclease will cut in exon 1 and exon 3 (indicated by red triangles). The deletion primers (green arrows) bind outside of the deletion region, whereas the non-deletion primers (orange arrows) bind inside the deletion region. **B.** Expected bands after PCR with deletion primers. In case of a negative clone (non-deletion), the primers outside of the deletion region will produce a large DNA fragment of 10,237 bp. In case of a positive clone (deletion), the produced fragment lacks the deleted region and will be smaller (1458 bp). **C.** Expected bands after PCR with non-deletion primers. In case of a negative clone (non-deletion), the primers inside the deletion region will produce a medium sized DNA fragment of 2,377 bp. In case of a positive clone (deletion), the primers cannot bind, and no product will be obtained.

Using gDNA from bulk cells after CRISPR-Cas treatment, the screening primers were optimized regarding the annealing temperature for the PCR (Figure 48B). The displayed results were obtained at an annealing temperature of 58 °C and confirm that both positive (band at approx. 1,500 bp) and negative (band at approx. 2,500 bp) clones are present within the bulk population.

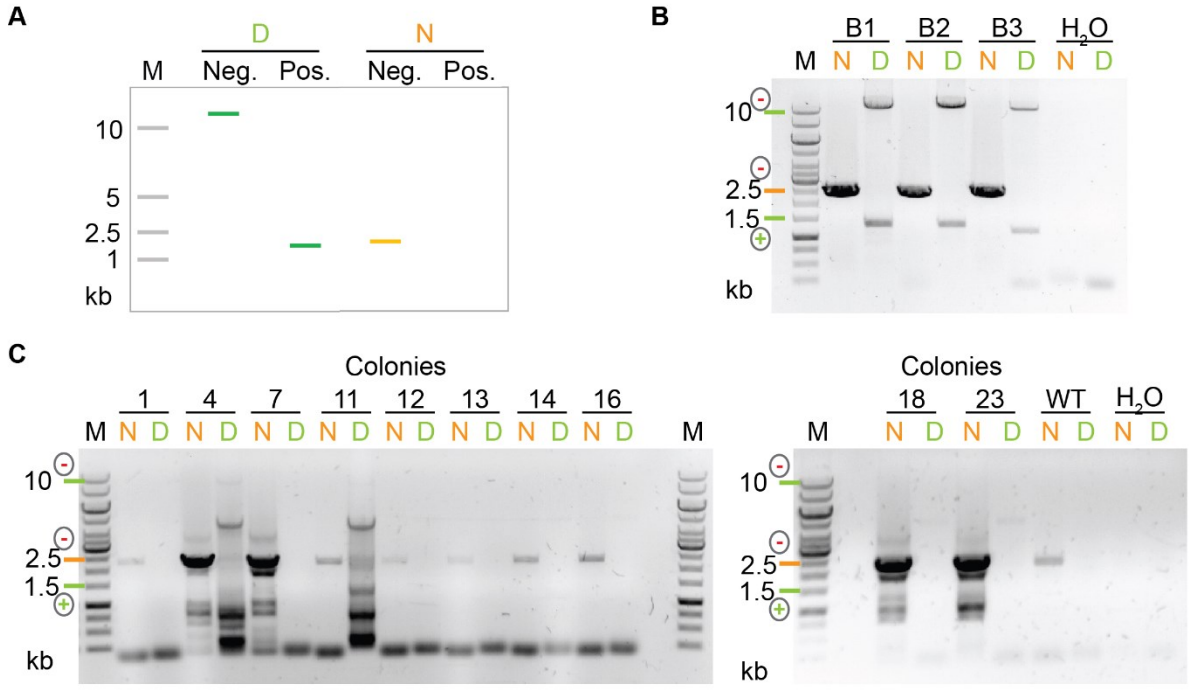

Figure 48. Generation of NIH/3T3-PI4KB-KD cells – evaluation on DNA level. A. Illustration of expected DNA bands for negative (neg.) and positive (pos.) clones when using deletion (D) and non-deletion (N) primers. **B.** Optimization of deletion screening primers. NIH/3T3 cells were transfected with two CRISPR-Cas-GFP-sgRNA constructs (used sgRNAs: bulk 1 (B1): 2a and 4b, bulk 2 (B2): 5a and 5b, bulk 3 (B3): 7a and 8b) to induce a large deletion inside the PI4KB genomic sequence. After 48 h of transfection, cells were sorted for GFP intensity and the top 10% were re-plated. After growing to confluence, cells were detached and genomic DNA (gDNA) was isolated. A PCR was carried out using the isolated gDNA as a template and non-deletion (N) or deletion (D) primers at an annealing temperature of 58 °C to test for a successful deletion (n=1). **C.** Single cell clone screening. Cells of bulk 3 were seeded at very low density to allow the formation of single cell colonies. After colonies reached sufficient size, cells were detached and expanded in single wells. Upon confluence, cells were detached, gDNA was isolated and PCR was carried out as detailed in B (WT=wildtype, n=1).

The bulk cells were then seeded at low density to isolate single cell clones and retrieve a homogenous monoclonal PI4KB knockout cell line. Genomic DNA, which was isolated from several single cell clones, was then again amplified in a PCR employing D and N primers (Figure 48C). All single cell clones were positive for the 2,500 bp in the non-deletion PCR, suggesting that the deletion was not successful. The PCR reaction using D primers, however, did not yield the expected bands, not even for the wildtype control. As a secondary approach, the same clones were also screened for PI4KB protein levels using the immunoblot technique (Figure 49A and B). Here, clone 14 displayed the lowest PI4KB abundance (7%). When another batch of cells from clone 14 was lysed and analyzed via immunoblotting, the protein level was only decreased to approx. 40% (Figure 49C). Fluctuating protein levels and the absence of a complete knockout suggested that the cell population of clone 14 was not monoclonal after all. Therefore, cells from clone 14 were again seeded at low density to

retrieve single cell colonies and expand these for another round of clone screening (Figure 49D). Here, clone 21 showed the lowest level of PI4KB (24.6%).

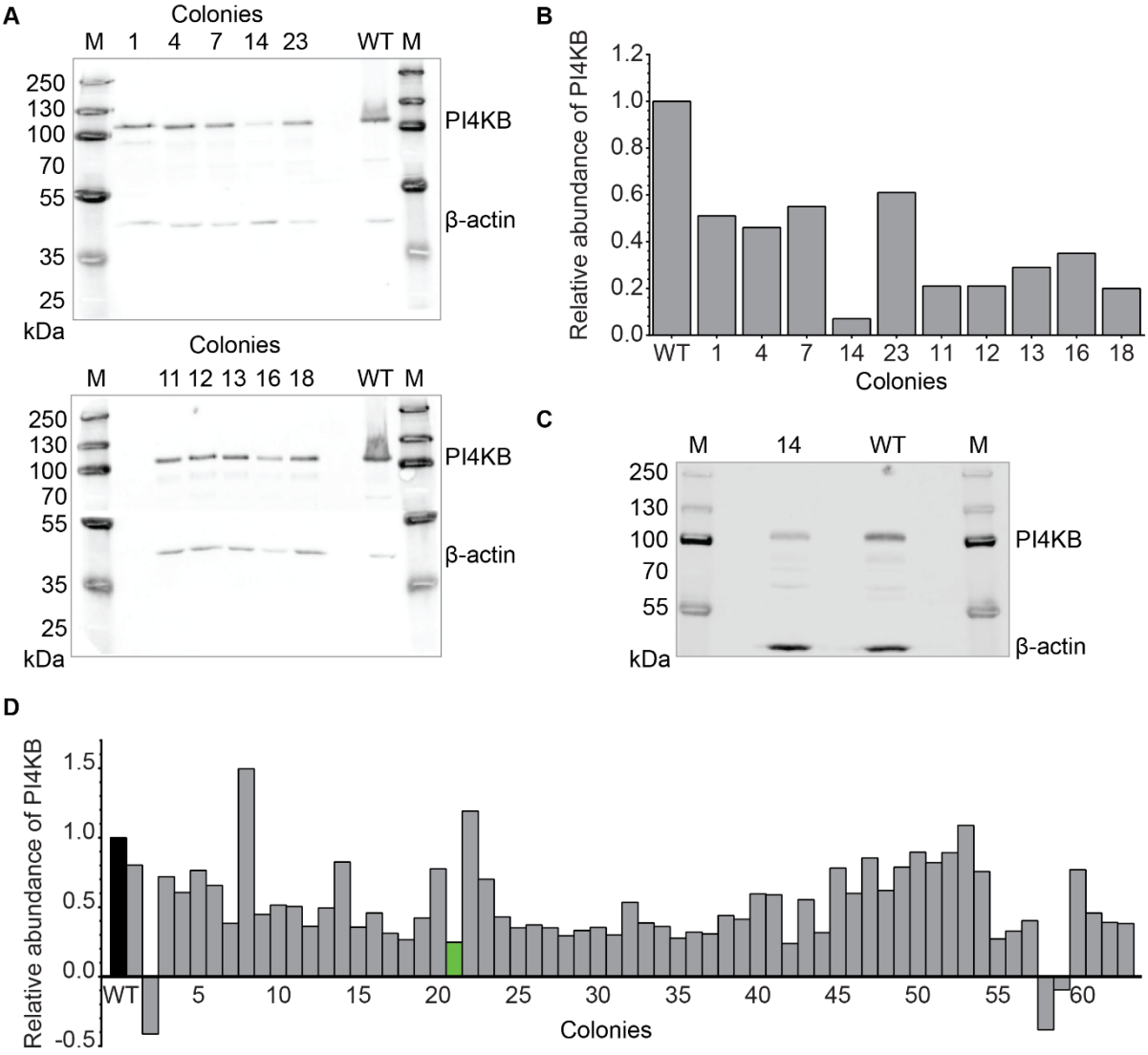

Figure 49. Generation of NIH/3T3-PI4KB-KD cells – evaluation on protein level. A.-D. PI4KB abundance for single cell clones. NIH/3T3 cells were transfected with two CRISPR-Cas-GFP-sgRNA constructs (7a and 8b) to induce a large deletion in the PI4KB gene. After 48 h of transfection, cells were sorted for GFP and the top 10% were seeded at very low density to allow the formation of single cell colonies. After colonies reached sufficient size, cells were detached and expanded in single wells and grown into confluence. Cells were then lysed, proteins were separated via SDS-PAGE, transferred onto a PVDF membrane, blocked and incubated with primary (PI4KB, β-Actin) and secondary (anti-rabbit-800CW) antibodies. **A.** First screen of single cell clones. **B.** Quantification of bands from A. The PI4KB signal was normalized to the β-Actin signal and levels are displayed relative to the wildtype (WT) control (n=1). **C.** Re-evaluation of PI4KB abundance of clone 14 (n=1). **D.** Screen of single cell clones from clone 14. The PI4KB signal was normalized to the β-Actin signal and levels are displayed relative to the wildtype (WT) control (n=1). Corresponding immunoblots can be found in the appendix (12.4).

Another round of CRISPR-Cas treatment was attempted to achieve a full knockout, but the cells died directly after transfection. PI4KB is part of the essantialome[185], i.e. a set of genes that was shown to be needed for viability or optimal fitness in a large scale experiment in two haploid cell lines[185]. Thus, a complete knockout of PI4KB might be lethal to the cells. Because of this, only cells with an incomplete knockout would survive the CRISPR-Cas nuclease treatment. Clone 21 (labelled in green) was selected for genetic validation of PI4KB and was entitled as 3T3-PI4KB-KD cell line. Throughout all repetitions of the experiment, an average knockdown of 61.6 ± 5.3 % (Figure 50A and B) was observed.

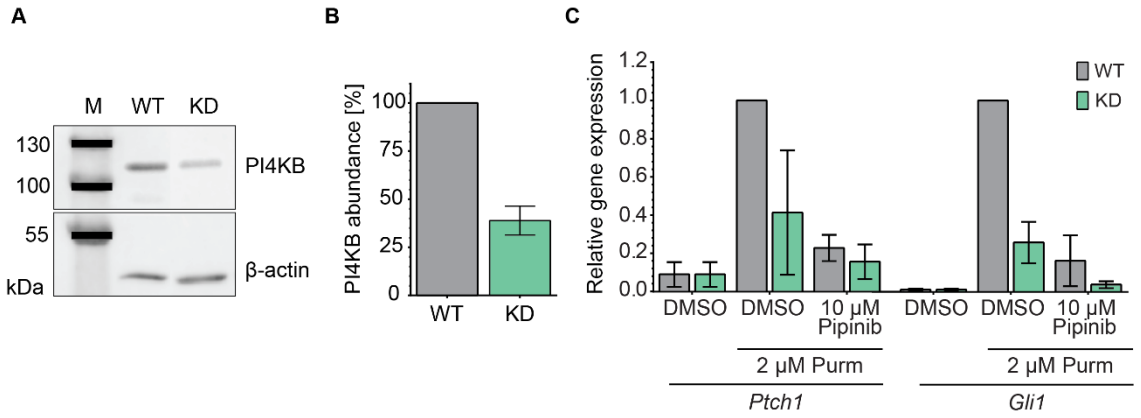

Figure 50. Evaluation of Hh target gene expression after CRISPR-Cas-mediated knockdown of PI4KB. A. Knockdown efficiency. NIH/3T3-PI4KB-KD (KD) and wildtype NIH/3T3 (WT) cells were treated with DMSO for 48 h. After this, cells were lysed, proteins were separated via SDS-PAGE and transferred onto a PVDF membrane that was blocked and incubated with primary (PI4KB, β-Actin) and secondary (anti-rabbit-800CW) antibodies. **B.** Quantification of bands from A. The PI4KB signal was normalized to the β-Actin signal and levels are displayed relative to the wildtype (WT) control. Data are mean values of biological replicates (n=3) ± SD. **C.** Hh target gene expression. NIH/3T3-PI4KB-KD (KD) and wildtype NIH/3T3 (WT) cells were treated with 2 µM Purmorphamine and the compound or DMSO as a control for 48 h. After this, the cells were lysed, RNA was isolated and transcribed into cDNA: Using primers for *Ptch1* and *Gli1* as Hh target genes and *Gapdh* as a reference gene, qRT-PCR was carried out to retrieve gene expression levels. Data are mean values of biological replicates (n=3) ± SD.

Hh signaling pathway activity as measured by expression of Hh target genes *Ptch1* and *Gli1* was decreased in the knockdown cell line (Figure 50C). Similar to the siRNA experiment, 10 µM Pipinib leads to a slightly increased inhibition in 3T3-PI4KB-KD cells. In conclusion, all genetic experiments so far are coherent and suggest that PI4KB is a positive regulator of Hh signaling. Additionally, the titration of Pipinib after siRNA-mediated depletion of PI4KB suggests a sensitization of the cells towards Pipinib treatment.

5.4.7 Overexpression of PI4KB

Another approach to validate a target is to increase its protein abundance. In theory, the increased protein amount should scavenge the inhibitor, thus reducing its potency. To assess whether this is true for PI4KB and Pipinib, C3H10T1/2 cells were transfected with a nEGFP-PI4KB expression construct and an empty control vector (Figure 51A) as *part of the Master thesis of M.Sc. Elisabeth Hennes, MPI Dortmund*.

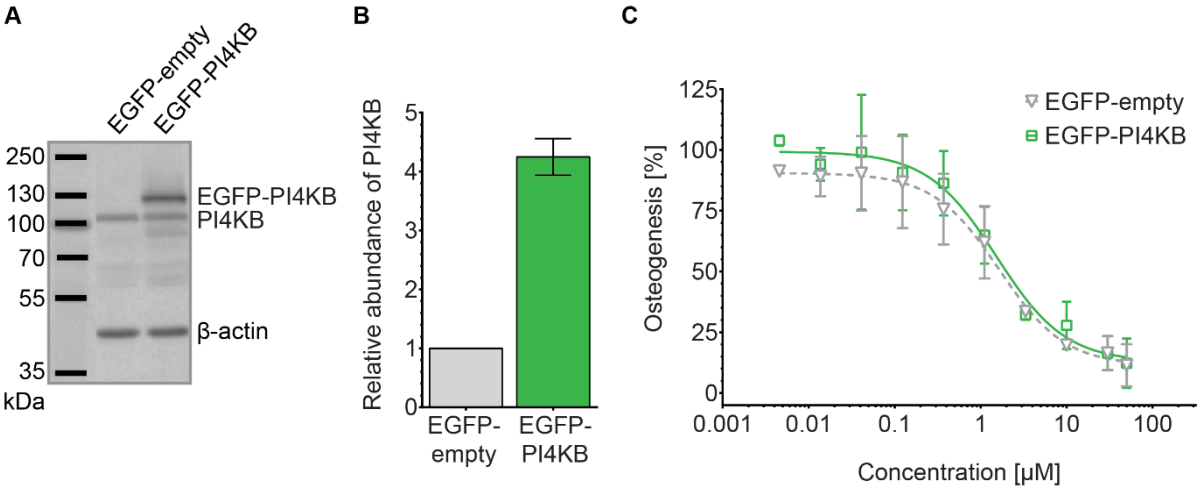

Figure 51. Evaluation of the effects of EGFP-PI4KB overexpression on osteogenesis. A. Fold overexpression. C3H10T1/2 cells were transfected with 0.58 µg/ml EGFP-PI4KB construct (PI4KB) or the empty EGFP control vector (empty) for 24 h in bulk. Afterwards, cells were detached and seeded in a 96-well plate before addition of DMSO 5 h later. After incubation for 96 h, cells were lysed, proteins were separated via SDS-PAGE and transferred onto a PVDF membrane that was blocked and incubated with primary (PI4KB, β-actin) and secondary (anti-rabbit-800CW) antibodies. **B.** Quantification of bands from A and one further blot. The PI4KB signal was normalized to the β-actin signal and levels are displayed relative to the wildtype (WT) control. Data are mean values of independent experiments (n=2) ± SD. **C.** Osteoblast differentiation assay. Cells were treated as described in A. Additionally, Hh signaling was activated with 2 µM Purmorphamine. After an incubation of 96 h, cells were lysed and, as a measure of osteogenesis, alkaline phosphatase activity was detected. Data were normalized to DMSO-Purmorphamine-treated cells and are mean values of biological replicates (n=3) ± SD.

Here, an overexpression of 4.3 ± 0.2-fold was achieved (Figure 51B). When these cells were evaluated in an osteoblast differentiation assay, overexpressing cells show slightly higher differentiation values. The inhibitory potency of Pipinib, however, as measured by IC_{50} values of 2.2 ± 0.4 µM for control cells and 1.9 ± 0.2 µM for overexpressing cells, did not change. Since EGFP is a large protein and might impair proper protein folding, activity and/or localization, nFlag-cHis-PI4KB, whose small protein tags should have lesser impact on proper protein function, was additionally evaluated in C3H10T1/2 cells. Several plasmid concentrations were applied to evaluate concentration-dependent effects of protein dose.

Transfection of this construct led to lower PI4KB levels compared to nEGFP-PI4KB (Figure 52A and B).

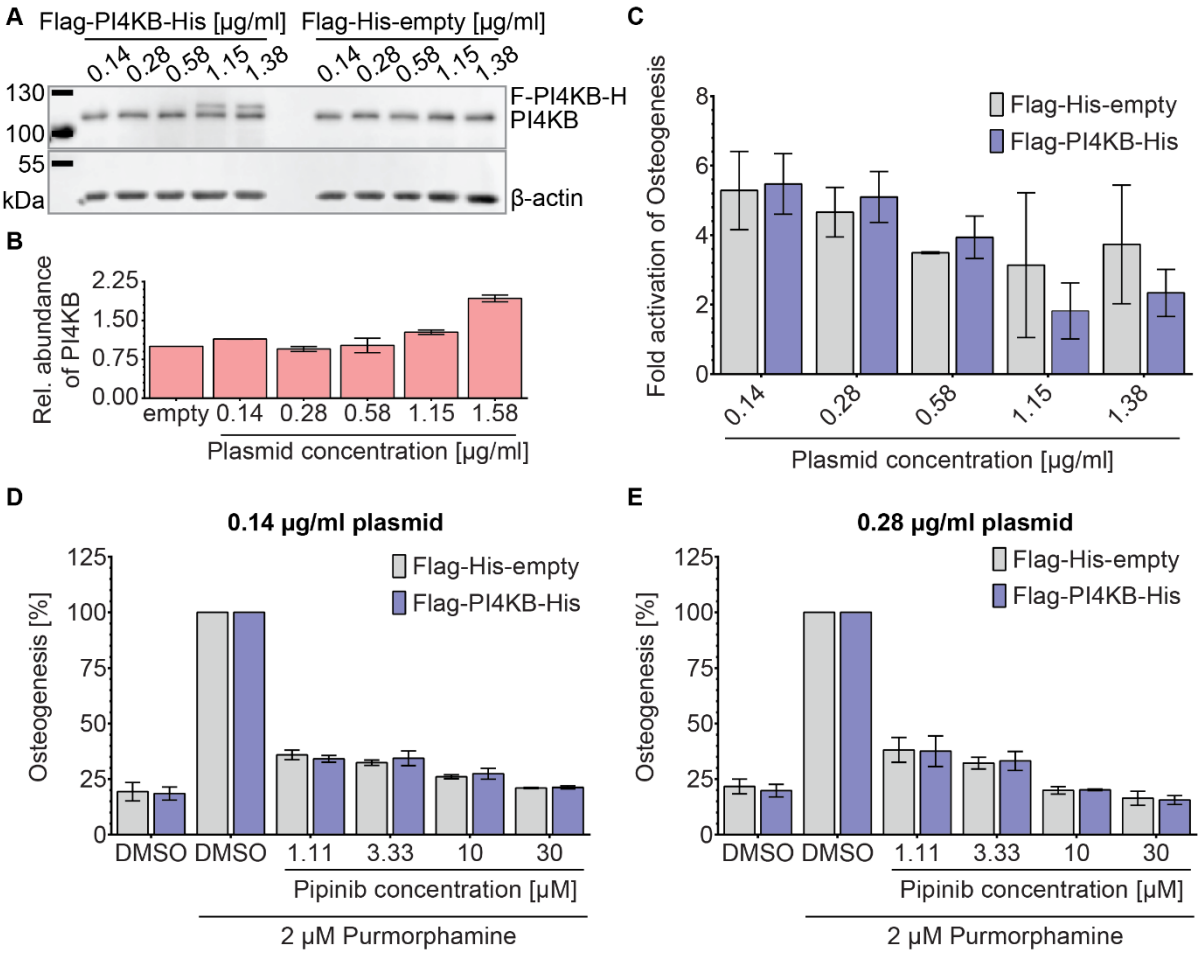

Figure 52. Evaluation of the effects of Flag-PI4KB-His overexpression on osteogenesis. A. Fold overexpression. C3H10T1/2 cells were transfected with an Flag-PI4KB-His construct (F-PI4KB-H) or the Flag-His-empty control vector for 24 h in bulk. Afterwards, cells were detached and seeded in a 96-well plate before addition of DMSO 5 h later. After an incubation of 96 h, cells were lysed, proteins were separated via SDS-PAGE and transferred onto a PVDF membrane that was blocked and incubated with primary (PI4KB, β-actin) and secondary (anti-rabbit-800CW) antibodies. The blot is representative for independent repetitions (n=2). **B.** Quantification of bands from A. The PI4KB signal was normalized to the β-actin signal and levels are displayed relative to the empty vector control. Data are mean values of independent experiments (n=2) ± SD. **C.** Osteoblast differentiation assay. Cells were treated as described in A, transfection was performed with different plasmid concentrations. Additionally, Hh signaling was activated with 2 µM Purmorphamine. After an incubation of 96 h, cells were lysed and, as a measure of osteogenesis, alkaline phosphatase activity was detected. For each plasmid concentration, values for DMSO-treated cells were set to 1 (not shown) to display fold activation of osteogenesis in the bar graph. Data are mean values of biological replicates (n=2) ± SD. **D-E.** Osteoblast differentiation assay. Cells were treated as described in C. Transfection was performed with a plasmid concentration of 0.14 µg/ml (D) or 0.28 µg/ml (E) and cells were additionally treated with different concentrations of Pipinib. Data were normalized to DMSO-Purmorphamine-treated cells and are mean values of biological replicates (n=2) ± SD.

At the highest plasmid concentration of 1.38 µg/ml, PI4KB was overexpressed 1.9 ± 0.1-fold. At lower plasmid concentrations, only slightly increased levels of PI4KB were observed. For

the highest plasmid concentrations of 1.15 and 1.38 µg/ml, osteogenesis was impaired (Figure 52C). Due to differences throughout the repetitions of the experiments, the standard errors are considerably high, and no clear effect can be concluded.

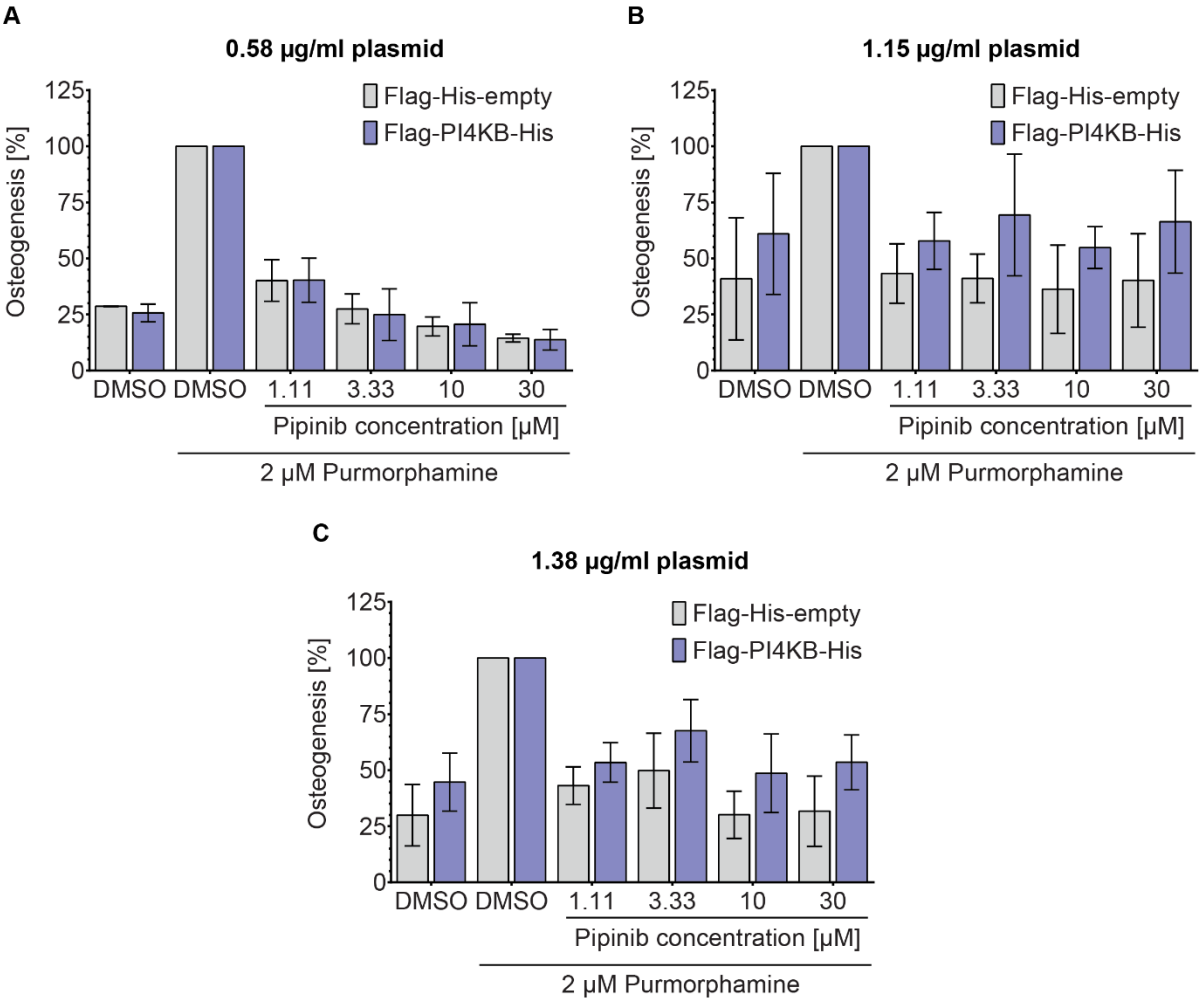

Figure 53. Evaluation of the effects of Flag-PI4KB-His overexpression on osteogenesis. A-C. Osteoblast differentiation assay. C3H10T1/2 cells were transfected with a Flag-PI4KB-His construct or the Flag-His-empty control vector for 24 h in bulk. Afterwards, cells were detached and seeded in a 96-well plate before addition of 2 µM Purmorphamine and the compound or DMSO as a control 5 h later. After an incubation of 96 h, cells were lysed and, as a measure of osteogenesis, alkaline phosphatase activity was detected. Transfection was performed with a plasmid concentration of 0.58 µg/ml (A), 1.15 µg/ml (B) or 1.38 µg/ml (C). Data were normalized to DMSO-Purmorphamine-treated cells and are mean values of biological replicates (n=2) ± SD.

Regarding the potency of Pipinib, evaluation of osteogenesis yielded similar results for PI4KB overexpressing and control cells for plasmid concentrations of 0.14 and 0.28 µg/ml (Figure 52D and E). Considering the PI4KB protein levels, which are almost unchanged under these conditions (Figure 52B), this result is not unexpected. The same holds true for a plasmid concentration of 0.58 µg/ml (Figure 53A). For concentrations of 1.15 and 1.38 µg/ml,

however, protein levels of PI4KB are increased and also compound potency is impaired (Figure 53B and C). For all evaluated concentrations of Pipinib, cells that are overexpressing PI4KB show increased osteogenesis. While showing a trend, the observed differences were not significant as determined with an unpaired t-test and a confidence interval of 95%.

To further investigate whether Hh signaling is affected by PI4KB overexpression, target gene expression of NIH/3T3 cells was monitored as *part of the Master thesis of M.Sc. Elisabeth Hennes, MPI Dortmund*. In this cell line, an overexpression of 33.1 ± 4.8-fold was achieved with the EGFP-PI4KB vector (Figure 54A and B).

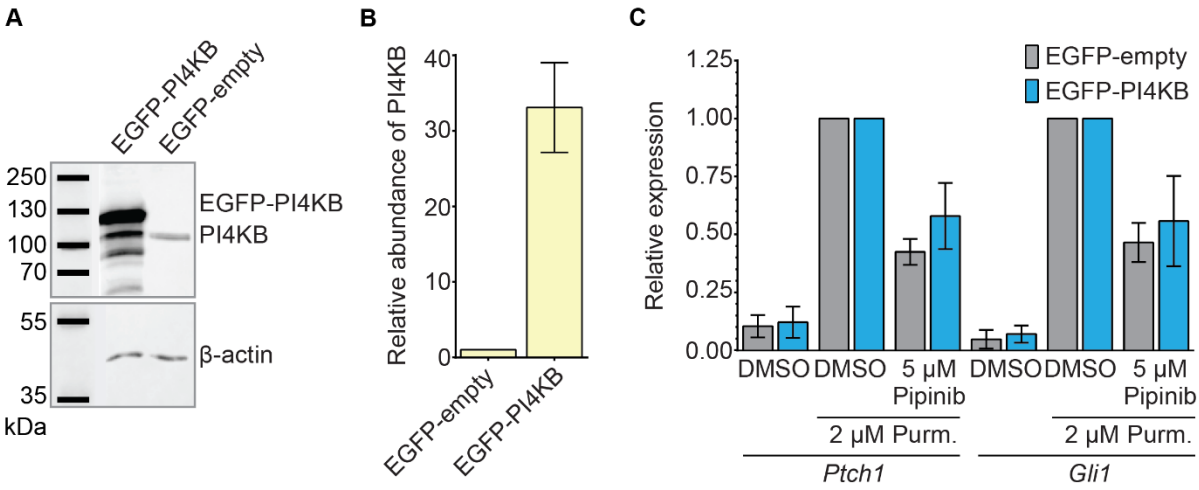

Figure 54. Evaluation of Hh target gene expression after overexpression of EGFP-PI4KB. A. Fold overexpression of PI4KB. NIH/3T3 cells were transfected with 0.5 µg/ml of an EGFP-PI4KB construct or an EGFP-empty vector 48 h before cells were treated with DMSO and incubated for another 48 h. Cells were then lysed, proteins were separated via SDS-PAGE and transferred onto a PVDF membrane that was blocked and incubated with primary (PI4KB, β-actin) and secondary (anti-rabbit-800CW) antibodies. The blot is representative of independent repetitions (n=3). **B.** Quantification of bands from A. The PI4KB signal was normalized to the β-actin signal and levels are displayed relative to the wildtype (WT) control. Data are mean values of independent experiments (n=3) ± SD. **C.** Hh target gene expression. Cells were treated as described in A. Additionally, Hh signaling was activated with 2 µM Purmorphamine and 5 µM of Pipinib was applied. After an incubation time of 48 h, cells were lysed, RNA was isolated and transcribed into cDNA: Using primers for *Ptch1* and *Gli1* as Hh target genes and *Gapdh* as a reference gene, qRT-PCR was carried out to retrieve gene expression levels. Data are mean values of biological replicates (n=3) ± SD.

For both *Ptch1* and *Gli1* target genes, a slight tendency towards a decreased potency of Pipinib was observed at a concentration of 5 µM (Figure 54C). However, according to an unpaired t-test with a confidence interval of 95%, these differences were not significant.

5.4.8 Evaluation of other possible kinase targets

While having thoroughly evaluated a possible relevance of PI4KB for both Hh signaling and osteogenesis, the effect of the other possible kinase targets must be investigated as well. In chapter 5.4.3.1 four other potential targets were introduced: PIP5K1C, PIK3C2G, GAK and TTK. To assess the influence of these kinases on Hh signaling, siRNA-mediated depletion of protein expression was attempted. For PIP5K1C, GAK and TTK, a knockdown was achieved (Figure 55A). *These experiments were performed by Alexandra Brause*.

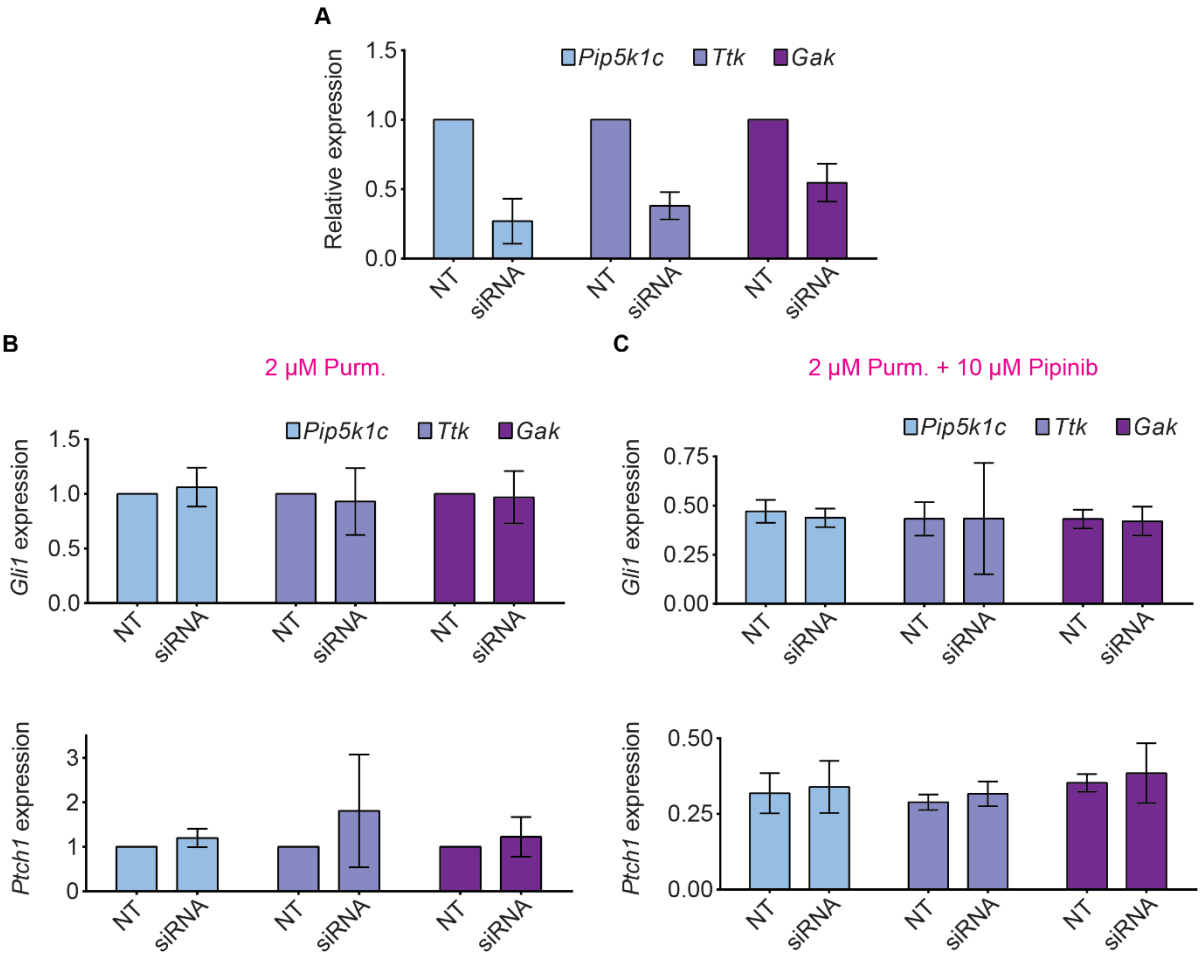

Figure 55. Evaluation of Hh target gene expression after siRNA-mediated knockdown of PIP5K1C, TTK or GAK. A. Knockdown efficiency. NIH/3T3 cells were transfected with 50 nM siRNA or non-targeting control (NT) for 48 h before DMSO treatment for another 48 h. Cells were then lysed, RNA was isolated, transcribed into cDNA and employed in qRT-PCR using primers for Hh target genes *Ptch1* and *Gli1* as well as *Gapdh* (reference). Data are mean values of biological replicates (n=3) ± SD. **B and C.** Evaluation of Hh target gene expression. NIH/3T3 cells were treated as described in A. Additionally, Hh signaling was activated with 2 µM Purmorphamine (B) and 10 µM Pipinib was applied (C). Data were normalized to NT-Purmorphamine-DMSO-treated samples and are mean values of biological replicates (n=3) ± SD.

At a maximum siRNA concentration of 50 nM, a knockdown of 73.1 ± 0.2%, 62 ± 0.1% and 45.4 ± 0.1% was achieved for PIP5K1C, TTK and GAK, respectively. Despite the high siRNA concentration, it was not possible to further reduce protein levels for GAK. Nevertheless, Hh signaling pathway activity measured by means of target gene expression was evaluated. Depletion of these kinases did not have an effect on the expression of *Gli1* and *Ptch1* (Figure 55B). For TTK, an increased expression of *Ptch1* was observed. However, since the standard deviation was high, and this behavior was not observed for *Gli1*, it was not considered as a significant effect. Addition of Pipinib did not lead to distinct effects in depleted or control cells, furthermore confirming that these kinases are not relevant for Hh signaling pathway activity or inhibition. For PIK3C2G, a sufficient knockdown was not achieved. To still evaluate this kinase, published and selective inhibitors of PIK3C2G[186] (Figure 56A) were *synthesized by Dr. Lucas Robke, MPI Dortmund*, and evaluated for inhibition of Hh signaling.

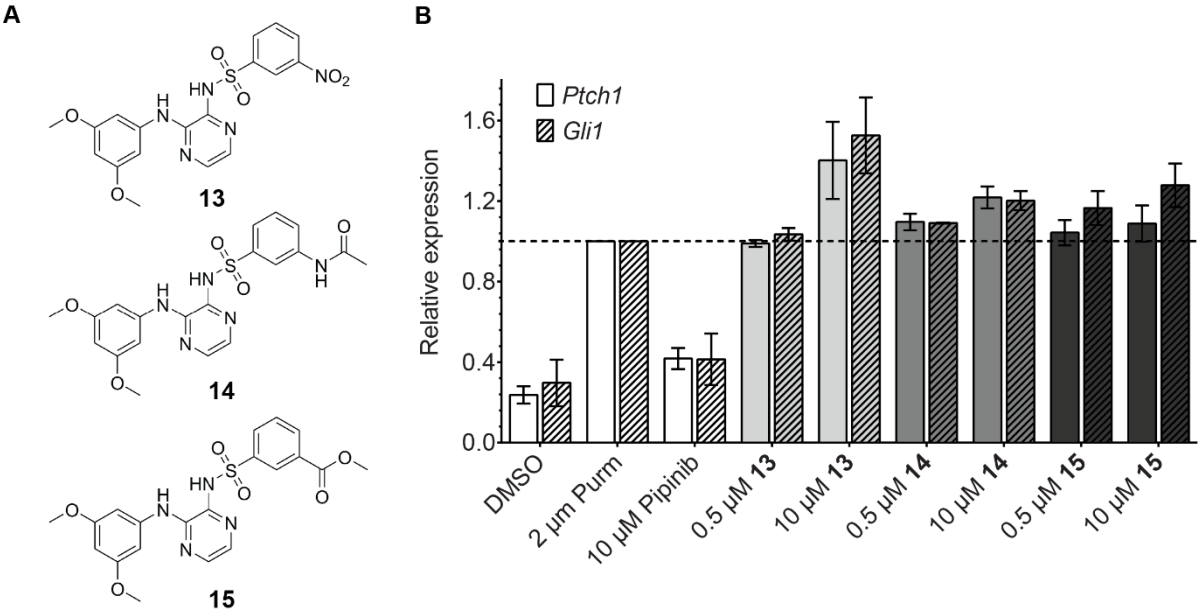

Figure 56. Evaluation of PIK3C2G as a Hh regulator by means of chemical inhibition. A. Chemical structures of the applied PIK3C2G inhibitors. **B.** Hh target gene expression. NIH/3T3 cells were treated with 2 µM Purmorphamine and the compounds or DMSO as a control for 48 h. After this, the cells were lysed, RNA was isolated and transcribed into cDNA. Using primers for *Ptch1* and *Gli1* as Hh target genes and *Gapdh* as a reference gene, qRT-PCR was carried out to retrieve expression levels. Data were normalized to DMSO-Purmorphamine-treated cells and are mean values of biological replicates (n=3) ± SD.

None of the tested inhibitors inhibited expression of the Hh target genes *Ptch1* and *Gli1*, while Pipinib led to reduced expression levels (Figure 56B). These results demonstrate that inhibition of PIK3C2G does not impair Hh signaling. Thus, it is unlikely that this kinase is relevant for Hh signaling or a mediator of Pipinib's effect on this pathway.

5.4.9 Pipinib inhibits growth of medulloblastoma cells

The Hedgehog signaling pathway plays an important role in the development and progression of cancer, the most prominent examples thereof are basal cell carcinoma and medulloblastoma.[15] To investigate whether Pipinib modulates cancer cell growth, its effect on the growth of the Hh responsive medulloblastoma DAOY cell line[187] was assessed. Using the IncuCyte live cell analysis system, cells were imaged over time and confluence was quantified as a measure of cell growth using the ZOOM software. Pipinib led to a growth reduction at the highest applied concentration of 30 µM. At 10 µM, no effect was observed (Figure 57A and B). The known GLI antagonist, GANT61[112], inhibited cell growth already at a concentration of 10 µM, displaying a higher potency compared to Pipinib (Figure 57A and C). The SMO antagonist Vismodegib did not reduce or inhibit growth of DAOY cells (Figure 57A and D). The known PI4KB inhibitor, compound **12**, however, reduced cell growth but did not reach the same extent of growth inhibition compared to Pipinib (Figure 57A and E).

To evaluate specificity of the growth inhibitory effects of Pipinib and compound **12**, a specific PI4KA inhibitor, compound **16**[76], was evaluated for growth inhibition as well. Although PI4KB and PI4KA both generate PI4P, due to their distinct localization within the cell (PM and Golgi), they have different functions[188]. Thus, a similar effect on cell growth could indicate a general growth inhibition due to PI4P depletion. Inhibition of PI4KA also caused mild growth inhibition at the highest applied concentration of 30 µM but variations among experiments was high (Figure 57A and F). This result suggests that Pipinib's growth inhibitory effect might not be specifically related to Hh inhibition, while inhibition of PI4KB has stronger effects on cell viability than inhibition of PI4KA.

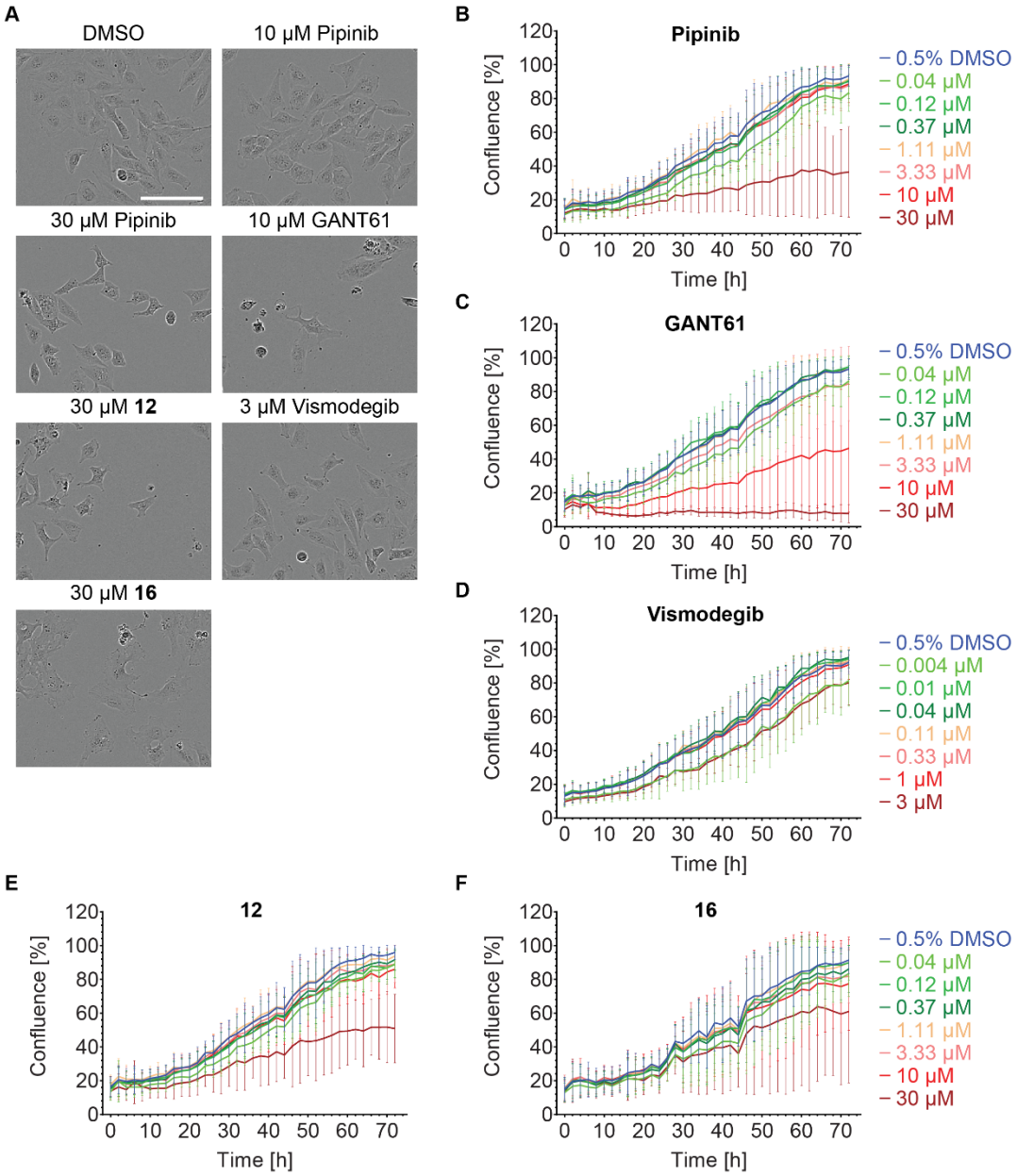

Figure 57. Influence of Hh signaling inhibitors on the growth of DAYO cells in the absence of a Hh activator. A. Phase-contrast images after compound treatment. DAOY cells were treated with the compounds or DMSO as a control and were incubated in the IncuCyte ZOOM for 72 h, while images were acquired every two hours. Images show a time point of 48 h and are representative of biological replicates (n≥2, scale bar: 150 µm). **B-F.** Quantification of cell confluence. Cells were treated as described in A. Confluence was quantified for each time point using the ZOOM software and plotted against the time to derive growth curves. Data are mean values of biological replicates ± SD. Titrations of Pipinib (B, n=4), GANT61 (C, n=4), Vismodegib (D, n=3), PI4KB inhibitor 12 (E, n=3) and PI4KA inhibitor 16 (F, n=2) were applied.

To evaluate this assumption, the same experiment was repeated with simultaneous activation of the Hh signaling pathway with 2 µM Purmorphamine. Here, similar results were obtained (Figure 58).

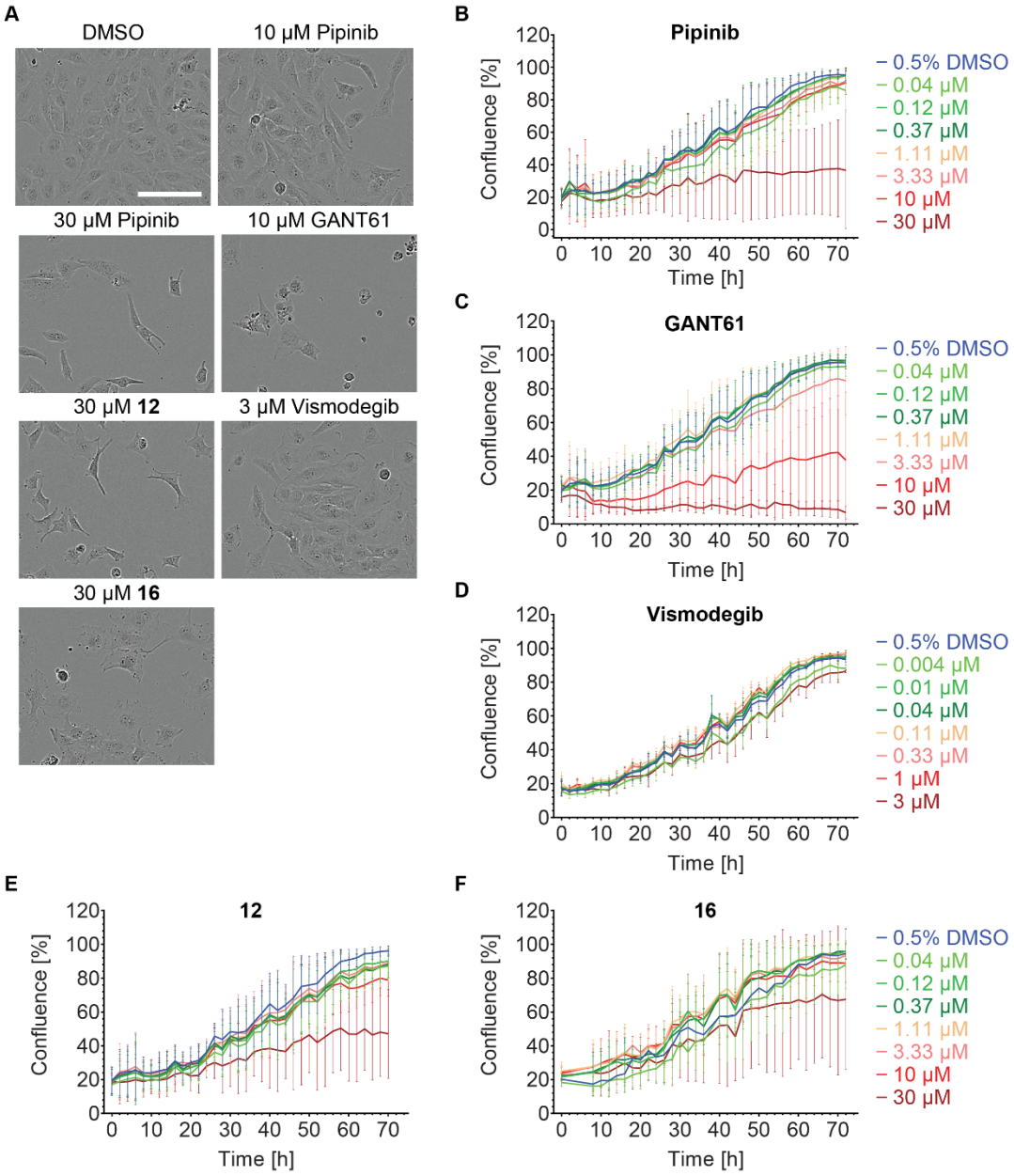

Figure 58. Influence of Hh signaling inhibitors on the growth of DAOY cells after Hh signaling pathway activation with Purmorphamine. A. Phase-contrast images after compound treatment. DAOY cells were treated with 2 µM Purmorphamine and the compounds or DMSO as a control and were incubated in the IncuCyte ZOOM for 72 h, while images were acquired every two hours. Images show a time point of 48 h and are representative of biological replicates (n≥2, scale bar: 150 µm). **B-E.** Quantification of cell confluence. Cells were treated as described in A. Confluence was quantified for each time point using the ZOOM software and plotted against the time to derive growth curves. Data are mean values of biological replicates ± SD. Titrations of Pipinib (B, n=4), GANT61 (C, n=4), Vismodegib (D, n=3), PI4KB inhibitor 12 (E, n=3) and PI4KA inhibitor 16 (F, n=2) were applied.

Purmorphamine co-treatment did not lead to different effects, indicating that Hh signaling pathway activity is not relevant for the growth inhibitory effect of Pipinib, GANT61 or

compounds **12** and **16**. To find out whether Pipinib's growth inhibitory effect is specific for medulloblastoma cells or affects non-cancer cells as well, growth of NIH/3T3 cells was monitored (Figure 59). When Hh signaling pathway was inactive and cells were maintained in full growth medium containing 10% FBS, Pipinib did not impair growth of NIH/3T3 cells (Figure 59A and B). When serum was reduced to 0.5%, Pipinib inhibited cell growth at 30 µM (Figure 59A and C). Even though the average of both curves of the independent experiments would have led to high standard deviations, which is why the curves are shown separately in Figure 59D, a similar trend can be observed.

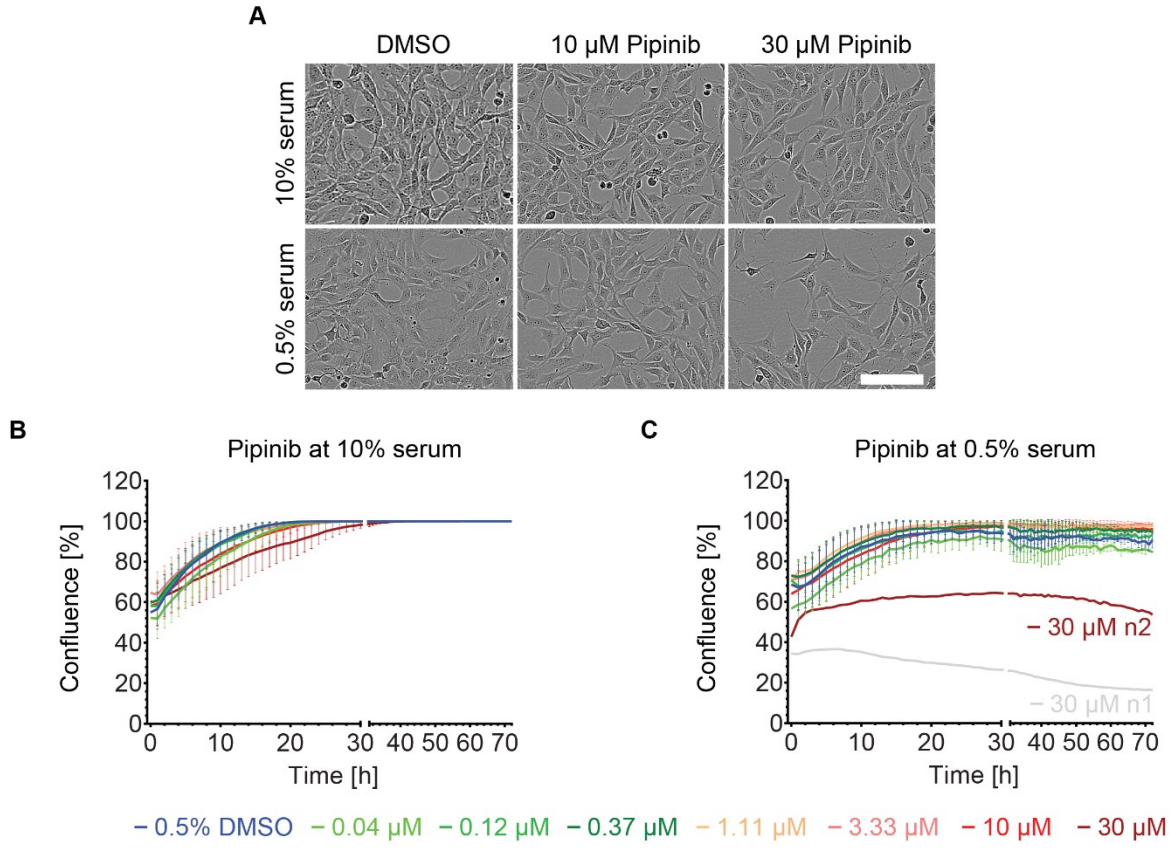

Figure 59. Influence of Pipinib on the growth of NIH/3T3 cells in absence of a Hh signaling pathway activator. A. Phase contrast images. NIH/3T3 cells were treated with the compound or DMSO as a control for 72 hours, while images were acquired every hour. Representative images of biological replicates (n=2) are shown. Scale bar: 150 µm. **B.-C.** Quantification of confluence. NIH/3T3 cells were treated as described in A. For each image, confluence was quantified with the ZOOM software and plotted against the time to derive growth curves. Data are mean values of biological replicates (n=2) ± SD. The cells were maintained at 10% (C) or 0.5% (D) serum.

As observed for DAOY cells, similar growth curves were obtained when Hh signaling was activated with 2 µM Purmorphamine in NIH/3T3 cells (Figure 60). Taken together, these

results indicate that Pipinib does not unselectively inhibit growth. It rather inhibits cell growth of DAOY cells and non-cancer NIH/3T3 cells only under starvation conditions. Cancer cells have an enhanced metabolism and thereby an increased energy consumption, which could explain why Pipinib shows a growth inhibitory effect even in full growth medium in medulloblastoma cells.

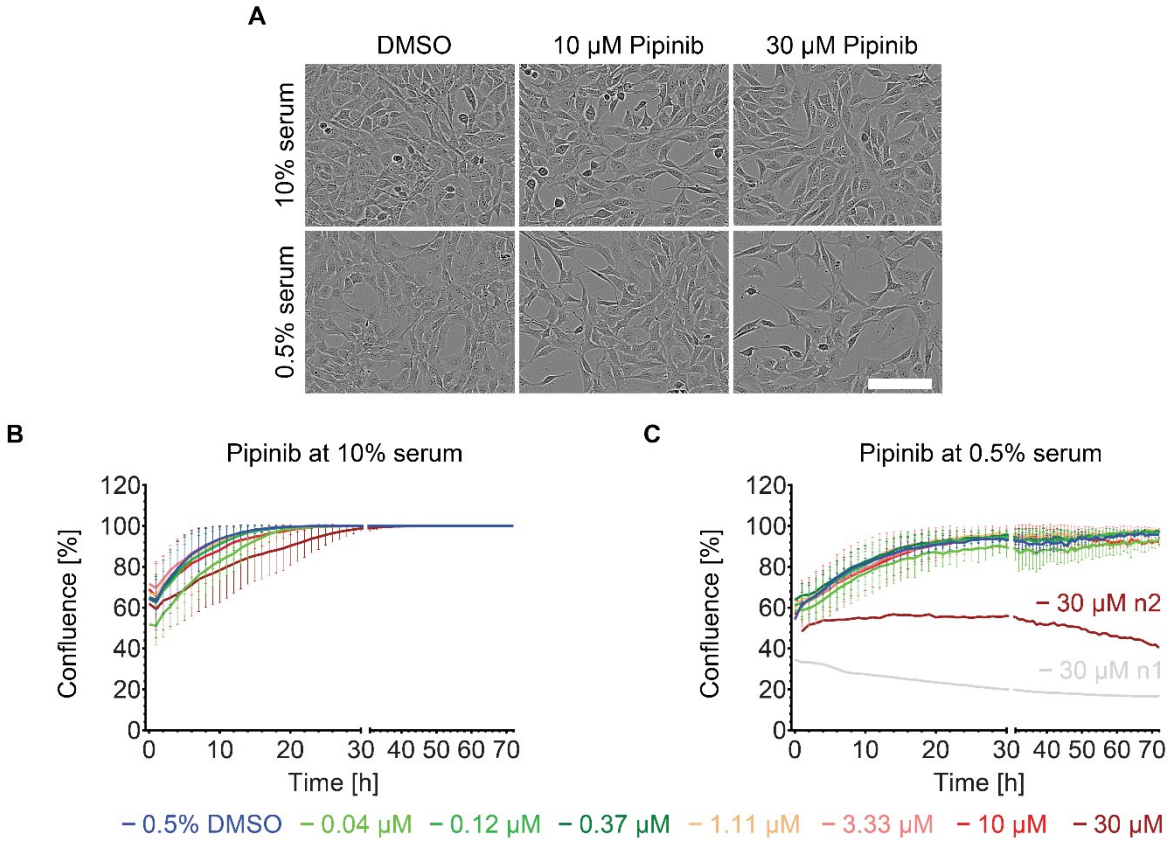

Figure 60 Influence of Pipinib on growth of NIH/3T3 cells in presence of 2 µM Purmorphamine. A. Phase contrast images. NIH/3T3 cells were treated with 2 µM Purmorphamine and the compound or DMSO as a control for 72 hours, while images were acquired every hour. Representative images of biological replicates (n=2) are shown. Scale bar: 150 µm. **B.-C.** Quantification of confluence. NIH/3T3 cells were treated as described in A. For each image, confluence was quantified with the ZOOM software and plotted against the time to derive growth curves. Data are mean values of biological replicates (n=2) ± SD. The cells were maintained at 10% (C.) or 0.5% (D.) serum.

Since Hh signaling pathway activation by means of Purmorphamine treatment did not change the phenotype in NIH/3T3 and in DAOY cells, growth inhibition might be independent of Hedgehog signaling. Additionally, PI4KA inhibition reduced growth of DAOY cells, suggesting that reduction of intracellular PI4P in general leads to growth inhibition of medulloblastoma cells.

5.4.10 Mechanistic considerations

To elucidate how Pipinib-mediated inhibition of PI4KB leads to inhibition of Hh signaling, further experiments were performed to characterize Hh inhibition in NIH/3T3 cells.

5.4.10.1 Pipinib impairs ciliary entry of SMO

It has been shown that PI4P treatment leads to ciliary accumulation of SMO and activation of the Hh signaling pathway.[35] Since Pipinib inhibits PI4KB and reduces intracellular levels of PI4P, impairment of ciliary trafficking of SMO could be a possible mode of action. Therefore, the intracellular localization of SMO was monitored via immunofluorescence in fixed NIH/3T3 cells. To this end, the cells were first starved for 24 h to induce ciliation, then pre-treated with Pipinib alone for another 24 h and co-treated with Pipinib and ShhN-protein for an additional incubation of 24 h before fixation and antibody staining. To mark the primary cilium, an antibody against acetylated tubulin was used and to stain SMO, an anti-SMO antibody was employed. The ciliary amount of SMO increased upon pathway activation with Purmorphamine and decreased upon simultaneous treatment with Pipinib (Figure 61). For better visualization, zoom-in images of selected cilia are displayed in Figure 62, confirming the initial hypothesis.

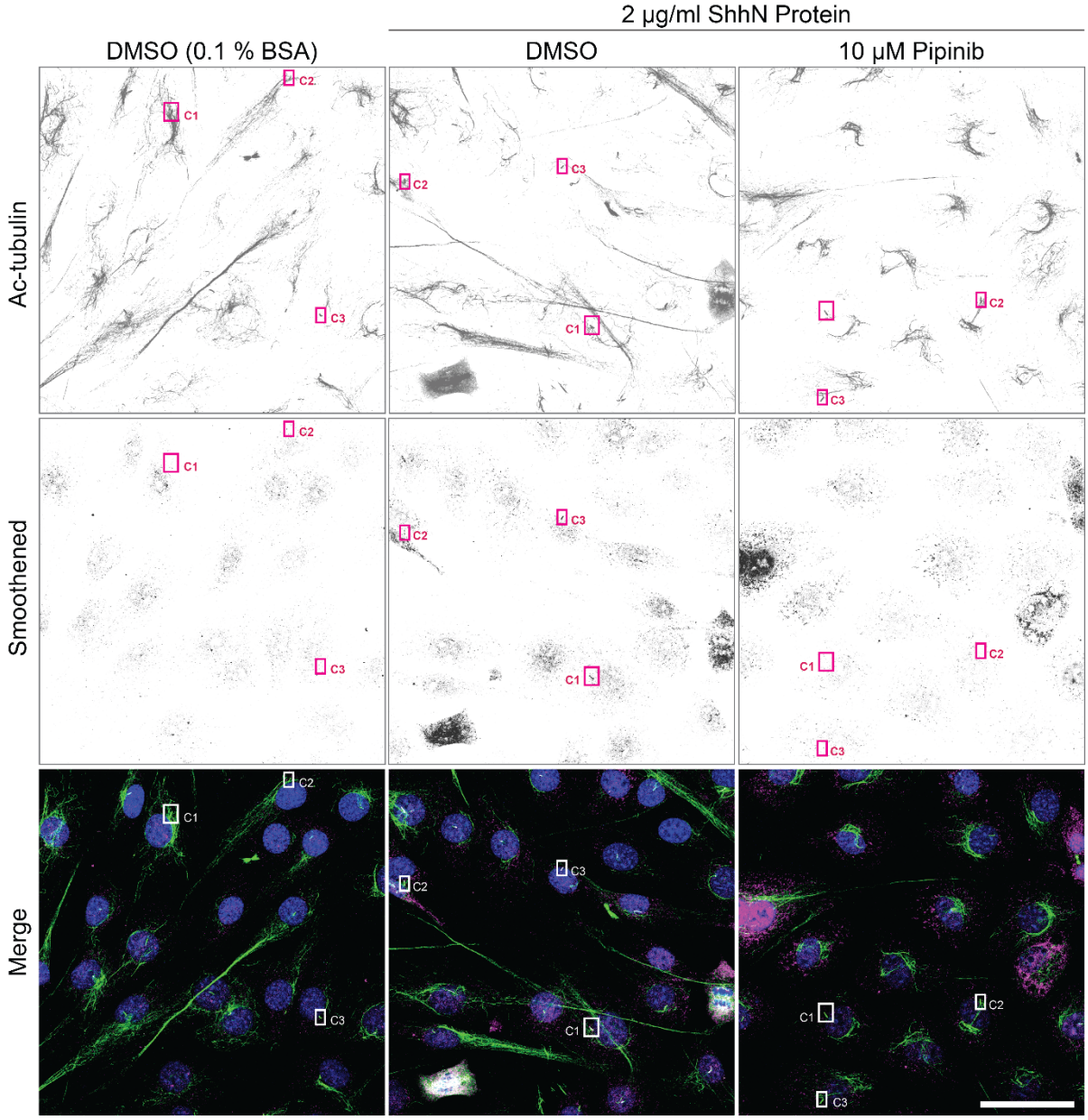

Figure 61. Pipinib impairs trafficking of Smoothened to the cilium. A. Smoothened trafficking assay. NIH/3T3 cells were serum starved for 24 h and then pre-incubated with Pipinib or DMSO for another 24 h before co-treatment with 2 µg/ml ShhN and Pipinib or DMSO as a control for 24 h. Cells were then fixed, permeabilized, blocked and incubated with antibodies against acetylated tubulin (Ac-tubulin, green) and SMO (magenta) as well as DAPI (blue) to visualize the nucleus. Representative images of biological replicates (n=3) are shown. Scale bar: 50 µm. Rectangles labelled with C1, C2 and C3 indicate enlarged cilia displayed in Figure 62.

Using the software ImageJ, the intensity of ciliary SMO was quantified to validate the visual impression. Indeed, the ciliary intensity increased upon pathway activation with ShhN and decreased when cells were simultaneously treated with Pipinib. To ascertain that overall ciliogenesis was not impaired by Pipinib, ciliary size and the percentage of ciliated cells was

determined. Neither Pipinib, nor ShhN decreased ciliary size or ciliation, verifying that Pipinib interferes with the transport of Smoothened to the cilium.

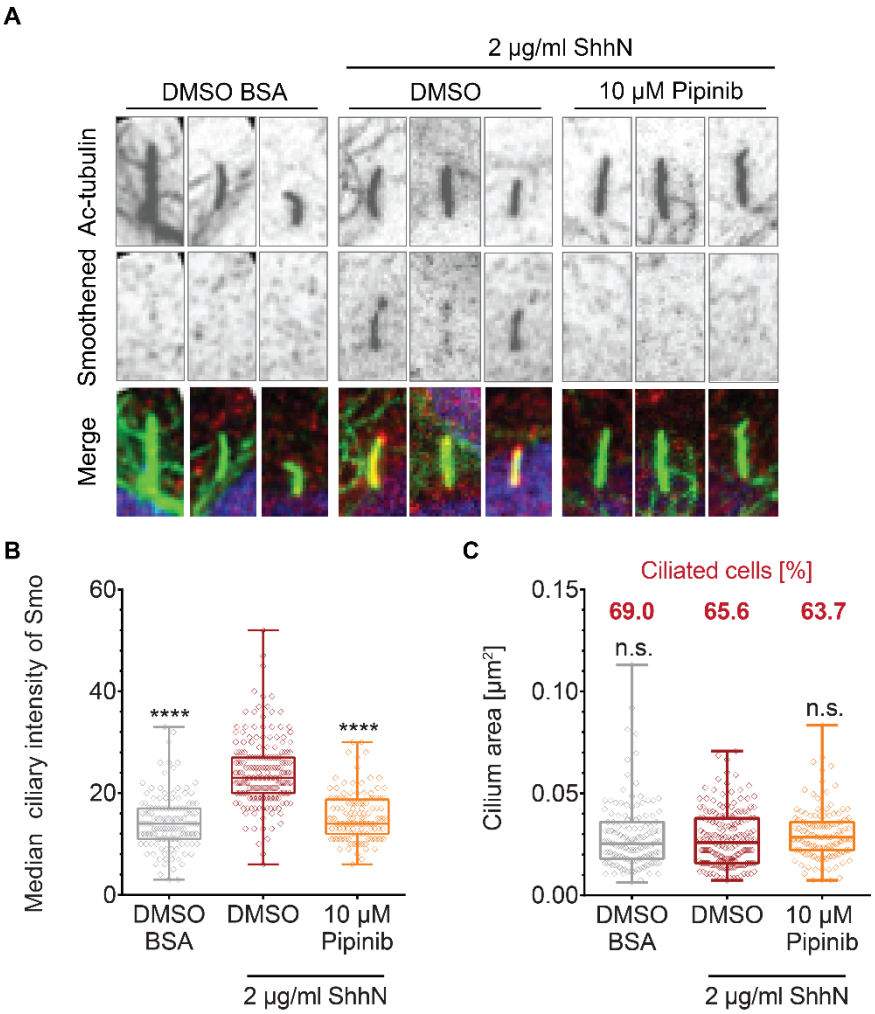

Figure 62. Evaluation of Smoothened trafficking to the cilium. A. Zoom-in on exemplary cilia from Figure 61. C1, C2 and C3 are displayed from left to right for each condition. **B.** Quantification of SMO ciliary intensity. More than 100 cilia were quantified using the software ImageJ. For this, each cilium was marked according to the ac-tubulin stain and the pixel intensity of SMO was quantified. Data are displayed as median intensity throughout the cilium, each dot represents a single cilium. The shown plot is representative of biological replicates (n=3). Statistical significance was assessed using an unpaired t-test with a confidence level of 95% (****: p<0.0001). n.s.: not significant. **C.** Assessment of ciliogenesis. Cilium area was determined by measuring the size of each cilium quantified in panel B using the software ImageJ. Each dot represents a single cilium and the plot is representative of biological replicates (n=3). Statistical significance was assessed using an unpaired t-test with a confidence level of 95%. The percentage of ciliated cells was calculated by counting cilia per image (Ac-tubulin stain) and relating this number to the total number of cells (DAPI stain).

5.4.10.2 Pipinib does not have an influence on interaction of SMO and PI4P as measured by PLA

Jiang and coworkers published that PI4P interacts with the C-terminal tail of SMO and thereby mediates its phosphorylation and activation.[35] To investigate whether Pipinib indirectly interferes with this interaction by reducing PI4P levels inside the cell, the interaction of PI4P and SMO was analyzed by means of the proximity ligation assay (PLA) in NIH/3T3 cells (Figure 63). This assay monitors the close proximity of two entities, which can be detected with an antibody using a combination of immunolabelling and PCR techniques.

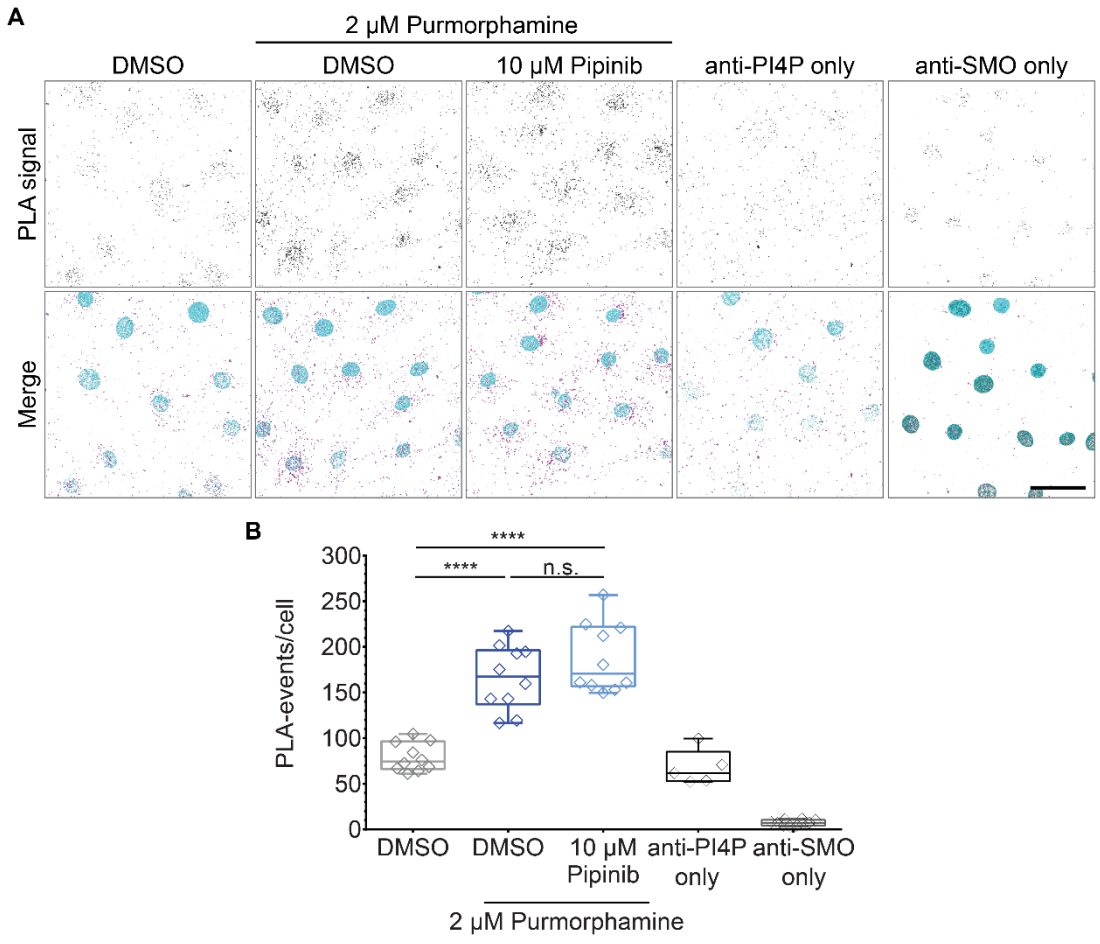

Figure 63. Assessment of PI4P-SMO proximity by means of proximity ligation assay. A. Fluorescence microscopy images. NIH/3T3 cells were serum starved for 24 h and subsequently treated with Pipinib or DMSO as a control. After another 24 h, cells were co-treated with 2 µM Purmorphamine and Pipinib or DMSO as a control for an additional period of 24 h. Cells were then fixed and blocked before addition of PLA probes, ligase, polymerase and rolling circle amplification to incorporate fluorescent nucleotides that produce the PLA signal (black, magenta in the merged images). Nuclei were stained with DAPI (cyan). Images are representative of biological replicates (n=3). To improve visibility, the background color in the merged images was changed to white. **B.** Quantification of PLA events per cell. PLA events (dots) per image were counted using the software ImageJ and divided by the number of nuclei per image to retrieve the number of PLA events per cell. Each data point represents one image. Data are representative for biological replicates (n=3). Statistical significance was assessed using an unpaired t-test with a confidence level of 95% (****: p<0.0001).

In cells that have not been treated with the Hh activator Purmorphamine, the amount of PLA events per cell resembles the number in the anti-PI4P only sample (Figure 63A and B). In this sample, only the primary antibody against PI4P is applied. All PLA events that are detected in these samples are unspecific and can be caused by unspecific binding of the PLA probes. Activation of Hh signaling with 2 µM Purmorphamine leads to a statistically significant increase in PLA events/cell, confirming that PI4P and SMO are in close proximity when Hh signaling pathway is active. The PLA events are uniformly distributed throughout the cell body. If Pipinib is added simultaneously, the number of PLA events per cell increases slightly but not significantly. Based on these results, no interference of Pipinib with the overall close proximity of PI4P and SMO can be detected.

It is important to note, however, that the proximity ligation assay, as already referenced by the name, only monitors close proximity but not interaction. The maximum distance that will results in a PLA signal is 40 nm, whereas the minimum distance can be 0 nm, assumed that the antibodies can bind and are not impaired by steric hindrance. PI4P is a small molecule which is distributed throughout the whole cell in high abundance. This might explain the high background in the PI4P control sample and questions whether PLA is a suitable technique to detect its interaction with proteins. Due to its high abundance, it can easily be close to another protein by chance. Even if the results of the PLA reflect the interaction of PI4P and SMO, the absence of an impairment by Pipinib might result from a spatial regulation that is not detectable in this kind of assay.

5.4.10.3 PI4KB is the major source for Hh-relevant PI4P

Pipinib selectively inhibits PI4KB over the other PI 4-kinases (5.4.3.1) and thereby reduces Hh signaling activity. However, Yavari and co-workers have shown by means of a siRNA-mediated knockout that both PI4KB and its isoenzyme PI4KA are relevant for Hh signaling. To investigate whether, indeed, both kinases are required for Hh signaling, a selective PI4KA inhibitor (IC_{50}=6.3 nM), compound **16**[76], was tested for inhibition of Hh target gene expression.

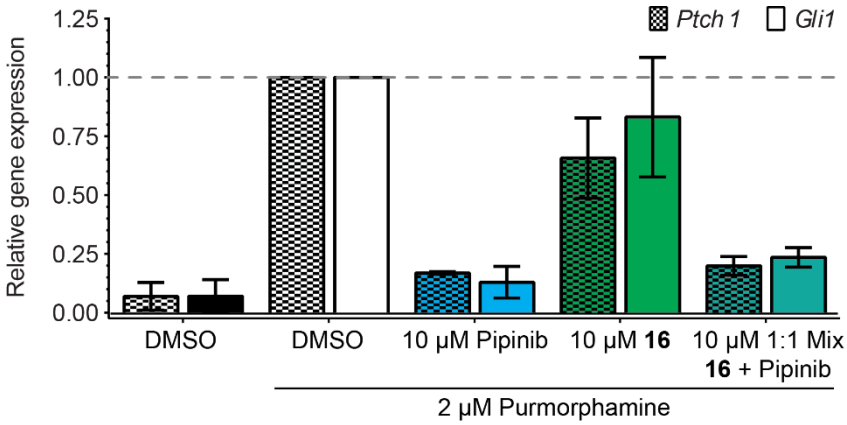

Figure 64. PI4KA inhibition leads to minor inhibition of Hh signaling. Evaluation of Hh target gene expression. NIH/3T3 cells were treated with 2 µM Purmorphamine and the compounds or DMSO as a control for 48 h. Cells were then lysed, RNA was isolated, transcribed into cDNA and used as a template for qRT-PCR using primers for the Hh target genes *Ptch1* and *Gli1* and for *Gapdh* as a reference gene. Data were normalized to Purmorphamine-DMSO-treated cells and are mean values of biological replicates (n=3) ± SD.

While 10 µM Pipinib caused the usually observed inhibition of both *Ptch1* and *Gli1* expression by 83 and 87%, respectively, compound **16** only led to an inhibition of 44 and 17% (Figure 64). Application of an equimolar mixture of compound **16** and Pipinib did not further inhibit target gene expression compared to Pipinib alone. These results suggest that PI4KB is the major PI 4-kinase required for Hh signaling and that it does not act in synergism with PI4KA.

6 DISCUSSION

6.1 Quinoline, indoline and azepinone derivatives inhibit Hh signaling and do not bind to SMO

Compounds **1**, **2** and **3** were identified as inhibitors of osteogenesis with IC_{50} values of 1.0 ± 0.9 µM, 0.2 ± 0.01µM and 0.5 ± 0.6 µM, respectively. The small molecules were confirmed to be Hh pathway inhibitors by means of a GLI reporter gene assay with IC_{50} values of 5.7 ± 3.4 µM, 45 ± 9.5 µM and 31.6 ±6.7 µM, respectively. Even compound **1**, which displayed a one-digit micromolar IC_{50}, only led to a pathway inhibition of 60% at the highest applied concentration. It is not uncommon that compound activity is lower in the GLI reporter gene assay compared to the osteogenesis assay. This can be explained by the complexity of osteogenesis. This process is not only dependent on Hh signaling but also on other developmental signaling pathways like Wnt, Notch and bone morphogenetic protein (BMP) signaling as well as cytokines, vitamin D, parathyroid hormone (PTH) and histone deacetylases (HDACs)[189]. On the one hand, the mesenchymal stem cells used in the osteogenesis assay are more sensitive to Hh inhibitors than the reporter cell line. On the other hand, if the compounds also inhibit the other mentioned processes, they are more potent inhibitors of osteogenesis than they are inhibitors of Hh signaling (i.e. GLI reporter expression). For compounds **1**, **2** and **3**, the drop in potency is too drastic to be explained by reduced cell line sensitivity and rather suggests that these compounds are not selective Hh inhibitors. This is also supported by the results of the target gene expression analysis. Compounds **2** and **3** led to an inhibition of target gene expression of approx. 40% when 30 and 20 µM were applied, whereas compound **1**, being the most potent of these compounds, led to an inhibition of 80% at a concentration of 20 µM. Compared to other compounds that have been characterized in this thesis and known Hh pathway inhibitors, these small molecules can be regarded as low potency Hh inhibitors.

Furthermore, it was found that none of the compounds displaces BODIPY-cyclopamine from SMO, suggesting that these compounds do not bind to the Cyclopamine binding site within the heptahelical bundle of SMO. Considering their low potency, it is rather unlikely that the compounds selectively target any cell membrane receptor because such inhibitors are expected to possess higher potency due to the target location and easy accessibility. In the microscopy images, an effect on fluorescence distribution was observed for compounds **2** and **3**, whereas overall intensity as measured by flow cytometry was not decreased. These

results lead to the assumption that the compounds might have a general effect on protein localization.

In conclusion, compounds **1**, **2** and **3** are Hh inhibitors that do not target SMO and, based on their low potency, might not be selective for this signaling pathway. Strikingly, all compounds were inactive for the other tested signaling pathways or cellular processes, e.g. autophagy, firefly luciferase activity, glucose uptake, formation of lipid droplets, Notch signaling, induction of reactive oxygen species (ROS) or Wnt signaling. Within this range of assays, the compounds seemed to be selective for inhibition of Hh signaling. Nevertheless, evaluation of further pathways that are connected to osteogenesis, like TGFβ or BMP signaling could give further insights into selectivity and might reveal reasons for the potency difference between osteogenesis and GLI-dependent transcription. Additionally, direct inhibition of alkaline phosphatase should be tested to exclude this as a reason for high compound activity in osteogenesis.

A SciFinder search for similar structures (>85% similarity) revealed four related molecules for compound **1**. As an example, the most similar structure is shown in Figure 65A. No biological activity was referenced for the retrieved similar compounds. For compound **2**, five similar structures were found (the most similar compound can be found in Figure 65B). Also for these compounds, no biological activity is known. The similarity search returned 2 similar compounds for compound **3**, none of whom were reported to be biologically active (see Figure 65C for the most similar compound). Interestingly, all similar compounds (>85% similarity) found by SciFinder are part of the original synthesis project[160]. No other publication or patent reported similar structures, which emphasizes the uniqueness of the compounds.

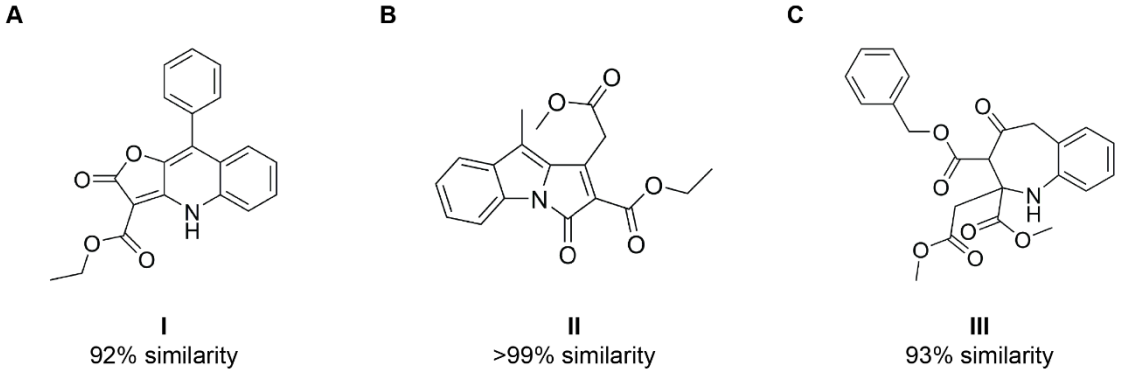

Figure 65. Most similar molecules according to a SciFinder similarity search for compounds 1 (A), 2 (B) and 3 (C).

Since only high potency compounds are suitable for linker attachment, which is necessary for proteomics-based target identification, the compounds presented in this chapter were not chosen for further experiments. Still, a possible mode of action of compounds **2** and **3** could be connected to the impairment of protein localization observed in the SMO displacement assay. A SMO trafficking assay could be performed to investigate whether the ciliary trafficking of SMO, which is necessary for proper Hh pathway activation, is reduced.

6.2 Withanolide A derivative is a Hh inhibitor and SMO binder

The Withanolide A derivative compound **4** was identified as an inhibitor of osteogenesis (IC_{50}=1.8 ± 0.6 µM) and confirmed as a Hh inhibitor in the GLI reporter gene assay (IC_{50}=3.2 ± 0.7 µM). Inhibition of Hh signaling pathway activity was further validated by evaluating *Ptch1* target gene expression that was reduced to 40% upon addition of compound **4** at a concentration of 2 µM. Additionally, the compound was found to displace BODIPY-cyclopamine from SMO almost as efficiently as the known SMO binder Vismodegib. It can be concluded, that Hh pathway inhibition by compound **4** is mediated through its interaction with Smoothened. Published Hh inhibitors that bind to SMO either inhibit or promote its ciliary localization.[15,106,190] To analyze the exact mode of action, ciliary trafficking of SMO could be analyzed by means of immunofluorescence to elucidate whether compound **4**, like Vismodegib, impairs SMO's translocation to the cilium[191] or if it acts like Cyclopamine, a SMO antagonist that induces ciliary localization of SMO[190]. The structural similarity of compound **4** and Budesonide (Figure 66), a published Hh inhibitor that impairs the ciliary localization of SMO[106], gives a hint that they might share this mode of action. Strikingly, Budesonide does not displace BODIPY-cyclopamine from SMO, which is why the authors suggested an allosteric mode of action. Cyclopamine, however, is structurally similar to both Budesonide and compound **4** while binding to SMO and inducing its ciliary accumulation. These observations highlight that regulation of SMO by small molecules is a very complex process and that structural similarities do not necessarily indicate a shared binding site. By now, several small molecule SMO agonists and antagonists have been co-crystallized with SMO. Sharpe *et al.*[192] and Wang *et al.*[28] have analyzed the observed binding modes and their findings confirm the complexity of SMO regulation. Even though most small molecules target the heptahelical bundle of SMO, interaction with distinct amino acids within this binding pocket determines if SMO is inhibited or activated[28,192]. A molecular docking study or co-crystallization experiments could also shed light on the exact binding modes of compound **4** and Budesonide.

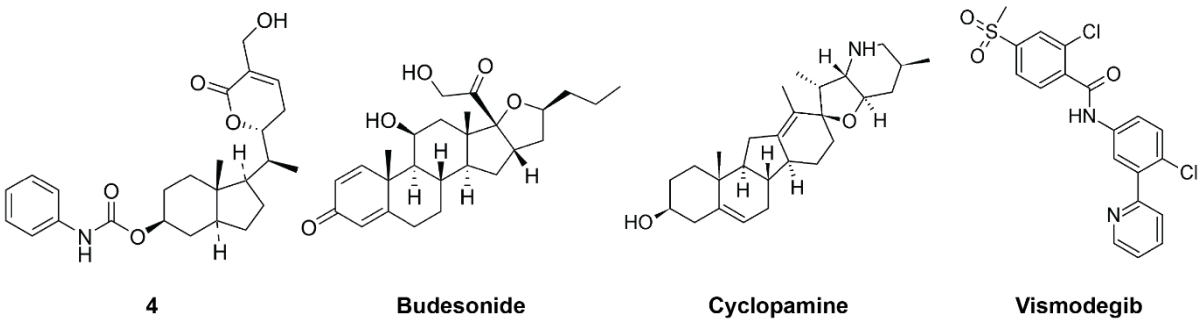

Figure 66. Chemical structures of compound 4, Budesonide, Cyclopamine and Vismodegib.

In the light of acquired resistance to Vismodegib treatment[123], the structurally distinct compound **4** (see Figure 66) could be a starting point for the development of an alternative treatment. To elucidate whether compound **4** can also inhibit ligand binding pocket (LBQ) mutants of SMO, i.e. D473H, D473G, W281C or Q477E[124], SMO variants that contain these mutations could be expressed in cells that have been depleted of wildtype SMO via siRNA and tested for Hh pathway activity upon treatment with compound **4**. Being an allosteric regulator of SMO, Budesonide was able to inhibit Hh signaling in cells that expressed mutated versions of SMO, i.e. D473H and W535L.[106] Since compound **4** contains structural elements that can be found in Budesonide and Cyclopamine, it might possess a different binding mode that would likewise enable it to overcome point-mutation-conferred resistance.

6.3 Smoothib, a pyrazolo-imidazole derivative, is a Hh inhibitor that binds to SMO and impairs its ciliary trafficking

Smoothib, a pyrazolo-imidazole derivative of the LDC compound library, was identified as an inhibitor of Hh-induced osteogenesis. With an IC_{50} value of 46 ± 10 nM, it is the most potent inhibitor of osteogenesis that was characterized in this thesis. Smoothib was confirmed as an inhibitor of Hh signaling, exhibiting a reduced potency (IC_{50}=1.4 ± 1.0 µM) in the GLI reporter gene assay. A 30-fold drop in potency between osteogenesis and GLI reporter gene assay was observed. While Smoothib remains to be a potent Hh inhibitor, this drop could imply that the compound might also inhibit other osteogenesis-relevant pathways and processes. However, the expression of Hh target genes *Ptch1* and *Gli1* was inhibited to 70% at a concentration of 2 µM. The observed potency of Smoothib in this experiment indicates that the Hh signaling pathway is its main target.

Computational target prediction suggested SMO as a possible target of Smoothib, which is why the compound was evaluated for SMO binding in the BODIPY-cyclopamine displacement assay. Here, Smoothib induced a dose-dependent displacement of BODIPY-cyclopamine from SMO, demonstrating almost complete displacement at a concentration of 30 µM. When comparing inhibition of GLI reporter gene expression after Hh signaling activation with the SMO binder SAG, either at a concentration of 0.1 µM or at an excess of 1 µM, a reduced compound potency was observed for 1 µM SAG, confirming a competition for binding to SMO. This was confirmed in a proliferation assay that employs *Ptch*$^{+/-}$ medulloblastoma cells. In these cells, Smoothib inhibited cell growth but showed reduced potency when it was co-administered with SAG, confirming again a competitive behavior. It was further found that Smoothib, like Vismodegib, inhibits ciliary entry of SMO resulting in a strongly reduced ciliary abundance of this receptor. So far, it is not clear how and why some SMO antagonists inhibit its ciliary entry while others do not. SMO regulation remains the most poorly characterized part of Hedgehog signaling. Upon relief of PTC-mediated inhibition, SMO is first activated through posttranslational modifications and conformational changes and then transported to the cilium by a ciliary targeting complex consisting of Kinesin-like protein Kif3b, Pitchfork (Pifo) and G protein-coupled receptor associated sorting protein 2 (Gprasp2).[193] It has been reported that SMO is phosphorylated by Casein Kinase 1α (CK1α) and GRK2 upon pathway activation.[33] Phosphatidylinositol-4-phosphate (PI4P) levels regulate this process through direct binding to an arginine motif of SMO and the pleckstrin homology (PH) domain of GRK2[35]. Another study shows that SMO is also phosphorylated by Gilgamesh (Gish)/ Casein kinase 1γ (CK1γ) at the carboxyl-terminal intracellular tail.[194] Recently, Ma and coworkers provided evidence that SMO activity and ciliary localization also depend on sumoylation of SMO.[195] Thus, the regulation of SMO is a highly complex process that is synergistically orchestrated by several factors, modifications and enzymes. Most likely, Smo antagonists impair one or all of these processes, e.g., they could prevent conformational changes that are necessary to activate Smo or initiate its ciliary localization. SMO agonists would rather induce a beneficial conformational change that promotes SMO activation. Another theory is based on the assumption that SMO itself is autoinhibited when the pathway is inactive. Autoinhibition is achieved through a PTC1-dependent mechanism and an unknown ligand that binds the ligand binding pocket (LBP) of SMO[124]. Common SMO antagonists stabilize the autoinhibited state through interaction with the LBP. However, this theory does not explain why Purmorphamine and SAG, which also target the heptahelical bundle of SMO, do not inhibit but activate SMO. A possible explanation could be that only slightly different binding modes and positions alter the effect on SMO activity from inhibition to activation. Wang and

colleagues have analyzed several ligand-bound structures of SMO and could identify differences between agonist and antagonist-bound SMO conformations that explain the different modes of action despite the similar binding sites.[28] They reveal that SAG binding disrupts the interaction of D473 and E518 while the guanidine group of R400 interacts with Q477.[28] SMO antagonists, in contrast, stabilize a conformation in which D473 and E581 interact with each other, while R400 interacts with D473, H470 and/or the ligand.[28]

Docking studies with a crystal structure of SMO in complex with the SMO antagonist and Hh inhibitor SANT-1 revealed that Smoothib delves deep into the pocket, similar to SANT-1, and forms a hydrogen bond with H470. Additionally, π-π stacking interactions with W281, F391, and H470 were observed. Common carcinogenic mutations in the ligand binding pocket are D473H, D473G, W281 and Q477E[124]. Based on the docking model, Smoothib only targets W281 but not the most common mutation D473H. It could therefore be a possible complementary treatment to Vismodegib whose activity is abolished by mutations in D473. This is supported by the fact that SANT-1 was unaffected by a D473A mutation in a ^{3}H-cyclopamine competition binding assay.[28] Assuming that Smoothib binds in a mode similar to SANT-1, it might indeed be another alternative to Vismodegib. To evaluate whether these assumptions are true, similar to compound **4**, mutants of SMO, i.e. D473H, D473G, W281C or Q477E[124], could be expressed in cells that have been depleted of wildtype SMO via siRNA and tested for Hh pathway activity upon treatment with Smoothib. Additionally, a co-crystallization of SMO and Smoothib could be performed to validate the proposed binding mode.

6.4 In-depth characterization, target identification and target validation of Pipinib, a thienopyrimidine derivative

6.4.1 Characterization of Hh inhibition

As another member of the LDC compound library, the thienopyrimidine derivative Pipinib was identified as an inhibitor of osteogenesis with an IC_{50} of 0.6 ± 0.3 µM. Inhibition of Hh signaling was confirmed by means of the GLI reporter gene assay (IC_{50}=1.7 ± 0.1 µM) and evaluation of *Ptch1* and *Gli1* Hh target gene expression yielded IC_{50} values of 3.1 ± 0.9 µM and 4.1 ± 1.6 µM, respectively. For Pipinib, only a 3-fold activity drop between osteogenesis and reporter gene assay was observed, suggesting that this compound is fairly selective for inhibition of Hh signaling. As a comparison, Vismodegib, a highly selective SMO antagonist, showed the same activity in both assays, with an IC_{50} value of 26 ± 10 nM in the osteoblast

differentiation assay and an IC_{50} value of 24 ± 6 nM in the GLI reporter gene assay. Further proof for Hh inhibition was obtained when monitoring the levels and truncation of the GLI3 transcription factor that meditates downstream effects of Hh signaling.[15] Here, Pipinib lead to increased levels of the truncated GLI3-R repressor version. Interestingly, the full-length version of GLI3 (GLI3-FL) was decreased upon pathway inhibition and slightly increased upon treatment with Pipinib. At a first glance, this is contradictory. If GLI3 truncation is abolished upon pathway activation, full-length GLI3 levels should increase and likewise decrease again if the pathway is inhibited. This phenomenon has been observed before by Wen et al[129], within the publication that described the generation of the anti-GLI3 antibody that has been used in this thesis. The authors also observed that GLI3-FL decreased upon Hh stimulation and have shown that this is caused by posttranslational degradation via speckle type POZ protein (SPOP) and Cullin-3 (CUL-3) E3 ubiquitin ligase. They have further shown that this mechanism is distinct from the regulatory processing of GLI3-FL to GLI3-R[129]. Thus, the observed behavior of GLI3 processing is consistent with the findings of others and the proposed mechanism of GLI3 protein turnover.

Also for Pipinib, binding to SMO was evaluated in the SMO displacement assay. Here, no displacement of BODIPY-cyclopamine could be observed, neither via the microscopy nor via the flow cytometry read-out. It was therefore concluded that Pipinib does not bind to the cyclopamine binding site of SMO. Nevertheless, Pipinib could still be a SMO binder that targets other binding sites on SMO. So far, there are four known binding sites for SMO agonists and antagonists, which are illustrated in Figure 67. Compounds like LY2940680 bind to the extracellular loops of the 7-transmembrane (7TM) domain.[27] Most substances, though, bind to the heptahelical bundle, a narrow and hydrophobic pocket inside the membrane part of the receptor, e.g., Cyclopamine[96], Vismodegib[103] and Purmorphamine[116] as well as the two SMO antagonists that were identified in this thesis, compound **4** and Smoothib. Oxysterols, activators of SMO, bind to the extracellular cysteine-rich domain (CDR) of the protein.[26] In 2015, a slightly different binding mode has been identified for the acylguanidine derivative MRT-92, which binds to both the extracellular loop and the heptahelical bundle, thereby overcoming the frequent resistance-mediating SMO mutation D473H[196]. Recently, PI4P was found to bind the cytosolic tail and induce phosphorylation by GRK2 and PKA that leads to SMO activation and ciliary migration[35].

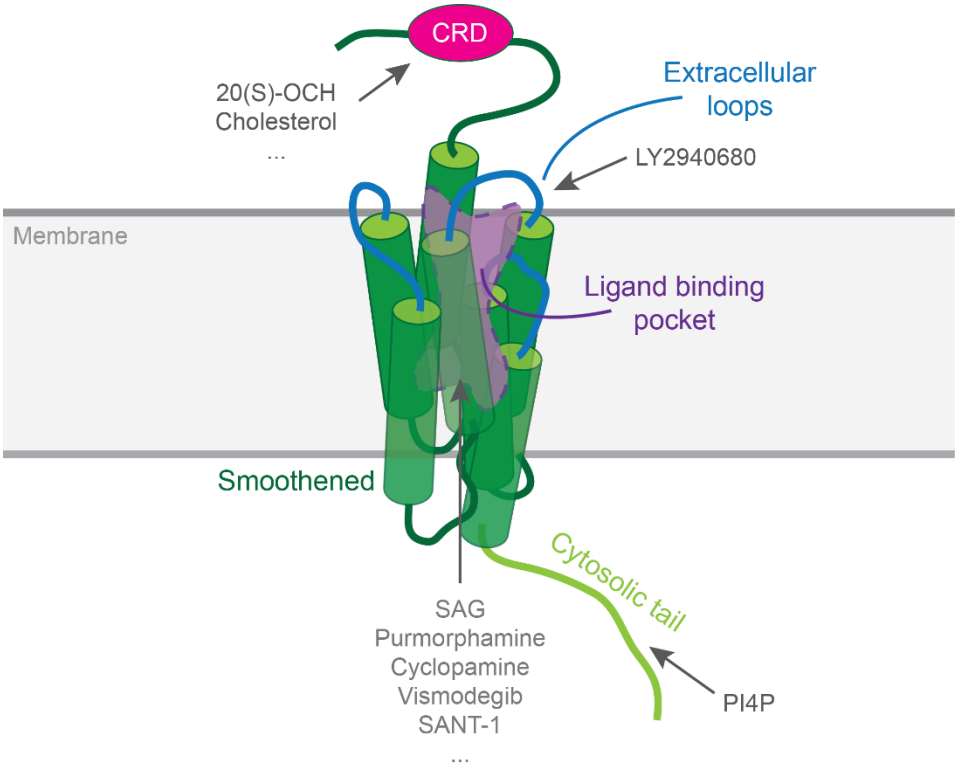

Figure 67. Overview of SMO binding sites and identified ligands. The TM domains form the heptahelical bundle that contains the ligand binding pocket (purple), to which most small molecule ligands bind. The cysteine-rich domain (CRD, pink) on the extracellular part of the protein is known to bind oxysterols like 20(S)-OCH and cholesterol. The extracellular loops (blue) are targeted by LY2940680. The cytosolic tail (light green) is known to be bound by PI4P.

To evaluate binding to other binding sites than the heptahelical bundle, one could synthesize further compound probes, employing other already known antagonists, i.e. LY2940680 for the extracellular loops and oxysterols for the CRD. To gain information on whether Pipinib binds to SMO at all, biophysical binding assays with the purified protein would be appropriate. Possible methods include differential scanning fluorimetry (DSF), fluorescence polarization (FP) and surface plasmon resonance (SPR). Additionally, CETSA could be used to study SMO binding in lysates or even living cells.

6.4.2 Target identification

Pipinib contains structure motifs that are common for kinase inhibitors, i.e. the typical hinge region binding motif that shares similarity with the purine ring of adenine from adenosine triphosphate (ATP). When screening a kinase panel of 456 kinases, nine kinases were found to be inhibited or bound to more than 50% by Pipinib at a concentration of 10 µM. Three kinases were excluded because they were either not expressed in mouse cells (GRK7) or

because they were only bound but not inhibited to more than 50% (MAPK8 and MYLK4). Furthermore, when a dose-response analysis using Pipinib was performed for NUAK1, an IC_{50} value of more than 16.7 µM was retrieved which also led to exclusion of this kinase as a main target of Pipinib. The remaining kinases, PI4KB, PIP5K1C, PIK3C2G and TTK were potently inhibited by Pipinib with IC_{50} values of 2.2 ± 0.8 µM, 4.1 ± 0.9 µM, 3.5 ± 0.7 µM and 2.5 ± 0.7 µM, respectively. For GAK, only a binding assay was available. Here, a tracer, which was based on an ATP-competitive kinase inhibitor, was displaced by Pipinib with an EC_{50} of 0.8 ± 0.2 µM. Since literature reports suggested a possible role for PI4KB and its product PI4P in Hh signaling[35,50] and the remaining kinases were excluded by means of siRNA knockdown and known inhibitors, PI4KB was selected to be investigated in detail.

6.4.2.1 Characterization of PI4KB inhibition *in vitro*

Kinetic measurements revealed an ATP-competitive inhibition of PI4KB by Pipinib. According to Michaelis Menten kinetics, only a minor decrease of V_{max} was observed, while K_m increased with increasing concentrations of Pipinib. When plotting the data in a Lineweaver Burk plot, all curves except the 50 µM curve intercept close and right to the y-axis. The 50 µM curve intersects the DMSO curve close and left to the y-axis. There are three types of inhibition: competitive, uncompetitive and noncompetitive. A competitive inhibitor competes with the substrate for binding to the enzyme. Here, the substrate has a higher affinity for binding to the free enzyme than to the complex of enzyme and inhibitor, i.e. inhibitor binding impairs the formation of an enzyme-substrate complex[197]. For very high substrate concentrations, the inhibitor will not be able to bind[198]. For this inhibition mode, application of an inhibitor will not change V_{max} while K_m will be increased[199]. Translated into a double-reciprocal Lineweaver-Burk plot (inverse of substrate concentration against inverse of velocity), curves for DMSO and inhibitor-treated samples should intercept at the y-axis[199]. An uncompetitive inhibitor only binds to the enzyme-substrate complex and decreases both K_m and V_{max}, resulting in parallel curves in a Lineweaver-Burk plot. Here, no binding of the inhibitor will be observed for very low substrate concentrations.[198] This mode is the rarest form of enzyme inhibition observed in cellular systems[198]. A non-competitive inhibitor binds to the enzyme independent of its substrate, resulting in an unchanged K_m and a decreased V_{max}, resulting in curves that intercept left to the y-axis.[199] Due to the different intercepts in the Lineweaver-Burk plot and the unclear behavior of V_{max}, a definite decision for the inhibition mode of Pipinib is not possible. Still, the most probable mode of inhibition can be concluded via exclusion of less possible modes. Considering the K_m value, an uncompetitive mode of inhibition can be excluded because this would require a decrease of K_m with increasing inhibitor concentration,

which is not observed for Pipinib. This is confirmed by the Lineweaver-Burk plot, which does not show parallel curves that would be expected for an uncompetitive inhibitor. Due to the outlier, a definite conclusion for V_{max}, would be uncertain. However, when comparing the Lineweaver-Burk plot with the two possible modes, the overview image of Pipinib (Figure 34C) suggests a competitive mode of inhibition but the zoom-in reveals that not all curves intersect exactly at the y-axis. Still, the close proximity to the y-axis and the fact that a noncompetitive inhibition would require an unchanged K_m for increasing compound concentrations, which is not observed for Pipinib, suggests a competitive mode of inhibition.

6.4.2.2 Proteome-wide screen for target proteins of Pipinib

Being an ATP-competitive kinase inhibitor, Pipinib is well suited for an ATP-based affinity isolation experiment. This technique employs an ATP probe to enrich all ATP-binding proteins from a cell lysate. Competition with a kinase inhibitor like Pipinib will reduce the amount of enriched proteins that interact with the inhibitor and thereby enables identification of possible targets. In three different runs of the experiment, PI4KB was the only ATP-binding protein that was significantly enriched in the DMSO-treated sample compared to the compound-treated sample. It has to be mentioned, though, that, except for GAK, the other kinases, which were found to be inhibited by Pipinib, have not been identified in any repetition of the pull-down, i.e. the pull-down probe did not enrich these proteins during the affinity chromatography. GAK was identified in one experiment, but was not enriched in the DMSO sample. However, this observation could not be confirmed or reproduced because the kinase was not identified in the other experiments. An additional limitation of this assay is the restriction to ATP-binding proteins. To increase the amount of assessed proteins, a compound-probe based pull-down was applied. Here, the compound itself is used as a bait to enrich its binding partners. Additionally, free compound can be used as a competitor to verify interaction of the small molecule and its target protein. In order to use Pipinib as a bait, a linker had to be attached to the compound to enable coupling of the probe to a solid support. To retain compound activity after linker attachment, relating structure to activity (structure-activity relationship, SAR) is required. To analyze the SAR of Pipinib, the structure was varied at two positions, revealing that an increase of the steric bulkiness at the isopropyl position (R^1) reduces bioactivity while all other substitutions did neither improve nor increase compound activity. Despite the observed decrease of biological activity, variation on the ester (R^2) decreased bioactivity even further. Therefore, R^1 was chosen for linker attachment. Due to increased synthetic effort, substitution of the thieno-ring was not explored. Nevertheless,

evaluation of this position could yield further insights and might even reveal another suitable position for linker attachment.

To exclude unspecific binding of proteins to the linker, a negative probe has to be included. For this, a Pipinib core scaffold was equipped with a linker and both negative (inactive) and positive (active) probe were evaluated for inhibition of Hh signaling. Here, it could be confirmed that the active probe was inhibiting Hh pathway activity while the inactive probe caused inhibition as well but to a lesser extent. The inactive probe showed reduction of GLI reporter expression but only induced medium inhibition of Hh target gene expression, suggesting that the observed inhibition of reporter gene activity was caused by unspecific inhibition of protein expression or luciferase activity. Evaluation of PI4KB enzyme inhibition by both probes confirmed this observation: only the active probe reduced enzyme activity. Even though Pipinib could have other targets than PI4KB, the binding mode to other proteins might be similar to that of Pipinib and PI4KB and the confirmation of the probes for this enzyme, in combination with the results for Hh pathway inhibition, suggest that the chosen site for linker attachment is appropriate. In the following pull-down experiments, neither PI4KB nor the other possible kinase targets were enriched or identified in any repetition. Since the active probe inhibits PI4KB in a biochemical assay and thus should bind to PI4KB in a lysate, a possible reason could be unsuitable experimental conditions that reduce binding affinity and/or prevent efficient enrichment. To evaluate binding of PI4KB, further pulldowns could be carried out with different buffers, lysate concentrations, incubation times and probe concentrations before detection via immunoblotting. A possible strategy would include performing the pull-down in a similar manner as the ATP probe-based pulldown, since this procedure is optimized for the enrichment of kinases. Even though PI4KB was not identified, the pull-down results were analyzed for further binding partners. None of the twelve enriched proteins has a known implication in Hh signaling. Seven potential targets could be excluded because they were either not competed by the free compound or, regarding the two kinases (MAPK9 and 10), were not inhibited by Pipinib in the kinase panel.

The remaining five proteins were ribosyldihydronicotinamide dehydrogenase (NQO2), a detoxification oxidoreductase, heme-binding protein 1 (HEBP1), a scavenger for possibly toxic free porphyrinogens, GRAM domain-containing protein 4 (GRAMD4), a mitochondrial pro-apoptotic protein, transmembrane 7 superfamily member 3 (TM7SF3), an orphan transmembrane receptor connected to cytokine activity, and ferrochelatase (mitochondrial, FECH), which catalyzes the insertion of iron into protoporphyrin IX[175]. The first two proteins, NQO2 and HEBP1, are the only two proteins that were enriched in both pulldowns and competed by the free compound. Due to the lack of any connection to Hh signaling and no

possible implication of how they could influence the Hh signaling pathway, they were not considered as Hh relevant targets of Pipinib. Still, they have to be acknowledged as compound binding partners. Likewise, it has to be considered that not all proteins were pulled down due to direct interaction with Pipinib but due to interaction with each other, i.e. as a protein complex. However, string analysis, a database-analysis on known, predicted and functional interactions of proteins[200], has revealed that the five proteins do not interact with each other. To verify that these proteins are also bound by Pipinib in a cellular context, several techniques could be applied. Since NQO2 is supposed to protect cells from oxidative stress[201], evaluation of this process, e.g. by monitoring formation of reactive oxygen species (ROS) after Pipinib treatment would shed light on a possible cellular inhibition of NQO2 by Pipinib. In fact, the compound was inactive in a ROS induction assay at COMAS. As formation of ROS is a hallmark of oxidative stress[202], and NQO2 inhibition should increase oxidative stress, it is rather unlikely that Pipinib impairs the cellular function of NQO2. Nevertheless, Pipinib could still bind to the protein without impairing its enzymatic function. However, so far, no interaction partners are known, therefore it is implausible that this has an effect on Hh signaling. HEBP1 is a protein that binds and scavenges free porphyrinogens and a precursor for F2L, a high-affinity agonist of the formyl peptide receptor (FPR).[203] Thus, only binding can be monitored in cells. For this, a fluorescence resonance energy transfer (FRET) experiment could be carried out. If both the small molecule and the protein of interest, e.g. HEBP1, are coupled to fluorophores of a FRET-pair, this technique could be employed to detect close proximity of both fluorophores upon binding of the small molecule to the protein. A variant of this technique is fluorescence lifetime imaging (FLIM)-FRET, which yields high spatial and temporal resolution. Here, not FRET is measured but the decrease of the fluorescence lifetime of the donor fluorophore during FRET. Every fluorophore has a specific fluorescence lifetime that describes the time the molecule remains in its excited state after absorbing a photon. If cells are imaged over time, fluorescence lifetime can be measured. If a FRET acceptor is in close proximity to its donor partner fluorophore and FRET occurs, the fluorescence lifetime of the donor is affected.[204] The same technique could be applied to investigate interaction of Pipinib with GRAMD4 and TM7SF3. It is noteworthy that a majority of the other potential target proteins share either location or function. HEBP1 and FECH bind to heme[175]. FECH and GRAMD4 are mitochondrial proteins[171], whereas GRAMD4 and TM7SF3 are both controlled by apoptotic proteins (p73 and p53, respectively) and are relevant for either cell survival or cell death[171,173]. In conclusion, none of the proteins, which were identified as possible binding partners of Pipinib have a known implication in Hh

signaling. Since PI4KB was, in comparison to the other possible targets, the most plausible Hh-relevant target of Pipinib, it was followed up for further characterization.

6.4.2.3 Pipinib interferes with cellular PI4P levels and distribution

If PI4KB is a cellular target of Pipinib, the compound should reduce its cellular activity after treatment. To evaluate this hypothesis, NIH/3T3 cells were treated with different concentrations of Pipinib up to 15 µM for 6, 24 or 48 h and generation of PI4P, the product of PI4KB, was assessed using an anti-PI4P antibody in combination with a fluorescence microcopy or flow cytometry read-out. After six and 24 h, microscopy revealed decreased PI4P staining around the nucleus and especially in the cellular periphery, while flow cytometry after 48 h confirmed an overall decrease of PI4P-antibody staining. Additionally, detection of PI4P using a EYFP-PH(FAPP1)-PI4P sensor with 75 µM Pipinib showed that cytosolic levels of PI4P are increased while Golgi levels of PI4P are slightly decreased 10 to 30 min after compound treatment. First of all, these results confirm an impairment of PI4P distribution by PI4KB. In all experiments, clear changes in PI4P sensor intensity compared to the DMSO control were observed. Since PI4KB is mainly localized at the Golgi apparatus[75], an inhibition of this enzyme is expected to decrease PI4P levels in this organelle. It is important to note, though, that PI4Ps migrate between organelles and membranes and can be found almost everywhere within the cell, i.e. on the plasma membrane, the ER, the Golgi apparatus, trafficking vesicles, and lysosomes[65]. Even though the four PI 4-kinases have distinct locations and therefore are responsible for different pools of PI4P[65], it is not possible to track the origin of PI4Ps within the cell without affecting cell physiology. Furthermore, PI4P can also be generated via dephosphorylation of other phosphatidylinositols, i.e. phosphatidylinositol 4,5 bisphosphate ($PI(4,5)P_2$) or phosphatidylinositol 3,4 bisphosphate ($PI(3,4)P_2$) by different phosphatases like the inositol polyphosphate 5-phosphatase (INPP5E) or the phosphatidylinositol 3,4,5-trisphosphate 3-phosphatase and dual-specificity protein phosphatase (PTEN).[68] PI4P generation and distribution is a very complex field and it becomes clear that monitoring PI4P can only be considered as an indirect measure of PI4KB inhibition. Nevertheless, since PI4KB is the only PI 4-kinase that is affected by Pipinib, it is very likely that reduction and re-distribution of PI4P is caused by Pipinib-mediated inhibition of PI4KB. Still, it is interesting that cytosolic PI4P increased during the real-time sensor experiment and decreased when detecting PI4P with an antibody in fluorescence microscopy after six and 24 h. This different behavior can be attributed to the use of different detection methods. An antibody might be more or less specific than a fusion protein. Additionally, cell fixation might alter the physiological distribution of phosphatidylinositols. It

has been found that formaldehyde fixation is not sufficient to stabilize $PI(4,5)P_2$ within membranes and causes membrane blebbing.[205] It is unknown whether this is also true for PI4P. For samples used in this thesis, no changes in PI4P distribution were observed over time while storing fixed samples. Still, it has to be acknowledged that fixed cells can display different characteristics than living cells. Nevertheless, also the expression of fusion proteins can have an impact on cell physiology. Transfection alone is already a perturbation of cell integrity and metabolism. Additionally, PH domains of FAPPs have been shown to also bind ADP-ribosylation factor 1 (Arf1) and, at high expression levels, scavenge the lipid and prevent is physiological distribution and function.[65] With drawbacks on both sides, the application of these two complementary approaches and careful comparison of the results can still give meaningful insights. PI4P is a lipid membrane component and free diffusion of this molecule is unlikely. Therefore, the dispersed effect observed for the sensor experiment could be caused by an overall effect on endomembranes and vesicles which might be caused by the application of a high compound concentration (75 µM). Here, the application of lower concentrations could reveal if this effect is unspecific or related to inhibition of PI4KB. In the antibody-based experiment, the PI4P-positive dots in the cell periphery, which were observed in DMSO-treated samples and could be PI4P containing vesicles that originate from the Golgi, are reduced upon compound treatment. In the context of reduced PI4KB activity at the Golgi, this effect is to be expected. Nevertheless, further experiments that confirm the observed dots as vesicles and assign their identity would be necessary to validate this assumption. For this, further immunofluorescence experiments using antibodies against vesicular markers like Rab5 (early endosome)[206] and Rab11 (post-Golgi vesicles, secretory pathway)[207] would be required.

6.4.2.4 Pipinib induces morphological changes at mitochondria and the Golgi apparatus

The cell painting assay, which monitors morphological changes in various cellular compartments upon compound treatment, revealed that Pipinib induces alterations in the morphology of mitochondria and the Golgi apparatus. The intensity of the mitochondrial stain and the overall size of the organelle was increased after compound treatment. Indeed, it is known that Hh signaling affects mitochondria. Yao and colleagues reported that SHH treatment leads to an increased mitochondrial mass in neurons.[183] Additionally, Hh signaling induces mitochondrial fragmentation in medulloblastoma[182] and Cyclopamine tartrate, a SMO antagonist, was found to inhibit mitochondrial respiration in lung cancer cells.[184] So far, no influence of mitochondrial function on Hh signaling is known. This indicates that the observed

change in mitochondrial morphology might be a consequence of Hh inhibition and not a direct effect of Pipinib target interaction. To prove this hypothesis, a screening of known Hh inhibitors, like Vismodegib or Cyclopamine, in the cell painting assay could be performed.

The most drastic morphological change in comparison to the DMSO control was observed for the Golgi apparatus. Here, fluorescently labelled wheat germ agglutinin was used as a marker. This lectin preferentially labels the Golgi complex and post-Golgi vesicles[208,209]. Upon treatment with Pipinib, a decreased size of the Golgi apparatus was observed. This could be caused by inhibition of PI4KB because this kinase is not only required for generation of PI4P but also for the structural integrity of the Golgi apparatus.[180] Additionally, numerous dot-like structures, resembling vesicles, appeared in the cytoplasm. According to the literature, these dot-like structures could be post-Golgi vesicles.[209] If so, this accumulation of post-Golgi vesicles could be induced by an impaired post-Golgi secretion, which, in turn, could be caused by inhibition of PI4KB. Kinase function is required for trafficking from the trans-Golgi network (TGN) to the plasma membrane: PI4KB synthesizes PI4P, which is required for overall trafficking from the TGN to the membrane[66], and recruits Rab11, a small GTPase that is also required for cargo transport to the PM, to the Golgi apparatus[210]. Thus, the accumulation of post-Golgi vesicles could indicate insufficient membrane delivery of vesicles that were generated at the TGN. This hypothesis could be evaluated by repeating the WGA staining after knockdown of PI4KB by means of siRNA or inhibition of PI4KB via treatment with compound **12**, a known PI4KB inhibitor. The observed effect of vesicle accumulation is in line with the previously observed decrease of PI4P positive vesicles. A reduced amount of PI4P on vesicles, caused by Pipinib-mediated inhibition of PI4KB, might be the reason for impaired vesicle delivery and concomitant accumulation of such vesicles in the cytoplasm.

Comparison of Pipinib's morphological profile with the profiles of reference compounds identified four compounds that display a profile similarity of more than 40%. Those compounds are PD1730747, ketoconazole, benztropine mesylate and methotrimeprazine maleat salt. They target several different proteins, speaking in categories, these were receptors, kinases, cytochrome enzymes, steroid 5α-reductase-2, UDP-glucuronosyltransferase 1-1 (UGT1A1), mitochondrial permeability transition pore, geminin, Lysine-specific demethylase 4A (KDM4A) and Isocitrate dehydrogenase NADP (cytoplasmic). Table 8 summarizes all targets, their function, tissue-specific expression and possible implications in Hh signaling. The highest similarity of 50% was observed for PD173074.

Table 8. Target proteins of reference compounds with morphological profiles similar to the profile of Pipinib. Information on function and expression was retrieved from www.uniprot.org. Some gene expression information was retrieved from Expression Atlas (EA), Bgee or genevisible (G,specified).

Reference compound	Target protein	Function	Tissue expression	Implication in Hh signaling?
PD173074 (50% similarity)	FGFR	• receptor tyrosine kinase • embryonic development • cell proliferation • RAS/RAF/MEK/ERK signaling	ubiquitous	Activates Hh signaling in neocortical precursors[211]
	VEGF	• growth factor • angiogenesis • vasculogenesis • endothelial cell growth	adult kidney glomeruli & choroid plexus	Hh signaling regulates vessel growth[212]
	EGFR	• receptor tyrosine kinase • RAS/RAF/MEK/ERK signaling • PI3 kinase-AKT signaling • PLCγ-PKC signaling	various tissues (EA)	Cooperation of both EGFR and Hh signaling, activation of Hh target genes via PI3K/AKT and MAPK cascade[213]
	Insulin receptor	• receptor tyrosine kinase • PI3K-AKT/PKB signaling • RAS-MAPK signaling • Glucose transporter translocation to membrane • anti-apoptotic effects via phosphorylation of BAD • mTORC1 signaling	various tissues (EA)	• Hh signaling increases levels of insulin receptor substrate 1 (IRS1) via inhibiting mTOR dependent IRS1 turnover[214] • Hh signaling induces osteogenesis via insulin-like growth factors[215]
	MAP2K1	• component of MAPK cascade • activation of MAPK3 and MAPK1 • endosome cycling • Golgi fragmentation during mitosis	various tissues (EA)	Stabilization of GLI2 (see also ref. 189)[216]
	Src	• non-receptor tyrosine kinase • cytoskeletal organization • phosphorylation of target proteins at adherens and gap junctions • RAS signaling • EGFR internalization • phosphorylation and activation of GRK2	various tissues (EA)	Non-canonical Hh signaling activates Src via SMO[217]
	PKC	• serine/threonine protein kinase • Ca^{2+} activated • MAPK signaling • anti-apoptotic • cell proliferation, migration • inflammation	various tissues (PubMed search)	PKC directly regulates Hh signaling and GLI activity[218]
Ketoco-nazole (41.7% similarity)	Cytochrome enzymes	• heme-thiolate monooxygenases • NADPH-dependent electron transport pathway • oxidation of various compounds • 2-hydroxylation	high expression in liver, olfactory epithelium, gastrointestinal system, kidney and immune cells (EA)	Responsible for oxidation of cholesterol to form oxysterols[219,220]

Reference compound	Target protein	Function	Tissue expression	Implication in Hh signaling?
	Steroid 5α-reductase-2	• testosterone and progesterone conversion • sexual differentiation and androgen physiology	high expression in adrenal gland and olfactory epithelium (G)	Hedgehog signaling is required for sexual differentiation of the genitalia[221]
	UGT1A1	• glucuronosyltransferase • elimination of toxic xenobiotics/endogenous compounds	liver (high), colon, kidney, stomach and intestine (EA)	GLI1 stimulates UGT1A1 activity resulting in drug resistance[222]
	Androgen receptor (AR)	• ligand-activated transcription factor • cell proliferation and differentiation	high in lacrimal gland, prostate, uterine horn, seminal gland, adrenal gland, uterus, brainstem, uterine cervix, (G)	• Androgen stimulates GLI1 mRNA expression[223] • GLI1 blocks AR-mediated transactivation[224]
Benztropine mesylate (40.9% similarity)	Muscarinic acetylcholine receptor M1 (CHRM1)	• neuromuscular synaptic transmission • inhibition of adenylate cyclase • breakdown of phosphoinositides • G protein activation to modulate K^+-channels	various brain tissues, olfactory tubercle (G & EA)	Hh pathway activation promotes *Chrm1* expression leading to salivary gland regeneration in irradiation-induced hyposalivation[225,226]
Methotrimeprazine maleat salt (40.6% similarity)	Mitochondrial permeability transition pore (mPTP)	• pore in the inner mitochondrial membrane[227] • forms upon increased levels of calcium and phosphate or ROS[227] • increases permeability of the mitochondrial membrane[227] • results in swelling and depolarization of mitochondria leading to rupture and release of mitochondrial death factors[227] • putative components[228]: 1. Voltage-dependent anion channel (VDAC) 2. Adenine nucleotide translocase (ANT) 3. Mitochondrial phosphate carrier (SLC25A3) 4. Cyclophilin D 5. *c*-subunit of ATP synthase (Atp5g3)	• VDAC: high in heart, kidney, brain and skeletal muscle, not in testis • ANT: high in neurons but expressed in various tissues (G) • SLC25A3: various tissues (G & EA) • Cyclophilin D: various tissues (G) • Atp5g3: various tissues (Bgee)	Hh and PI3K/Akt signaling have anti-inflammatory and neuroprotective effects in a mPTP-induced Parkinson mouse model[229]
	Geminin	• inhibitor of DNA replication • prevents incorporation of the minichromosome maintenance complex • degraded during mitotic phase of the cell cycle	various tissues (EA)	no link found
	KDM4A	• histone demethylase • demethylation of H9 and H36 of histone H3 • transcriptional repression	widely expressed	KDM4A knockout leads to aggravation of vein disruption in the developing wing of

Reference compound	Target protein	Function	Tissue expression	Implication in Hh signaling?
				Drosophila flies expressing a constitutively active SMO mutant[230]
	Isocitrate dehydrogenase NADP (cytoplasmic) (IDH1)	• oxidative decarboxylation of isocitrate to 2-oxoglutarate and CO_2 • tricarboxylic acid (TCA) cycle[231]	various tissues (G & EA)	IDH1 mutations are associated with Hh responsiveness in glioma[232]
	Glucagon-like peptide receptor	• G-protein coupled receptor • Ligand: Glucagon-like peptide • activation of adenylyl cyclase, increase of cAMP • insulin secretion	pancreatic islets and lung	no link found

Several targets of the reference compounds are expressed in various tissues and it is likely that they are also expressed in the fibroblast cell line (NIH/3T3) that was used for characterization of Pipinib. For Geminin and glucagon-like peptide receptor (highlighted in grey), no link to Hh signaling was found. Of course, this does not exclude these proteins as Hh relevant targets but concerning their function in DNA replication and cell cycle (Geminin) or their mode of activation (glucagon-like peptide receptor), they are not a good fit for an inhibitor of Hh signaling. FGFR, EGFR, MAP2K1 and PKC (grey), despite having an implication in Hh signaling, can be excluded as possible targets of Pipinib because they were not inhibited in a biochemical assay (see kinase panel results in 12.2). For various targets, it was found that they are regulated by Hh signaling (highlighted in yellow). It is not known whether they also have a feedback influence on Hh signaling, which is why also these proteins are rather unlikely to be Hh relevant targets. For KDM4A and IDH1, only indirect correlation with or influence on Hh signaling has been reported. Based on this literature, it is not possible to decide whether their inhibition would lead to inhibition of Hh signaling. Further experiments, employing siRNA-mediated knockdown or published and selective inhibitors, would be necessary. A first hint could be obtained by evaluating the reference compounds (Ketoconazole, Benztropine mesylate and Methotrimeprazine maleat salt) for inhibition of Hh signaling. Ketoconazole has been reported to inhibit *Gli1* expression via inhibition of cholesterol synthesis,[233] highlighting that also Cytochrome enzymes could be Hh relevant targets. Furthermore, the androgen receptor might have an influence on Hh signaling through GLI1. To evaluate whether these proteins are effectors of Pipinib-mediated Hh inhibition, a first step would include testing them for inhibition by Pipinib *in vitro*. If Pipinib inhibits both proteins, a relevance for Hh signaling could be assessed via siRNA-mediated knockdown

and co-treatment with Pipinib. Here, an increased potency of Pipinib after siRNA knockdown would suggest a functional correlation for inhibition of Hh signaling.

While it is not clearly defined which similarity score can be considered as significant, it can be argued that significance should be higher than 75% to derive meaningful target hypotheses based on the reference compounds. It is also noteworthy, that all reference compounds lead to a similar morphological profile compared to Pipinib while presumably targeting entirely different proteins. This observation emphasizes that various inhibition profiles can lead to a similar phenotype and also suggests that similar morphology does not necessarily implicate similar targets. Further knowledge on this method can be generated, if several inhibitors of PI4KB and Hh signaling are screened in the cell painting assay. Additionally, one could plot the phenotypic profiles as heat maps to easily spot differences and similarities among reference and query compounds. Bearing the described limitations in mind, PI4KB was still considered as the most promising Hh relevant target of Pipinib.

6.4.3 Target validation for PI4KB

6.4.3.1 Proof of target engagement in cellular lysates via CETSA

Employing the ATP probe-based pull-down technique, it was shown that Pipinib competes with ATP for binding to PI4KB in cellular lysates. To obtain further proof for target engagement under physiological conditions, a cellular thermal shift assay (CETSA) was performed. The DMSO control revealed a melting temperature of 52.6 ± 0.6 °C. In the Proteome DB, data for human PI4KB results in a melting temperature of approx. 55 °C. Even though human and mouse PI4KB protein sequences are 99% identical, the different melting temperatures could be explained by the usage of a different cell line and thus different lysate composition, experimental settings and equipment. Addition of Pipinib induced a shift of the melting temperature to higher values, resulting in a ΔT_m of +2.8 ± 0.6 °C. The ΔT_m induced upon ligand binding varies per target and ligand. For a large number of kinases, shifts between 4 and 7 °C have been observed[234]. The decision on what can be considered as a significant shift is difficult. Some research groups consider thermal shifts of more than 1 °C as significant[235] others select a threshold of 4 °C[234]. Since the resolution of the assay is also dependent on the step size between the applied temperatures, a thermal shift that was 1.5-fold higher than the step size was regarded as significant. Within the range of the melting temperature of PI4KB, a step size of 1.5 °C was applied, setting the significance threshold to 2.25 °C. Thus, the thermal shift of 2.8 ± 0.6 °C for PI4KB, which was induced by Pipinib, can

be considered as a significant shift. In comparison, Dasatinib and Staurosporine induced thermal shifts of -0.1 °C and 1.3 °C for PI4KB (Proteomics DB, PRDB004185[236]). Dasatinib is a kinase inhibitor selective for ABL/SRC tyrosine kinases[237] and has not been reported to inhibit PI4KB, which is in accordance with the absence of a thermal shift. In contrast, Staurosporine is a broad-spectrum kinase inhibitor that targets a high number of different protein kinases in an ATP-competitive manner[238] and thus could inhibit PI4KB as well. It was already shown that Staurosporine can also inhibit lipid kinases, namely a Class IA PI3K, with an IC_{50} value of 9 µM, and binds to PI3Kγ with a K_D of 0.29 ± 0.06 µM[239]. The authors concluded that this to be a low-affinity interaction[239]. The thermal shift caused by Staurosporine treatment (1.3 °C) further validates the significance of the observed shift of 2.8 °C that has been induced by Pipinib.

Additionally to the melting curve, an isothermal dose-response fingerprinting (ITDRF) was performed to evaluate dose dependency of Pipinib-mediated PI4KB stabilization. Here, the concentration at which 50% of the protein was stabilized (i.e. occupied, OC_{50}[240]) was 3.1 ± 2.0 µM. This concentration is in the same range as the IC_{50} value for inhibition of PI4KB (2.2 ± 0.8 µM) and once more confirms binding of Pipinib to PI4KB.

6.4.3.2 Chemocopy of PI4KB-mediated Hh pathway inhibition

To prove that PI4KB is not only a target of Pipinib but also mediates its inhibitory effect on Hh signaling, several approaches can be applied. One of them is the employment of structurally unrelated and selective inhibitors of PI4KB. Using inhibitors published by Mejdrová *et al.* (compounds **10**, **11** and **12**)[78], inhibition of Hh signaling activity was assessed by measuring osteogenesis and target gene expression. For all three inhibitors, low micromolar IC_{50} values were obtained for inhibition of osteogenesis. In this assay, all compounds displayed cytotoxicity in a similar range. This could be caused by a possibly increased sensitivity of mesenchymal stem cells towards PI4KB inhibition or by the long incubation time of 96 h. Pipinib did not cause these strong effects on toxicity but still showed a slightly decreased cell viability in the osteogenesis assay. Still, the IC_{50} value for viability was higher than 10 µM thus leaving a large window between Hh inhibition and effects on viability. The decreased window for the known PI4KB inhibitors could be caused by their increased potency compared to Pipinib. For Hh target gene expression, dose-dependent inhibition of *Ptch1* and *Gli1* expression was observed while no toxic effects could be detected. These results confirm an implication of PI4KB in Hh signaling and emphasize that PI4KB inhibition impairs Hh signaling. However, despite being nanomolar PI4KB inhibitors, compounds **10** and **11** only reduced target gene expression by approx. 50% at 10 µM. This could be explained by

reduced membrane permeability. Indeed, compound **12**, which was most potently inhibiting Hh target gene expression, was also more potent than compound **10** and **11** in a cellular antiviral screening[78], confirming the difference between biochemical and cellular inhibition.

6.4.3.3 siRNA-mediated depletion of PI4KB and phenocopy of Hh pathway inhibition

An alternative approach to chemical inhibition is genetic depletion. Here, PI4KB expression is impaired due to siRNA-induced mRNA degradation. Using this technique, a knockdown of PI4KB was achieved in C3H10T1/2 mesenchymal stem cells, which were used for the osteoblast differentiation assay, and NIH/3T3 cells that were tested for Hh target gene expression. PI4KB knockdown led to a reduction of Hh target gene expression. For osteogenesis, a hint towards reduced osteogenesis was observed. As stated before, reduced pathway activity upon siRNA treatment proves that PI4KB is a positive regulator of Hh signaling but it does not prove that PI4KB inhibition by Pipinib causes Hh inhibition. This can be verified by testing compound potency after knockdown. If Pipinib is the main and Hh relevant target of Pipinib, reduced protein amounts will require less inhibitor to achieve a certain effect, thereby reducing the IC_{50} value. Figure 68 illustrates the effects of protein knockdown on compound potency.

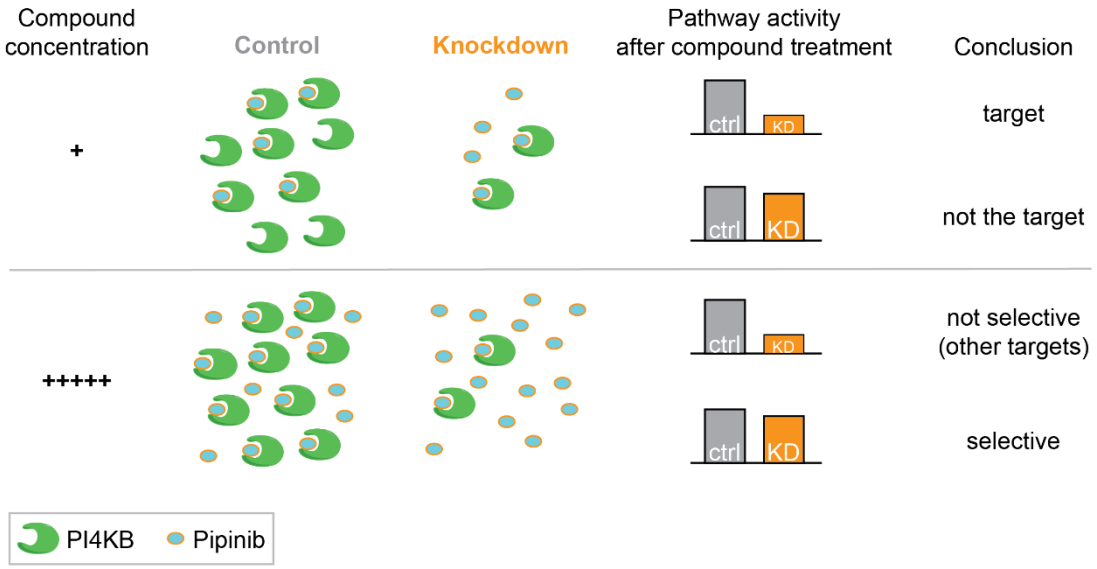

Figure 68. Effects of target knockdown on compound potency. If a low compound concentration is added after knockdown of a target protein, less of the compound will be needed to establish a phenotypic effect, i.e. compound potency is increased if the protein is the target of this compound. If an excess of compound is applied, a selective compound will not be more active compared to the control because it can already establish its maximum/threshold effect under wildtype protein levels. If additional activity is observed, the compound also targets other proteins that contribute to the phenotypic effect, thus, it is not selective.

A special case is a very efficient knockdown (>95%) that reduces protein abundance to almost undetectable amounts. If hardly any protein is present within the cell, the compound cannot establish any effect and thus should not produce a phenotype. Indeed, the potency of Pipinib was increased in the osteoblast differentiation assay, suggesting that PI4KB knockdown sensitized the cells for Pipinib treatment. Even at very low compound concentrations, e.g. 1 nM, osteoblast differentiation was reduced by approx. 75% in presence of siRNA, whereas control cells were not inhibited. This result was confirmed when IC_{50} values were determined for inhibition of Hh target gene expression. Also here, PI4KB knockdown led to reduced IC_{50} values, again suggesting sensitization towards Pipinib treatment. For high compound concentrations, the curves of knockdown and control cells converge to similar values, showing that the maximum activity of the compound, i.e. osteogenesis inhibition of approx. 85%, cannot be increased further. This suggests that a maximum threshold of pathway inhibition by Pipinib is reached and emphasizes selectivity of Pipinib for PI4KB.

6.4.3.4 CRISPR-Cas-mediated depletion of PI4KB and phenocopy of Hh pathway inhibition

The CRISPR-Cas technique is used to induce double strand breaks (DSBs) in specific regions of the DNA and thereby abolish gene expression. Like this, a knockout of a gene can be achieved if all alleles are successfully targeted. This method was performed as a complementary approach to the siRNA-mediated knockdown since both techniques can produce off-targets. If both experiments lead to the same results, it is very unlikely that these results have been caused by off-target effects.

Before testing CRISPR-Cas-mediated depletion of PI4KB, a knock-out cell line had to be generated. Using two sgRNAs, which would induce DSBs at two distinct sites in exon 1 and exon 3 of the PI4KB genomic sequence, creation of a large deletion was attempted. Several clones were screened for the large deletion by means of PCR using specifically designed primers to detect the deletion in the isolated genomic DNA (gDNA). While gDNA from the bulk cells was positive for the desired deletion, this could not be observed for the screened single cell colonies. However, comparison of the bands suggests that the PCR reaction using the deletion primers was not successful because no band at all, not even the control band for a negative clone, was detected. Here, a repetition of the PCR could clarify whether a deletion was achieved or not. When screening the clones for protein levels of PI4KB, clone 14 showed significantly reduced protein amounts of PI4KB but a complete knock-out was not observed. Retrieving new single cell clones from clone 14, clone 21 showed a reproducible reduction of

PI4KB protein levels. Yet, a complete knock-out was still not achieved. Literature search revealed that PI4KB is part of the essantialome[185]- Thus, complete removal of the protein leads to cell death, resulting in the selection of cells that still express PI4KB. Thus, the selected 3T3-PI4KB-KD cell line is a knockdown (KD) cell line, in which not all alleles of PI4KB were inactivated. The parent cell line was found to be mostly tri- (26.2%) to tetraploid (60%)[241], indicating that, within the KD cell line generated in this thesis, 2 of 3 or 3 of 4 PI4KB-alleles have been inactivated.

Evaluation of Hh target gene expression in CRISPR-Cas knockdown cells and comparison to wildtype NIH/3T3 cells revealed reduced target gene expression in knockdown cells, confirming the results obtained after siRNA-mediated depletion of PI4KB. Since 10 µM is a high concentration of Pipinib, the absence of a strong increase of compound potency could be explained with the threshold effect. This means that at this concentration of Pipinib, the achieved inhibition is close to the maximum compound activity, meaning a decrease of protein will not change the inhibitory effect of Pipinib. Here, testing lower concentrations of Pipinib should reveal an increased compound potency.

6.4.3.5 Overexpression of PI4KB

Increasing the protein amount of a target via overexpression should, in theory, scavenge the compound and thereby reduce the effective amount of compound which in turn will lead to reduced compound potency. To evaluate whether this is also true for Pipinib and PI4KB, the protein was overexpressed using an EGFP-PI4KB expression construct. Overexpressing cells did not show reduced compound potency in the osteoblast differentiation assay. To evaluate whether the EGFP fusion protein hinders correct folding, localization or activity, the same assay was repeated with a Flag-PI4KB-His construct. Due to smaller protein size, the Flag and His fusion proteins should not interfere with correct folding and localization. Using this construct, the overexpression was less efficient leading to lower protein amounts compared to the EGFP-PI4KB construct. This could be caused by use of different promoters. EGFP-PI4KB expression is controlled by a CMV enhancer fused to the chicken beta-actin promoter (CAG), while Flag-PI4KB-His expression is regulated by a human cytomegalovirus (CMV) immediate early enhancer and promoter. It has been reported that a CMV promoter induced poor transgene expression in murine embryonic stem cells in comparison to a CMV enhancer/chicken β actin (CAG) promoter which led to sufficient transgene expression[242]. Nevertheless, the overexpression using Flag-PI4KB-His showed a slight reduction of compound potency for high plasmid and compound concentrations, suggesting a possible scavenger effect. However, due to large variations between the experimental repetitions,

further repetitions and maybe the application of higher plasmid concentrations would be necessary to confirm this observation.

Assessment of Hh target gene expression after overexpression of PI4KB using the EGFP-PI4KB construct, yielded similar results. Here, only a tendency towards reduced compound potency was found. Further experiments employing the Flag-PI4KB-His plasmid and a titration of Pipinib would be necessary to verify a possible effect of overexpression of PI4KB on potency of Pipinib. It has to be noted that target overexpression does not always cause a scavenger effect. Protein overexpression can have drastic effects on cellular physiology and metabolism[11] and the impact on compound potency depends on the mode of inhibition and the effect of the protein itself as well as the overexpression on the cellular system.[12] Thus, the absence of a scavenger effect after protein overexpression does not imply that the respective protein is not the target of a compound. Based on the results obtained after chemical and genetic depletion of PI4KB activity or protein amount, PI4KB can be considered as a validated target of Pipinib and a mediator of Hh inhibition.

6.4.3.6 Evaluation of further kinase targets

So far, PI4KB was evaluated as the main target of Pipinib. The kinase panel, however, has also revealed further kinase targets, namely PIP5K1C, TTK, GAK and PIK3C2G. To assess whether these kinases also contribute to inhibition of Hh signaling, siRNA was employed to reduce expression of PIP5K1C, TTK and GAK. Upon siRNA treatment, Hh signaling was unchanged for each of the three kinases. Co-treatment with Pipinib did not lead to an increase of compound potency, suggesting that these kinases are neither positive regulators of Hh signaling nor mediators of Pipinib-induced Hh inhibition. According to literature, PIP5K1C was found to be required for ciliogenesis[243] and thus could be a positive regulator of Hh signaling. Still, this was not observed for the accomplished siRNA knockdown of 73.1 ± 0.2%. This could be caused by compensation of the knockdown mediated by isoenzymes of PIP5K1C, e.g. PIP5K1A or PIP5K1B, that also generate $PI(4,5)P_2$, the product of PIP5K1C. TTK, also called MPS1, was reported to be a negative regulator of ciliogenesis[244], which might explain the observed slight increase in *Ptch1* target gene expression. Nevertheless, inhibition of TTK would rather lead to pathway activation, if at all, than pathway inhibition. Thus, it cannot be responsible for mediating Pipinib-induced inhibition of Hh signaling pathway activity. So far, no implication of GAK in Hh signaling has been reported. Since only binding of Pipinib was assessed, it might be that Pipinib does not inhibit its activity after all. The siRNA experiment shows that depletion of GAK does not interfere with Hh signaling or increase compound

potency, suggesting that it does not mediate Hh inhibition. Even if Pipinib would inhibit GAK, it is very unlikely that this would affect Hh signaling.

For PIK3C2G, siRNA treatment did not induce a knockdown in NIH/3T3 cells. This could be caused by an overall low expression level of the protein. Highest expression of PIK3C2G is found in the BA/F3 cell line, a murine pro-B cell line, and even in these cells, only medium expression levels were found (information retrieved from Genevestigator, illustrated in Figure 69A and Figure 70A). Of all assessed 52 cell lines, NIH/3T3 cells exhibit the lowest PIK3C2G mRNA expression, even though the variation across measurements is quite high, indicated by the error bars.

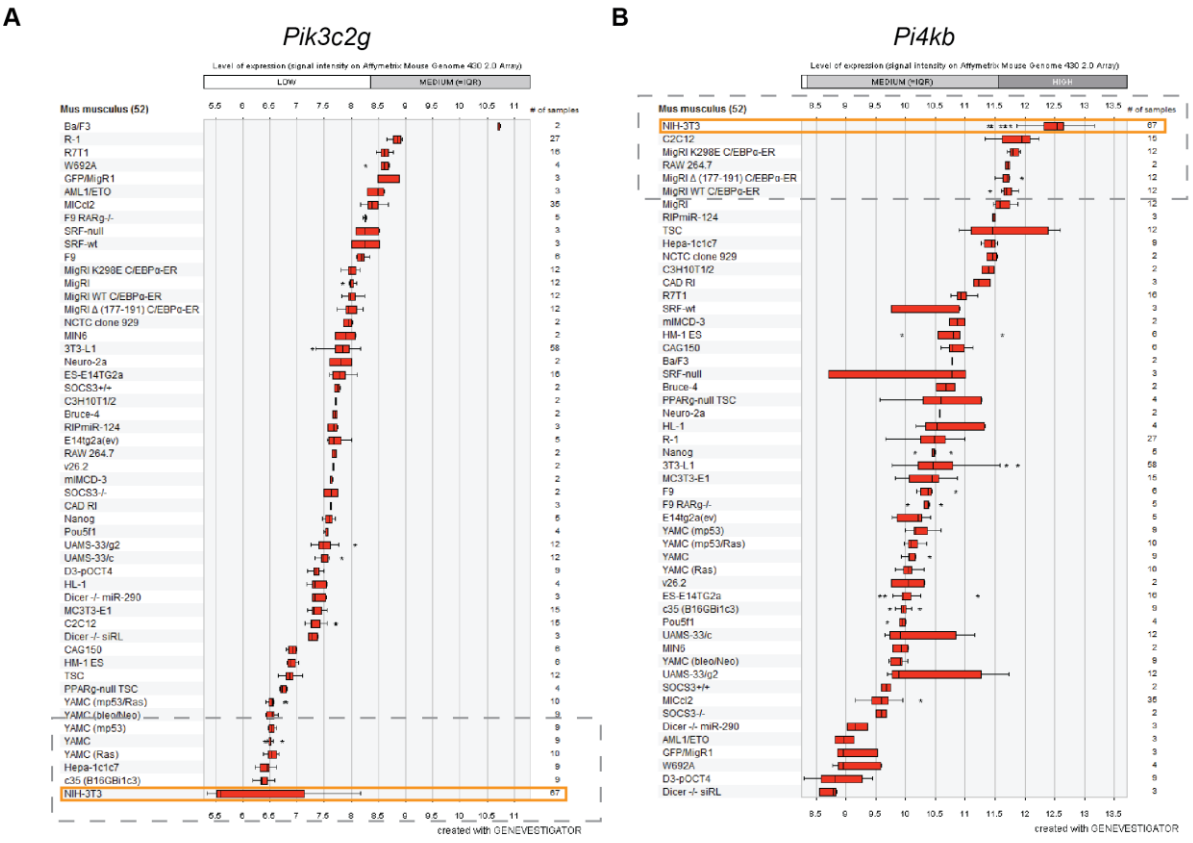

Figure 69. Expression levels of *Pik3c2g* and *Pi4kb* across 52 murine cell lines. Data were obtained by means of the Genevestigator tool. The orange box indicates expression levels of the NIH/3T3 cell line **A.** Expression levels of *Pik3c2g*. **B.** Expression levels of *Pi4kb*. Zoom-in images of the indicated areas (dashed grey rectangle) can be found in Figure 52.

As a comparison, NIH/3T3 cells have the highest expression of PI4KB compared to the other 51 cell lines (Figure 69B and Figure 70B). This emphasizes that protein levels of PIK3C2G are already at a minimum and further reduction via siRNA might not be feasible. To still

investigate whether PIK3C2G is a regulator of Hh signaling, published inhibitors of this kinase were evaluated for Hh inhibition.

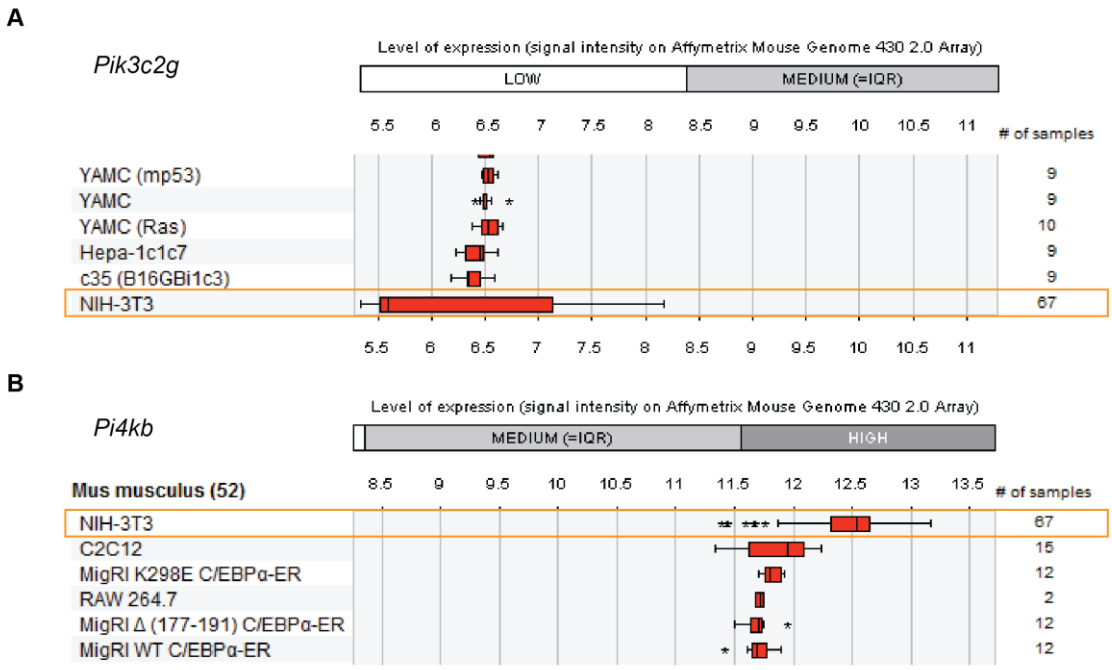

Figure 70. Expression levels of *Pik3c2g* and *Pi4kb* across 52 murine cell lines- zoom-in. Data were obtained by means of the Genevestigator tool. The orange box indicates expression levels of the NIH/3T3 cell line **A.** Expression levels of *Pik3c2g*. **B.** Expression levels of *Pi4kb*.

Here, none of the tested inhibitors led to a reduction of Hh target gene expression, suggesting that this kinase is not relevant for Hh signaling. It has been reported that Shh-responsive medulloblastoma (MB) carry mutations in PIK3C2G, amongst others[245]. Generally, PI3K signaling is implicated in Hh signaling via AKT[246] and since PIK3C2G belongs to the family of PI3 kinases, it could also contribute to AKT-mediated influence of Hh signaling. However, since expression levels of PIK3C2G are very low in NIH/3T3 cells and published inhibitors did not impair Hh target gene expression, it is very unlikely that this enzyme mediates Pipinib's inhibitory effect on Hh signaling.

6.4.4 Pipinib inhibits growth of medulloblastoma cells and serum-starved fibroblasts

To evaluate a possible implication of Pipinib for exploration in medicinal chemistry projects, its effect on the growth of DAOY medulloblastoma cells was monitored. One molecular

subgroup of medulloblastoma (SHH, group 2) is characterized by activated Hh signaling and an intermediate prognosis[247], i.e. a 5-year overall survival of approx. 75% under standard therapy[248]. Common mutations within this subgroup are found in PTC and SUFU, gene amplifications of GLI2 have been reported as well while mutations in SMO are only found in adults[247]. Sonidegib and Vismodegib, both SMO antagonists, have shown efficacy in clinical trials, highlighting the responsiveness of SHH-MB to treatment with Hh signaling inhibitors. The DAOY cell line was isolated from a human infant desmoplastic cerebellar medulloblastoma. This type of medulloblastoma belongs to the SHH subgroup[249]. Additionally, Götschel *et al.* have shown that this cell line is Hh responsive.[187,249]

Pipinib reduced growth of DAOY cells at a concentration of 30 µM. Lower concentrations did not inhibit cell growth, i.e. no dose-response was observed. Similar results were obtained for compounds **12** and **16**, inhibitors of PI4KB and PI4KA, respectively. PI4KA inhibition, however, led to a milder phenotype as compared to inhibition of PI4KB. GANT61, a GLI antagonist, also inhibited cell growth at concentrations of 10 and 30 µM. The SMO antagonist Vismodegib, however, did not impair cell growth. Co-treatment with the Hh pathway activator and SMO binder Purmorphamine did not change these results. Since Pipinib and GANT61 are both Hh inhibitors that do not target SMO while Vismodegib is a SMO binder, one could argue that only Hh inhibitors that do not target SMO are effective in DAOY cells. Contradictory to that, it has been found that Vismodegib successfully inhibits expression of the Hh target genes *Ptch1* and *Gli1* in DAOY cells[250]. Nevertheless, the results presented herein are in line with previous findings showing that DAOY cell growth is not affected by Cyclopamine, Vismodegib or LDE-225 (Sonidegib), all of whom are SMO binders.[251] In the same publication, a novel chemotype was identified that binds to SMO as well but is not affected by the common resistance mutations of the receptor. This compound is able to inhibit growth of DAOY cells, suggesting that DAOY cells might be resistant to common SMO binders. Still, if resistance mechanisms apply, it is questionable how Vismodegib treatment would lead to Hh pathway inhibition as reported[250]. So far, SMO mutations in DAOY cells have not been published. The cancer cell line encyclopedia (CCLE) has not listed any SMO mutations, either. Since DAOY cells were isolated from an infant tumor and, within this subgroup of medulloblastoma, SMO mutations are only found in adults[247], it is rather unlikely that this cell line carries mutations in SMO. If SMO is not mutated and growth would be Hh dependent, it can be assumed that pathway activation should increase growth and pathway inhibition should have the opposite effect. Since this has not been observed and both PI 4-kinases, PI4KA and PI4KB, reduce growth of DAOY cells, a more general and Hh-independent mechanism can be assumed for Pipinib. Accordingly, PI4KB has been found to be

upregulated in breast cancer and PI4P is generally involved in regulation of cell survival and proliferative signaling.[66] Additionally, Golgi phosphoprotein 3 (GOLPH3), a PI4P-specific effector, was found to be an oncogene that acts through mTOR[66]. Thus, the reduction of cellular PI4P levels alone could reduce proliferative signaling resulting in a lower growth rate. This is supported by the fact that no increase in dead cells was observed for neither Pipinib, nor compounds **12** or 1**6**, even though cell shape was affected, suggesting rather a growth inhibitory than a toxic effect. How GANT61 induces cell death is unknown. It could be an unknown toxic side effect that is not connected to its inhibitory effect on Hh signaling.

To evaluate whether Pipinib's growth inhibitory effect is specific to cancer cell lines, growth of the non-cancer NIH/3T3 cell line was evaluated. In this cell line, Pipinib only induced cell death in serum-reduced medium, independent of Hh signaling pathway activity, suggesting that nutrient deprivation induces inhibition of cell growth. Here, a parallel to the phenotype in cancer cells can be found. Since cancer cells have a deregulated metabolism and increased energy consumption, their demand for nutrients is increased compared to non-malignant cells. To compensate this, cancer cells perform macropinocytosis, a form of bulk endocytosis, which requires several membrane phospholipids, PI4P being one of them.[252] Due to this, DAOY cells could be more sensitive to reduced PI4P levels caused by inhibition of PI4KB or PI4KA. Additionally, observations within the group have shown that cancer cells are often more sensitive to compound treatment than cell lines from non-malignant tissues, which might be caused by the plethora of mutations that have accumulated in these cells. Considering the high concentrations at which effects are observed, they might be altogether unspecific.

6.4.5 Mode of action analysis

Several experiments were performed to unravel how Pipinib inhibits Hedgehog signaling. The obtained results will be discussed in the following chapters.

6.4.5.1 Pipinib impairs ciliary trafficking of SMO

To elucidate at which stage of the pathway Pipinib interferes with Hh signaling, trafficking of SMO to the primary cilium was monitored. It was found that Pipinib efficiently impairs the migration of SMO to the cilium. So far, only few Hh signaling inhibitors are known that interfere with SMO trafficking without binding to the protein itself, which is why Pipinib inhibits Hh signaling through an alternative mode of action.

Several compounds are known to impair ciliary trafficking of SMO, among them the well-known SMO antagonist Vismodegib and its derivatives. Recently, assessment of the trafficking of a constitutively active mutant of SMO that harbors the common W535L point mutation (SMO-M2), revealed ten novel small-molecule inhibitors of SMO ciliary trafficking[253]. Eight compounds were found to target the ciliary targeting complex of G protein-coupled receptor associated sorting protein 2 (Gprasp2) and SMO-M2, thereby interfering with SMO's transport to the cilium, while one compound impaired overall intracellular trafficking of SMO by inhibiting ionotropic receptors.[253] These publications emphasize that there are several mechanisms and routes that can be employed by small molecules to modulate Hh signaling.

It has been reported that PI4P binding is required to induce conformational changes in SMO that lead to its phosphorylation, activation and transport into the cilium.[35] Thus, impairment of SMO's ciliary trafficking could be caused by lowering cellular levels of PI4P and thereby reducing conformational change which is necessary for the subsequent transport of SMO. Two approaches would be suitable to validate this hypothesis. On the one hand, phosphorylation of SMO could be monitored by means of antibodies that specifically recognize the phosphorylated version of SMO. On the other hand, interaction of SMO and PI4P could be monitored in cells. The first approach was attempted but not successful due to insufficient performance of the SMO antibody in immunoblot detection. Future experiments could use a tagged version of SMO that could be detected using an antibody against the respective tag. The second proposed experiment was performed and will be discussed in 6.5.4.2.

While Pipinib could act specifically on the interaction of PI4P and SMO, it could likewise interfere with general protein trafficking to the membrane and the cilium. It is known that PI4P generated by PI4KB is necessary for protein trafficking from the TGN to the PM[66,75]. To evaluate whether Pipinib specifically inhibits transport of SMO to the cilium, trafficking of other G-protein coupled receptors (GPCRs) that are transported to the cilium, presumably using a similar mechanism, could be monitored. A possible candidate for such an experiment is the G-protein coupled receptor 161 (GPR161), a receptor that is known to negatively regulate Hh signaling via increasing cyclic adenosine monophosphate (cAMP) levels[254]. If Pipinib generally targets ciliary transport of membrane proteins, ciliary amounts of GPR161 should be reduced after Pipinib treatment. Like this, the mode of action of Pipinib can be elucidated in further detail.

6.4.5.2 Pipinib does not inhibit interaction of SMO and PI4P as measured by PLA

The interaction of SMO and PI4P was approximated by measuring close proximity using the proximity ligation assay (PLA). Using this technique, an increase of PLA-detected interaction of PI4P and SMO was observed for pathway activation with Purmorphamine. Treatment with Pipinib, however, did not lead to a reduction of proximity. There are four possible explanations for this outcome. First, Pipinib does not reduce the interaction of SMO and PI4P, even though it impairs its ciliary trafficking and reduces cellular levels of PI4P. If this is true, Pipinib might act more generally and thus could act on receptor trafficking to the cilium as a whole (see also 6.5.4.1). Second, Pipinib does reduce interaction of SMO and PI4P but PLA is not a suitable technique to detect this event. Since PLA is measuring close proximity and PI4P is highly abundant throughout the cell, proximity could be coincidental thereby falsifying experimental results obtained with this technique. Third, Pipinib does not decrease overall interaction but impairs interaction in certain parts of the cell that are not detectable by a whole-cell measurement. Considering that Pipinib reduced PI4P on vesicle structures, it might be that only the interaction between PI4P and SMO, which takes place during vesicular transport of SMO from the Golgi to the cilium or the plasma membrane, is affected and this effect is superimposed with the PLA events distributed all over the cell body. To assess interaction in (living) cells, other approaches than PLA are necessary. Possible methods could include FLIM-FRET experiments employing either a directly fluorescently labeled Phosphoinositide paired with a fluorescent SMO fusion protein or the use of a fluorescent PI4P sensor paired with the aforementioned SMO fusion protein. Even though this technique also measures proximity and not interaction, the Förster radius that is required for FRET to occur is considerably lower than the maximum tolerated distance for PLA (approx. 10 nM versus 40 nM), thus arguing that FLIM-FRET will be more accurate and less prone to abundance-based false positive detection. Here, the disadvantage lies within the ectopic protein expression that could have an impact on cell physiology. Additionally, the use of a PI4P sensor could cause false positive results due to increased size when engaging PI4P. Nevertheless, this approach is the most suitable technique to monitor protein-protein or protein-small molecule interactions inside cells.

6.4.5.3 Inhibition of PI4KA only induces minor inhibition of Hh signaling

Previously, an implication of both PI4KB and PI4KA in Hh signaling was assumed.[50] This thesis has validated PI4KB as a positive regulator of Hh signaling. Previously, both PI4KA and PI4KB were suggested as Hh regulators based on siRNA-mediated depletion of the

proteins and measurement of GLI reporter gene activity[50]. Hence, the possible implication of PI4KA in Hh signaling was re-assessed by means of Hh target gene expression using a published inhibitor for this PI 4-kinase[186]. This compound showed lower inhibition of Hh target gene expression compared to Pipinib. Additionally, an equimolar mixture with Pipinib did not lead to increased inhibition, i.e. a synergistic effect, suggesting that PI4KA is not the primary PI4-kinase, which is required for Hh signaling. PI4KA is localized at the plasma membrane were it generates PI4P[188]. The fact that inhibition of PI4KA does not have a major impact on Hh signaling pathway activity emphasizes that the PI4P, which is generated at the plasma membrane, might not have a high relevance for SMO trafficking to the primary cilium. It is possible, that mainly PI4KB-generated PI4P is relevant for Hh signaling because it is located on post-Golgi vesicles that transport receptors and membrane proteins to the plasma membrane and the primary cilium.

6.4.5.4 Proposed mode of action

Based on the results presented in this thesis, three modes of action for Pipinib-mediated inhibition of Hh signaling can be proposed. Pipinib inhibits PI4KB, resulting in reduced PI4P levels at the Golgi apparatus and especially on post-Golgi vesicles that transport membrane proteins, e.g. SMO, to the primary cilium.

1. Due to a low concentration of PI4P on post-Golgi vesicles, not enough of this phosphoinositide is available to bind to SMO and enable its conformational switch, resulting in a retention of SMO in the cytoplasm.

2. Due to decreased PI4P production at the Golgi, also membrane levels of PI4P are reduced. Thus, less PI4P is available at the PM to bind to SMO, resulting in a retainment of SMO in the cytoplasm or the PM.

3. Due to a low concentration of PI4P on post-Golgi vesicles, these cannot fuse with the membrane, resulting in general inhibition of vesicle-mediated transport of proteins to the plasma membrane.

Figure 71 summarizes the possible modes of action. It is also possible that proteins are transported directly to the cilium and fuse with the membrane inside the cilium. This process could be likewise inhibited by lowered PI4P levels in the same manner as described above (1.-3.). For the sake of simplicity, only the plasma membrane theory is depicted in the figure.

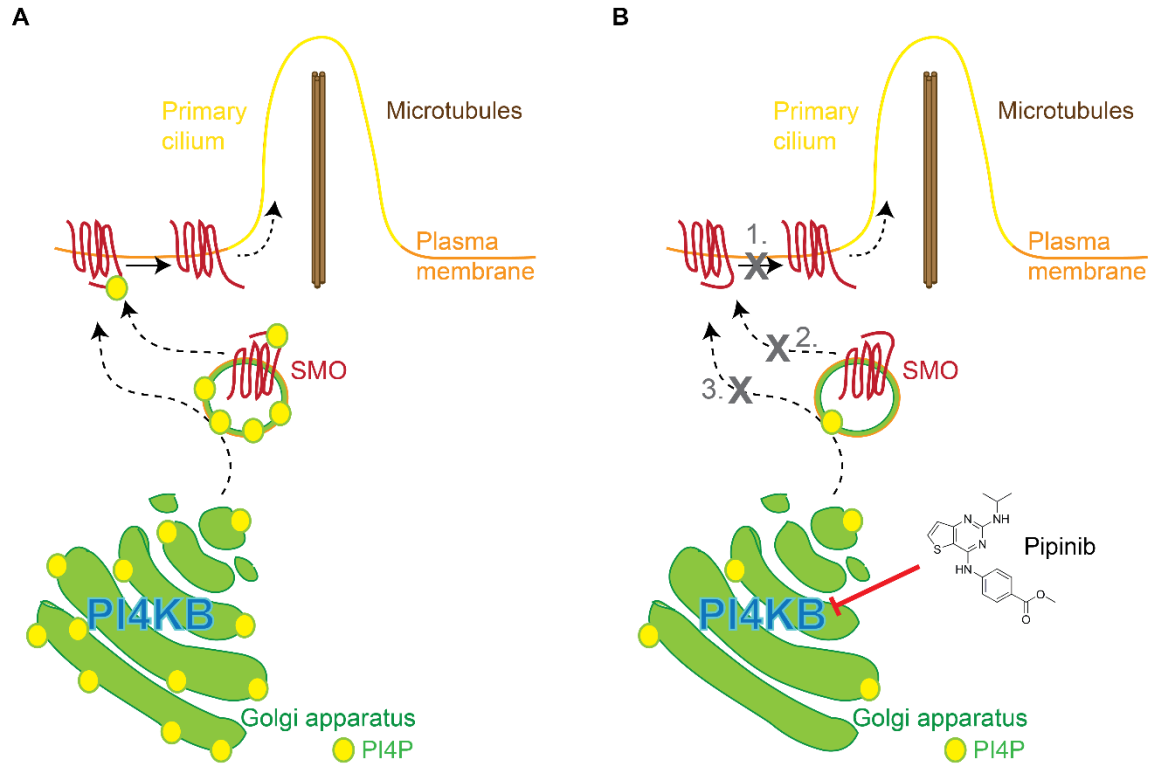

Figure 71. Possible modes of action of Pipinib. A. Simplified scheme of SMO trafficking in absence of Pipinib. PI4KB generates PI4P at the Golgi. SMO is transported to the membrane/the primary cilium on post-Golgi vesicles. PI4P present on these vesicles binds to SMO and facilitates a conformational switch or the fusion with the plasma membrane. **B.** Simplified scheme of SMO trafficking in the presence of Pipinib. Pipinib inhibits PI4KB, thereby reducing PI4P levels at the Golgi and on post-Golgi vesicles. Due to low PI4P levels, SMO does not interact with PI4P and its activation is impaired (1.) and/or vesicles cannot fuse with the plasma membrane (2.) and/or overall vesicle trafficking to the membrane is impaired (3.), leading to reduced migration of SMO to the primary cilium.

Recently, Klink *et al.* reported that the BBSome, a complex that transports proteins into cilia, binds to SMO peptides[255]. Thus, the BBSome could be involved in the complex process of SMO trafficking. A possible series of events could include PI4P binding, which enables phosphorylation and a conformational switch that exposes SMO's ciliary targeting sequence to the BBSome, which in turn induces binding of this transport complex and transport into the cilium. To prove this hypothesis, several approaches could be applied. Fluorescently tagged versions of BBSome components and SMO could be applied in FLIM-FRET experiments to prove binding and transport of SMO upon pathway activation. Furthermore, cells harboring a dysfunctional BBSome, e.g. cell lines derived from patients with the Bardet-Biedl syndrome (BBS), a disease that is based on mutations in 19 genes[255,256], eight of which are known to form the BBSome[255,257], could be evaluated for SMO trafficking to validate an implication of this complex in ciliary transport of SMO. In fact, it has been reported that BBS mutations in mice and hTERT-RPE1 cells lead to accumulation of SMO and PTC in cilia and inhibition of

Hh signaling[258,259]. This suggests that the BBSome might rather be implicated in SMO ciliary export or shuttling. Nevertheless, Pipinib and PI4P levels might have a possible implication in these events.

Additionally, it is unknown how PI4KB is implicated in Hh signaling. This thesis has shown that PI4KB activity is necessary for Hh signaling and that its inhibition impairs SMO ciliary trafficking. Furthermore, it is known that PTCH inhibits SMO by restricting its ciliary abundance[15]. A possible conclusion would be that PTCH might control PI4KB and thereby interfere with PI4P production. However, it is unclear how a membrane protein could influence the activity of PI4KB which is recruited to the Golgi and activated by the GTPase ADP-ribosylation factor 1 (Arf1), whose binding might be mediated by Acyl-CoA-binding domain containing protein 3 (ACBD3).[48] Activity of PI4KB is additionally controlled by the neuronal calcium sensor 1 (NCS-1) and increased after phosphorylation at Ser^{294} by protein kinase D (PKD), which leads to recruitment of 14-3-3 proteins that stabilize PI4KB activity.[48] On the basis of this information, it is unlikely that PTCH can influence the activity of PI4KB. Additionally, this thesis has revealed that Pipinib inhibits Hh signaling upon pathway activation with Purmorphamine. The SMO agonist activates Hh signaling downstream of PTC thereby circumventing any influence of PTCH on Hh signaling. Since Pipinib inhibits Hh signaling via PI4KB, PI4KB's role in Hh signaling has to be, at least in part, independent of PTCH. Furthermore, PI4KB is required for several general cellular processes like protein trafficking and Golgi integrity. Thus, it would be rather inconvenient if the activity of this protein is influenced by Hh signaling since this would affect the trafficking of various membrane proteins. In conclusion, it is more likely that PTCH sequesters PI4P without affecting PI4KB activity and thereby induces a local reduction in PI4P levels that prevents activation of SMO[35]. Indeed, Jiang *et al.* have shown that PTCH binds to PI4P, proving the overall applicability of this hypothesis. It has been proposed that SMO is bound by a priming ligand that does not have activating properties and enables SMO activation upon binding of another activating ligand that is yet unknown[260]. Since PI4P binds the cytosolic tail of SMO[35], it could fulfill the role of such a priming ligand. Under these circumstances, Pipinib treatment would decrease cellular PI4P, thereby preventing priming of SMO. Binding of Purmorphamine, which, in this setting, is the activating ligand, would not be sufficient for proper SMO activation, resulting in Pipinib-induced inhibition of Hh signaling.

7 CONCLUSION AND PERSPECTIVES

The Hedgehog signaling pathway is of major importance for embryonic development and tissue homeostasis. Its implication in several cancers, e.g. medulloblastoma and basal cell carcinoma, makes it one of the most studied pathways in biological research. So far, several inhibitors have been published, some of which are in clinical use. Nevertheless, due to frequent occurrence of therapy resistance, the demand for novel compounds with alternative modes of action is high.

Within this thesis, several inhibitors of Hedgehog signaling have been identified and characterized. Quinoline-, indole- and azepinone derivatives moderately inhibited Hh signaling pathway activity while not binding to the cyclopamine binding site of SMO. A withanolide A derivative and Smoothib, a pyrazolo-imidazole derivative, were identified as SMO antagonists. Future studies could be aimed at characterizing the withanolide A derivative by means of the SMO trafficking assay to assess whether its binding to SMO causes impairment of SMO's migration to the cilium. Smoothib impairs ciliary trafficking of SMO. A molecular docking study suggested that Smoothib delves deep into the ligand binding pocket of SMO, occupying a binding site similar to that of the resistance overcoming SMO binder SANT-1. Further experiments for this compound could include co-crystallization of Smoothib an SMO to verify the binding mode. Additionally, assessment of Smoothib's binding to mutated versions of SMO could enable evaluation whether Smoothib indeed could overcome common resistances, which are observed in the clinic. If so, Smoothib could represent an alternative to common clinically applied SMO antagonists like Vismodegib.

Pipinib, a thienopyrimidine derivative is a potent inhibitor of Hh signaling that increases protein levels of GLI3-R. Via kinase panel screening and protein affinity chromatography, the following potential targets were identified for Pipinib: PI4KB, NQO2, HEBP1, GRAMD4, TM7SF3, FECH, PIP5K1C, PIK3C2G, GAK and TTK. Except for PI4KB, none of these proteins was found to be implicated in Hh signaling. Based on literature reports that link PI4KB and its product PI4P to Hh signaling,[35,50] PI4KB was chosen for further characterization and validation. Pipinib inhibits PI4KB in an ATP-competitive manner and engages the kinase in cellular lysates. Pipinib induced changes in the morphology of the Golgi apparatus and mitochondria and reduced intracellular levels of PI4P. In DAOY cells, Pipinib treatment lead to reduced cell growth independent of Hh signaling activation, suggesting that the compound affects cell growth via a general mechanism that could involve PI4P signaling. In NIH/3T3 cells, growth was only inhibited upon serum starvation, a condition that increases cellular

stress and might sensitize cells for Pipinib treatment and PI4P deprivation. Previously reported inhibitors of PI4KB as well as genetic depletion confirmed PI4KB as a positive regulator of Hh signaling and sensitized NIH/3T3 cells for Pipinib treatment resulting in increased compound potency for Hh signaling inhibition. The proposed mode of action involves inhibition of PI4KB and reduction of cellular PI4P levels, which impairs SMO ciliary trafficking. Inhibition of PI4KA only leads to minor inhibition of Hh signaling, suggesting that PI4KB might be a major source for Hh relevant PI4KB.

To pin down the mode of action of Pipinib, additional experiments would be necessary. First of all, the evaluation of the transport of other membrane proteins to the primary cilium could reveal whether overall or only SMO transport to the cilium is affected by Pipinib. Additionally FLIM-FRET experiments for SMO and PI4P would be required to prove the interaction of those two entities inside living cells and determine whether Pipinib interferes with this interaction. Since PI4P interaction with SMO is followed by phosphorylation of SMO by CK1α and GRK2[33], monitoring these phosphorylation events using phospho-specific antibodies against SMO could confirm an impact of PI4P on this series of events.

Furthermore, a crystal structure of PI4KB and Pipinib would enable identification of the exact binding site of the compound. On the one hand, this information could facilitate medicinal chemistry-based improvement of the compound structure to retrieve more potent derivatives and comparison of the binding mode to that of already published PI4KB inhibitors. On the other hand, information on the binding site of Pipinib could enable generation of mutated compound-resistant PI4KB versions. If PI4KB is the main target of Pipinib, the expression of these mutants in cells that have been depleted of native PI4KB should abolish Pipinib activity as a Hh inhibitor.

With its novel mode of action, Pipinib is an interesting tool compound to study the Hh signaling pathway and PI4KB function. Due to PI4KB's implication in viral infections, it could be equally interesting to study antiviral therapies. Due to SMO mutations and resistances against clinically approved Hh inhibitors like Vismodegib[123], Pipinib could be a starting point for the development of alternative treatments which might be applicable in cancer therapy.

8 REFERENCES

1. Kostic, M. A Shout Out to Chemical Biology, a Multidisciplinary Field Par Excellence. *Cell chemical biology* **24,** 427 (2017).
2. Stockwell, B.R. Frontiers in chemical genetics. *Trends in biotechnology* **18,** 449–455 (2000).
3. Kawasumi, M. & Nghiem, P. Chemical genetics. Elucidating biological systems with small-molecule compounds. *The Journal of investigative dermatology* **127,** 1577–1584 (2007).
4. Haasen, D. *et al.* How Phenotypic Screening Influenced Drug Discovery. Lessons from Five Years of Practice. *Assay and drug development technologies* **15,** 239–246 (2017).
5. Ziegler, S., Pries, V., Hedberg, C. & Waldmann, H. Target Identification for Small Bioactive Molecules. Finding the Needle in the Haystack. *Angewandte Chemie International Edition* **52,** 2744–2792 (2013).
6. Kapoor, S., Waldmann, H. & Ziegler, S. Novel approaches to map small molecule-target interactions. *Bioorganic & medicinal chemistry* **24,** 3232–3245 (2016).
7. Mateus, A., Määttä, T.A. & Savitski, M.M. Thermal proteome profiling. Unbiased assessment of protein state through heat-induced stability changes. *Proteome science* **15,** 13 (2016).
8. Schneider, G., Tanrikulu, Y. & Schneider, P. Self-organizing molecular fingerprints. A ligand-based view on drug-like chemical space and off-target prediction. *Future medicinal chemistry* **1,** 213–218 (2009).
9. Bray, M.-A. *et al.* Cell Painting, a high-content image-based assay for morphological profiling using multiplexed fluorescent dyes. *Nature protocols* **11,** 1757–1774 (2016).
10. Martinez Molina, D. & Nordlund, P. The Cellular Thermal Shift Assay: A Novel Biophysical Assay for In Situ Drug Target Engagement and Mechanistic Biomarker Studies. *Annual review of pharmacology and toxicology* **56,** 141–161 (2016).
11. Gibson, T.J., Seiler, M. & Veitia, R.A. The transience of transient overexpression. *Nature methods* **10,** 715–721 (2013).
12. Palmer, A.C. & Kishony, R. Opposing effects of target overexpression reveal drug mechanisms. *Nature communications* **5,** 4296 (2014).
13. Nüsslein-Volhard, C. & Wieschaus, E. Mutations affecting segment number and polarity in Drosophila. *Nature* **287,** 795–801 (1980).
14. Briscoe, J. & Thérond, P.P. The mechanisms of Hedgehog signalling and its roles in development and disease. *Nature reviews. Molecular cell biology* **14,** 416–429 (2013).
15. Wu, F., Zhang, Y., Sun, B., McMahon, A.P. & Wang, Y. Hedgehog Signaling. From Basic Biology to Cancer Therapy. *Cell chemical biology* **24,** 252–280 (2017).
16. Venkatesh, D. Primary cilia. *Journal of oral and maxillofacial pathology : JOMFP* **21,** 8–10 (2017).

17. Rohatgi, R., Milenkovic, L. & Scott, M.P. Patched1 regulates hedgehog signaling at the primary cilium. *Science* **317,** 372–376 (2007).

18. Kogerman, P. *et al.* Mammalian suppressor-of-fused modulates nuclear-cytoplasmic shuttling of Gli-1. *Nature cell biology* **1,** 312–319 (1999).

19. Hui, C.-C. & Angers, S. Gli proteins in development and disease. *Annual review of cell and developmental biology* **27,** 513–537 (2011).

20. Tukachinsky, H., Petrov, K., Watanabe, M. & Salic, A. Mechanism of inhibition of the tumor suppressor Patched by Sonic Hedgehog. *Proceedings of the National Academy of Sciences of the United States of America* **113,** E5866-E5875 (2016).

21. Corbit, K.C. *et al.* Vertebrate Smoothened functions at the primary cilium. *Nature* **437,** 1018–1021 (2005).

22. Yang, C., Chen, W., Chen, Y. & Jiang, J. Smoothened transduces Hedgehog signal by forming a complex with Evc/Evc2. *Cell research* **22,** 1593–1604 (2012).

23. Tukachinsky, H., Lopez, L.V. & Salic, A. A mechanism for vertebrate Hedgehog signaling. Recruitment to cilia and dissociation of SuFu-Gli protein complexes. *The Journal of cell biology* **191,** 415–428 (2010).

24. Katoh, Y. & Katoh, M. Hedgehog target genes. Mechanisms of carcinogenesis induced by aberrant hedgehog signaling activation. *Current molecular medicine* **9,** 873–886 (2009).

25. Rana, R. *et al.* Structural insights into the role of the Smoothened cysteine-rich domain in Hedgehog signalling. *Nature communications* **4,** 2965 (2013).

26. Nedelcu, D., Liu, J., Xu, Y., Jao, C. & Salic, A. Oxysterol binding to the extracellular domain of Smoothened in Hedgehog signaling. *Nature chemical biology* **9,** 557–564 (2013).

27. Wang, C. *et al.* Structure of the human smoothened receptor bound to an antitumour agent. *Nature* **497,** 338–343 (2013).

28. Wang, C. *et al.* Structural basis for Smoothened receptor modulation and chemoresistance to anticancer drugs. *Nature communications* **5,** 4355 (2014).

29. Xie, J. *et al.* Activating Smoothened mutations in sporadic basal-cell carcinoma. *Nature* **391,** 90–92 (1998).

30. Arensdorf, A.M., Marada, S. & Ogden, S.K. Smoothened Regulation. A Tale of Two Signals. *Trends in Pharmacological Sciences* **37,** 62–72 (2016).

31. Moreira, I.S. Structural features of the G-protein/GPCR interactions. *Biochimica et biophysica acta* **1840,** 16–33 (2014).

32. Chen, W. *et al.* Activity-dependent internalization of smoothened mediated by beta-arrestin 2 and GRK2. *Science* **306,** 2257–2260 (2004).

33. Chen, Y. *et al.* Sonic Hedgehog dependent phosphorylation by CK1α and GRK2 is required for ciliary accumulation and activation of smoothened. *PLoS biology* **9,** e1001083 (2011).

34. Chen, Y. & Jiang, J. Decoding the phosphorylation code in Hedgehog signal transduction. *Cell research* **23,** 186–200 (2013).

35. Jiang, K. *et al.* PI(4)P Promotes Phosphorylation and Conformational Change of Smoothened through Interaction with Its C-terminal Tail. *PLoS biology* **14,** e1002375 (2016).

36. Rohatgi, R. & Snell, W.J. The ciliary membrane. *Current opinion in cell biology* **22,** 541–546 (2010).

37. Kim, J. *et al.* The role of ciliary trafficking in Hedgehog receptor signaling. *Science signaling* **8,** ra55 (2015).

38. Benmerah, A. The ciliary pocket. *Current opinion in cell biology* **25,** 78–84 (2013).

39. Milenkovic, L., Scott, M.P. & Rohatgi, R. Lateral transport of Smoothened from the plasma membrane to the membrane of the cilium. *The Journal of cell biology* **187,** 365–374 (2009).

40. Milenkovic, L. *et al.* Single-molecule imaging of Hedgehog pathway protein Smoothened in primary cilia reveals binding events regulated by Patched1. *Proceedings of the National Academy of Sciences of the United States of America* **112,** 8320–8325 (2015).

41. Mukhopadhyay, S. & Rohatgi, R. G-protein—coupled receptors, hedgehog signaling and primary cilia. *Seminars in cell & developmental biology* **0,** 63–72 (2014).

42. Davies, J.P., Chen, F.W. & Ioannou, Y.A. Transmembrane molecular pump activity of Niemann-Pick C1 protein. *Science (New York, N.Y.)* **290,** 2295–2298 (2000).

43. Dorn, K.V., Hughes, C.E. & Rohatgi, R. A Smoothened-Evc2 complex transduces the Hedgehog signal at primary cilia. *Developmental cell* **23,** 823–835 (2012).

44. Pusapati, G.V. *et al.* EFCAB7 and IQCE regulate hedgehog signaling by tethering the EVC-EVC2 complex to the base of primary cilia. *Developmental cell* **28,** 483–496 (2014).

45. Polizio, A.H. *et al.* Heterotrimeric Gi proteins link Hedgehog signaling to activation of Rho small GTPases to promote fibroblast migration. *The Journal of biological chemistry* **286,** 19589–19596 (2011).

46. Belgacem, Y.H. & Borodinsky, L.N. Sonic hedgehog signaling is decoded by calcium spike activity in the developing spinal cord. *Proceedings of the National Academy of Sciences of the United States of America* **108,** 4482–4487 (2011).

47. Teperino, R. *et al.* Hedgehog partial agonism drives Warburg-like metabolism in muscle and brown fat. *Cell* **151,** 414–426 (2012).

48. Dornan, G.L., McPhail, J.A. & Burke, J.E. Type III phosphatidylinositol 4 kinases. Structure, function, regulation, signalling and involvement in disease. *Biochemical Society transactions* **44,** 260–266 (2016).

49. Balla, T. Phosphoinositides. Tiny lipids with giant impact on cell regulation. *Physiological reviews* **93,** 1019–1137 (2013).

50. Yavari, A. *et al.* Role of lipid metabolism in smoothened derepression in hedgehog signaling. *Developmental cell* **19,** 54–65 (2010).

51. Chávez, M. *et al.* Modulation of Ciliary Phosphoinositide Content Regulates Trafficking and Sonic Hedgehog Signaling Output. *Developmental cell* **34,** 338–350 (2015).

52. Garcia-Gonzalo, F.R. *et al.* Phosphoinositides Regulate Ciliary Protein Trafficking to Modulate Hedgehog Signaling. *Developmental cell* **34,** 400–409 (2015).

53. Brown, J.R. & Auger, K.R. Phylogenomics of phosphoinositide lipid kinases. Perspectives on the evolution of second messenger signaling and drug discovery. *BMC evolutionary biology* **11,** 4 (2011).

54. Blumental-Perry, A. *et al.* Phosphatidylinositol 4-phosphate formation at ER exit sites regulates ER export. *Developmental cell* **11,** 671–682 (2006).

55. Balla, A. *et al.* Maintenance of hormone-sensitive phosphoinositide pools in the plasma membrane requires phosphatidylinositol 4-kinase IIIalpha. *Molecular biology of the cell* **19,** 711–721 (2008).

56. Sridhar, S. *et al.* The lipid kinase PI4KIIIβ preserves lysosomal identity. *The EMBO journal* **32,** 324–339 (2013).

57. Brill, J.A., Hime, G.R., Scharer-Schuksz, M. & Fuller, M.T. A phospholipid kinase regulates actin organization and intercellular bridge formation during germline cytokinesis. *Development (Cambridge, England)* **127,** 3855–3864 (2000).

58. Tóth, B. *et al.* Phosphatidylinositol 4-kinase IIIbeta regulates the transport of ceramide between the endoplasmic reticulum and Golgi. *The Journal of biological chemistry* **281,** 36369–36377 (2006).

59. Godi, A. *et al.* ARF mediates recruitment of PtdIns-4-OH kinase-beta and stimulates synthesis of PtdIns(4,5)P2 on the Golgi complex. *Nature cell biology* **1,** 280–287 (1999).

60. Sasaki, J., Ishikawa, K., Arita, M. & Taniguchi, K. ACBD3-mediated recruitment of PI4KB to picornavirus RNA replication sites. *The EMBO journal* **31,** 754–766 (2012).

61. Zhao, X. *et al.* Interaction of neuronal calcium sensor-1 (NCS-1) with phosphatidylinositol 4-kinase beta stimulates lipid kinase activity and affects membrane trafficking in COS-7 cells. *The Journal of biological chemistry* **276,** 40183–40189 (2001).

62. Hausser, A. *et al.* Protein kinase D regulates vesicular transport by phosphorylating and activating phosphatidylinositol-4 kinase IIIbeta at the Golgi complex. *Nature cell biology* **7,** 880–886 (2005).

63. Hausser, A. *et al.* Phospho-specific binding of 14-3-3 proteins to phosphatidylinositol 4-kinase III beta protects from dephosphorylation and stabilizes lipid kinase activity. *Journal of cell science* **119,** 3613–3621 (2006).

64. Graaf, P. de *et al.* Phosphatidylinositol 4-kinasebeta is critical for functional association of rab11 with the Golgi complex. *Molecular biology of the cell* **15,** 2038–2047 (2004).

65. Tan, J. & Brill, J.A. Cinderella story. PI4P goes from precursor to key signaling molecule. *Critical reviews in biochemistry and molecular biology* **49,** 33–58 (2014).

66. Matteis, M.A. de, Wilson, C. & D'Angelo, G. Phosphatidylinositol-4-phosphate: the Golgi and beyond. *BioEssays : news and reviews in molecular, cellular and developmental biology* **35,** 612–622 (2013).

67. Bowser, R. & Novick, P. Sec15 protein, an essential component of the exocytotic apparatus, is associated with the plasma membrane and with a soluble 19.5S particle. *The Journal of cell biology* **112,** 1117–1131 (1991).

68. Craene, J.-O. de, Bertazzi, D.L., Bär, S. & Friant, S. Phosphoinositides, Major Actors in Membrane Trafficking and Lipid Signaling Pathways. *International journal of molecular sciences* **18** (2017).

69. Mesmin, B. *et al.* A four-step cycle driven by PI(4)P hydrolysis directs sterol/PI(4)P exchange by the ER-Golgi tether OSBP. *Cell* **155,** 830–843 (2013).

70. Chung, J. *et al.* INTRACELLULAR TRANSPORT. PI4P/phosphatidylserine countertransport at ORP5- and ORP8-mediated ER-plasma membrane contacts. *Science* **349,** 428–432 (2015).

71. Lenoir, M. *et al.* Structural basis of dynamic membrane recognition by trans-Golgi network specific FAPP proteins. *Journal of molecular biology* **427,** 966–981 (2015).

72. Knight, Z.A. *et al.* A pharmacological map of the PI3-K family defines a role for p110alpha in insulin signaling. *Cell* **125,** 733–747 (2006).

73. Spickler, C. *et al.* Phosphatidylinositol 4-kinase III beta is essential for replication of human rhinovirus and its inhibition causes a lethal phenotype in vivo. *Antimicrobial agents and chemotherapy* **57,** 3358–3368 (2013).

74. Lamarche, M.J. *et al.* Anti-hepatitis C virus activity and toxicity of type III phosphatidylinositol-4-kinase beta inhibitors. *Antimicrobial agents and chemotherapy* **56,** 5149–5156 (2012).

75. Boura, E. & Nencka, R. Phosphatidylinositol 4-kinases. Function, structure, and inhibition. *Experimental cell research* **337,** 136–145 (2015).

76. Waring, M.J. *et al.* Potent, selective small molecule inhibitors of type III phosphatidylinositol-4-kinase α- but not β-inhibit the phosphatidylinositol signaling cascade and cancer cell proliferation. *Chemical communications (Cambridge, England)* **50,** 5388–5390 (2014).

77. Arita, M. *et al.* Phosphatidylinositol 4-kinase III beta is a target of enviroxime-like compounds for antipoliovirus activity. *Journal of virology* **85,** 2364–2372 (2011).

78. Mejdrová, I. *et al.* Rational Design of Novel Highly Potent and Selective Phosphatidylinositol 4-Kinase IIIβ (PI4KB) Inhibitors as Broad-Spectrum Antiviral Agents and Tools for Chemical Biology. *Journal of medicinal chemistry* **60,** 100–118 (2017).

79. Hahn, H. *et al.* Mutations of the human homolog of Drosophila patched in the nevoid basal cell carcinoma syndrome. *Cell* **85,** 841–851 (1996).

80. Johnson, R.L. *et al.* Human homolog of patched, a candidate gene for the basal cell nevus syndrome. *Science (New York, N.Y.)* **272,** 1668–1671 (1996).

81. Gailani, M.R. *et al.* The role of the human homologue of Drosophila patched in sporadic basal cell carcinomas. *Nature genetics* **14,** 78–81 (1996).

82. Reifenberger, J. *et al.* Missense mutations in SMOH in sporadic basal cell carcinomas of the skin and primitive neuroectodermal tumors of the central nervous system. *Cancer research* **58,** 1798–1803 (1998).

83. Unden, A.B. *et al.* Mutations in the human homologue of Drosophila patched (PTCH) in basal cell carcinomas and the Gorlin syndrome: different in vivo mechanisms of PTCH inactivation. *Cancer research* **56,** 4562–4565 (1996).

84. Ellison, D.W. *et al.* Medulloblastoma: clinicopathological correlates of SHH, WNT, and non-SHH/WNT molecular subgroups. *Acta neuropathologica* **121,** 381–396 (2011).

85. Kool, M. *et al.* Molecular subgroups of medulloblastoma: an international meta-analysis of transcriptome, genetic aberrations, and clinical data of WNT, SHH, Group 3, and Group 4 medulloblastomas. *Acta neuropathologica* **123,** 473–484 (2012).

86. Onishi, H. & Katano, M. Hedgehog signaling pathway as a new therapeutic target in pancreatic cancer. *World journal of gastroenterology* **20,** 2335–2342 (2014).

87. Bertrand, F.E., Angus, C.W., Partis, W.J. & Sigounas, G. Developmental pathways in colon cancer: crosstalk between WNT, BMP, Hedgehog and Notch. *Cell cycle (Georgetown, Tex.)* **11,** 4344–4351 (2012).

88. Geng, L. & Wang, X. New insight into hedgehog signaling in hematological malignancies. *Leukemia & lymphoma* **56,** 858–865 (2015).

89. Xin, M., Ji, X., La Cruz, L.K. de, Thareja, S. & Wang, B. Strategies to target the Hedgehog signaling pathway for cancer therapy. *Medicinal research reviews* (2018).

90. Singh, S. *et al.* Hedgehog-producing cancer cells respond to and require autocrine Hedgehog activity. *Cancer research* **71,** 4454–4463 (2011).

91. Yauch, R.L. *et al.* A paracrine requirement for hedgehog signalling in cancer. *Nature* **455,** 406–410 (2008).

92. Gupta, S., Takebe, N. & Lorusso, P. Targeting the Hedgehog pathway in cancer. *Therapeutic advances in medical oncology* **2,** 237–250 (2010).

93. Batlle, E. & Clevers, H. Cancer stem cells revisited. *Nature medicine* **23,** 1124–1134 (2017).

94. Merchant, A.A. & Matsui, W. Targeting Hedgehog--a cancer stem cell pathway. *Clinical cancer research : an official journal of the American Association for Cancer Research* **16,** 3130–3140 (2010).

95. Bryden, M.M., Evans, H.E. & Keeler, R.F. Cyclopia in sheep caused by plant teratogens. *Journal of anatomy* **110,** 507 (1971).

96. Chen, J.K., Taipale, J., Cooper, M.K. & Beachy, P.A. Inhibition of Hedgehog signaling by direct binding of cyclopamine to Smoothened. *Genes & development* **16,** 2743–2748 (2002).

97. Wang, J. *et al.* Identification of a novel Smoothened antagonist that potently suppresses Hedgehog signaling. *Bioorganic & medicinal chemistry* **20,** 6751–6757 (2012).

98. Wu, T.-M. *et al.* Synthesis and biological evaluation of novel benzamide derivatives as potent smoothened antagonists. *Bioorganic & medicinal chemistry letters* **24,** 1426–1431 (2014).

99. Pan, S. *et al.* Discovery of NVP-LDE225, a Potent and Selective Smoothened Antagonist. *ACS medicinal chemistry letters* **1,** 130–134 (2010).

100. Chen, J.K., Taipale, J., Young, K.E., Maiti, T. & Beachy, P.A. Small molecule modulation of Smoothened activity. *Proceedings of the National Academy of Sciences of the United States of America* **99,** 14071–14076 (2002).

101. Roudaut, H. *et al.* Identification and mechanism of action of the acylguanidine MRT-83, a novel potent Smoothened antagonist. *Molecular pharmacology* **79,** 453–460 (2011).

102. Cooper, M.K. Teratogen-Mediated Inhibition of Target Tissue Response to Shh Signaling. *Science* **280,** 1603–1607 (1998).

103. Robarge, K.D. *et al.* GDC-0449-a potent inhibitor of the hedgehog pathway. *Bioorganic & medicinal chemistry letters* **19,** 5576–5581 (2009).

104. Dlugosz, A., Agrawal, S. & Kirkpatrick, P. Vismodegib. *Nature reviews. Drug discovery* **11,** 437–438 (2012).

105. Burness, C.B. Sonidegib: First Global Approval. *Drugs* **75,** 1559–1566 (2015).

106. Wang, Y. *et al.* Glucocorticoid compounds modify smoothened localization and hedgehog pathway activity. *Chemistry & biology* **19,** 972–982 (2012).

107. Sever, N. *et al.* Endogenous B-ring oxysterols inhibit the Hedgehog component Smoothened in a manner distinct from cyclopamine or side-chain oxysterols. *Proceedings of the National Academy of Sciences of the United States of America* **113** (2016).

108. Bijlsma, M.F. *et al.* Repression of smoothened by patched-dependent (pro-)vitamin D3 secretion. *PLoS biology* **4,** e232 (2006).

109. Linder, B. *et al.* A Functional and Putative Physiological Role of Calcitriol in Patched1/Smoothened Interaction. *The Journal of biological chemistry* **290,** 19614–19628 (2015).

110. Stanton, B.Z. *et al.* A small molecule that binds Hedgehog and blocks its signaling in human cells. *Nature chemical biology* **5,** 154–156 (2009).

111. Petrova, E., Rios-Esteves, J., Ouerfelli, O., Glickman, J.F. & Resh, M.D. Inhibitors of Hedgehog acyltransferase block Sonic Hedgehog signaling. *Nature chemical biology* **9,** 247–249 (2013).

112. Lauth, M., Bergström, A., Shimokawa, T. & Toftgård, R. Inhibition of GLI-mediated transcription and tumor cell growth by small-molecule antagonists. *Proceedings of the National Academy of Sciences of the United States of America* **104,** 8455–8460 (2007).

113. Hyman, J.M. *et al.* Small-molecule inhibitors reveal multiple strategies for Hedgehog pathway blockade. *Proceedings of the National Academy of Sciences of the United States of America* **106,** 14132–14137 (2009).

114. Infante, P. *et al.* Gli1/DNA interaction is a druggable target for Hedgehog-dependent tumors. *The EMBO journal* **34,** 200–217 (2015).

115. Wu, X., Ding, S., Ding, Q., Gray, N.S. & Schultz, P.G. A Small Molecule with Osteogenesis-Inducing Activity in Multipotent Mesenchymal Progenitor Cells. *J. Am. Chem. Soc.* **124,** 14520–14521 (2002).

116. Sinha, S. & Chen, J.K. Purmorphamine activates the Hedgehog pathway by targeting Smoothened. *Nature chemical biology* **2,** 29–30 (2006).

117. Frank-Kamenetsky, M. *et al. J Biol* **1,** 10 (2002).

118. Nachtergaele, S. *et al.* Oxysterols are allosteric activators of the oncoprotein Smoothened. *Nature chemical biology* **8,** 211–220 (2012).

119. Nachtergaele, S. *et al.* Structure and function of the Smoothened extracellular domain in vertebrate Hedgehog signaling. *eLife* **2,** e01340 (2013).

120. Huang, P. *et al.* Cellular Cholesterol Directly Activates Smoothened in Hedgehog Signaling. *Cell* **166,** 1176-1187.e14 (2016).

121. Myers, B.R. *et al.* Hedgehog pathway modulation by multiple lipid binding sites on the smoothened effector of signal response. *Developmental cell* **26,** 346–357 (2013).

122. Blassberg, R., Macrae, J.I., Briscoe, J. & Jacob, J. Reduced cholesterol levels impair Smoothened activation in Smith-Lemli-Opitz syndrome. *Human Molecular Genetics* **25,** 693–705 (2016).

123. Yauch, R.L. *et al.* Smoothened mutation confers resistance to a Hedgehog pathway inhibitor in medulloblastoma. *Science (New York, N.Y.)* **326,** 572–574 (2009).

124. Atwood, S.X. *et al.* Smoothened variants explain the majority of drug resistance in basal cell carcinoma. *Cancer cell* **27,** 342–353 (2015).

125. Pan, Y., Bai, C.B., Joyner, A.L. & Wang, B. Sonic hedgehog signaling regulates Gli2 transcriptional activity by suppressing its processing and degradation. *Molecular and Cellular Biology* **26,** 3365–3377 (2006).

126. Nagao-Kitamoto, H. *et al.* GLI2 is a novel therapeutic target for metastasis of osteosarcoma. *International journal of cancer* **136,** 1276–1284 (2015).

127. Kramann, R. *et al.* Pharmacological GLI2 inhibition prevents myofibroblast cell-cycle progression and reduces kidney fibrosis. *The Journal of clinical investigation* **125,** 2935–2951 (2015).

128. K. Kompoliti & L. Verhagen Metman eds. *Encyclopedia of Movement Disorders* (Elsevier, 2010).

129. Wen, X. *et al.* Kinetics of Hedgehog-Dependent Full-Length Gli3 Accumulation in Primary Cilia and Subsequent Degradation ▿†‡. *Molecular and Cellular Biology* **30,** 1910–1922 (2010).

130. Taipale, J. *et al.* Effects of oncogenic mutations in Smoothened and Patched can be reversed by cyclopamine. *Nature* **406,** 1005–1009 (2000).

131. Ran, F.A. *et al.* Genome engineering using the CRISPR-Cas9 system. *Nature protocols* **8,** 2281–2308 (2013).

132. Hsu, P.D. *et al.* DNA targeting specificity of RNA-guided Cas9 nucleases. *Nature biotechnology* **31,** 827–832 (2013).

133. Doench, J.G. *et al.* Optimized sgRNA design to maximize activity and minimize off-target effects of CRISPR-Cas9. *Nature biotechnology* **34,** 184–191 (2016).

134. Heigwer, F., Kerr, G. & Boutros, M. E-CRISP. Fast CRISPR target site identification. *Nature methods* **11,** 122–123 (2014).

135. Sasaki, H., Hui, C., Nakafuku, M. & Kondoh, H. A binding site for Gli proteins is essential for HNF-3beta floor plate enhancer activity in transgenics and can respond to Shh in vitro. *Development (Cambridge, England)* **124,** 1313–1322 (1997).

136. Arens, J. *et al.* Exploration of biosynthetic access to the shared precursor of the fusicoccane diterpenoid family. *Chemical communications (Cambridge, England)* **49,** 4337–4339 (2013).

137. Ryan, K.J. & Ray, C.G. *Sherris medical microbiology. An introduction to infectious diseases.* 4th ed. (McGraw-Hill, New York, 2004).

138. Sorek, R., Kunin, V. & Hugenholtz, P. CRISPR--a widespread system that provides acquired resistance against phages in bacteria and archaea. *Nature reviews. Microbiology* **6,** 181–186 (2008).

139. Jinek, M. *et al.* A programmable dual-RNA-guided DNA endonuclease in adaptive bacterial immunity. *Science (New York, N.Y.)* **337,** 816–821 (2012).

140. Hsu, P.D., Lander, E.S. & Zhang, F. Development and applications of CRISPR-Cas9 for genome engineering. *Cell* **157,** 1262–1278 (2014).

141. Doudna, J.A. & Charpentier, E. Genome editing. The new frontier of genome engineering with CRISPR-Cas9. *Science (New York, N.Y.)* **346,** 1258096 (2014).

142. Kim, H. & Kim, J.-S. A guide to genome engineering with programmable nucleases. *Nature reviews. Genetics* **15,** 321–334 (2014).

143. Bauer, D.E., Canver, M.C. & Orkin, S.H. Generation of genomic deletions in mammalian cell lines via CRISPR/Cas9. *Journal of visualized experiments : JoVE,* e52118 (2015).

144. Livak, K.J. & Schmittgen, T.D. Analysis of relative gene expression data using real-time quantitative PCR and the 2(-Delta Delta C(T)) Method. *Methods (San Diego, Calif.)* **25,** 402–408 (2001).

145. Schindelin, J., Rueden, C.T., Hiner, M.C. & Eliceiri, K.W. The ImageJ ecosystem. An open platform for biomedical image analysis. *Molecular reproduction and development* **82,** 518–529 (2015).

146. Fredriksson, S. *et al.* Protein detection using proximity-dependent DNA ligation assays. *Nature biotechnology* **20,** 473–477 (2002).

147. LOWRY, O.H., ROSEBROUGH, N.J., FARR, A.L. & RANDALL, R.J. Protein measurement with the Folin phenol reagent. *The Journal of biological chemistry* **193,** 265–275 (1951).

148. Johnson, C.M. Differential scanning calorimetry as a tool for protein folding and stability. *Archives of Biochemistry and Biophysics* **531,** 100–109 (2013).

149. Huynh, K. & Partch, C.L. Analysis of protein stability and ligand interactions by thermal shift assay. *Current protocols in protein science* **79,** 28.9.1-14 (2015).

150. Jafari, R. *et al.* The cellular thermal shift assay for evaluating drug target interactions in cells. *Nature protocols* **9,** 2100–2122 (2014).

151. Cox, J. & Mann, M. MaxQuant enables high peptide identification rates, individualized p.p.b.-range mass accuracies and proteome-wide protein quantification. *Nature biotechnology* **26,** 1367–1372 (2008).

152. Tyanova, S. *et al.* The Perseus computational platform for comprehensive analysis of (prote)omics data. *Nature methods* **13,** 731–740 (2016).

153. Rappsilber, J., Mann, M. & Ishihama, Y. Protocol for micro-purification, enrichment, pre-fractionation and storage of peptides for proteomics using StageTips. *Nature protocols* **2,** 1896–1906 (2007).

154. Kremer, L. *et al.* Discovery of a Novel Inhibitor of the Hedgehog Signaling Pathway through Cell-based Compound Discovery and Target Prediction. *Angewandte Chemie (International ed. in English)* **56,** 13021–13025 (2017).

155. Reker, D., Rodrigues, T., Schneider, P. & Schneider, G. Identifying the macromolecular targets of de novo-designed chemical entities through self-organizing map consensus. *Proceedings of the National Academy of Sciences of the United States of America* **111,** 4067–4072 (2014).

156. Schneider, P. & Schneider, G. Collection of Bioactive Reference Compounds for Focused Library Design. *QSAR Comb. Sci.* **22,** 713–718 (2003).

157. Reutlinger, M. *et al.* Chemically Advanced Template Search (CATS) for Scaffold-Hopping and Prospective Target Prediction for 'Orphan' Molecules. *Molecular informatics* **32,** 133–138 (2013).

158. Chemical Computing Group ULC. *Molecular Operating Environment (MOE)* (Chemical Computing Group ULC, 1010 Sherbooke St. West, Suite #910, Montreal, QC, Canada, H3A 2R7, 2017).

159. Schneider, G. & Schneider, P. Macromolecular target prediction by self-organizing feature maps. *Expert opinion on drug discovery* **12,** 271–277 (2017).

160. Garcia-Castro, M. *et al.* De novo branching cascades for structural and functional diversity in small molecules. *Nature communications* **6,** 6516 (2015).

161. James, A.W. Review of Signaling Pathways Governing MSC Osteogenic and Adipogenic Differentiation. *Scientifica* **2013,** 684736 (2013).

162. Chen, L.-X., He, H. & Qiu, F. Natural withanolides. An overview. *Natural product reports* **28,** 705–740 (2011).

163. van Hattum, H. & Waldmann, H. Biology-oriented synthesis. Harnessing the power of evolution. *Journal of the American Chemical Society* **136,** 11853–11859 (2014).

164. Švenda, J. *et al.* Biology-oriented synthesis of a withanolide-inspired compound collection reveals novel modulators of hedgehog signaling. *Angewandte Chemie (International ed. in English)* **54,** 5596–5602 (2015).

165. Frank-Kamenetsky, M. *et al.* Small-molecule modulators of Hedgehog signaling: identification and characterization of Smoothened agonists and antagonists. *Journal of biology* **1,** 10 (2002).

166. Urich, R. *et al.* De novo design of protein kinase inhibitors by in silico identification of hinge region-binding fragments. *ACS chemical biology* **8,** 1044–1052 (2013).

167. Weiss, E.R. *et al.* Species-specific differences in expression of G-protein-coupled receptor kinase (GRK) 7 and GRK1 in mammalian cone photoreceptor cells: implications for cone cell phototransduction. *The Journal of neuroscience : the official journal of the Society for Neuroscience* **21,** 9175–9184 (2001).

168. Lineweaver, H. & Burk, D. The Determination of Enzyme Dissociation Constants. *Journal of the American Chemical Society* **56,** 658–666 (1934).

169. Cornish-Bowden, A. *Principles of Enzyme Kinetics* (Elsevier Science, 2014).

170. Shoichet, B.K. Interpreting steep dose-response curves in early inhibitor discovery. *Journal of medicinal chemistry* **49,** 7274–7277 (2006).

171. John, K., Alla, V., Meier, C. & Pützer, B.M. GRAMD4 mimics p53 and mediates the apoptotic function of p73 at mitochondria. *Cell death and differentiation* **18,** 874–886 (2011).

172. Katoh, Y. & Katoh, M. Integrative genomic analyses on GLI2: mechanism of Hedgehog priming through basal GLI2 expression, and interaction map of stem cell signaling network with P53. *International journal of oncology* **33,** 881–886 (2008).

173. Beck, A. *et al.* An siRNA screen identifies transmembrane 7 superfamily member 3 (TM7SF3), a seven transmembrane orphan receptor, as an inhibitor of cytokine-induced death of pancreatic beta cells. *Diabetologia* **54,** 2845–2855 (2011).

174. Isaac, R. *et al.* TM7SF3, a novel p53-regulated homeostatic factor, attenuates cellular stress and the subsequent induction of the unfolded protein response. *Cell death and differentiation* **24,** 132–143 (2017).

175. Magness, S.T., Maeda, N. & Brenner, D.A. An exon 10 deletion in the mouse ferrochelatase gene has a dominant-negative effect and causes mild protoporphyria. *Blood* **100,** 1470–1477 (2002).

176. Mejdrová, I. *et al.* Highly Selective Phosphatidylinositol 4-Kinase IIIβ Inhibitors and Structural Insight into Their Mode of Action. *Journal of medicinal chemistry* **58,** 3767–3793 (2015).

177. DOWLER, S. *et al.* Identification of pleckstrin-homology-domain-containing proteins with novel phosphoinositide-binding specificities. *Biochemical Journal* **351,** 19–31 (2000).

178. Strous, G.J. Golgi and secreted galactosyltransferase. *CRC critical reviews in biochemistry* **21,** 119–151 (1986).

179. Chazotte, B. Labeling membrane glycoproteins or glycolipids with fluorescent wheat germ agglutinin. *Cold Spring Harbor protocols* **2011,** pdb.prot5623 (2011).

180. Minogue, S. & Waugh, M.G. The phosphatidylinositol 4-kinases. Don't call it a comeback. *Sub-cellular biochemistry* **58,** 1–24 (2012).

181. Mimeault, M. & Batra, S.K. Frequent deregulations in the hedgehog signaling network and cross-talks with the epidermal growth factor receptor pathway involved in cancer progression and targeted therapies. *Pharmacological reviews* **62,** 497–524 (2010).

182. Malhotra, A., Dey, A., Prasad, N. & Kenney, A.M. Sonic Hedgehog Signaling Drives Mitochondrial Fragmentation by Suppressing Mitofusins in Cerebellar Granule Neuron Precursors and Medulloblastoma. *Molecular cancer research : MCR* **14,** 114–124 (2016).

183. Yao, P.J. *et al.* Sonic hedgehog pathway activation increases mitochondrial abundance and activity in hippocampal neurons. *Molecular biology of the cell* **28,** 387–395 (2017).

184. Alam, M.M., Sohoni, S., Kalainayakan, S.P., Garrossian, M. & Zhang, L. Cyclopamine tartrate, an inhibitor of Hedgehog signaling, strongly interferes with mitochondrial function and suppresses aerobic respiration in lung cancer cells. *BMC cancer* **16,** 150 (2016).

185. Blomen, V.A. *et al.* Gene essentiality and synthetic lethality in haploid human cells. *Science (New York, N.Y.)* **350,** 1092–1096 (2015).

186. Freitag, A. *et al.* Development of first lead structures for phosphoinositide 3-kinase-C2γ inhibitors. *Journal of medicinal chemistry* **58,** 212–221 (2015).

187. Götschel, F. *et al.* Synergism between Hedgehog-GLI and EGFR signaling in Hedgehog-responsive human medulloblastoma cells induces downregulation of canonical Hedgehog-target genes and stabilized expression of GLI1. *PloS one* **8,** e65403 (2013).

188. Waugh, M.G. Phosphatidylinositol 4-kinases, phosphatidylinositol 4-phosphate and cancer. *Cancer letters* **325,** 125–131 (2012).

189. Rutkovskiy, A., Stensløkken, K.-O. & Vaage, I.J. Osteoblast Differentiation at a Glance. *Med Sci Monit Basic Res* **22,** 95–106 (2016).

190. Wilson, C.W., Chen, M.-H. & Chuang, P.-T. Smoothened adopts multiple active and inactive conformations capable of trafficking to the primary cilium. *PloS one* **4,** e5182 (2009).

191. Wu, V.M., Chen, S.C., Arkin, M.R. & Reiter, J.F. Small molecule inhibitors of Smoothened ciliary localization and ciliogenesis. *Proceedings of the National Academy of Sciences of the United States of America* **109,** 13644–13649 (2012).

192. Sharpe, H.J., Wang, W., Hannoush, R.N. & Sauvage, F.J. de. Regulation of the oncoprotein Smoothened by small molecules. *Nature chemical biology* **11,** 246–255 (2015).

193. Jung, B. *et al.* Pitchfork and Gprasp2 Target Smoothened to the Primary Cilium for Hedgehog Pathway Activation. *PloS one* **11** (2016).

194. Li, S. *et al.* Regulation of Smoothened Phosphorylation and High-Level Hedgehog Signaling Activity by a Plasma Membrane Associated Kinase. *PLoS biology* **14,** e1002481 (2016).

195. Ma, G. *et al.* Regulation of Smoothened Trafficking and Hedgehog Signaling by the SUMO Pathway. *Developmental cell* **39,** 438–451 (2016).

196. Hoch, L. *et al.* MRT-92 inhibits Hedgehog signaling by blocking overlapping binding sites in the transmembrane domain of the Smoothened receptor. *FASEB journal : official publication of the Federation of American Societies for Experimental Biology* **29,** 1817–1829 (2015).

197. Whiteley, C.G. Mechanistic and kinetic studies of inhibition of enzymes. *Cell Biochem Biophys* **33,** 217–225 (2000).

198. Bisswanger, H. *Enzyme Kinetics* (Wiley-VCH Verlag GmbH & Co. KGaA, Weinheim, Germany, 2008).

199. Waldrop, G.L. A qualitative approach to enzyme inhibition. *Biochemistry and molecular biology education : a bimonthly publication of the International Union of Biochemistry and Molecular Biology* **37,** 11–15 (2009).

200. Szklarczyk, D. *et al.* STRING v10. Protein-protein interaction networks, integrated over the tree of life. *Nucleic acids research* **43,** D447-52 (2015).

201. Long, D.J. & Jaiswal, A.K. NRH:quinone oxidoreductase2 (NQO2). *Chemico-biological interactions* **129,** 99–112 (2000).

202. Schieber, M. & Chandel, N.S. ROS function in redox signaling and oxidative stress. *Current biology : CB* **24,** R453-62 (2014).

203. Devosse, T. *et al.* Processing of HEBP1 by cathepsin D gives rise to F2L, the agonist of formyl peptide receptor 3. *Journal of immunology (Baltimore, Md. : 1950)* **187,** 1475–1485 (2011).

204. Krishnan, R.V., Masuda, A., Centonze, V.E. & Herman, B. Quantitative imaging of protein-protein interactions by multiphoton fluorescence lifetime imaging microscopy using a streak camera. *Journal of biomedical optics* **8,** 362–367 (2003).

205. Zhao, S. *et al.* Fixation-induced cell blebbing on spread cells inversely correlates with phosphatidylinositol 4,5-bisphosphate level in the plasma membrane. *FEBS open bio* **4,** 190–199 (2014).

206. Hutagalung, A.H. & Novick, P.J. Role of Rab GTPases in membrane traffic and cell physiology. *Physiological reviews* **91,** 119–149 (2011).

207. Welz, T., Wellbourne-Wood, J. & Kerkhoff, E. Orchestration of cell surface proteins by Rab11. *Trends in cell biology* **24,** 407–415 (2014).

208. Tartakoff, A.M. & Vassalli, P. Lectin-binding sites as markers of Golgi subcompartments. Proximal-to-distal maturation of oligosaccharides. *The Journal of cell biology* **97,** 1243–1248 (1983).

209. Kanazawa, T., Takematsu, H., Yamamoto, A., Yamamoto, H. & Kozutsumi, Y. Wheat germ agglutinin stains dispersed post-golgi vesicles after treatment with the cytokinesis inhibitor psychosine. *Journal of cellular physiology* **215,** 517–525 (2008).

210. D'Angelo, G., Vicinanza, M., Di Campli, A. & Matteis, M.A. de. The multiple roles of PtdIns(4)P -- not just the precursor of PtdIns(4,5)P2. *Journal of cell science* **121,** 1955–1963 (2008).

211. Kessaris, N., Jamen, F., Rubin, L.L. & Richardson, W.D. Cooperation between sonic hedgehog and fibroblast growth factor/MAPK signalling pathways in neocortical precursors. *Development (Cambridge, England)* **131,** 1289–1298 (2004).

212. Moran, C.M., Myers, C.T., Lewis, C.M. & Krieg, P.A. Hedgehog regulates angiogenesis of intersegmental vessels through the VEGF signaling pathway. *Developmental dynamics : an official publication of the American Association of Anatomists* **241,** 1034–1042 (2012).

213. Mangelberger, D., Kern, D., Loipetzberger, A., Eberl, M. & Aberger, F. Cooperative Hedgehog-EGFR signaling. *Frontiers in bioscience (Landmark edition)* **17,** 90–99 (2012).

214. Parathath, S.R., Mainwaring, L.A., Fernandez-L, A., Campbell, D.O. & Kenney, A.M. Insulin receptor substrate 1 is an effector of sonic hedgehog mitogenic signaling in cerebellar neural precursors. *Development (Cambridge, England)* **135,** 3291–3300 (2008).

215. Shi, Y., Chen, J., Karner, C.M. & Long, F. Hedgehog signaling activates a positive feedback mechanism involving insulin-like growth factors to induce osteoblast differentiation. *Proceedings of the National Academy of Sciences of the United States of America* **112,** 4678–4683 (2015).

216. Liu, Z., Li, T., Reinhold, M.I. & Naski, M.C. MEK1-RSK2 contributes to Hedgehog signaling by stabilizing GLI2 transcription factor and inhibiting ubiquitination. *Oncogene* **33,** 65–73 (2014).

217. Brennan, D., Chen, X., Cheng, L., Mahoney, M. & Riobo, N.A. Noncanonical Hedgehog signaling. *Vitamins and hormones* **88,** 55–72 (2012).

218. Li, J. & Evers, B.M. in *Hedgehog signaling activation in human cancer and its clinical implications,* edited by J. Xie (Springer New York, New York, NY, 2011), pp. 77–83.

219. Blassberg, R. & Jacob, J. Lipid metabolism fattens up hedgehog signaling. *BMC biology* **15,** 95 (2017).

220. Schroepfer, G.J. Oxysterols: modulators of cholesterol metabolism and other processes. *Physiological reviews* **80,** 361–554 (2000).

221. Cohn, M.J. Development of the external genitalia: conserved and divergent mechanisms of appendage patterning. *Developmental dynamics : an official publication of the American Association of Anatomists* **240,** 1108–1115 (2011).

222. Osherovich, L. Hedgehog joins the resistance. *Science-Business eXchange* **7,** 776 (2014).

223. Chen, M. *et al.* Androgenic regulation of hedgehog signaling pathway components in prostate cancer cells. *Cell cycle (Georgetown, Tex.)* **8,** 149–157 (2009).

224. Chen, G. *et al.* GLI1, a crucial mediator of sonic hedgehog signaling in prostate cancer, functions as a negative modulator for androgen receptor. *Biochemical and biophysical research communications* **404,** 809–815 (2011).

225. Liu, F. & Wang, S. Molecular cues for development and regeneration of salivary glands. *Histology and histopathology* **29,** 305–312 (2014).

226. Hai, B. *et al.* Transient activation of hedgehog pathway rescued irradiation-induced hyposalivation by preserving salivary stem/progenitor cells and parasympathetic innervation. *Clinical cancer research : an official journal of the American Association for Cancer Research* **20,** 140–150 (2014).

227. Kinnally, K.W., Peixoto, P.M., Ryu, S.-Y. & Dejean, L.M. Is mPTP the gatekeeper for necrosis, apoptosis, or both? *Biochimica et biophysica acta* **1813,** 616–622 (2011).

228. Ong, S.-B., Dongworth, R.K., Cabrera-Fuentes, H.A. & Hausenloy, D.J. Role of the MPTP in conditioning the heart - translatability and mechanism. *British journal of pharmacology* **172,** 2074–2084 (2015).

229. Shao, S. *et al.* Activation of Sonic hedgehog signal by Purmorphamine, in a mouse model of Parkinson's disease, protects dopaminergic neurons and attenuates inflammatory response by mediating PI3K/AKt signaling pathway. *Molecular Medicine Reports* **16,** 1269–1277 (2017).

230. Shalaby, N.A. *et al.* Systematic discovery of genetic modulation by Jumonji histone demethylases in Drosophila. *Scientific Reports* **7** (2017).

231. Fujii, T., Khawaja, M.R., DiNardo, C.D., Atkins, J.T. & Janku, F. Targeting isocitrate dehydrogenase (IDH) in cancer. *Discovery medicine* **21,** 373–380 (2016).

232. Valadez, J.G. *et al.* Identification of Hedgehog pathway responsive glioblastomas by isocitrate dehydrogenase mutation. *Cancer letters* **328,** 297–306 (2013).

233. Cunningham, D. *et al.* Analysis of hedgehog signaling in cerebellar granule cell precursors in a conditional Nsdhl allele demonstrates an essential role for cholesterol in postnatal CNS development. *Human Molecular Genetics* **24,** 2808–2825 (2015).

234. Fedorov, O. *et al.* A systematic interaction map of validated kinase inhibitors with Ser/Thr kinases. *Proceedings of the National Academy of Sciences of the United States of America* **104,** 20523–20528 (2007).

235. Wahlberg, E. *et al.* Family-wide chemical profiling and structural analysis of PARP and tankyrase inhibitors. *Nature biotechnology* **30,** 283 (2012).

236. Savitski, M.M. *et al.* Tracking cancer drugs in living cells by thermal profiling of the proteome. *Science* **346,** 1255784 (2014).

237. Lindauer, M. & Hochhaus, A. Dasatinib. *Recent results in cancer research. Fortschritte der Krebsforschung. Progres dans les recherches sur le cancer* **201,** 27–65 (2014).

238. Nakano, H. & Ōmura, S. Chemical biology of natural indolocarbazole products. 30 years since the discovery of staurosporine. *The Journal of Antibiotics* **62,** 17 (2009).

239. Walker, E.H. *et al.* Structural Determinants of Phosphoinositide 3-Kinase Inhibition by Wortmannin, LY294002, Quercetin, Myricetin, and Staurosporine. *Molecular Cell* **6,** 909–919 (2000).

240. Xu, H. *et al.* Cellular thermal shift and clickable chemical probe assays for the determination of drug-target engagement in live cells. *Organic & biomolecular chemistry* **14,** 6179–6183 (2016).

241. Leibiger, C. *et al.* First molecular cytogenetic high resolution characterization of the NIH 3T3 cell line by murine multicolor banding. *The journal of histochemistry and cytochemistry : official journal of the Histochemistry Society* **61,** 306–312 (2013).

242. Alexopoulou, A.N., Couchman, J.R. & Whiteford, J.R. The CMV early enhancer/chicken beta actin (CAG) promoter can be used to drive transgene expression during the differentiation of murine embryonic stem cells into vascular progenitors. *BMC cell biology* **9,** 2 (2008).

243. Xu, Q. *et al.* Phosphatidylinositol phosphate kinase PIPKIγ and phosphatase INPP5E coordinate initiation of ciliogenesis. *Nature communications* **7,** 10777 (2016).

244. Majumder, S. & Fisk, H.A. VDAC3 and Mps1 negatively regulate ciliogenesis. *Cell Cycle* **12,** 849–858 (2013).

245. Pak, E. & Segal, R.A. Hedgehog Signal Transduction: Key Players, Oncogenic Drivers, and Cancer Therapy. *Developmental cell* **38,** 333–344 (2016).

246. Riobó, N.A., Lu, K., Ai, X., Haines, G.M. & Emerson, C.P. Phosphoinositide 3-kinase and Akt are essential for Sonic Hedgehog signaling. *Proceedings of the National Academy of Sciences of the United States of America* **103,** 4505–4510 (2006).

247. Kieran, M.W. Targeted treatment for sonic hedgehog-dependent medulloblastoma. *Neuro-oncology* **16,** 1037–1047 (2014).

248. Kijima, N. & Kanemura, Y. Molecular Classification of Medulloblastoma. *Neurologia medico-chirurgica* **56,** 687–697 (2016).

249. Taylor, M.D. *et al.* Molecular subgroups of medulloblastoma: the current consensus. *Acta neuropathologica* **123,** 465–472 (2012).

250. Gruber, W. *et al.* DYRK1B as therapeutic target in Hedgehog/GLI-dependent cancer cells with Smoothened inhibitor resistance. *Oncotarget* **7,** 7134–7148 (2016).

251. Infante, P. *et al.* Inhibition of Hedgehog-dependent tumors and cancer stem cells by a newly identified naturally occurring chemotype. *Cell death & disease* **7,** e2376 (2016).

252. Recouvreux, M.V. & Commisso, C. Macropinocytosis: A Metabolic Adaptation to Nutrient Stress in Cancer. *Frontiers in endocrinology* **8,** 261 (2017).

253. Jung, B. *et al.* Novel small molecules targeting ciliary transport of Smoothened and oncogenic Hedgehog pathway activation. *Scientific Reports* **6** (2016).

254. Mukhopadhyay, S. *et al.* The ciliary G-protein-coupled receptor Gpr161 negatively regulates the Sonic hedgehog pathway via cAMP signaling. *Cell* **152,** 210–223 (2013).

255. Klink, B.U. *et al.* A recombinant BBSome core complex and how it interacts with ciliary cargo. *eLife* **6** (2017).

256. Khan, S.A. *et al.* Genetics of human Bardet-Biedl syndrome, an updates. *Clinical genetics* **90,** 3–15 (2016).

257. Forsythe, E. & Beales, P.L. Bardet-Biedl syndrome. *European journal of human genetics : EJHG* **21,** 8–13 (2013).

258. Zhang, Q., Seo, S., Bugge, K., Stone, E.M. & Sheffield, V.C. BBS proteins interact genetically with the IFT pathway to influence SHH-related phenotypes. *Human Molecular Genetics* **21,** 1945–1953 (2012).

259. Seo, S. *et al.* A Novel Protein LZTFL1 Regulates Ciliary Trafficking of the BBSome and Smoothened. *PLoS Genetics* **7** (2011).

260. Byrne, E.F. *et al.* Structural basis for Smoothened regulation by its extracellular domains. *Nature* **535,** 517–522 (2016).

261. Taipale, J. *et al.* Effects of oncogenic mutations in Smoothened and Patched can be reversed by cyclopamine. *Nature* **406,** 1005–1009 (2000).

9 FIGURES

10 TABLES

11 ABBREVIATIONS

Abbreviation	Definition
µg	Microgram
µL	Microliter
3' UTR	3’ untranslated region
ACBD3	Acyl-CoA-binding domain containing protein 3
AcN	Acetonitrile
Ac-Tubulin	Acetylated Tubulin
Akt	Protein kinase B
ALP	Alkaline phosphatase
APS	Ammoniumpersulfate
Arf1	ADP-ribosylation factor 1
BBS	Bardet-Biedl syndrome
BCC	Basal cell carcinoma
BMP	Bone morphogenic protein
bp	Basepairs
BSA	Bovine Serum Albumine
$CaCl_2$	Calciumchloride
CAG	CMV early enhancer/chicken β actin
Cat. No.	Catalogue number
CATS	Chemical advanced template search
CCLE	Cancer cell line encyclopedia
CCVs	Clathrin-coated vesicles
CETSA	Cellular Thermal Shift Assay
CFP	Cyan fluorescent protein
CHAPS	3-[(3-Cholamidopropyl)dimethylammonio]-1-propanesulfonate
Chrm1	Muscarinic acetylcholine receptor M1
CK1	Casein kinase 1
CLS	Ciliary localization sequence
CMV	Cytomegalovirus
COMAS	Compound Management and Screening Center
Cpd	Compound
CSCs	Cancer stem cells
C-tail	C-terminal tail
CYP1A2	Cytochrom P450 1A2
CYP2D6	Cytochrom P450 2D6
DAPI	4',6-diamidino-2-phenylindole
DAPI	4‘,6-Diamidin-2-phenylindol
DHH	Desert hedgehog
DMEM	Dulbecco’s modified eagle medium
DMSO	Dimethylsulfoxide
DNA	Deoxyribonucleic acid
DPF	Dortmund Protein Facility
DSBs	Double strand breaks

DSC	Differential scanning calorimetry
DTE	Dithioerythritol
DTT	Dithiothreitol
EA	Expression Atlas
EC	Extracellular loop
EDTA	Ethylenediaminetetraacetic acid
EGF	Epidermal growth factor
EGFR	Epidermal growth factor receptor
EGTA	Ethylene glycol-bis(β-aminoethyl ether)-N,N,N',N'-tetraacetic acid
ER	Endoplasmic reticulum
EtOH	Ethanol
EVC2	Ellis-van-Creveld 2
EYFP	Enhanced yellow fluorescent protein
FAPP1	Phosphatidylinositol-four-phosphate adapter protein 1
FBS	Fetal bovine serum
FCS	Fetal calf serum
FDA	Food and drug administration
FECH	Ferrochelatase, mitochondrial
FGFR	Fibroblast growth factor receptor
Fz	Frizzled
G418	Geneticin
gDNA	genomic DNA
G	Genevisible
GLI1 (*Gli1*)	Glioma-associated oncogene 1
GLI2/3	Glioma-associated oncogene 2 and 3
GOLPH3	Golgi phosphoprotein 3
GPCR	G-protein coupled receptor
GPP	Genetic Perturbation Platform
GPR161	G-protein coupled receptor 161
GRAMD4	GRAM domain-containing protein 4
GSK3β	Glykocen-synthase kinase 3β
GT	β1,4-galactosyltransferase
h	Hour
HCl	Hydrochloric acid
HEBP1	Heme-binding protein 1
HEPES	2-(4-(2-Hydroxyethyl)-1-piperazinyl)-ethansulfonsäure
Hh	Hedgehog
HPSF	High Purity Salt Free
HRP	horse reddish peroxidase
IB	Immunoblot
IC	Intracellular loop
ICC	Immunocytochemistry
IHH	Indian hedgehog
INPP5E	Inositol polyphosphate-5-phosphatase E
IP	Immunoprecipitation
ITDRF	Isothermal dose response fingerprinting
KCl	Potassiumchloride

kDa	Kilodalton
KDM4A	Lysine-specific demethylase 4A
KRas	Kirsten rat sarcoma
LIC	Ligation Independent Cloning
LYN	Tyrosine-protein kinase Lyn
LysC	Lysyl Endopeptidase
MAP2K1	Dual specificity mitogen-activated protein kinase kinase 1
MAPK	Mitogen activated protein kinase
MAPK10	Mitogen-activated protein kinase 10
MAPK9	Mitogen-activated protein kinase 9
MB	Medulloblastoma
MeOH	Methanol
MgCl2	Milligram
$MgCl_2$	Magnesiumchloride
mH_2O	Millipore filtered deionized water
min	Minute
mL	Milliliter
MOPS	3-(N-morpholino)propanesulfonic acid
mRNA	messenger RNA
MVB	Multivesicular bodies
NaCl	Sodiumchloride
NADP	Nicotinamide adenine dinucleotide phosphate
NaOH	Sodiumhydroxide
NCS-1	Neuronal calcium sensor 1
NH_4HCO_3	Ammoniumbicarbonate
non-palm.	Non-palmitoylated
NP-40	Nonidet P-40
NQO2	Ribosyldihydronicotinamide dehydrogenase [quinone]
OMM	Outer mitochondrial membrane
OSBP	Oxysterol-binding protein
PBS	Phosphate buffered saline
PCR	Polymerase chain reaction
PDB	Protein Data Bank
PenStrep	Penicillin/Streptomycin
PH	Pleckstrin homology domain
PI3K	Phosphoinositide 3-kinase
PI4K2A	Phosphatidylinositol 4-kinase IIα
PI4K2B	Phosphatidylinositol 4-kinase IIβ
PI4KA	Phosphatidylinositol 4-kinase IIIα
PI4KB	Phosphatidylinositol 4-kinase IIIβ
PI4P	Phosphatidylinositol-4-phosphate
PKA	Protein kinase A
PKC	Protein kinase C
PKD	Protein kinase D
PLA	Proximity ligation assay
PM	Plasma membrane

PTC(1)/*Ptch(1)*	Patched (1)
Purm	Purmorphamine
qRT-PCR	Quantitative reverse transcription PCR
Ras	Rat sarcoma
RLU	Relative light units
RMS	Rhabdomyosarcoma
RNA	Ribonucleic acid
RNA	Ribonucleic acid
RT	Room temperature
s	Second
SAG1.3	Smoothened Agonist
SAR	structure activity relationship
SD	Standard deviation
SDF	Structure-data file
SDS	Sodiumdodecylsulfate
SDS-PAGE	SDS-polyacrylamide gel electrophoresis
SEM	Standard error of the mean
SHH	Sonic hedgehog
SILAC	Stable isotope labeling by amino acids in cell culture
SMO	Smoothened
SPiDER	Self-organizing map–based prediction of drug equivalence relationships
SRC	Tyrosinkinase Src (from sarcoma)
Stage	Stop-and-go-extraction
SUFU	Suppressor of fused
TAE	TRIS-Acetat-EDTA
TBS	Tris buffered saline
TEMED	Tetramethylethylendiamin
TFA	Trifluoroacetic acid
TGFβ	Transforming growth factor β
TGN	Trans-Golgi network
TIGER	Target Inference GEneRator
TM	Transmembrane
TM7SF3	Transmembrane 7 superfamily member 3
TNF-α	Tumor necrosis factor-α
TPP	Thermal proteome profiling
TULP3	Tubby like protein 3
UDP	Uridine diphosphate
UGT1A1	UDP-glucuronosyltransferase 1-1
UPR	Unfolded protein response
VEGF	Vascular endothelial growth factor
Vismo	Vismodegib
WB	Western blot
WGA	Wheat germ agglutinin

12 APPENDIX

12.1 Vector maps

Flag-PI4KB-His

The cHis-nFlag-PI4KB plasmid was cloned by the Dortmund Protein Facility (DPF).

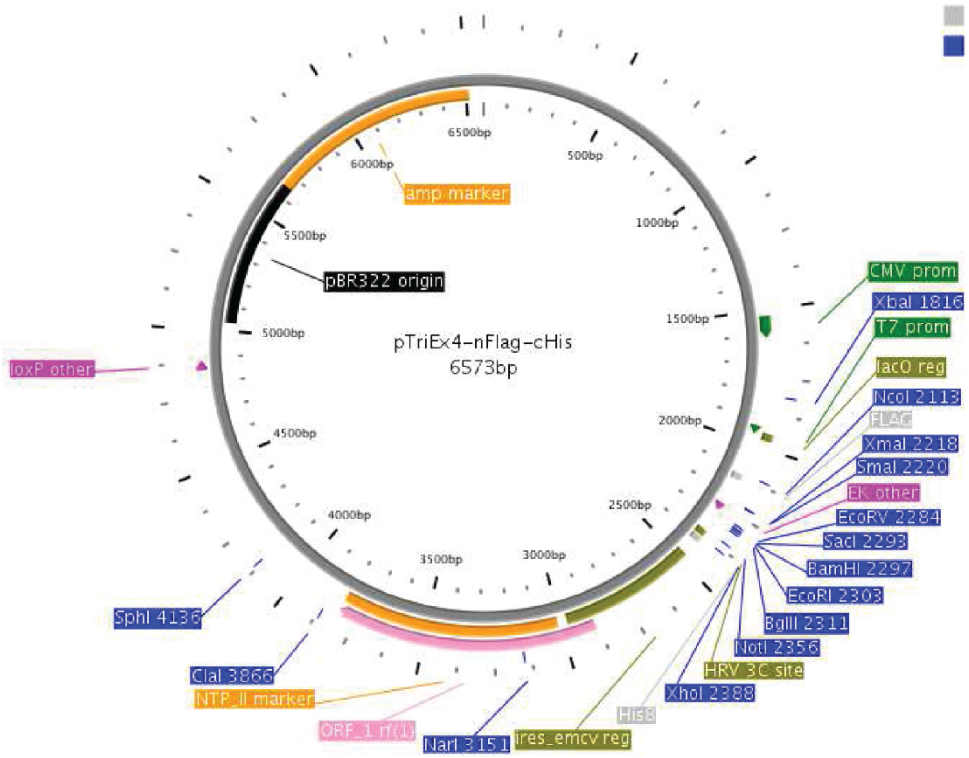

FEATURE	EXPRESSED SEQUENCE	ADDED SIZE TO PROTEIN (kDa)
Nterminal Fusion → FLAGtag	MADYKDDDDRTSGene	1.4 kDa
Cterminal Fusion → HRV 3C ("/" = cleavage site) → 8 x His	GeneAAALEVLFQG/PLEHHHHHHHH	2.5 kDa

pTriEx4-nFlag-cHis Vector backbone used for cloning.

Sequence of PI4KB:

ATGGGAGACATGGTAGTGGAGCCTGCCACCCTGAAGCCAACTTCTGAGCCTACTCCTA
GCCCATCAGGGAATAATGGGGGCTCCCTACTAAGCGTCATCACGGAGGGGGTCGGG
GAACTGTCAGTGATTGACCCTGAGGTGGCCCAGAAGGCCTGCCAGGAGGTACTGGAG
AAAGTCAAGCTTTTGCATGGAGGTGTAGCCATCTCTAGCAAAGGCACCCCGCTGGAGT
TGGTTAATGGGGATGGTGTGGACAATGAAATCCGTTGCCTAGATGATCCACCTGCCCA
GATCAGGGAGGAAGAAGATGAGATGGGGGCTGGTGTGGCCTCTGGCACAGCCAAAG
GAGCAAGACGACGACGACAGAACAACTCAGCCAAACAGTCTTGGCTCCTGAGGCTGT
TTGAGTCAAAACTATTTGACATCTCTATGGCTATTTCATACTTGTATAACTCCAAGGAGC
CTGGAGTGCAAGCCTACATTGGCAACCGGCTCTTCTACTTTCGCAATGAGGATGTGGA
CTTCTATTTGCCCCAGTTGCTTAACATGTATATCCACATGGATGAGGATGTGGGCGATG
CCATTAAGCCCTACATAGTCCACCGCTGTCGCCAGAGCATCAACTTTTCCCTCCAGTG
TGCCCTGTTGCTTGGGGCCTACTCTTCAGACATGCACATTTCCACTCAGCGACACTCG
CGAGGGACCAAGTTACGGAAGCTAATCCTCTCAGATGAGCTGAAGCCAGCTCACCGA
AAGAGGGAGCTGCCCACATTAAGCCCAGCCCCTGACACAGGGCTGTCTCCCTCTAAA
AGGACTCACCAGCGTTCTAAGTCAGATGCTACGGCCAGCATAAGTCTCAGCAGCAACC
TGAAACGAACAGCCAGCAACCCTAAAGTGGAGAATGAGGATGAGGAGCTCTCCTCCA
GCACCGAGAGTATTGATAATTCATTCAGTTCCCCTGTCCGGCTGGCCCCTGAGCGAGA
ATTCATCAAGTCTTTGATGGCAATCGGCAAACGGCTGGCCACGCTCCCCACTAAAGAG
CAAAAAACACAAAGGCTGATCTCAGAGCTTTCCCTGCTCAACCATAAGCTCCCTGCCC
GAGTCTGGCTGCCCACGGCTGGCTTTGACCACCACGTGGTCCGTGTGCCCCACACAC
AAGCTGTTGTTCTCAATTCCAAGGATAAGGCTCCCTACCTGATCTACGTGGAAGTTCTC
GAATGTGAAAACTTTGACACAACTAGTGTTCCTGCCCGGATTCCTGAAAACCGAATTCG
GAGTACACGGTCTGTAGAGAACCTGCCTGAATGTGGTATCACTCATGAGCAGCGAGCT
GGCAGCTTCAGCACTGTGCCCAATTATGACAATGATGATGAAGCCTGGTCAGTGGATG
ATATAGGCGAGCTGCAAGTGGAGCTCCCTGAAGTGCACACCAACAGCTGTGACAACAT
CTCCCAGTTCTCGGTGGACAGCATCACCAGCCAGGAGAGCAAGGAGCCTGTGTTCAT
TGCAGCAGGGGACATCCGACGGCGCCTTTCAGAACAGCTGGCTCATACTCCTACAGC
CTTCAAACGAGACCCTGAAGACCCTTCTGCAGTTGCCCTCAAAGAGCCCTGGCAGGA
GAAAGTGCGGAGGATCAGAGAAGGTTCCCCGTATGGCCATCTTCCCAATTGGCGACT
CCTTTCAGTCATTGTCAAGTGTGGAGATGACCTTCGCCAGGAGCTGCTGGCTTTCCAG
GTGTTGAAACAACTGCAGTCCATTTGGGAACAGGAGCGAGTGCCTCTTTGGATCAAGC
CATATAAGATTCTTGTGATTTCAGCTGACAGTGGCATGATTGAACCAGTAGTCAACGCT
GTGTCCATCCACCAGGTGAAGAAACAGTCACAGCTCTCCTTGCTCGATTACTTCCTACA
GGAACATGGCAGTTATACCACTGAGGCATTCCTCAGTGCCCAGCGCAATTTTGTGCAA
AGCTGTGCTGGCTACTGCTTGGTCTGCTACCTATTGCAAGTCAAGGACAGGCACAACG
GGAACATCCTTCTGGACGCAGAAGGTCACATCATCCACATCGACTTTGGCTTCATCCTT
TCCAGCTCACCCCGAAACCTGGGCTTCGAGACATCAGCCTTTAAGCTGACCACAGAAT
TTGTGGATGTAATGGGTGGCCTGAACGGTGATATGTTCAACTACTACAAGATGCTCAT
GCTGCAAGGGCTGATTGCTGCTCGGAAGCACATGGACAAGGTGGTACAGATTGTGGA
GATCATGCAGCAAGGTTCTCAGCTTCCTTGCTTCCATGGCTCCAGCACCATTCGCAAC
CTCAAAGAGAGGTTCCACATGAGCATGACTGAGGAGCAGCTGCAGCTGCTGGTGGAG
CAGATGGTGGACGGCAGCATGAGGTCCATCACCACCAAACTCTACGATGGCTTCCAGT
ACCTCACCAATGGCATCATGTGA

EGFP-PI4KB

The EGFP-PI4KB plasmid was cloned by the Dortmund Protein Facility (DPF).

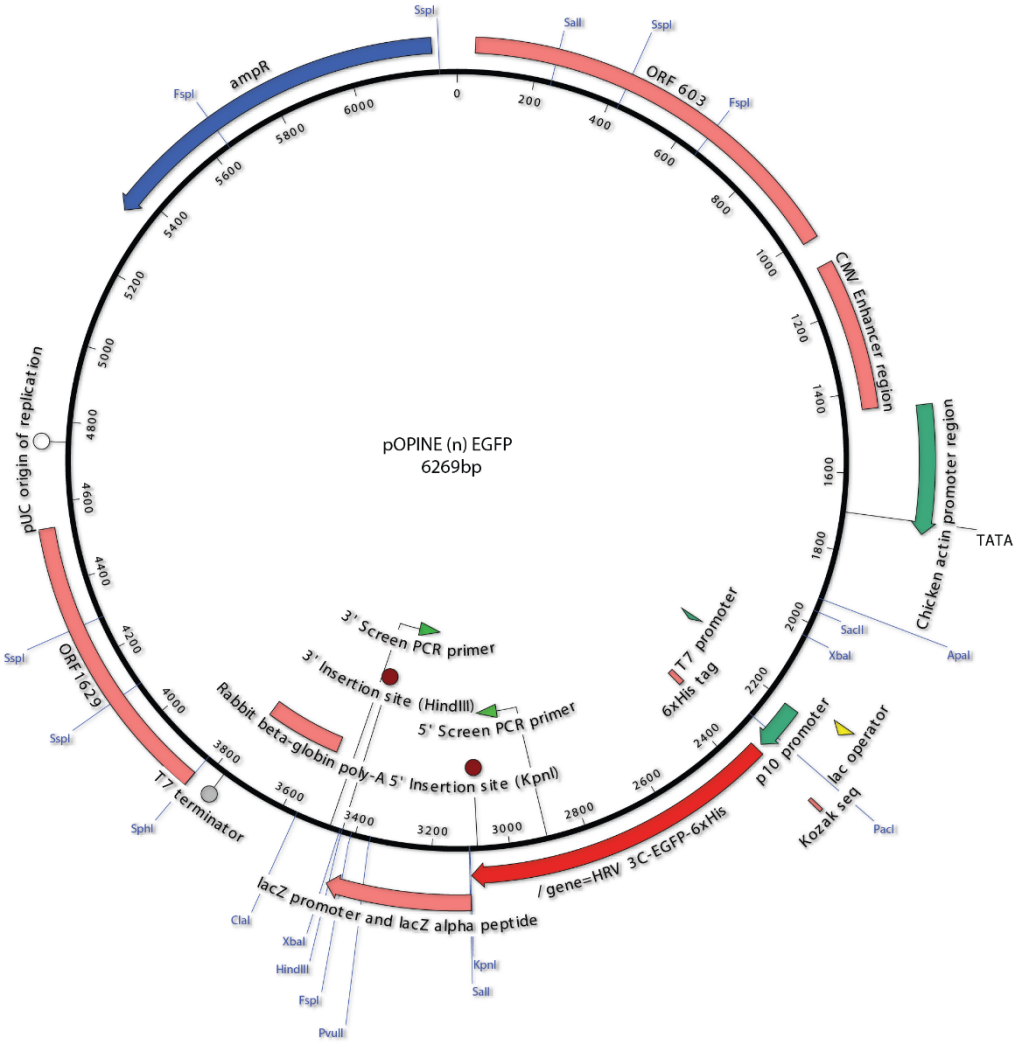

pOPIN(n)EGFP

FEATURE	EXPRESSED SEQUENCE	ADDED SIZE TO PROTEIN * (KDA)
N-terminal Fusion ⇒ Enhanced Green Fluorescent Protein ⇒ 6 x His ⇒ HRV 3C (❙/❙ = cleavage site)	*MAHHHHHHSSGVSKGEELFTGVVPILVELDGDVNGHKFSVS GEGEGDATYGKLTLKFICTTGKLPVPWPTLVTTLTYGVQCFS RYPDHMKQHDFFKSAMPEGYVQERTIFFKDDGNYKTRAEVKF EGDTLVNRIELKGIDFKEDGNILGHKLEYNYNSHNVYIMADK QKNGIKVNFKIRHNIEDGSVQLADHYQQNTPIGDGPVLLPDN HYLSTQSALSKDPNEKRDHMVLLEFVTAAGITLGMDELYKLE VLFQ/G - Gene	28.9
C-Terminal Fusion	N/A	N/A

*Without cleavage by HRV 3C

pOpine(n)EGFP Vector backbone used for cloning.

For sequence of PI4KB please see Flag-PI4KB-His.

pGEN-mSmo

The pGEN-mSmo plasmid was obtained from Addgene (#37673), where it was deposited by Philip Beachy[261].

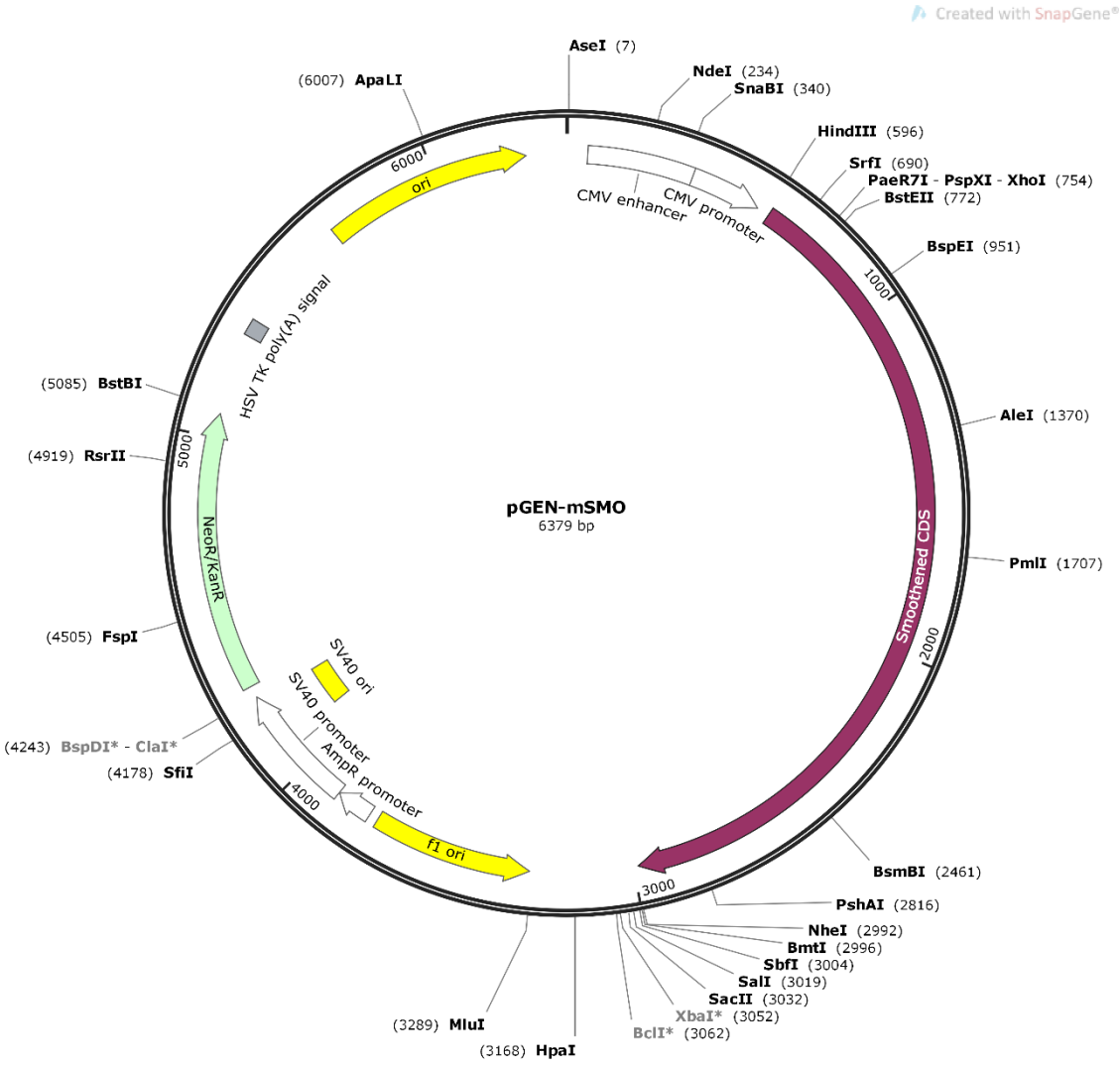

Vector map of pGEN-mSMO.

pSpCas9(BB)-2A-GFP (PX458)

The pSpCas9(BB)-2A-GFP (PX458) plasmid was obtained from Addgene (#48138), where it was deposited by Feng Zhang[131].

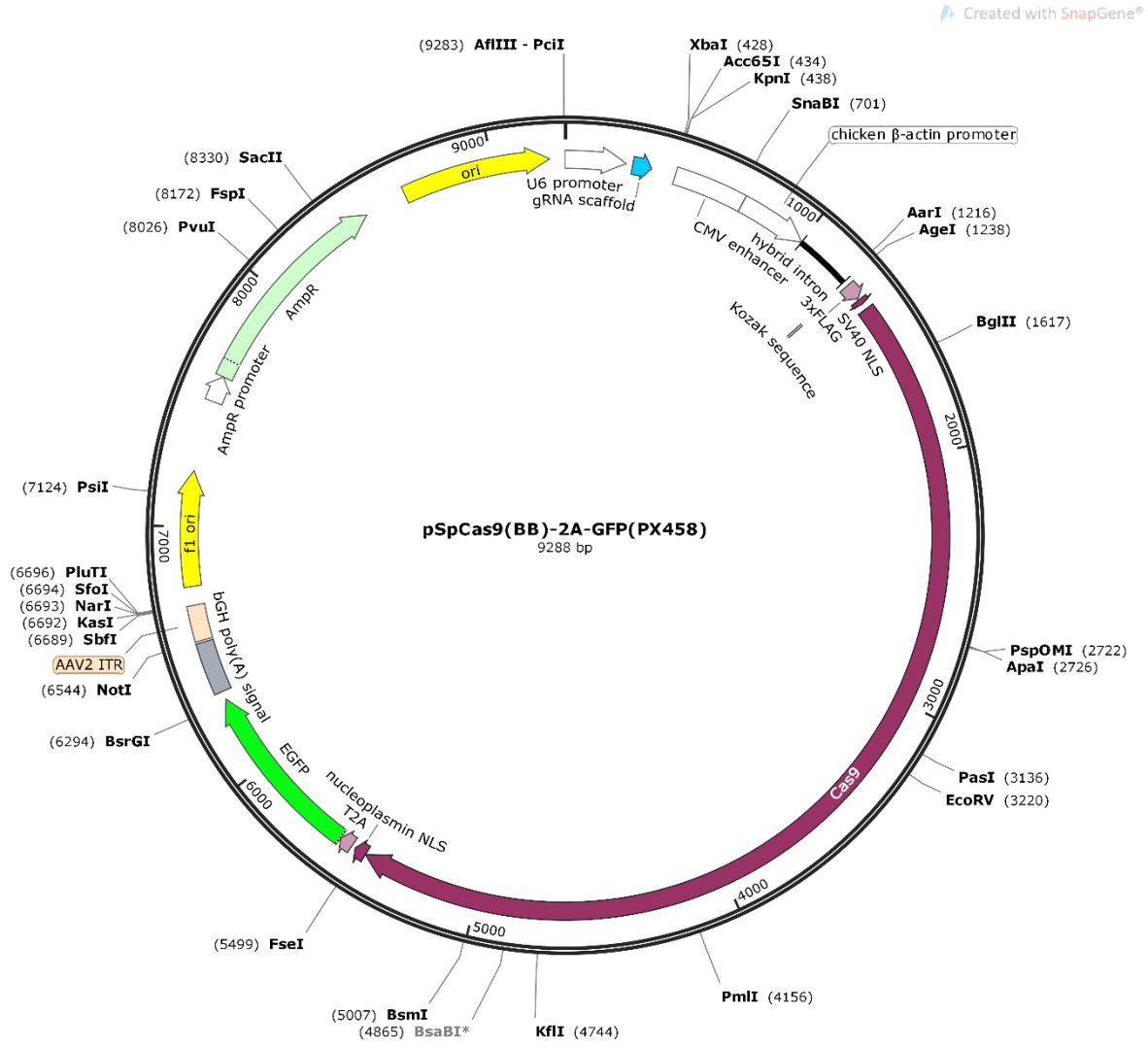

Vector map of pSpCas9(BB)-2A-GFP (PX458).

Smo-BFP

Smo-BFP was cloned by inserting the SMO-Sequence from the pGEN-mSMO plasmid into an pTagBFP-N vector (evrogen, #FP172) via LIC cloning.

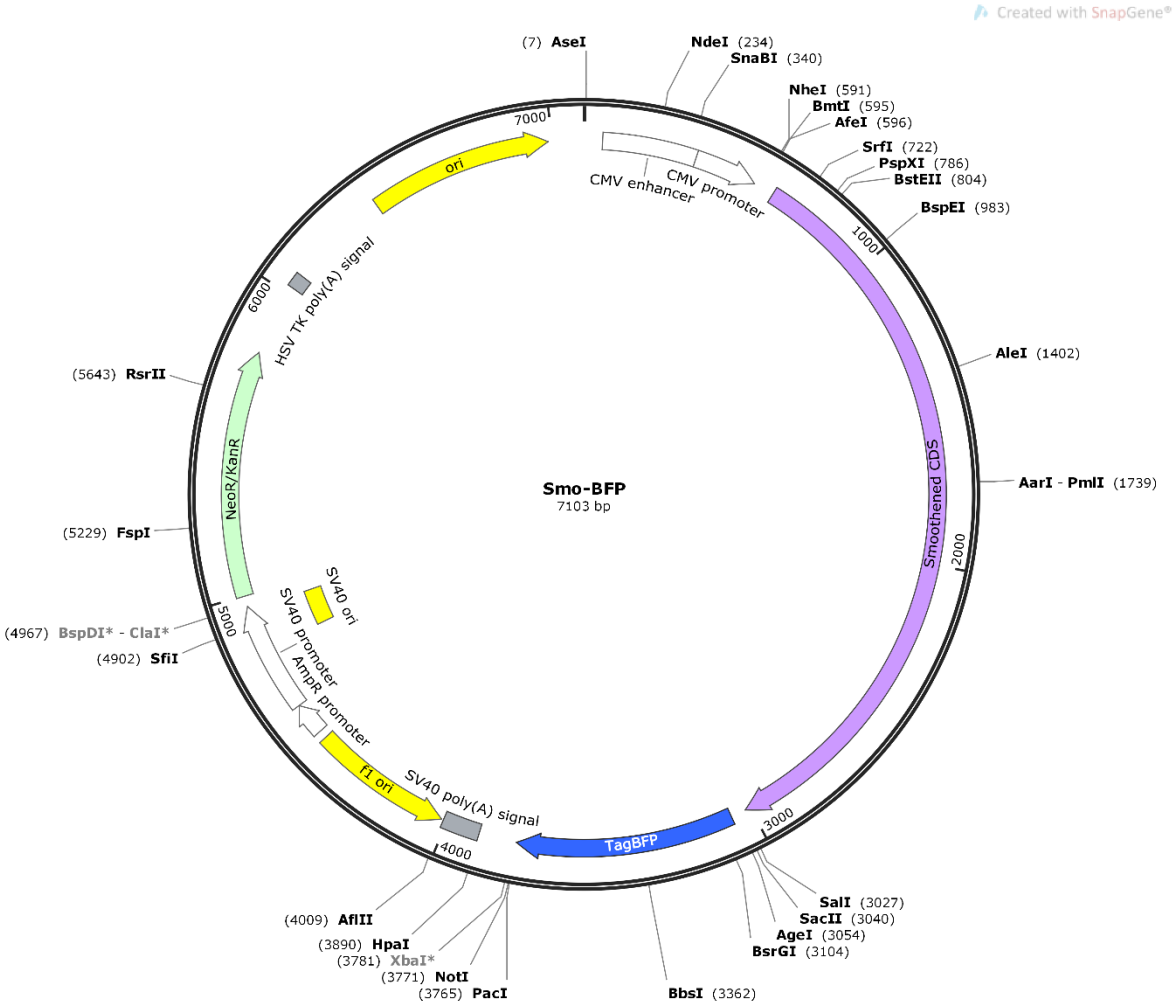

Vector map of Smo-BFP.

12.2 Kinase panel results

The kinase panel was measured at SelectScreen. All inhibition (i)/displacement (d) values >50% are highlighted in orange.

Kinase	ATP Tested [µM]	inhibition(i)/ displacement (d) [%]	SD	assay format	i/d
AAK1	n.a.	31.14	0.23	Lantha	d
ABL1	Km app	12.63	1.17	Z'Lyte	i
ABL1 E255K	Km app	-0.53	2.12	Z'Lyte	i
ABL1 F317I	Km app	-1.00	0.94	Z'Lyte	i
ABL1 G250E	Km app	-0.86	0.47	Z'Lyte	i
ABL1 H396P	n.a.	6.57	4.36	Lantha	d
ABL1 M351T	n.a.	5.83	2.11	Lantha	d
ABL1 Q252H	n.a.	2.88	3.39	Lantha	d
ABL1 T315I	Km app	-1.95	1.08	Z'Lyte	i
ABL1 Y253F	Km app	-9.27	0.84	Z'Lyte	i
ABL2 (Arg)	Km app	1.26	2.60	Z'Lyte	i
ACVR1 (ALK2)	n.a.	-4.69	3.09	Lantha	d
ACVR1 (ALK2) R206H	n.a.	8.81	4.58	Lantha	d
ACVR1B (ALK4)	Km app	3.33	0.57	Z'Lyte	i
ACVR1C (ALK7)	n.a.	17.21	2.16	Lantha	d
ACVR2A	n.a.	-18.41	0.65	Lantha	d
ACVR2B	n.a.	4.17	3.13	Lantha	d
ACVRL1 (ALK1)	n.a.	3.44	6.48	Lantha	d
ADCK3	n.a.	13.97	1.60	Lantha	d
ADRBK1 (GRK2)	Km app	7.40	1.96	Z'Lyte	i
ADRBK2 (GRK3)	Km app	5.01	1.33	Z'Lyte	i
AKT1 (PKB alpha)	Km app	-6.47	1.26	Z'Lyte	i
AKT2 (PKB beta)	Km app	1.38	2.19	Z'Lyte	i
AKT3 (PKB gamma)	Km app	-3.79	2.07	Z'Lyte	i
ALK	Km app	-3.21	2.45	Z'Lyte	i
ALK C1156Y	n.a.	15.90	0.74	Lantha	d
ALK F1174L	n.a.	16.25	0.63	Lantha	d
ALK L1196M	n.a.	2.58	2.18	Lantha	d
ALK R1275Q	n.a.	10.55	2.72	Lantha	d
AMPK (A1/B1/G2)	n.a.	11.79	3.94	Lantha	d
AMPK (A1/B1/G3)	n.a.	13.62	1.48	Lantha	d
AMPK (A1/B2/G1)	n.a.	16.87	3.86	Lantha	d
AMPK (A1/B2/G3)	Km app	6.97	1.58	Z'Lyte	i
AMPK (A2/B1/G2)	Km app	-0.87	1.64	Z'Lyte	i
AMPK (A2/B1/G3)	Km app	4.54	3.50	Z'Lyte	i
AMPK (A2/B2/G1)	n.a.	3.57	0.78	Lantha	d
AMPK (A2/B2/G2)	n.a.	4.05	0.05	Lantha	d

Kinase	ATP Tested [µM]	inhibition(i)/ displacement (d) [%]	SD	assay format	i/d
AMPK (A2/B2/G3)	Km app	3.35	0.38	Z'Lyte	i
AMPK A1/B1/G1	Km app	4.07	1.81	Z'Lyte	i
AMPK A2/B1/G1	Km app	1.16	1.42	Z'Lyte	i
ANKK1	n.a.	1.80	1.74	Lantha	d
AURKA (Aurora A)	Km app	-13.06	0.28	Z'Lyte	i
AURKB (Aurora B)	Km app	1.12	0.63	Z'Lyte	i
AURKC (Aurora C)	Km app	-0.57	0.23	Z'Lyte	i
AXL	Km app	-15.71	0.91	Z'Lyte	i
AXL R499C	n.a.	5.76	0.31	Lantha	d
BLK	Km app	-14.47	0.05	Z'Lyte	i
BMPR1A (ALK3)	n.a.	-9.61	1.52	Lantha	d
BMPR1B (ALK6)	n.a.	6.06	4.06	Lantha	d
BMPR2	n.a.	37.85	0.84	Lantha	d
BMX	Km app	8.52	6.31	Z'Lyte	i
BRAF	n.a.	12.47	2.90	Lantha	d
BRAF	100	-4.51	1.00	Z'Lyte	i
BRAF V599E	n.a.	4.69	0.11	Lantha	d
BRAF V599E	100	14.10	1.86	Z'Lyte	i
BRSK1 (SAD1)	Km app	-3.15	0.68	Z'Lyte	i
BRSK2	n.a.	-11.62	0.94	Lantha	d
BTK	Km app	3.52	2.77	Z'Lyte	i
CAMK1 (CaMK1)	10	1.72	6.95	Adapta	i
CAMK1D (CaMKI delta)	Km app	1.71	0.44	Z'Lyte	i
CAMK1G (CAMKI gamma)	Km app	-3.33	1.38	Z'Lyte	i
CAMK2A (CaMKII alpha)	Km app	-4.92	5.94	Z'Lyte	i
CAMK2B (CaMKII beta)	Km app	-8.93	0.08	Z'Lyte	i
CAMK2D (CaMKII delta)	Km app	5.52	0.23	Z'Lyte	i
CAMK2G (CaMKII gamma)	n.a.	5.47	1.22	Lantha	d
CAMK4 (CaMKIV)	Km app	-5.76	0.64	Z'Lyte	i
CAMKK1 (CAMKKA)	n.a.	-5.94	2.24	Lantha	d
CAMKK2 (CaMKK beta)	n.a.	5.87	1.80	Lantha	d
CASK	n.a.	-18.13	2.40	Lantha	d
CDC42 BPA (MRCKA)	Km app	1.57	2.16	Z'Lyte	i
CDC42 BPB (MRCKB)	Km app	-9.28	10.87	Z'Lyte	i
CDC42 BPG (MRCKG)	Km app	-4.51	0.23	Z'Lyte	i
CDC7/DBF4	n.a.	28.49	6.82	Lantha	d
CDK1/cyclin A2	n.a.	-23.03	4.86	Lantha	d
CDK1/cyclin B	Km app	10.47	3.01	Z'Lyte	i
CDK11 (Inactive)	n.a.	-2.45	2.80	Lantha	d
CDK14 (PFTK1)/cyclin Y	n.a.	-14.13	2.15	Lantha	d
CDK16 (PCTK1)/cyclin Y	n.a.	-13.83	0.98	Lantha	d

Kinase	ATP Tested [µM]	inhibition(i)/ displacement (d) [%]	SD	assay format	i/d
CDK17/cyclin Y	Km app	2.37	7.86	Z'Lyte	i
CDK18/cyclin Y	Km app	-2.36	3.68	Z'Lyte	i
CDK2/cyclin A	Km app	3.10	4.53	Z'Lyte	i
CDK2/cyclin A1	n.a.	19.31	1.87	Lantha	d
CDK2/cyclin E1	n.a.	-1.80	2.97	Lantha	d
CDK2/cyclin O	n.a.	22.80	6.04	Lantha	d
CDK3/cyclin E1	n.a.	-6.99	7.99	Lantha	d
CDK5 (Inactive)	n.a.	-18.85	9.20	Lantha	d
CDK5/p25	Km app	5.27	5.05	Z'Lyte	i
CDK5/p35	Km app	4.88	6.73	Z'Lyte	i
CDK7/cyclin H/MNAT1	Km app	13.61	10.17	Adapta	i
CDK8/cyclin C	n.a.	-1.03	0.88	Lantha	d
CDK9 (Inactive)	n.a.	8.10	0.28	Lantha	d
CDK9/cyclin K	n.a.	0.67	0.76	Lantha	d
CDK9/cyclin T1	Km app	30.27	7.32	Adapta	i
CDKL5	Km app	-0.89	0.10	Z'Lyte	i
CHEK1 (CHK1)	Km app	-15.39	9.23	Z'Lyte	i
CHEK2 (CHK2)	Km app	4.44	0.54	Z'Lyte	i
CHUK (IKK alpha)	Km app	1.18	0.49	Adapta	i
CLK1	Km app	12.16	2.34	Z'Lyte	i
CLK2	Km app	-15.66	3.05	Z'Lyte	i
CLK3	Km app	0.35	1.62	Z'Lyte	i
CLK4	n.a.	39.36	2.35	Lantha	d
CSF1R (FMS)	Km app	6.40	2.93	Z'Lyte	i
CSK	Km app	-1.34	1.14	Z'Lyte	i
CSNK1A1 (CK1 alpha 1)	Km app	4.76	1.22	Z'Lyte	i
CSNK1A1L	Km app	5.16	0.21	Z'Lyte	i
CSNK1D (CK1 delta)	Km app	-1.67	0.62	Z'Lyte	i
CSNK1E (CK1 epsilon)	Km app	4.76	0.55	Z'Lyte	i
CSNK1G1 (CK1 gamma 1)	Km app	10.73	0.15	Z'Lyte	i
CSNK1G2 (CK1 gamma 2)	Km app	-5.50	1.25	Z'Lyte	i
CSNK1G3 (CK1 gamma 3)	Km app	-10.86	7.82	Z'Lyte	i
CSNK2A1 (CK2 alpha 1)	Km app	16.38	3.76	Z'Lyte	i
CSNK2A2 (CK2 alpha 2)	Km app	0.03	1.89	Z'Lyte	i
DAPK1	Km app	12.06	1.29	Adapta	i
DAPK2	n.a.	9.85	1.54	Lantha	d
DAPK3 (ZIPK)	Km app	0.84	2.23	Z'Lyte	i
DCAMKL1 (DCLK1)	Km app	1.65	1.45	Z'Lyte	i
DCAMKL2 (DCK2)	Km app	3.62	1.42	Z'Lyte	i
DDR1	n.a.	2.01	1.72	Lantha	d
DDR2	n.a.	1.68	0.57	Lantha	d

Kinase	ATP Tested [µM]	inhibition(i)/ displacement (d) [%]	SD	assay format	i/d
DDR2 N456S	n.a.	7.07	0.02	Lantha	d
DDR2 T654M	n.a.	18.98	1.10	Lantha	d
DMPK	n.a.	0.81	1.20	Lantha	d
DNA-PK	Km app	20.48	2.23	Z'Lyte	i
DYRK1A	Km app	5.03	0.62	Z'Lyte	i
DYRK1B	Km app	7.45	1.45	Z'Lyte	i
DYRK2	n.a.	-18.68	3.51	Lantha	d
DYRK3	Km app	-0.28	1.14	Z'Lyte	i
DYRK4	Km app	-5.41	1.05	Z'Lyte	i
EEF2K	Km app	5.25	3.48	Z'Lyte	i
EGFR (ErbB1)	Km app	-12.43	1.66	Z'Lyte	i
EGFR (ErbB1) d746-750	n.a.	-1.04	1.61	Lantha	d
EGFR (ErbB1) L858R	Km app	1.78	1.48	Z'Lyte	i
EGFR (ErbB1) L861Q	Km app	2.36	1.08	Z'Lyte	i
EGFR (ErbB1) T790M	Km app	7.02	4.39	Z'Lyte	i
EGFR (ErbB1) T790M L858R	Km app	-11.88	2.36	Z'Lyte	i
EIF2AK2 (PKR)	n.a.	-27.81	3.32	Lantha	d
EPHA1	Km app	1.44	0.63	Z'Lyte	i
EPHA2	Km app	-11.28	0.35	Z'Lyte	i
EPHA3	n.a.	1.91	3.02	Lantha	d
EPHA4	Km app	6.74	0.42	Z'Lyte	i
EPHA5	Km app	19.87	0.50	Z'Lyte	i
EPHA6	n.a.	-3.99	5.24	Lantha	d
EPHA7	n.a.	-13.97	2.08	Lantha	d
EPHA8	Km app	7.55	0.41	Z'Lyte	i
EPHB1	Km app	2.74	1.11	Z'Lyte	i
EPHB2	Km app	3.25	0.63	Z'Lyte	i
EPHB3	Km app	5.72	0.22	Z'Lyte	i
EPHB4	Km app	2.42	0.33	Z'Lyte	i
ERBB2 (HER2)	Km app	1.34	2.67	Z'Lyte	i
ERBB4 (HER4)	Km app	1.20	2.78	Z'Lyte	i
ERN1	n.a.	-16.32	2.88	Lantha	d
ERN2	n.a.	-11.80	1.13	Lantha	d
FER	Km app	3.19	1.40	Z'Lyte	i
FES (FPS)	Km app	19.54	2.64	Z'Lyte	i
FGFR1	Km app	-1.60	2.20	Z'Lyte	i
FGFR1 V561M	n.a.	-11.47	5.25	Lantha	d
FGFR2	Km app	13.14	2.99	Z'Lyte	i
FGFR3	Km app	5.56	0.75	Z'Lyte	i
FGFR3 G697C	n.a.	-5.85	1.57	Lantha	d
FGFR3 K650E	Km app	1.87	12.28	Z'Lyte	i

Kinase	ATP Tested [µM]	inhibition(i)/ displacement (d) [%]	SD	assay format	i/d
FGFR3 K650M	n.a.	-8.91	0.31	Lantha	d
FGFR4	Km app	0.99	4.75	Z'Lyte	i
FGR	Km app	3.99	2.15	Z'Lyte	i
FLT1 (VEGFR1)	Km app	-3.62	2.14	Z'Lyte	i
FLT3	Km app	12.33	0.86	Z'Lyte	i
FLT3 D835Y	Km app	11.09	0.93	Z'Lyte	i
FLT3 ITD	n.a.	40.96	7.16	Lantha	d
FLT4 (VEGFR3)	Km app	2.39	1.50	Z'Lyte	i
FRAP1 (mTOR)	Km app	0.09	4.22	Z'Lyte	i
FRK (PTK5)	Km app	-5.13	0.62	Z'Lyte	i
FYN	Km app	1.30	4.02	Z'Lyte	i
FYN A	n.a.	-6.04	1.78	Lantha	d
GAK	n.a.	73.05	0.64	Lantha	d
GRK1	n.a.	25.22	0.50	Lantha	d
GRK4	Km app	0.77	4.42	Z'Lyte	i
GRK5	Km app	-0.63	2.29	Z'Lyte	i
GRK6	Km app	3.07	1.41	Z'Lyte	i
GRK7	Km app	53.22	3.20	Z'Lyte	i
GSG2 (Haspin)	Km app	15.11	4.09	Adapta	i
GSK3A (GSK3 alpha)	Km app	-7.49	1.09	Z'Lyte	i
GSK3B (GSK3 beta)	Km app	10.63	3.28	Z'Lyte	i
HCK	Km app	9.23	0.36	Z'Lyte	i
HIPK1 (Myak)	Km app	2.34	1.33	Z'Lyte	i
HIPK2	Km app	5.93	0.42	Z'Lyte	i
HIPK3 (YAK1)	Km app	2.08	0.29	Z'Lyte	i
HIPK4	Km app	0.26	0.22	Z'Lyte	i
HUNK	n.a.	1.90	1.48	Lantha	d
ICK	n.a.	5.56	2.25	Lantha	d
IGF1R	Km app	-4.65	3.25	Z'Lyte	i
IKBKB (IKK beta)	Km app	0.04	2.44	Z'Lyte	i
IKBKE (IKK epsilon)	Km app	1.69	4.16	Z'Lyte	i
INSR	Km app	2.86	2.39	Z'Lyte	i
INSRR (IRR)	Km app	7.87	1.41	Z'Lyte	i
IRAK1	Km app	14.69	8.89	Adapta	i
IRAK3	n.a.	32.42	4.43	Lantha	d
IRAK4	Km app	-3.56	0.30	Z'Lyte	i
ITK	Km app	11.96	6.22	Z'Lyte	i
JAK1	Km app	-1.45	0.32	Z'Lyte	i
JAK2	Km app	-1.76	1.21	Z'Lyte	i
JAK2 JH1 JH2	Km app	0.17	0.45	Z'Lyte	i
JAK2 JH1 JH2 V617F	Km app	-4.43	1.58	Z'Lyte	i

Kinase	ATP Tested [µM]	inhibition(i)/ displacement (d) [%]	SD	assay format	i/d
JAK3	Km app	4.93	0.67	Z'Lyte	i
KDR (VEGFR2)	Km app	-0.05	6.99	Z'Lyte	i
KIT	Km app	15.26	9.50	Z'Lyte	i
KIT A829P	n.a.	7.42	2.64	Lantha	d
KIT D816H	n.a.	25.89	2.40	Lantha	d
KIT D816V	n.a.	13.28	2.08	Lantha	d
KIT D820E	n.a.	3.55	0.44	Lantha	d
KIT N822K	n.a.	5.33	2.29	Lantha	d
KIT T670E	n.a.	-2.65	1.41	Lantha	d
KIT T670I	Km app	13.88	7.64	Z'Lyte	i
KIT V559D	Km app	-3.83	2.06	Z'Lyte	i
KIT V559D T670I	n.a.	3.73	1.81	Lantha	d
KIT V559D V654A	Km app	-3.69	3.12	Z'Lyte	i
KIT V560G	Km app	-11.34	3.69	Z'Lyte	i
KIT V654A	n.a.	-0.29	1.90	Lantha	d
KIT Y823D	n.a.	3.85	1.48	Lantha	d
KSR2	Km app	4.59	0.99	Z'Lyte	i
LATS1	n.a.	-49.49	2.06	Lantha	d
LATS2	n.a.	0.35	2.81	Lantha	d
LCK	Km app	-0.59	7.60	Z'Lyte	i
LIMK1	n.a.	-1.74	5.44	Lantha	d
LIMK2	n.a.	1.67	0.18	Lantha	d
LRRK2	Km app	27.07	4.75	Adapta	i
LRRK2 FL	Km app	30.81	3.96	Adapta	i
LRRK2 G2019S	Km app	34.89	6.05	Adapta	i
LRRK2 G2019S FL	Km app	35.15	0.41	Adapta	i
LRRK2 I2020T	Km app	10.08	1.25	Adapta	i
LRRK2 R1441C	Km app	22.44	1.78	Adapta	i
LTK (TYK1)	Km app	9.24	5.84	Z'Lyte	i
LYN A	Km app	1.02	5.38	Z'Lyte	i
LYN B	Km app	-0.50	0.13	Z'Lyte	i
MAP2K1 (MEK1)	n.a.	-0.83	0.78	Lantha	d
MAP2K1 (MEK1)	100	-2.04	1.39	Z'Lyte	i
MAP2K1 (MEK1) S218D S222D	n.a.	-1.74	2.73	Lantha	d
MAP2K2 (MEK2)	n.a.	-1.93	0.30	Lantha	d
MAP2K2 (MEK2)	100	1.54	1.68	Z'Lyte	i
MAP2K3 (MEK3)	n.a.	-48.29	1.88	Lantha	d
MAP2K4 (MEK4)	n.a.	1.55	0.99	Lantha	d
MAP2K5 (MEK5)	n.a.	2.32	1.17	Lantha	d
MAP2K6 (MKK6)	n.a.	-0.74	0.43	Lantha	d
MAP2K6 (MKK6)	100	-3.52	0.28	Z'Lyte	i

Kinase	ATP Tested [µM]	inhibition(i)/ displacement (d) [%]	SD	assay format	i/d
MAP2K6 (MKK6) S207E T211E	n.a.	1.20	1.07	Lantha	d
MAP3K10 (MLK2)	n.a.	3.25	1.59	Lantha	d
MAP3K11 (MLK3)	n.a.	3.47	0.47	Lantha	d
MAP3K14 (NIK)	n.a.	-5.87	2.42	Lantha	d
MAP3K19 (YSK4)	Km app	1.19	1.87	Z'Lyte	i
MAP3K2 (MEKK2)	n.a.	-20.24	0.61	Lantha	d
MAP3K3 (MEKK3)	n.a.	-22.31	3.98	Lantha	d
MAP3K5 (ASK1)	n.a.	-29.89	0.02	Lantha	d
MAP3K7/MAP3K7IP1 (TAK1-TAB1)	n.a.	43.00	1.80	Lantha	d
MAP3K8 (COT)	100	-6.27	1.38	Z'Lyte	i
MAP3K9 (MLK1)	Km app	-0.53	2.94	Z'Lyte	i
MAP4K1 (HPK1)	n.a.	7.09	0.41	Lantha	d
MAP4K2 (GCK)	Km app	-16.91	0.04	Z'Lyte	i
MAP4K3 (GLK)	n.a.	-4.33	3.67	Lantha	d
MAP4K4 (HGK)	Km app	-7.79	2.46	Z'Lyte	i
MAP4K5 (KHS1)	Km app	10.80	2.32	Z'Lyte	i
MAPK1 (ERK2)	Km app	3.00	0.23	Z'Lyte	i
MAPK10 (JNK3)	n.a.	40.79	1.63	Lantha	d
MAPK10 (JNK3)	100	-8.65	2.71	Z'Lyte	i
MAPK11 (p38 beta)	Km app	-2.68	1.59	Z'Lyte	i
MAPK12 (p38 gamma)	Km app	-1.84	0.56	Z'Lyte	i
MAPK13 (p38 delta)	Km app	4.65	1.60	Z'Lyte	i
MAPK14 (p38 alpha)	100	-19.37	1.32	Z'Lyte	i
MAPK14 (p38 alpha)	Km app	-4.14	3.20	Z'Lyte	i
MAPK15 (ERK7)	n.a.	7.97	1.02	Lantha	d
MAPK3 (ERK1)	Km app	5.99	0.07	Z'Lyte	i
MAPK7 (ERK5)	Km app	-2.26	1.91	Z'Lyte	i
MAPK8 (JNK1)	n.a.	65.20	2.17	Lantha	d
MAPK8 (JNK1)	100	8.47	3.83	Z'Lyte	i
MAPK9 (JNK2)	n.a.	34.73	5.64	Lantha	d
MAPK9 (JNK2)	100	8.65	2.21	Z'Lyte	i
MAPKAPK2	Km app	6.15	0.41	Z'Lyte	i
MAPKAPK3	Km app	-8.11	0.48	Z'Lyte	i
MAPKAPK5 (PRAK)	Km app	-3.71	1.42	Z'Lyte	i
MARK1 (MARK)	Km app	-1.09	0.60	Z'Lyte	i
MARK2	Km app	4.36	1.92	Z'Lyte	i
MARK3	Km app	6.32	0.78	Z'Lyte	i
MARK4	Km app	24.20	1.82	Z'Lyte	i
MASTL	n.a.	-1.47	2.51	Lantha	d
MATK (HYL)	Km app	-2.80	1.70	Z'Lyte	i
MELK	Km app	45.09	1.66	Z'Lyte	i

Kinase	ATP Tested [µM]	inhibition(i)/ displacement (d) [%]	SD	assay format	i/d
MERTK (cMER)	Km app	6.65	0.85	Z'Lyte	i
MERTK (cMER) A708S	n.a.	14.72	1.46	Lantha	d
MET (cMet)	Km app	1.97	2.40	Z'Lyte	i
MET D1228H	n.a.	8.38	4.66	Lantha	d
MET M1250T	Km app	7.14	3.02	Z'Lyte	i
MINK1	Km app	-3.36	1.48	Z'Lyte	i
MKNK1 (MNK1)	Km app	7.51	3.35	Z'Lyte	i
MKNK2 (MNK2)	n.a.	-16.64	5.19	Lantha	d
MLCK (MLCK2)	n.a.	-5.47	1.78	Lantha	d
MLK4	n.a.	-4.48	2.93	Lantha	d
MST1R (RON)	Km app	-0.36	3.23	Z'Lyte	i
MST4	Km app	-2.79	2.66	Z'Lyte	i
MUSK	Km app	-1.22	0.07	Z'Lyte	i
MYLK (MLCK)	n.a.	26.08	1.00	Lantha	d
MYLK2 (skMLCK)	Km app	-8.20	5.23	Z'Lyte	i
MYLK4	n.a.	52.99	0.69	Lantha	d
MYO3A (MYO3 alpha)	n.a.	-10.51	1.55	Lantha	d
MYO3B (MYO3 beta)	n.a.	8.07	1.40	Lantha	d
NEK1	Km app	1.73	0.56	Z'Lyte	i
NEK2	Km app	4.70	7.53	Z'Lyte	i
NEK4	Km app	10.21	2.96	Z'Lyte	i
NEK6	Km app	-7.85	1.82	Z'Lyte	i
NEK7	Km app	2.65	0.26	Z'Lyte	i
NEK8	n.a.	2.86	0.46	Lantha	d
NEK9	Km app	-11.98	3.76	Z'Lyte	i
NIM1K	Km app	1.90	3.02	Z'Lyte	i
NLK	n.a.	10.76	1.74	Lantha	d
NTRK1 (TRKA)	Km app	16.52	7.84	Z'Lyte	i
NTRK2 (TRKB)	Km app	4.24	0.11	Z'Lyte	i
NTRK3 (TRKC)	Km app	11.65	4.29	Z'Lyte	i
NUAK1 (ARK5)	Km app	51.08	1.78	Adapta	i
NUAK2	n.a.	22.01	0.12	Lantha	d
OXSR1	n.a.	-45.46	4.32	Lantha	d
PAK1	Km app	15.56	4.45	Z'Lyte	i
PAK2 (PAK65)	Km app	11.34	9.91	Z'Lyte	i
PAK3	Km app	28.97	7.23	Z'Lyte	i
PAK4	Km app	-5.77	6.50	Z'Lyte	i
PAK6	Km app	10.66	3.77	Z'Lyte	i
PAK7 (KIAA1264)	Km app	6.49	3.37	Z'Lyte	i
PASK	Km app	0.11	1.60	Z'Lyte	i
PDGFRA (PDGFR alpha)	Km app	-3.43	0.77	Z'Lyte	i

Kinase	ATP Tested [µM]	inhibition(i)/ displacement (d) [%]	SD	assay format	i/d
PDGFRA D842V	Km app	6.57	2.72	Z'Lyte	i
PDGFRA T674I	Km app	3.72	3.90	Z'Lyte	i
PDGFRA V561D	Km app	11.24	11.75	Z'Lyte	i
PDGFRB (PDGFR beta)	Km app	-1.79	0.99	Z'Lyte	i
PDK1	100	4.25	1.61	Z'Lyte	i
PDK1	Km app	-1.23	4.02	Z'Lyte	i
PEAK1	Km app	-8.29	6.40	Z'Lyte	i
PHKG1	Km app	1.00	2.18	Z'Lyte	i
PHKG2	Km app	5.73	1.99	Z'Lyte	i
PI4K2A (PI4K2 alpha)	10	11.25	0.63	Adapta	i
PI4K2B (PI4K2 beta)	10	-1.52	2.32	Adapta	i
PI4KA (PI4K alpha)	10	-7.91	1.04	Adapta	i
PI4KB (PI4K beta)	Km app	75.59	1.65	Adapta	i
PIK3C2A (PI3K-C2 alpha)	Km app	11.96	2.08	Adapta	i
PIK3C2B (PI3K-C2 beta)	10	10.38	3.56	Adapta	i
PIK3C2G (PI3K-C2 gamma)	10	53.18	2.62	Adapta	i
PIK3C3 (hVPS34)	Km app	24.69	4.88	Adapta	i
PIK3CA E545K/PIK3R1 (p110 alpha E545K/p85 alpha)	10	9.89	1.00	Adapta	i
PIK3CA/PIK3R1 (p110 alpha/p85 alpha)	Km app	-14.75	3.85	Adapta	i
PIK3CA/PIK3R3 (p110 alpha/p55 gamma)	10	1.27	7.16	Adapta	i
PIK3CB/PIK3R1 (p110 beta/p85 alpha)	Km app	7.75	0.34	Adapta	i
PIK3CB/PIK3R2 (p110 beta/p85 beta)	10	4.68	5.68	Adapta	i
PIK3CD/PIK3R1 (p110 delta/p85 alpha)	Km app	-2.24	0.98	Adapta	i
PIK3CG (p110 gamma)	Km app	22.77	4.19	Adapta	i
PIM1	Km app	-17.61	2.13	Z'Lyte	i
PIM2	Km app	-12.91	0.80	Z'Lyte	i
PIM3	Km app	-8.26	0.12	Z'Lyte	i
PIP4K2A	10	4.73	2.53	Adapta	i
PIP5K1A	10	12.57	3.42	Adapta	i
PIP5K1B	10	10.43	0.36	Adapta	i
PIP5K1C	10	56.08	0.04	Adapta	i
PKMYT1	n.a.	6.85	7.69	Lantha	d
PKN1 (PRK1)	Km app	-3.61	2.19	Z'Lyte	i
PKN2 (PRK2)	n.a.	-9.22	2.29	Lantha	d
PLK1	Km app	-0.58	2.33	Z'Lyte	i
PLK2	Km app	11.65	2.06	Z'Lyte	i
PLK3	Km app	-10.36	1.81	Z'Lyte	i
PLK4	n.a.	27.61	3.24	Lantha	d
PRKACA (PKA)	Km app	-0.03	0.31	Z'Lyte	i

Kinase	ATP Tested [µM]	inhibition(i)/ displacement (d) [%]	SD	assay format	i/d
PRKACB (PRKAC beta)	n.a.	10.67	0.62	Lantha	d
PRKACG (PRKAC gamma)	n.a.	-18.72	1.53	Lantha	d
PRKCA (PKC alpha)	Km app	-10.28	4.25	Z'Lyte	i
PRKCB1 (PKC beta I)	Km app	4.26	2.61	Z'Lyte	i
PRKCB2 (PKC beta II)	Km app	-0.48	11.10	Z'Lyte	i
PRKCD (PKC delta)	Km app	8.14	4.22	Z'Lyte	i
PRKCE (PKC epsilon)	Km app	-7.52	4.01	Z'Lyte	i
PRKCG (PKC gamma)	Km app	2.66	9.13	Z'Lyte	i
PRKCH (PKC eta)	Km app	16.06	9.28	Z'Lyte	i
PRKCI (PKC iota)	Km app	-5.70	2.88	Z'Lyte	i
PRKCN (PKD3)	Km app	8.31	0.38	Z'Lyte	i
PRKCQ (PKC theta)	Km app	-10.59	1.92	Z'Lyte	i
PRKCZ (PKC zeta)	Km app	-4.33	2.49	Z'Lyte	i
PRKD1 (PKC mu)	Km app	12.92	1.23	Z'Lyte	i
PRKD2 (PKD2)	Km app	-5.37	0.98	Z'Lyte	i
PRKG1	Km app	0.87	5.79	Z'Lyte	i
PRKG2 (PKG2)	Km app	-2.93	0.69	Z'Lyte	i
PRKX	Km app	7.50	1.28	Z'Lyte	i
PTK2 (FAK)	Km app	6.10	0.86	Z'Lyte	i
PTK2B (FAK2)	Km app	2.70	1.81	Z'Lyte	i
PTK6 (Brk)	Km app	2.28	1.96	Z'Lyte	i
RAF1 (cRAF) Y340D Y341D	n.a.	3.62	1.17	Lantha	d
RAF1 (cRAF) Y340D Y341D	100	-7.67	3.75	Z'Lyte	i
RET	Km app	5.84	0.45	Z'Lyte	i
RET G691S	n.a.	-27.39	5.38	Lantha	d
RET M918T	n.a.	12.36	11.86	Lantha	d
RET S891A	Km app	-19.56	6.22	Z'Lyte	i
RET V804L	Km app	2.48	1.64	Z'Lyte	i
RET V804M	n.a.	-5.89	6.32	Lantha	d
RET Y791F	Km app	0.97	0.33	Z'Lyte	i
RIPK2	n.a.	1.01	2.03	Lantha	d
RIPK3	n.a.	-4.22	3.03	Lantha	d
ROCK1	Km app	-2.75	0.79	Z'Lyte	i
ROCK2	Km app	-3.43	11.44	Z'Lyte	i
ROS1	Km app	1.12	1.14	Z'Lyte	i
RPS6KA1 (RSK1)	Km app	5.36	0.84	Z'Lyte	i
RPS6KA2 (RSK3)	Km app	-1.87	1.71	Z'Lyte	i
RPS6KA3 (RSK2)	Km app	-3.66	0.57	Z'Lyte	i
RPS6KA4 (MSK2)	Km app	-0.52	2.12	Z'Lyte	i
RPS6KA5 (MSK1)	Km app	-1.23	2.80	Z'Lyte	i
RPS6KA6 (RSK4)	Km app	-10.30	0.91	Z'Lyte	i

Kinase	ATP Tested [µM]	inhibition(i)/ displacement (d) [%]	SD	assay format	i/d
RPS6KB1 (p70S6K)	Km app	-12.99	1.80	Z'Lyte	i
RPS6KB2 (p70S6Kb)	Km app	-8.24	2.62	Z'Lyte	i
SBK1	Km app	3.75	0.73	Z'Lyte	i
SGK (SGK1)	Km app	-10.49	2.77	Z'Lyte	i
SGK2	Km app	-14.09	2.45	Z'Lyte	i
SGKL (SGK3)	Km app	-8.86	0.90	Z'Lyte	i
SIK1	n.a.	1.07	0.26	Lantha	d
SIK3	n.a.	-19.76	0.35	Lantha	d
SLK	n.a.	-3.35	1.79	Lantha	d
SNF1LK2	Km app	-0.18	0.34	Z'Lyte	i
SPHK1	Km app	-3.92	0.05	Adapta	i
SPHK2	10	17.63	4.24	Adapta	i
SRC	Km app	4.68	3.52	Z'Lyte	i
SRC N1	Km app	-8.78	0.65	Z'Lyte	i
SRMS (Srm)	Km app	-5.00	1.64	Z'Lyte	i
SRPK1	Km app	3.46	1.66	Z'Lyte	i
SRPK2	Km app	-12.68	7.51	Z'Lyte	i
STK16 (PKL12)	n.a.	6.12	1.91	Lantha	d
STK17A (DRAK1)	n.a.	41.39	0.78	Lantha	d
STK17B (DRAK2)	n.a.	33.49	1.46	Lantha	d
STK22B (TSSK2)	Km app	7.76	1.31	Z'Lyte	i
STK22D (TSSK1)	Km app	3.47	1.80	Z'Lyte	i
STK23 (MSSK1)	Km app	7.49	0.87	Z'Lyte	i
STK24 (MST3)	Km app	-15.45	1.63	Z'Lyte	i
STK25 (YSK1)	Km app	-1.35	0.69	Z'Lyte	i
STK3 (MST2)	Km app	1.31	0.42	Z'Lyte	i
STK32B (YANK2)	n.a.	-2.43	2.06	Lantha	d
STK32C (YANK3)	n.a.	-10.03	4.40	Lantha	d
STK33	n.a.	5.61	1.24	Lantha	d
STK38 (NDR)	n.a.	-4.16	6.46	Lantha	d
STK38L (NDR2)	n.a.	-38.95	3.34	Lantha	d
STK39 (STLK3)	n.a.	-4.07	7.47	Lantha	d
STK4 (MST1)	Km app	6.80	1.39	Z'Lyte	i
SYK	Km app	-1.59	1.75	Z'Lyte	i
TAOK1	n.a.	21.20	0.93	Lantha	d
TAOK2 (TAO1)	Km app	-0.54	3.46	Z'Lyte	i
TAOK3 (JIK)	n.a.	-12.81	1.03	Lantha	d
TBK1	Km app	5.95	3.22	Z'Lyte	i
TEC	n.a.	-0.71	2.00	Lantha	d
TEK (Tie2)	Km app	0.49	1.54	Z'Lyte	i
TEK (TIE2) R849W	n.a.	-6.58	4.06	Lantha	d

Kinase	ATP Tested [µM]	inhibition(i)/ displacement (d) [%]	SD	assay format	i/d
TEK (TIE2) Y1108F	n.a.	-5.07	2.19	Lantha	d
TEK (TIE2) Y897S	Km app	3.17	0.06	Z'Lyte	i
TESK1	n.a.	-45.95	12.46	Lantha	d
TESK2	n.a.	-8.24	5.95	Lantha	d
TGFBR1 (ALK5)	n.a.	3.79	0.05	Lantha	d
TGFBR2	n.a.	27.55	2.73	Lantha	d
TLK1	n.a.	1.96	1.11	Lantha	d
TLK2	n.a.	1.29	6.13	Lantha	d
TNIK	n.a.	11.53	0.20	Lantha	d
TNK1	Km app	-3.97	0.15	Z'Lyte	i
TNK2 (ACK)	n.a.	1.12	0.53	Lantha	d
TTK	n.a.	68.52	2.74	Lantha	d
TXK	Km app	5.65	7.71	Z'Lyte	i
TYK2	Km app	0.08	2.07	Z'Lyte	i
TYRO3 (RSE)	Km app	-11.53	1.05	Z'Lyte	i
ULK1	n.a.	-2.37	1.76	Lantha	d
ULK2	n.a.	-0.26	3.35	Lantha	d
ULK3	n.a.	-3.68	4.84	Lantha	d
VRK2	n.a.	11.49	1.41	Lantha	d
WEE1	n.a.	-19.00	3.16	Lantha	d
WNK2	n.a.	-14.28	1.79	Lantha	d
WNK3	n.a.	-10.45	5.33	Lantha	d
YES1	Km app	19.14	2.22	Z'Lyte	i
ZAK	n.a.	-1.95	1.40	Lantha	d
ZAP70	Km app	15.32	0.02	Z'Lyte	i

12.3 PI4KB - Kinetic measurements (SignalChem)

Raw data

N1

Raw data

ENZ ONLY		CTRL		0.1uM		1uM		10uM		50uM	
7,379	6,683	142,698	163,364	158,409	142,669	137,046	132,061	62,485	86,782	62,962	58,978
9,128	8,477	265,632	263,518	243,812	235,704	211,741	230,360	124,641	149,204	94,115	94,964
16,740	13,448	468,492	466,666	446,969	437,788	393,698	436,466	256,239	276,508	190,639	172,561
23,477	23,751	717,733	723,739	696,038	677,183	624,846	705,258	415,873	441,214	287,502	275,867
46,072	37,873	980,797	1,043,908	1,003,032	942,973	955,304	1,028,733	651,524	692,456	463,008	420,105
73,631	68,787	1,350,506	1,403,200	1,307,468	1,265,989	1,308,286	1,403,482	979,332	1,062,710	677,905	643,118

Average	EO	0µM	0.1µM	1µM	10µM	50µM
	7,031	153,031	150,539	134,554	74,634	60,970
	8,803	264,575	239,758	221,051	136,923	94,540
	15,094	467,579	442,379	415,082	266,374	181,600
	23,614	720,736	686,611	665,052	428,544	281,685
	41,973	1,012,353	973,003	992,019	671,990	441,557
	71,209	1,376,853	1,286,729	1,355,884	1,021,021	660,512

NET RLU	0µM	0.1µM	1µM	10µM	50µM	ATP conversion equation	Slope	Intercept
5µM	146,000	143,508	127,523	67,603	53,939	y = 412844x + 5364.1	412844	-5364.1
10µM	255,773	230,956	212,248	128,120	85,737	y = 765939x + 15005	765939	-15005
25µM	452,485	427,285	399,988	251,280	166,506	y = 2E+06x + 42919	2000000	-42919
50µM	697,122	662,997	641,438	404,930	258,071	y = 3E+06x + 63722	3000000	-63722
100µM	970,380	931,030	950,046	630,018	399,584	y = 7E+06x + 208472	7000000	-208472
200µM	1,305,644	1,215,520	1,284,675	949,812	589,303	y = 1E+07x + 230260	10000000	-230260

% ATP conversion	0µM	0.1µM	1µM	10µM	50µM
5µM	34.07	33.46	29.59	15.08	11.77
10µM	31.43	28.19	25.75	14.77	9.23
25µM	20.48	19.22	17.85	10.42	6.18
50µM	21.11	19.98	19.26	11.37	6.48
100µM	10.88	10.32	10.59	6.02	2.73
200µM	10.75	9.85	10.54	7.20	3.59

µM phosphate transferre	0 µM	0.1 µM	1 µM	10 µM	50 µM
5 µM	1.7033	1.6731	1.4795	0.7538	0.5883
10 µM	3.1434	2.8194	2.5752	1.4768	0.9235
25 µM	5.1196	4.8046	4.4634	2.6045	1.5448
50 µM	10.5567	9.9879	9.6286	5.6868	3.2391
100 µM	10.8844	10.3223	10.5939	6.0221	2.7302
200 µM	21.5077	19.7052	21.0883	14.3910	7.1809

V (pmol P transferred/L/s)					
[ATP]	LDC003472:02 Concentration				
	0 µM	0.1 µM	1 µM	10 µM	50 µM
5 µM	946	929	822	419	327
10 µM	1,746	1,566	1,431	820	513
25 µM	2,844	2,669	2,480	1,447	858
50 µM	5,865	5,549	5,349	3,159	1,800
100 µM	6,047	5,735	5,886	3,346	1,517
200 µM	11,949	10,947	11,716	7,995	3,989

N2

Raw data

ENZ ONLY		CTRL		0.1uM		1uM		10uM		50uM	
6,649	6,189	141,727	131,052	141,280	143,786	126,075	115,671	48,937	49,607	41,473	36,371
7,666	7,217	167,320	199,403	156,977	149,891	142,311	134,478	118,868	120,539	124,485	77,618
14,348	13,583	323,939	337,977	342,557	368,323	340,640	340,057	188,786	203,728	111,698	197,674
26,596	23,484	575,069	589,891	626,372	621,857	557,411	541,168	315,133	328,457	224,718	251,118
38,262	37,028	691,319	781,112	814,914	801,102	770,457	746,679	447,548	494,803	391,332	354,770
55,958	53,401	676,593	746,065	844,053	875,844	846,525	802,746	691,036	728,995	613,618	577,261

Average	EO	0µM	0.1µM	1µM	10µM	50µM
	6,419	136,390	142,533	120,873	49,272	38,922
	7,442	183,362	153,434	138,395	119,704	101,052
	13,966	330,958	355,440	340,349	196,257	154,686
	25,040	582,480	624,115	549,290	321,795	237,918
	37,645	736,216	808,008	758,568	471,176	373,051
	54,680	711,329	859,949	824,636	710,016	595,440

NET RLU	0µM	0.1µM	1µM	10µM	50µM	ATP conversion equation	Slope	Intercept
5µM	129,971	136,114	114,454	42,853	32,503	y = 412844x + 5364.1	412844	-5364.1
10µM	175,920	145,993	130,953	112,262	93,610	y = 765939x + 15005	765939	-15005
25µM	316,993	341,475	326,383	182,292	140,721	y = 2E+06x + 42919	2000000	-42919
50µM	557,440	599,075	524,250	296,755	212,878	y = 3E+06x + 63722	3000000	-63722
100µM	698,571	770,363	720,923	433,531	335,406	y = 7E+06x + 208472	7000000	-208472
200µM	656,650	805,269	769,956	655,336	540,760	y = 1E+07x + 230260	10000000	-230260

% ATP conversion	0µM	0.1µM	1µM	10µM	50µM
5µM	30.18	31.67	26.42	9.08	6.57
10µM	21.01	17.10	15.14	12.70	10.26
25µM	13.70	14.93	14.17	6.97	4.89
50µM	16.46	17.85	15.35	7.77	4.97
100µM	7.00	8.03	7.32	3.22	1.81
200µM	4.26	5.75	5.40	4.25	3.11

µM phosphate transferre	0 µM	0.1 µM	1 µM	10 µM	50 µM
5 µM	1.5091	1.5835	1.3212	0.4540	0.3287
10 µM	2.1009	1.7102	1.5138	1.2698	1.0263
25 µM	3.4259	3.7319	3.5433	1.7422	1.2225
50 µM	8.2286	8.9225	7.6755	3.8839	2.4859
100 µM	7.0014	8.0270	7.3207	3.2151	1.8133
200 µM	8.5278	11.5002	10.7939	8.5015	6.2100

V (pmol P transferred/L/s)					
[ATP]	LDC003472:02 Concentration				
	0 µM	0.1 µM	1 µM	10 µM	50 µM
5 µM	838	880	734	252	183
10 µM	1,167	950	841	705	570
25 µM	1,903	2,073	1,969	968	679
50 µM	4,571	4,957	4,264	2,158	1,381
100 µM	3,890	4,459	4,067	1,786	1,007
200 µM	4,738	6,389	5,997	4,723	3,450

N3

Raw data

ENZ ONLY		CTRL		0.1uM		1uM		10uM		50uM	
6,452	7,381	113,983	102,896	110,534	112,389	99,019	92,069	39,036	41,082	35,857	33,390
7,684	8,144	201,382	201,580	205,585	215,245	216,453	208,347	103,942	110,453	91,752	79,596
13,802	13,723	409,068	434,304	446,830	467,531	447,938	441,790	247,005	260,499	223,757	196,391
22,565	22,492	662,678	691,729	665,046	688,798	661,574	622,702	350,247	366,080	313,029	276,577
36,364	37,073	837,485	868,577	821,944	840,696	814,199	804,605	528,692	544,473	477,538	415,128
69,271	68,557	1,079,900	1,136,015	1,196,064	1,206,076	1,180,261	1,179,011	856,432	880,419	798,172	712,929

Average

EO	0µM	0.1µM	1µM	10µM	50µM
6,917	108,440	111,462	95,544	40,059	34,624
7,914	201,481	210,415	212,400	107,198	85,674
13,763	421,686	457,181	444,864	253,752	210,074
22,529	677,204	676,922	642,138	358,164	294,803
36,719	853,031	831,320	809,402	536,583	446,333
68,914	1,107,958	1,201,070	1,179,636	868,426	755,551

NET RLU

	0µM	0.1µM	1µM	10µM	50µM	ATP conversion equation	Slope	Intercept
5µM	101,523	104,545	88,628	33,143	27,707	y = 412844x + 5364.1	412844	-5364.1
10µM	193,567	202,501	204,486	99,284	77,760	y = 765939x + 15005	765939	-15005
25µM	407,924	443,418	431,102	239,990	196,312	y = 2E+06x + 42919	2000000	-42919
50µM	654,675	654,394	619,610	335,635	272,275	y = 3E+06x + 63722	3000000	-63722
100µM	816,313	794,602	772,684	499,864	409,615	y = 7E+06x + 208472	7000000	-208472
200µM	1,039,044	1,132,156	1,110,722	799,512	686,637	y = 1E+07x + 230260	10000000	-230260

% ATP conversion

	0µM	0.1µM	1µM	10µM	50µM
5µM	23.29	24.02	20.17	6.73	5.41
10µM	23.31	24.48	24.74	11.00	8.19
25µM	18.25	20.02	19.41	9.85	7.67
50µM	19.70	19.69	18.53	9.06	6.95
100µM	8.68	8.37	8.06	4.16	2.87
200µM	8.09	9.02	8.80	5.69	4.56

µM phosphate transferre

	0 µM	0.1 µM	1 µM	10 µM	50 µM
5 µM	1.1646	1.2012	1.0084	0.3364	0.2706
10 µM	2.3313	2.4479	2.4738	1.1003	0.8193
25 µM	4.5626	5.0062	4.8523	2.4634	1.9174
50 µM	9.8492	9.8445	9.2648	4.5319	3.4759
100 µM	8.6834	8.3733	8.0602	4.1627	2.8735
200 µM	16.1757	18.0379	17.6092	11.3850	9.1275

V (pmol P transferred/L/s)

[ATP]	LDC003472:02 Concentration				
	0 µM	0.1 µM	1 µM	10 µM	50 µM
5 µM	647	667	560	187	150
10 µM	1,295	1,360	1,374	611	455
25 µM	2,535	2,781	2,696	1,369	1,065
50 µM	5,472	5,469	5,147	2,518	1,931
100 µM	4,824	4,652	4,478	2,313	1,596
200 µM	8,986	10,021	9,783	6,325	5,071

Processed data for Lineweaver-Burk plots

n1	1/V (pmolP transferred/L/d)					
		Pipinib				
	1/[ATP]	0 µM	0.1 µM	1 µM	10 µM	50 µM
5	0.2	0.00105708	0.00107643	0.00121655	0.00238663	0.0030581
10	0.1	0.00057274	0.00063857	0.00069881	0.00121951	0.00194932
25	0.04	0.00035162	0.00037467	0.00040323	0.00069109	0.0011655
50	0.02	0.0001705	0.00018021	0.00018695	0.00031656	0.00055556
100	0.01	0.00016537	0.00017437	0.00016989	0.00029886	0.0006592
200	0.005	8.3689E-05	9.1349E-05	8.5353E-05	0.00012508	0.00025069
n2	1/V (pmolP transferred/L/d)					
		Pipinib				
	1/[ATP]	0 µM	0.1 µM	1 µM	10 µM	50 µM
	0.2	0.00119332	0.00113636	0.0013624	0.00396825	0.00546448
	0.1	0.0008569	0.00105263	0.00118906	0.00141844	0.00175439
	0.04	0.00052549	0.00048239	0.00050787	0.00103306	0.00147275
	0.02	0.00021877	0.00020173	0.00023452	0.00046339	0.00072411
	0.01	0.00025707	0.00022427	0.00024588	0.00055991	0.00099305
	0.005	0.00021106	0.00015652	0.00016675	0.00021173	0.00028986
n3	1/V (pmolP transferred/L/d)					
		Pipinib				
	1/[ATP]	0 µM	0.1 µM	1 µM	10 µM	50 µM
	0.2	0.0015456	0.00149925	0.00178571	0.00534759	0.00666667
	0.1	0.0007722	0.00073529	0.0007278	0.00163666	0.0021978
	0.04	0.00039448	0.00035958	0.00037092	0.00073046	0.00093897
	0.02	0.00018275	0.00018285	0.00019429	0.00039714	0.00051787
	0.01	0.0002073	0.00021496	0.00022331	0.00043234	0.00062657
	0.005	0.00011128	9.979E-05	0.00010222	0.0001581	0.0001972

mean values	1/V (pmolP transferred/L/d)				
	Pipinib				
1/[ATP]	0 µM	0.1 µM	1 µM	10 µM	50 µM
0.2	0.00126533	0.00123735	0.00145489	0.00390083	0.00506308
0.1	0.00073395	0.00080883	0.00087189	0.00142487	0.00196717
0.04	0.00042386	0.00040555	0.00042734	0.0008182	0.00119241
0.02	0.00019067	0.00018827	0.00020525	0.00039236	0.00059918
0.01	0.00020991	0.00020453	0.00021303	0.00043037	0.0007596
0.005	0.00013534	0.00011589	0.00011811	0.00016497	0.00024591

SD	1/V (pmolP transferred/L/d)				
	Pipinib				
1/[ATP]	0 µM	0.1 µM	1 µM	10 µM	50 µM
0.2	0.00020583	0.0001868	0.00024139	0.00120975	0.00150028
0.1	0.00011912	0.00017686	0.00022458	0.00017036	0.00018146
0.04	7.396E-05	5.4685E-05	5.8453E-05	0.00015277	0.00021875
0.02	2.0487E-05	9.585E-06	2.0911E-05	6.0041E-05	8.9672E-05
0.01	3.7481E-05	2.1665E-05	3.1862E-05	0.00010658	0.00016561
0.005	5.4711E-05	2.8938E-05	3.5078E-05	3.5707E-05	3.7977E-05

12.4 CRISPR-Cas clone screening (protein level)

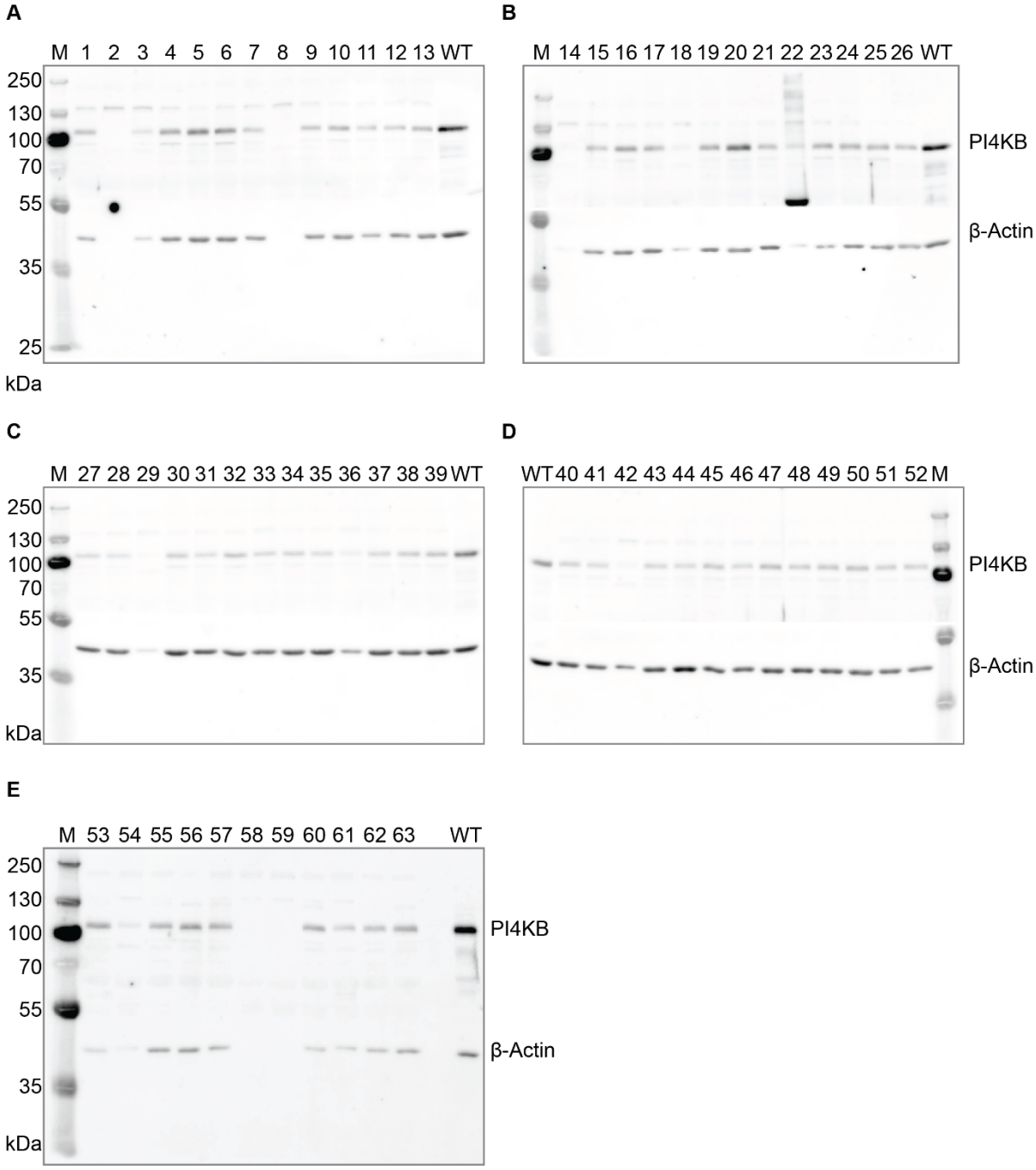

CRISPR-Cas Screening campaign. Bulk cells were seeded at low density to enable growth of single cell colonies. At sufficient size, colonies were detached and transferred to single wells of a -well plate. Here, clones were expanded and lysed upon confluence. Proteins were separated by means of SDS page and transferred onto PVDF-membranes, before blocking and incubation with primary (anti-PIKB and anti-β-Actin) and corresponding secondary antibodies (CW and RD IR-antibodies). The blots in A.-E. show all retrieved clones in ascending order (n=1). WT=wildtype NIH/3T3 lysate, M=marker.

CURRICULUM VITAE

PERSONAL INFORMATION

Surname:	Kremer
Name:	Lea
Date of Birth:	26.08.1989
Place of Birth:	Herdecke
Citizenship:	German

EDUCATION

10/2013 – 03/2018 **PhD student at the Max Planck Institute of Molecular Physiology**

Research topic: Identification and characterization of Hedgehog signaling inhibitors and their cellular targets

Advisor: Prof. Dr. Dr. h.c. Herbert Waldmann

10/2011 – 09/2013 **Master's at University Duisburg-Essen, Medical Biology**

Focus areas: Special bioinformatics, virology and internal medicine

Master thesis:

Research topic: Identification and Characterization of Wnt pathway modulators

Advisor: Prof. Dr. Dr. h.c. Herbert Waldmann

10/2008 – 09/2011 **Bachelor's at University Duisburg-Essen, Medical Biology**

Focus areas: Pharmacology and toxicology, microbiology and genetics

Bachelor thesis:

Research topic: Radiosensitization of non-small cell lung cancer and breast cancer stem cells via inhibition of glucose transporter GLUT1

Advisor: Prof. Dr. Monica Palmada

EIDESSTATTLICHE VERSICHERUNG (AFFIDAVIT)

Kremer, Lea
Name, Vorname
(Surname, first name)

173136
Matrikel-Nr.
(Enrolment number)

Belehrung:

Wer vorsätzlich gegen eine die Täuschung über Prüfungsleistungen betreffende Regelung einer Hochschulprüfungsordnung verstößt, handelt ordnungswidrig. Die Ordnungswidrigkeit kann mit einer Geldbuße von bis zu 50.000,00 € geahndet werden. Zuständige Verwaltungsbehörde für die Verfolgung und Ahndung von Ordnungswidrigkeiten ist der Kanzler/die Kanzlerin der Technischen Universität Dortmund. Im Falle eines mehrfachen oder sonstigen schwerwiegenden Täuschungsversuches kann der Prüfling zudem exmatrikuliert werden, § 63 Abs. 5 Hochschulgesetz NRW.

Die Abgabe einer falschen Versicherung an Eides statt ist strafbar.

Wer vorsätzlich eine falsche Versicherung an Eides statt abgibt, kann mit einer Freiheitsstrafe bis zu drei Jahren oder mit Geldstrafe bestraft werden, § 156 StGB. Die fahrlässige Abgabe einer falschen Versicherung an Eides statt kann mit einer Freiheitsstrafe bis zu einem Jahr oder Geldstrafe bestraft werden, § 161 StGB.

Die oben stehende Belehrung habe ich zur Kenntnis genommen:

Official notification:

Any person who intentionally breaches any regulation of university examination regulations relating to deception in examination performance is acting improperly. This offence can be punished with a fine of up to EUR 50,000.00. The competent administrative authority for the pursuit and prosecution of offences of this type is the chancellor of the TU Dortmund University. In the case of multiple or other serious attempts at deception, the candidate can also be unenrolled, Section 63, paragraph 5 of the Universities Act of North Rhine-Westphalia.

The submission of a false affidavit is punishable.

Any person who intentionally submits a false affidavit can be punished with a prison sentence of up to three years or a fine, Section 156 of the Criminal Code. The negligent submission of a false affidavit can be punished with a prison sentence of up to one year or a fine, Section 161 of the Criminal Code.

I have taken note of the above official notification.

Dortmund, 05.02.2018
Ort, Datum
(Place, date)

Unterschrift
(Signature)

Titel der Dissertation:
(Title of the thesis):

Identification and Biological Characterization of Novel Hedgehog Signaling Pathway Inhibitors and their Cellular Targets

Ich versichere hiermit an Eides statt, dass ich die vorliegende Dissertation mit dem Titel selbstständig und ohne unzulässige fremde Hilfe angefertigt habe. Ich habe keine anderen als die angegebenen Quellen und Hilfsmittel benutzt sowie wörtliche und sinngemäße Zitate kenntlich gemacht.
Die Arbeit hat in gegenwärtiger oder in einer anderen Fassung weder der TU Dortmund noch einer anderen Hochschule im Zusammenhang mit einer staatlichen oder akademischen Prüfung vorgelegen.

I hereby swear that I have completed the present dissertation independently and without inadmissible external support. I have not used any sources or tools other than those indicated and have identified literal and analogous quotations.

The thesis in its current version or another version has not been presented to the TU Dortmund University or another university in connection with a state or academic examination.*

*Please be aware that solely the German version of the affidavit ("Eidesstattliche Versicherung") for the PhD thesis is the official and legally binding version.

Dortmund, 05.02.2018
Ort, Datum
(Place, date)

Unterschrift
(Signature)